THE UNIVERSITY OF CALGARY

OPTIMIZATION AND KNOCK MODELING OF A GAS FUELED SPARK IGNITION ENGINE

by

Alireza Alizadeh Attar

A DISSERTATION
SUBMITTED TO THE FACULTY OF GRADUATE STUDIES
IN PARTIAL FULFILLMENT OF THE REQUIREMENTS FOR THE
DEGREE OF DOCTOR OF PHILOSOPHY

DEPARTMENT OF MECHANICAL ENGINEERING

CALGARY, ALBERTA

November, 1997

Abstract

The final design of an engine is normally the best compromise between various requirements achieved through lengthy and costly processes involving the use of experimental and analytical approaches.

Analytical techniques, primarily in the form of computer codes, are intended to reduce the time and resources needed for this purpose and provide an insight into the complex interacting processes which occur in the engine. The availability of such codes for the prediction of engine combustion and knock is limited and their scope of application is narrow mainly due to the complexity of the processes involved.

The present contribution describes a predictive procedure for the onset of knock and associated performance parameters of a spark ignition engine fueled with common gaseous fuels such as methane. The two-zone predictive combustion model is based on an estimate of the effective duration of the combustion period and the mass burning rate for any set of operating conditions. The unburned end gas preignition chemical reaction activity is described by a detailed chemical reaction kinetic scheme. The variation with time during a cycle of the value of a dimensionless knock criterion, K, is calculated. This parameter relates the total energy released within the end gas due to autoignition reaction activity per unit of the corresponding instantaneous volume relative to the total energy release per cylinder volume that would take place normally due to regular flame propagation. When knocking is encountered the value of K builds up to a sufficiently high value that exceeds an experimentally established acceptable limit. Under normal operating conditions, its value remains throughout the combustion period at comparatively low levels.

There is a need to provide effective guidelines for predicting the highest limit for acceptable power output for any spark ignition engine when operating on gaseous fuels. This is especially the case in relation to the encountering of knock that can impose a severe barrier to engine output and the efficient use of some fuel resources in engines. The results of a parametric study that investigates the influence of operational variables on engine performance and the knock intensity are presented. A relatively simple procedure for choosing an optimum operating condition close to an initial setting is also outlined.

A deterministic gradient based model and a simple genetic algorithm are described and shown to be capable of predicting analytically the changes in specified operating parameters to produce optimum output while maintaining knock free operation. A penalty based transformation method is used to convert the constrained engine optimization problem into an unconstrained one. The concepts of these two optimization methods are presented in detail with a number of typical illustrative examples.

There is no universal agreement on a satisfactory procedure for knock rating of gaseous fuels and their mixtures in spark ignition engines. The suitability of different procedures used in the past by different researchers is examined both analytically and experimentally. It is shown that a rating procedure based on a scale that uses n-butane-methane mixtures offers much promise.

Acknowledgments

I would like to thank my supervisor, Dr. G.A. Karim, for his support, guidance, corrections, and valuable suggestions. His encouragement allowed me to pursue my own ideas and to learn how to approach, cope, and solve a problem. I also wish to extend my thanks to all of the professors of the department, specially Dr. Ida Wierzba, whom I enjoyed their guidance during my studies.

Behind any valuable achievement, there exists some invisible family support. I must thank my parents, sisters, and brothers for their constant encouragement, help and support. Also, I wish to express my deepest appreciation to my wife and my children for their understanding, encouragement and support which made this work possible.

It has been a pleasure to work with fellow students, Reza Babayi, Mehrdad Farid, Bade Shrestha, M. Karbasi and other friends in the Department of Mechanical Engineering whose patience and help throughout my research remained constant.

Also, the contributions to this work of ex-graduate students Drs. Al-Alousi, Al-Himyary, Z. Liu, S. Klat, G. Zhou and J. Gao in providing analytical tools and experimental results cannot be overlooked.

The cooperation of the technical staff especially Mr. B.W. Stephens and Mr. R. Gustafson, and secretarial staff including Cecile Calverley, Maria Berry and Lynn Banach, in the Department of Mechanical Engineering is acknowledged.

Finally, the financial assistance of the Ministry of Petroleum and the Ministry of Culture and Higher Education of IRAN and the Natural Sciences and Engineering Research Council of Canada (NSERC) are greatly acknowledged.

Dedication

To my parents who devoted themselves to raise me,

my teachers to whom I owe all that I know,

and to my wife and children who patiently encouraged me throughout.

Nomenclature

Notation:

A, B	Constants, Eqs.3.46 and 3.61
ATDC	After Top Dead Center
ABDC	After Bottom Dead Center
BDC	Bottom Dead Center
BBDC	Before Bottom Dead Center
BTDC	Before Top Dead Center
C	Constant, Concentration
C_1, C_2	Constants, Eq. 3.25
Cp	Specific Heat at Constant Pressure
$\overline{Cp}$	Average Specific Heat at Constant Pressure
Cv	Specific Heat at Constant Volume
CR	Compression Ratio
D	Cylinder Bore Diameter
d_{ef}	Effective Flame Propagation Distance
E_{CD}	Error in Combustion Duration
E_{ig}	Error in Ignition Lag
E_{jf} and E_{jb}	Activation Energies of the j^{th} Reaction, Eq. 3.76
$e_{\vec{\theta_{st}}}$	Unit Vector in the Direction of Spark Timing, Eq. 6.2
$e_{\vec{CR}}$	Unit Vector in the Direction of Compression Ratio, Eq. 6.2
F	Scaled Fitness, Eq. 7.4

f	Any Function of Design Variables for Genetic Algorithm
f_1	Any Function of Design Variables for Gradient-Based Algorithm
g	Inequality Constraints, Eq. 7.1
$\overline{g}$	Equality Constraints, Eq. 7.1
H_u	Energy of End-Gas Self Reaction, Eq. 3.70
H_o	Energy of Normal Combustion, Eq. 3.71
$H_2\%$	Hydrogen Concentration in Fuel
h	Specific Enthalpy
I.O.C.	Initial Operating Conditions
K	Dimensionless Knock Criterion
K_{cr}	The Value of Knock Criterion at Knock Limit
K_{jf} and K_{jb}	Rate Constants for the j^{th} Reaction, Eqs. 3.73 and 3.76
K_{p1} to K_{p9}	Equilibrium Constant for Equations 3.36 to 3.44
KLCR	Knock Limited Compression Ratio
KLST	Knock Limited Spark Timing (Degrees BTDC)
L	Length of The Connecting Rod
L_i	Flammability Limit of a Species
L_{mix}	Flammability Limit of the Mixture
MBT	Minimum Timing for Best Power
M.O.C.	Modified Operating Conditions
m	Mass
m_a	Mass of Fresh Charge, Eq. 3.10
N	Population Size in Genetic Algorithm

$\overline{N}_{C/O}$	Carbon to Oxygen Atomic Ratio
$\overline{N}_{H/O}$	Hydrogen to Oxygen Atomic Ratio
$\overline{N}_{N/O}$	Nitrogen to Oxygen Atomic Ratio
$\overline{N}_{I/O}$	Inert to Oxygen Atomic Ratio
n_r	Number of Mole of Residuals
n_θ	Polytropic Index
P	Absolute Pressure
P_c	Crossover Probability
P_m	Mutation Probability
P_{mt}	Gas Pressure in the Motored Engine, Eq. 3.25
p_{sj}	Probability of a Particular Solution Survival
Q	Heat Transfer
$q(\vec{x})$	Typical Function Defined in Figures 7.6 and 7.7
R	Gas Constant, Crank Radius
R_{jf} and R_{jb}	Forward and Backward Reaction Rates of the j^{th} reaction, Eq. 3.75
$\overline{R}$	Universal Gas Constant
r	Penalty Multiplier
S	Stroke
S_f	Flame Speed
S_p	Average Piston Speed
$\vec{s}$	Search Direction Vector for Minimizing
T	Temperature (K)
T_o	Intake Temperature (K)

TDC	Top Dead Center
t	Time
U	Internal Energy
u	Specific Internal Energy
V	Volume
V_c	Clearance Volume
V_d	Swept Volume
v	Specific Volume
W	Power Output
W_o	Power Output for Initial Operating Conditions
X_i	Chemical Specie Formula, Equation 3.73
x	Function, Equation 3.46
$\vec{x}$	Set of Design Variables or Operational Parameters
$Y(\vec{x})$	Typical Function Defined in Figures 7.6 and 7.7
y	Fuel Molar Fraction, Equation 3.65
z	Function, Equation 3.46
σ	Mutiplier Function for Mass Burning Rate, Eq. 3.66
ϵ	Termination Criterion for Optimization Algorithm
λ	Heat Transfer Coefficient, Multiplier for Search Direction Vector
λ^*	A Critical Value for λ to Minimize Ψ
θ	Crank Angle (Degree)
θ_a	Crank Angle at the Time of Auto-Ignition (Degree)
$\theta_{e.i.}$	Crank Angle at the End of Ignition Lag (Degree)

$\theta_{e.c.}$	Crank Angle at the End of Combustion Duration (Degree)
α_{ijf} and α_{ijb}	Stoichiometric Coefficients, Eq. 3.73
ρ	Mixture Density
$\rho_{a,i}$	Inlet Air Density
ϕ	Fuel Equivalence Ratio
η	Thermal Efficiency
η_v	Volumetric Efficiency
Ψ	Objective Function
$\Delta\Psi$	Gradient of Ψ
$\lvert\Delta\Psi\rvert$	Norm of the Gradient of Ψ
$\Delta\theta$c	Combustion Duration
$\Delta\theta$c, m	Combustion Duration for a Mixture, Equation 3.65
$\Delta\theta$ig	Ignition Lag

Subscripts:

av	Average
b	Burned
c	Combustion, End of Combustion
e	Exhaust
f	Fuel
jf	Forward Reaction
jb	Backward Reaction

i	Species, Ignition
l	Lean Limit
m	Mean Value
max	Maximum
min	Minimum
o	Initial Conditions
p	Products
r	Rich Limit, Reactants
st	Spark Timing
t	Time
u	Unburned
w	Wall

Table of Contents

List of Tables

List of Figures

Chapter 1

Introduction

1.1 Prologue

Most of the energy produced for world consumption is currently from fossil fuels. The main contribution comes from crude oil followed by coal and natural gas. The increasing cost of liquid hydrocarbon fuels and the tightening of legislation on exhaust emission limits in recent years have stimulated interests in the use of alternative fuels in engine applications and automotive vehicles. Since natural gas, at present, has a favorable cost and supply advantages over gasoline and diesel fuel, engine conversion to natural gas has increased in recent years.

The lean burn natural gas approach in spark ignition engines has a number of positive features that make it attractive. It can provide in principle high thermal efficiency, low likelihood for knock, reduced emissions especially of NO_x, permit high compression ratio operation and low heat transfer. It may dispense with exhaust catalytic treatment and the need for precise control of the mixture quality. However, there are a number of difficulties associated with lean burn operation that require further research and development such as the associated slower flame propagation, less complete combustion, increased cyclic variations and encountering occasionally flame failure. These shortcomings can lead to poor efficiency, low power output and excessive emissions [1, 2].

1.2 Natural Gas and Hydrogen as a Vehicular Fuel

Natural gas has considerable potential as a *clean fuel* for motor vehicles. The technical advantages of natural gas include extremely low photochemical reactivity, zero evaporative emissions, reduced cold-start and low-temperature emissions due to the elimination of cold mixture enrichment and compatibility with fuel efficient lean-burn technology. Natural gas which has a high equivalent research octane number (RON) of 130 [3], the highest of any commonly used fuel as compared to 95 for a premium gasoline, allows the use of high compression ratios which increases engine efficiency. Its low lean operational limit and the absence of higher hydrocarbons makes it suitable for the optimization of an ultra-low pollution engine.

Natural gas is carried in vehicles as a compressed gas (called CNG) in high pressure cylinders which are built to rigorous and high quality standards. Studies conducted in the late 1970s could not identify a single instance of a CNG cylinder failure in a collision [4]. This is in contrast to the records of collision-caused fuel leakage and fires in gasoline and LPG fueled vehicles.

For equal volume of storage tank, the energy content of CNG at 20 MPa (3000 psig) and ambient temperature is about one-fifth that of diesel fuel or one-fourth that of gasoline. The low thermal energy storage capacity of CNG poses a significant problem in some applications such as in passenger cars. Recent developments in high-strength composite materials have made it possible to reduce the weight of CNG cylinders substantially which would enable a car to carry more fuel, compared to the past, without any substantial increase in the dead load.

The laminar flame speed of natural gas mixture is lower than that of other hy-

drocarbons mainly because of its relatively high effective activation energy. This is most significant under lean operation, which leads to an increase in the engine hydrocarbon emissions. The unburned hydrocarbons are mainly composed of methane, which has a low reactivity to form ozone and photochemical smog in an urban environment, but would contribute to the greenhouse effect. Effective measures need to be taken to minimize these emissions.

Recently, operation on lean mixtures has been extensively studied as a technique to reduce the exhaust emissions as well as to improve the fuel economy of spark ignition engines [5, 6]. However, there are two major problems hindering its widespread application to engines. These are the substantial decrease in the overall burning velocity and the increase in the tendency to misfire as the mixture is made leaner. In order to solve these problems, various measures have been attempted such as increasing the ignition energy [7], stratifying the mixture, intensifying the level of turbulence, modifications made to the design of the combustion chamber, intake ducts, piston shape, etc. [8, 9, 10, 11]. Although these methods may improve the combustion performance with lean mixtures to some extent, the burning of yet leaner mixtures at even higher burning velocities requires further measures.

Hydrogen has the lowest flammability limit and the highest burning velocity among common fuels [12] and the addition of a small amount of hydrogen to the fuel can contribute to the solution of the problems associated with lean operation. It can be expected also to burn mixtures that are leaner than the effective flammability limit of the hydrocarbon fuel. The addition of hydrogen to methane may affect the knock rating of the mixture significantly.

No satisfactory methods are available to evaluate the knock resistance character-

istics of a gaseous fuel. However, it has been proposed to use a method that employs a *Methane-Number*, which is somewhat analogous to the octane number for liquid fuels. *The methane number* is defined as the percentage by volume of methane in a blend with hydrogen that exactly matches the knock intensity of the unknown fuel sample under specified operating conditions in a CFR engine [13]. Pure methane has a knock rating of 100 and that of pure hydrogen is zero.

Engines are desired to be operated at their optimum performance. The optimization of performance involves many compromises. The final design is normally considered as the best compromise between various, often conflicting, requirements, achieved through lengthy and costly processes involving the use of experiment aided sometimes by analytical techniques. More recently, analytical techniques, primarily in the form of computer codes, are intended to reduce the time and resources needed for this purpose and to provide an insight into the complex interaction within the processes that occur in the engine. As to engine combustion and knock prediction, the availability of such codes tends to be limited and their scope of application is narrow mainly due to the complexity of the processes involved.

There is a need to provide effective guidelines for predicting the highest limit for acceptable power output for any spark ignition engine just before the onset of knock when operating on gaseous fuels. No specific guidelines are usually available to designers, engine converters and operators to show how to deal optimally with any specific engine installation when operating on a specific gaseous fuel. This is especially the case in relation to the encountering of knock which imposes a severe barrier to engine output and the efficient utilization of some fuel resources in engines.

Hence, the major objectives of the present research were:

1. To develop a predictive approach for the performance of a spark ignition engine operating on methane and its blend with other gaseous fuels notably hydrogen.

2. To predict the incidence of knock and its intensity for a spark ignition engine operating on gaseous fuels.

3. To evaluate the effectiveness of the *methane number* as a tool for the knock rating of gaseous fuels and to suggest, if possible, alternative approaches.

4. To propose some automated analytical models applicable to engine design and operation optimization.

5. To suggest guidelines for choosing operating parameters of a spark ignition engine to get maximum knock free power output or efficiency.

Much of the work carried out initially was in relation to the use of the common fuel methane, the main constituent of natural gas. This can be extended to consider the use of various gaseous fuel mixtures. Mainly methane-hydrogen mixtures were also considered. Various other approaches were tried to investigate the borderline knock operation when different fuel mixtures containing methane are employed.

1.3 Outline of Thesis

After this brief introduction in the current chapter, a literature review of the work relating to the modeling of the combustion, heat transfer, knock, optimization and other related subject-matter will be presented in Chapter 2.

Chapter 3 describes a semi-empirical two-zone predictive approach for simulation

of the performance and knock intensity of a spark ignition engine operating with methane, hydrogen and their mixtures.

Chapter 4 describes the experimental set-up of a CFR engine, which was used to get the required experimental data to support the two-zone predictive model. It includes the procedure for running tests and calibration of the equipment of the system.

Chapter 5 discusses the influence of some of the major operational and design parameters such as spark timing and compression ratio on the power output, efficiency, the tendency to knock and its intensity, and minimum spark timing for maximum power output (MBT timing) when methane-hydrogen mixtures are used as the fuel.

Chapter 6 deals with engine operation at borderline knock. It explains how to choose, for an initially knocking engine, a set of optimum operating conditions that takes it out of knock with the least undermining of key performance parameters. A parametric study is then presented and some guidelines for engine operation just before the onset of knock are suggested.

Chapter 7 describes the application of two well-established automated optimization algorithms, a gradient-based and a genetic algorithm method, which may be applied to the engine optimization problems.

Chapter 8 evaluates the suitability of applying the *methane number* to the knock rating of gaseous fuels, based on the model developed, and compares it with alternative approaches.

Chapter 9 presents a brief general discussion of this study, summarizes the results and suggests areas for further research.

Publication list and appendices are attached at the end of this work.

Chapter 2

Literature Survey

2.1 Introduction

Optimization is concerned with achieving the best outcome of a given operation while satisfying certain constraints. Human beings, guided and influenced by their natural surroundings, almost instinctively, usually tend to perform all functions in a manner that economizes in energy or minimizes discomfort and pain. The motivation is to exploit the available limited resources in a manner that maximizes output or profit. For example, engine designers always aim at maximizing power output and/or efficiency. The use of a high compression ratio, required for improvement of spark ignition engine efficiency and fuel economy, unfortunately promotes also the incidence of knock. Here, the term knock is identified with the physical manifestations of in cylinder pressure oscillations and noise. Under knock conditions, engine performance is impaired and prolonged operation may lead to serious engine damage [14, 15, 16]. Modern engine control systems modify the spark ignition advance to maximize output and efficiency at any given engine condition; in doing so they may require operation close to the knock boundary. Therefore, it is necessary not only to understand fully the combustion mechanisms that promote knock, but also to devise effective methods for its control.

Knock is defined as the abnormal combustion of part of the end-gas ahead of the arrival of the turbulent flame front following spark ignition. The sudden and rapid

heat release due to this abnormal combustion leads to a rapid pressure rise followed by pressure fluctuations within the chamber, objectionable noise and excessive local heat loss to the walls. Knock is acknowledged to be caused by the autoignition of this unburned mixture. In order to model and predict the incidence of knock, it is necessary to model and predict variations in the unburned gas state parameters and the unburned gas preignition reaction activity. Therefore, there is a need to build up a suitable combustion model that provides unburned gas state parameters with an appropriate chemical reaction mechanism for modeling the unburned gas preignition reactions.

The optimization of engine performance involves many compromises through lengthy and costly processes involving the use of experimental and analytical techniques. The experimental part involves efforts such as component design and matching, choice of controllers and control strategies, aerodynamic design, etc. All these involve a high degree of trial and error. Obviously, any means that can reduce the time and resources needed for these tasks will be indispensable to the engine designer and fully cost effective to the engine manufacturer.

Analytical techniques are intended to reduce the time and resources needed for this purpose while providing an insight into the complex interacting processes which occur in an engine. Because of the complexity of processes involved in internal combustion engines, the availability of such codes for the prediction of engine combustion and knock is limited and the scope of their application is quite narrow. This is why this field of engine research until very recently has been dominated by costly, sophisticated, elaborate and time consuming experimental techniques.

Accordingly, this literature survey is divided into three sections, the first deals

with the modeling of engine combustion processes, the second with engine knock and the third with theory of optimization.

2.2 Combustion Models

The air standard cycle modeling [17] of an engine, unlike the real process, considers neither combustion nor time with property changes in the working fluid accomplished by heat or work transfer. In spite of its obvious lack of correspondence with the real processes in engines, these models were used originally to predict some useful general trends of a qualitative nature, such as the effects of changes in compression ratio, initial temperature and pressure on engine work output and efficiency.

The development of digital computers provided the opportunity for researchers to develop more realistic internal combustion engine models. These could for example evaluate more realistically the effects of the combustion process instead of an assumed equivalent heat addition process at different times. These developments gradually made mathematical modeling an increasingly useful tool in engine activities. Combustion models can be considered under two categories:

- Quasi Single-Zone and Multi-Zone models
- Computational Fluid Dynamics (CFD) models

The quasi-zone models perform an analysis of the contents of the engine cylinder during the engine operating cycle, in which unburned and burned mixtures are assumed to be made up of air, fuel, products and a mixture of residual gas. All the gases are usually assumed to be ideal with combustion calculations based on thermodynamics

and conservation of mass. In a single-zone model, it is assumed that the mixture properties throughout the cylinder remain homogeneous and uniform as time is varied independently. The combustion processes are simplified usually by being treated as an equivalent heat addition or heat release phenomenon established on the basis of analysis of the First Law of Thermodynamics and experimental data. This heat release rate is usually taken to be equal to the product of the mass burning rate of the fuel and its lower heating value. The employment of an empirically based correlation of the heat release rate variations with time in the single-zone model approach can make the predicted results of reasonable value within acceptable appropriate error limits. A major weakness in the single-zone model is the need for a specification of the mass burning rate.

A quasi multi-zone model can provide sufficient data for the variations of in-cylinder temperature and concentration. This type of model tends to employ some conceptualizing of the various individual processes occurring in the engine cycle such as fuel injection, mixture formation, heat release and heat transfer. All of these individual processes together with the equations for mass and energy conservation within each zone provide the detailed data necessary for calculating some features of the performance of internal combustion engines. The rate of burning is derived usually from a physical sub-model of the turbulent combustion processes or an empirical heat release correlation.

Computational Fluid Dynamics (CFD) models, on the other hand, are based on the simultaneous numerical solution of mass, momentum, energy and species-conservation equations in either one, two or three dimensions to follow the flame propagation or combustion front through the engine combustion chamber. A de-

tailed CFD model can provide a formidable amount of predicted detailed data regarding the flow field for the operating engine. But, its validity is still very limited due to the complexity and lack of complete understanding of the processes involved such as turbulent flow, reaction rates, heat and mass transfer and how accurately the boundary conditions can be set. Meanwhile, this type of model requires a significant amount of computer power even for the prediction of turbulent fluid flow, with a simplistic description of the complex chemical reactions which take place during combustion. As a result, the use of a CFD model with full chemistry as part of a routine cycle simulation program is not feasible at this stage, especially with the current incomplete understanding of the combustion processes in spark ignition engines. Consequently, most of the combustion models being used are either of the single-zone or quasi multi-zone types.

From the pioneering work of Ricardo [18] and Withrow and Rassweiler [19, 20], there has been a long and distinguished history of spark ignition engine combustion research. This has been extensively reviewed by others such as in reference [21].

For many years, single-zone models were the main approach available for modeling the performance of internal combustion engines. For example, Gatowski and Heywood [8] used a single zone to represent the cylinder charge to research the blow-by gases in crevice flow and their effects on engine operation. This model relies on the pressure-time history of the engine through a heat release analysis that includes the effects of heat transfer, crevice flows and spark ignition. Although this model seems very simple in modeling the combustion process in the engine, it demonstrated that the complicated combustion phenomena in engine operation could be examined with simple experimental set-ups and moderate computing requirements.

The application of single-zone models can often be found in the simulation of combustion processes in motored engines. The whole charge in the motored engine can be treated as the end gas being compressed and sensitized to autoignition condition in a single zone model to research the effects of the chemical and physical processes on the autoignition characteristics of the charge. Westbrook, Pitz and other researchers [22, 23, 24, 25, 26] have used motored engine techniques to develop the detailed chemical kinetic mechanism of hydrocarbon oxidation which provides a fundamental understanding of autoignition chemistry and other combustion problems involving commercial hydrocarbon fuels.

Krieger and Borman [27] presented a diagnostic thermodynamic model for spark ignition engine heat release calculations. In their model, the combustion chamber was divided into two-zones, burned zone and unburned zone. The flame front was assumed to be infinitesimally thin. The mass burning rate was estimated by pressure-time experimental data. Heat transfer was also considered. In an effort by Peters and Borman [28], the mass burning rates from the experimental pressure-time diagram and the effects of various parameters on cyclic variations in the engine were studied using a similar model.

Benson et. al. [29] developed a two-zone model for the spark ignition engine that included the intake and exhaust systems. A laminar flame speed correlation is used to simulate empirically turbulent flame propagation without a clear indication of the basis for this determination. The model was employed to simulate the whole power cycle and predict NO emissions.

Hong [30] used a Weibe-type mathematical function to represent the fuel burning rate and examined single-zone and two-zone models. The ignition lag and combustion

duration were determined by curve-fitting. Based on this approach, he claimed that the effects of choosing different combustion models, single-zone or two-zone models, on the development of the pressure-time diagram are small.

Al-Alousi [31] and Al-Himyary [32] at the University of Calgary carried out an extensive experimental work on a CFR engine using methane and various mixtures with other fuels such as hydrogen and propane and diluents such as carbon dioxide and nitrogen. They used the measured pressure variations with time in single and two-zone models to calculate the corresponding duration for flame initiation (ignition lag) and propagation (combustion duration). They compiled much information about the variations of these periods and the effective heat release rate with common operating parameters and fuel composition.

Later on, Gao [33] developed a two-zone model and used Al-Himyary's [32] data to validate the predicted performance of a spark ignition engine using methane as a fuel. He was able to estimate well the variations of pressure and temperature in the burned and unburned zones. Then, he incorporated such data in a chemical kinetic scheme to consider the reaction activity of the unburned zone and the possibility of autoignition and knock. He defined an energy based knock criterion to estimate whether knock is to take place and its intensity when it occurs.

Turbulent flame modeling is an important aspect in engine combustion research. Some models simulated turbulent flame propagation by a laminar flame propagation speed correlation multiplied by a turbulent factor, such as Benson et. al. [29]. Hires et. al. [34] developed the correlation for ignition delay and combustion duration in a spark ignition engine by using a turbulent eddy entrainment concept of Tabaczynski [35]. They assumed that the turbulent integral scale is proportional to

the instantaneous chamber height prior to flame initiation, and the turbulent intensity scales proportional to the mean piston speed. Blumberg and Kummer's conic function of mass burning rate [36] was used to produce the correlation. In order to give the necessary parameter values at the point of 50% mass burned, a relationship between burned volume and burned mass must be assumed. However, some references such as Al-Himyary [32] showed that this relationship is not always true for all the operating conditions.

The k-ϵ turbulent model has been employed where the turbulent kinetic energy, k, is integrated over the whole combustion chamber to provide spatially average turbulence predictions and the dissipation rate, ϵ, is related to the integral length scale. The advantage of such models is that they are straight forward computationally, while the disadvantage is the ad hoc nature of the turbulence which involve plausible but arbitrary assumptions. The application of this model to spark ignition engines is complicated and the reader is referred to references [37, 38] for details.

2.2.1 The Intake and Exhaust Strokes Models

The objectives of any modeling of the intake and exhaust strokes is to provide the input or boundary conditions to the detailed modeling of the cylinder processes. When the manifold flows are the primary focus, such as for turbo-charger-engine matching, then models that adequately describe the unsteady gas-flow phenomena are normally required. Three types of models for calculating details of the intake and exhaust flows have been developed and used [21]:

1. Quasi-steady models for flow through the restrictions that the valve and port (and other components) provide.

2. Filling and emptying models, which account for the finite volume of critical manifold components.

3. Gas dynamic models, which describe the spatial variations in flow and pressure throughout the manifolds.

In the first type, the manifolds are considered as a series of interconnected components, which each constitutes a significant flow restriction, e.g. air cleaner, throttle, port and valve for the intake system. The actual flow is assumed to be quasi steady. These components are connected by the gas flow passing through them and the pressure ratio across them. Mass accumulation between components is neglected.

A quasi-steady model is often used to calculate the flow into and out of the cylinder through the inlet and exhaust valves. This approach has been used extensively with engine cycle simulations which predict engine performance characteristics from a thermodynamics-based analysis to estimate the mass flow rates into and out of the cylinder [39].

In the filling and emptying models, the manifolds are represented by finite volumes where the mass of gas can increase or decrease with time. Such models can range from treating the whole intake or exhaust system as a single volume to dividing these systems into many sections. Each volume is then treated as a control volume that contains gas at a uniform state. Watson [40] discusses the application of this model to a manifold in more detail. Such models can characterize the time-varying phenomena, spatially averaged over each manifold region corresponding to each volume analyzed: however, they cannot describe the spatial variation of pressure (and other gas properties) due to unsteady gas dynamics in the manifolds.

Many induction and exhaust system design variables determine overall performance. These variables include the length and cross sectional area of each part, the entrance or exit angles of the runners at junctions, the number of cylinders and their dimensions, intake and exhaust ports, valve design and valve lift and timing. Most of these details are beyond the level that can be incorporated into the models discussed above. Coupled with the pulsating nature of the flow into and out of each cylinder, these details create significant gas dynamic effects on intake and exhaust flows which require a more complete modeling approach. Gas dynamic models have been in use for a number of years to study engine gas exchange processes. These models use the mass, momentum, and energy conservation equations for the unsteady compressible flow in the intake and exhaust [41]. As an example, the work carried out by Bulaty et. al. [42] can be mentioned.

Because of its simplicity and due to the nature of this research, a filling and emptying model which uses a correlation for volumetric efficiency is considered to be suitable for modeling the intake and exhaust strokes.

2.2.2 Heat Transfer

Heat transfer to the combustion chamber surfaces of firing spark ignition engines has been the subject of many previous investigations. A concise review is given by Heywood [21]. The Woschni [43] correlation provides an instantaneous, spatially averaged, heat transfer coefficient for the evaluation of heat transfer rate to the cylinder walls. The correlation was developed from the results of combustion bomb studies and experiments carried out on a direct injection diesel engine. In subsequent work, Woschni and Fieger [44] (Quoted in [45, 46]) suggested that this could be

applied to spark ignition engines. They measured heat transfer at the cylinder head in a gasoline engine and showed that the local heat transfer in the near knocking region is slightly increased.

Other earlier correlations proposed by Annand [47] and Eichelburg [48] have also been widely used. However, these suffer from the fact that they require the assignment of suitable values to constants and their predictions are higher than the experimental data. Hence, they do not appear to be suitable for investigating the knock limit.

Shayler [49] investigated these models on three types of spark ignition engine. He claimed that the Woschni and Annand forms of correlation gave predicted heat transfer rates which were similar and in agreement with rates implied by energy balance considerations.

Lu et. al. [50] measured instantaneous wall heat flux at positions near and away from the end gas zone. They found phase and magnitude relationships between local heat-flux and knock intensity. Near the end-gas zone, the maximum heat-flux was found to increase linearly with the magnitude of pressure fluctuation for pressure fluctuations higher than 0.5 MPa. Away from the end-gas, the peak heat-flux was found to be insensitive to pressure fluctuations. Two other good papers in this field are published by Harigaya et. al. [51] and Michlis Syrimis et. al. [45]. They measured the instantaneous heat-flux from a cylinder and showed an increase in heat transfer from the cylinder when the engine began to knock, causing a drop in power output.

Borgnakke and Arpaci [37] developed another heat transfer model that depends on the local turbulent field and flame propagation. A compressibility factor is included in calculating the turbulent intensity and length scale. Turbulent flame

propagation was modeled using Tabaczynski's entrainment model [35]. Recently, Morell et. al. [52] developed a detailed model of cylinder heat transfer in spark ignition engines based on a flow model and boundary layer concepts. Unlike the old heat transfer coefficients, their coefficients may vary from surface to surface within the combustion chamber, reflecting the effects of local flow conditions.

The application of these complicated models is more suitable for a CFD model rather than a quasi-zone model, assuming a homogenous mixture in each zone. Consequently, the relatively simple model described by Woshni [43] is used in this work.

2.3 Knock Modeling

Knock has been studied for as long as the internal combustion engine itself. The sudden rapid heat release due to the abnormal combustion through autoignition leads to a rapid pressure rise followed by pressure fluctuations in the chamber, rapid heat transfer locally, and objectionable noise. During knock the normal development of combustion, characterized by a smooth rise in pressure, ceases when the pressure rises suddenly and high-frequency pressure fluctuations can be observed on an oscilloscope screen. These frequencies are governed by the size and shape of the combustion chamber, the velocity of sound in the charge and the engine operating conditions. The knock phenomenon varies substantially cycle-by-cycle, and does not necessarily occur every cycle. This type of knock, commonly called spark knock, is controllable to some extent by retarding the spark to reduce its occurrence, frequency and intensity. Knock studies may be categorized into:

1-Knock Detection:

A wide range of approaches have been employed for the detection of onset of knock and for categorizing its intensity. These involved various experimental investigations of knock phenomena. Some detection methods were developed based on these observation [53, 54, 55].

2-Effects of Fuels and Knock Rating:

From the outset of internal combustion engine development, it was clear that the onset of knock is strongly related to the nature and composition of the fuel [56, 57]. Lovell [58] found that the tendency to knock and its intensity are related to the molecular structure of that fuel. Individual hydrocarbon compounds vary enormously in their ability to resist knock, depending on their molecular size and structure. Hydrocarbons are grouped into three families of Paraffins, Olefins and Napthenes-Aromatics. Increasing the length of the carbon chain in Paraffins increases the knock intensity. The knock intensity decreases generally when the fuel is changed from Paraffins to Olefins and Aromatics. Napthenes have significantly greater knocking tendency than have the corresponding size aromatics. The use of isomers and the addition of some additives can reduce the knock intensity of hydrocarbon fuels. The discovery of antiknock properties of tetraethyl lead additives [59] was one of the most important findings of early research into fuels and knock.

Karim and Klat [57] established the knock limits for different common gaseous fuels including methane, propane, ethylene, hydrogen and their mixtures. They presented experimental results obtained in the CFR engine showing the effects of mixture strength, compression ratio and intake temperature on the knock limits.

Another contribution is that due to Annand and Sulaiman [60] who presented experimental results in terms of critical spark ignition timing for borderline knock at constant compression ratio.

To consider the knock resistance of a gaseous fuel in spark ignition engine, an analogy to the octane number was devised by German workers albeit less effectively. This was *the methane number* which was defined as the percentage by volume of methane in a blend with hydrogen that exactly matches the knock intensity of the unknown fuel sample under specified operating conditions in a CFR engine. Leiker et. al. [61] and Ryan et. al. [13] studied this experimentally under a specified set of test conditions. They suggested that the methane number can be used as a good indication of knock resistance of gaseous fuels. However, this view is not widely shared since there are shortcomings associated with the practice that need further investigation.

3-Knock Modeling:

Over the years, a number of theories have been put forward to explain the basis for the onset of knock. However, in recent years, it is accepted that the incidence of knock is due to autoignition in the end gas. The older proposition that knock may be due to the acceleration of the normal flame front to supersonic speeds (detonation) is essentially ruled out. Numerous recent high speed schlieren and shadow graph photographic studies support the autoignition theory [62, 63, 64]. They show that autoignition commonly occurs in one or more discrete locations within the end gas and then propagates to the other parts of the charge inside the cylinder. This end gas autoignition has also been detected by optical fiber techniques and correlated with Schlieren methods [65, 66, 67]. In some of these studies the flame front from the

end-gas autoignition sites was found to propagate at slightly supersonic speeds (developing detonation). It has been argued that the rapid release of energy occurs because of the acceleration of the advancing flame front to sonic velocity which in typical engine conditions would be of the order of 700 m/s. However, high speed film studies of knock have shown no evidence of flame front speeds approaching sonic velocity before knock [64, 67, 68]. Hence, it is now widely accepted that knock originates from the spontaneous autoignition of one or more local regions in the end gas. Additional regions then ignite till the whole end-gas is fully reacted. The rate of spread of these autoignited combustion centers can vary significantly. Under some conditions, this spread could be sufficiently slow for no pressure oscillations to be detected; thus autoignition does not necessarily lead to knock [62, 64]. Under heavy knock conditions, the spread of the auto-ignited region and hence the energy release is extremely rapid and high-amplitude pressure fluctuations may result.

In order to predict the onset of knock in engines, it is necessary to model and predict the unburned gas state parameter variations and the unburned gas preignition reaction activity. Therefore, there is a need to build up a combustion model to provide unburned gas state parameters such as pressure and temperature, and an appropriate chemical reaction mechanism for modeling the unburned gas preignition reactions.

Karim [69] developed a simple analytical approach to predict knock in spark ignition engines. A criterion for knock based on a gross chemical reaction of the fuel-air mixture in the end gas was used to predict the onset of knock. After adjusting some rate constants in the reaction mechanism, the calculated model gave a good agreement between predicted and experimental results. He suggested that more

reactions steps needed to be added to the kinetics scheme to predict a wider range of knocking observed experimentally.

Livengood and Wu [70] developed a simple model for engine knock, using the pressure and temperature data of a fired engine. A good agreement was obtained in predicting the results for n-heptane and a blend of n-heptane and iso-octane.

Westbrook and his colleagues [23, 24, 25, 71] developed comprehensive mechanisms for the combustion reactions of different common fuels and attempted to use them in the modeling of knock and self-ignition of some hydrocarbons. They reported relatively good agreement with their experimental results in estimating the ignition delay times under relatively simple situations such as constant volume reactor.

Dimpelfeld and Foster [72] used the mechanism of Westbrook to simulate knock in spark ignition engines with the assumption that end gas is adiabatically compressed, and the end gas temperature is only a function of cylinder pressure.

Karim and coworkers [73, 74] were able to develop a comprehensive detailed chemical kinetic scheme, including 155 reaction steps and 39 species to predict the autoignition of common gaseous fuels such as methane, propane, hydrogen and their mixtures. Karim and Gao [33, 75] applied this scheme and simulated the onset of knock in a CFR engine for methane operation. They defined a criterion for the onset of knock based on the specific volumetric energy release due to auto-ignition reactions relative to the total energy release to be expected from the combustion of the fuel. They developed a two-zone model to estimate the variations of pressure and temperature within the burned and unburned zones and used an empirical correlation for the corresponding combustion duration and heat release rate due to flame propagation profile.

In contrast to these approaches, some researchers have been trying to combine a very simplified and limited chemical kinetic representation with CFD codes such as those of KIVA to simulate the knock phenomena [76, 77, 78] as well as pressure oscillations [79]. These models tend so far to benefit from the detailed fluid mechanics calculations and to consider the variations of temperature and pressure within the volume of cylinder, but suffer from long computation times and gross inadequacy of the chemical representation with the required scales for engine modeling. That is why, normally, the chemical kinetic schemes in these models remain insufficiently comprehensive in comparison to the multi-zone models.

2.4 Optimization Methods

The engine design and development engineers have a task of fulfilling a comprehensive set of requirements such as reliability, fuel economy, drivability and conformity to exhaust emissions legislation. To design such systems, analytical, numerical and experimental tools are needed.

The optimization of the performance is not a straight forward process due to the complexity of the phenomena and the effect of different parameters on the engine performance and its knock intensity. Most optimization attempts were carried out experimentally. The final design is normally considered as the best compromise between various requirements, achieved through a lengthy and costly process involving the use of experimental and occasionally some very simple analytical techniques.

A comprehensive experimental investigation of a multi-cylinder engine performance was carried out recently by Asit Das [3]. After conducting a tremendous

amount of testing of the variations of power output, efficiency and emissions with operational parameters, he suggested that there is an optimum value for compression ratio between 15 to 16 for the best performance of the engine available to him.

Bazari and French [80] developed a model to predict the performance of a highly supercharged diesel engine (HSDI) and compared their results with experimental data. After carrying out a parametric study, they tried to use the results to find optimum operating conditions for the engine. Their model included an enormous amount of graphs and data, that were quite difficult to handle and specify a reliable optimum solution.

Some researchers [81, 82, 83] applied Taguchi [84] and Monte Carlo [85] methods to the engine optimization problem. These methods are more suitable for optimization of the engine performance experimentally. By monitoring the variations of the engine performance with changing one operational variable at a time, and giving weight to each variable, a function (usually statistical) can be established to relate the engine performance to the operational variables. Optimizing this function leads to a good approximation for optimum operating condition for the engine. Yan et. al. [83] suggested that the Taguchi method is effective in simultaneously optimizing multiple combustion parameters and identifying the significance of the effect of each parameter on the performance, while the Monte-Carlo simulation can be used as a useful statistical tool for predicting the performance. The main weakness of these methods is that they need comprehensive experimental efforts to provide a reliable correlation for engine performance.

Mathematical programming can provide a significant capability for the automated optimum engine design. A typical optimum design requires a minimization or

maximization of a stated objective function and simultaneous satisfaction of several design constraints. Perhaps, Shroff and Hodgetts [86] are the pioneers in introducing mathematical programming to engine performance optimization. They developed a quasi-zone model to predict engine performance and employed a linear function to relate the influence of each parameter on the engine performance. Actually, the effects of operational parameters on the engine performance are not linear for all the operating conditions, especially if the engine is operated at borderline knock. Also, they did not consider the occurrence of knock nor of its intensity.

The problems of optimization can be categorized as constrained and unconstrained problems. Most of the real life problems, including engine performance optimization, are considered to be constrained problems. The constraints divide the design space into two domains, the feasible domain where the constraints are satisfied and the nonfeasible domain where at least one of the constraints is violated. Constrained problems can be converted to unconstrained ones using the penalty function method [87]. Therefore, the analytical approaches developed for an unconstrained problem may be used for a constrained problem such as that relating to engine design.

Optimization algorithms could be grouped into deterministic and stochastic (random) algorithms. The most important type of deterministic algorithms is gradient-based, where the gradient of the objective function is used to search for an optimum solution. Among the stochastic methods, genetic algorithms may be named as the most powerful method, which uses a random operator combined with a statistical model to search for an optimum condition.

2.4.1 Gradient-Based Methods

The most efficient deterministic algorithms are gradient-based, which require at least the first derivative of the objective function, which is going to be optimized, and constraints with respect to the design variables [88]. The negative of the gradient of the objective function is used to find the minimum and/or maximum of that function and corresponding independent parameters. These algorithms are extremely efficient in locating a relative optimum value, close to a starting point in the design space. In applications where the design space is known to have multiple minima and/or maxima, the optimum value may be obtained by starting the search from several initial points in the design space and then comparing the final results. The reader is referred to references [89, 90, 91] for more details on the gradient based optimization theory.

Only a very few applications of these type of automated optimization approaches in the internal combustion engines have been reported. Mu et. al. [92] attempted to apply the gradient-based optimization method to optimize the performance of a diesel engine. They employed different gradient based algorithms and made some suggestions about the applicability of each of these methods to the diesel optimization problems, without providing sufficient details of their model.

2.4.2 Genetic Methods

A *genetic algorithm* is based on the principles of natural selection and survival of the fittest. The genetic algorithm developed by Holland [93] provides the capability to search for optimum solution with either disjoint or nonconvex spaces with several minimum or maximum points. These methods have since been adapted for a large

number of applications in game theory, inductive systems and other aspects of human cognition such as pattern recognition and natural language processing [94, 95, 96]. Such algorithms are generally regarded in the same category as stochastic (random) search methods [97].

Genetic search methods have their philosophical basis in Darwin's theory of survival of the fittest [98]. A set of design alternatives representing a population in a given generation is allowed to reproduce and cross among the alternatives with bias allocated to the most fit members of the population. Combination of the most desirable characteristics of mating members of the population results in progeny that are more fit than the parents. Hence, if a measure that indicates the fitness of a generation is also the desired goal of a design process, successive generations produce better values of the objective function. An obvious advantage in this approach is that the search is not based on the gradient information, therefore, it has no requirements on the continuity or convexity of the design space which makes it suitable for engineering applications, specially engine optimization.

Genetic algorithms have been used extensively in mechanical engineering [99, 100], civil engineering [101, 102], chemical engineering [103], neural network and fuzzy logic [104, 105].

Only one example has been reported of the application of genetic algorithm to optimizing engine performance. Edwards et. al. [106] used a genetic algorithm combined with a statistical model for predicting the engine performance from its experimental data. Their work suffers from the need for tremendous experimental efforts to develop the required statistical correlations to predict the engine performance and the scope of its application is both narrow and limited to the available

experimental data.

Due to the complexity of engine processes and our current lack of their full understanding particularly at the fundamental level, most engine models remain incomplete. At present, it is impractical to construct models that attempt to describe all the important aspects of engine operation. But models developed so far have their advantages and disadvantages. However, most of the reported engine optimization attempts involved either experimentally or semi-empirically based approaches with only a few attempts at applying automated optimization theory to engine optimization problems. To our knowledge, no one has employed any such models to predict engine performance at borderline knock. The present work aims at contributing to knock modeling and predicting optimum design and operating conditions for a gas fueled spark ignition engine.

Chapter 3

Simulation of Knock Phenomena and Performance of Spark Ignition Engines

3.1 Introduction

Experimental research into the knock phenomenon in engines is limited by the relative lack of suitable detection and measurement methods and the ever present risk of damage to the engine. Accordingly, the development of suitable comprehensive simulation models is needed to understand the knock mechanism and predict the knock limits in a spark ignition engine. These comprehensive simulation models must include a full understanding of the combustion process related to flame propagation as well as a suitable chemical kinetic mechanism to describe the oxidation of the fuel and autoignition of the end-gas.

This chapter describes a two-zone combustion model for predicting the performance of a gas fueled spark ignition engine and its knock intensity.

3.2 General Description of the Model

In order to be able to model the knock phenomenon in spark ignition engines, some relevant research on a number of related fronts was carried out by Karim and his co-workers to obtain needed supporting information . One of these was to provide improved description of the full kinetics of methane oxidation in air over a wide range

of operating conditions [107, 108].

It has been shown earlier that knock in spark ignition engines results from the autoignition of part of the charge ahead of the propagating turbulent flame and intense knocking is usually encountered when autoignition occurs regularly in every cycle and involves a significant portion of the charge [109]. Past attempts to predict the onset of knock in spark ignition engines [30, 110, 111] tend to be generally inadequate. Specific guidelines need to be developed which are convenient and easy to use yet faithful in representing the distinctive chemical reaction features of the different fuels within the end-gas region in a spark ignition engine. A special advantage would be avoiding the need for modeling turbulent flame propagation phenomena in detail at the same time. Accordingly, the onset of knock in a spark ignition engine can be predicted in principle by assuming that knock is due to the autoignition of a region of the gaseous charge yet to be consumed by the flame when its temperature variations with time is made known. Obviously, a representation of the autoignition reactions in a model based on a simple Arrhenius gross reaction is inadequate since the oxidation of the fuel-air charge for common fuels proceeds through chain reactions involving numerous intermediate species, both stable and unstable. For a relatively simple fuel such as methane, the nature and rates of these reactions have been established fairly reliably to yield good agreement with experimental observations. Kinetic schemes of other common fuels, that are more complex than methane, are becoming increasingly available and their reliability is being steadily improved. Obviously, such approaches add much to the computational complexity of the relatively simple conceptual model for knock but they are needed if the chemically controlled phenomenon of autoignition is to be simulated sufficiently reliably.

The reactions of the end-gas charge will be critically dependent on the temperature and pressure variations with time. These variations are mainly controlled by the energy release rate due to turbulent flame development, a function of not only operating conditions but also engine design parameters. In the present contribution based on the model developed by Gao [112] and earlier contribution of Al-Himyary [32] the effective temperature of the reactive end-gas is established using for the cylinder charge a relatively simple two-zone model. The mass transfer from the unburned to the burned zones at any instant through turbulent flame propagation is assumed to take place over an appropriate combustion period according to a deduced energy release rate function. These coupled parameters can be either known beforehand or established experimentally for a specific engine by employing a diagnostic two-zone model that analyses the corresponding pressure-time development records [113]. The decision as to whether knock is to take place or not and its intensity for any engine installation and operating conditions with any fuel is a complex and unknown function of the cumulative effects of the reactions proceeding within the end-gas and how they are influenced by flame propagation and the resulting changes in the size of the end-gas. Cycle variability is also a common recurring factor. The temperature distribution within the end-gas, unlike that of the pressure, can be complex and non-uniform, especially once the engine begins to knock. Accordingly, only average values of operating parameters need to be considered in any simple model for knock prediction and establishing the effectiveness of changes in operating and design conditions on the onset of knock and its intensity.

The two-zone model developed at the University of Calgary avoids predicting the detailed features of turbulent flame propagation. Instead, through an appropriately

assumed combustion period and associated mass burning and energy release rates, the changes in cylinder pressure and mean temperatures of the end-gas and burned regions are established at any instant of time. These results are then employed to evaluate the extent of reaction activity ahead of the flame within the end gas and the associated energy release by such reactions. This would permit establishing in time whether autoignition will take place and the likely intensity of the resulting knock.

A typical reciprocating piston engine with known dimensions, compression ratio and valve timing is the basis for the simulation of the model. The fresh charge of the intake mixture is assumed to be initially homogeneous and mixed thoroughly during the induction stroke with the residuals from the previous cycle. The composition of the residual gases, which are assumed to fill the clearance volume when a new cycle began, was considered to be of the same composition as that for the exhaust gases at the end of expansion to atmospheric pressure.

The resulting mixture following intake valve closure is then compressed, combusted and subsequently expanded to the exhaust stage. During these stages, reaction kinetics were used to predict in detail the changes in the concentrations and properties of the mixture in the end-gas and the consequent changes of the energy release rates with time.

The kinetic scheme employed in the present analysis was based largely on that described in reference [108]. It can describe the preignition and combustion reactions of common gaseous fuels such as propane, methane and hydrogen within the operating range of engines that involves lean mixtures and relatively high temperatures and pressures. The scheme employed, consisted of 155 elementary reaction steps and the following 39 chemical species:

C2H, C2H2, C3H8, C2H3, C2H4, C2H5, C2H6, CH, CH2, CH2CO, CH2O, CH3, CH3CHO, CH3CO, NC3H7, CH4, IC3H7, CO, CO2, H, H2, H2O, H2O2, HCO, HO2, N2, O, O2, OH, C3H6, CH3O, N2O, NO, N, CHCO, C3H4, C3H5, NO2, CH3O2.

The corresponding thermo-chemical data were obtained mainly from JANAF tables [114]. The scheme, when necessary, can include additional reactions and species accounting for the detailed reactions of nitrogen and/or fuel mixtures that may contain more fuel components.

For heat transfer, the mean wall temperature has been assumed for convenience to remain constant, while convective heat transfer is accounted for by Woschini's formulations [43] reported in the literature based on the analysis of a wide range of experimental data in engines.

3.3 Mathematical Treatment

The ideal thermodynamic cycle for a naturally aspirated engine is shown schematically in Figure 3.1. P_i and P_e are the intake manifold and exhaust pressures, respectively. Process (7-1-2) is the intake process. The intake valve opens at TDC (point 7). At the beginning of the intake stroke, the residual gas from the previous cycle is assumed to expand under an isentropic process to the intake pressure (point 1), then the fresh charge enters into the cylinder and mixes with the residual gas instantaneously, under a constant pressure process (1-2). The intake valve closes at bottom dead center (point 2). The charge is then compressed in the compression stroke (process 2-3). At point (3a), the combustion process is started and ends at state (4a).

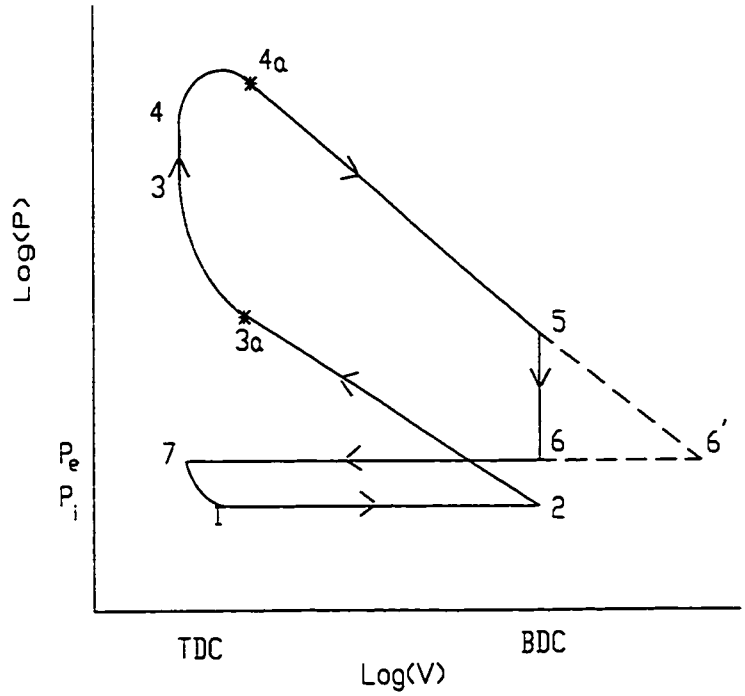

Figure 3.1: Ideal thermodynamic cycle for a naturally aspirated engine.

After that the combustion products will be expanded approximately polytropically to the point (5), when the exhaust valve opens at bottom dead center (BDC). Then, the gases are assumed to expand isentropically to the exhaust pressure (point 6′). Later on, the gases pushed out of the cylinder (process 6-7), except for some that will remain as residual gas at the thermodynamic state of point (7). More realistic valve timing consistent with engine operation can be considered instead when deemed necessary.

The cylinder charge is assumed during the combustion process to be divided into two zones: burned products and unburned reactants which comprise the end-gas region, as shown in Figure 3.2. The composition of the mixture of the unburned reactants is assumed known at all times up to the instant of spark ignition, since

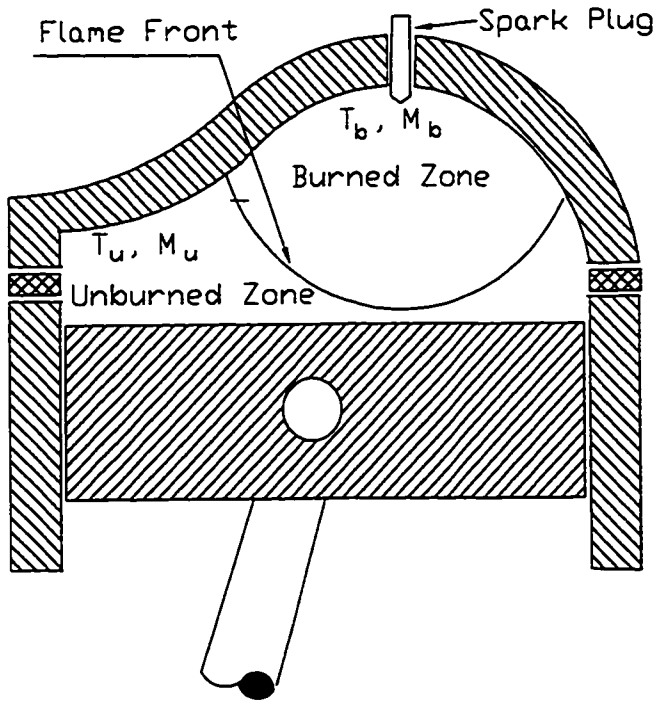

Figure 3.2: Schematic diagram of the two-zone model.

the fuel and air flow rates into the engine are closely metered and the presence of residual gases accounted for. However, when considering the reactivity of the end-gas, detailed reaction rates and the associated reactive species are accounted for, together with the energetic consequences of such reactions [75]. The composition of the burnt products is calculated using a dissociation scheme [115]. While the transient composition of the unburned zone is established throughout the chemical kinetic calculations. The following are the main assumptions in the model:

- The systems of burned and unburned zones are considered to be homogenous and have uniform properties.
- The pressure at any time is uniform throughout the cylinder.
- Flame thickness is negligible.

- Gases behave as ideal.
- Leakage from the cylinder is negligible.

Equation of State and Thermodynamic Relations:

$$PV = mRT, \qquad dh_i = Cp_i dT, \qquad du_i = Cv_i dT \tag{3.1}$$

where m is the total mass of the charge, V is the cylinder volume determined from the dimensions of the engine and its movement, T is mean temperature, h_i, u_i, Cp_i and Cv_i are enthalpy, internal energy, specific heat capacity at constant pressure and specific heat capacity at constant volume, respectively for a species i.

Mass Conservation:

$$m = m_u + m_b \qquad \Rightarrow \frac{dm_u}{d\theta} = -\frac{dm_b}{d\theta} \tag{3.2}$$

where subscript u indicates unburned mixture and subscript b is for the burned mixture. θ is crank angle.

Volume Conservation:

$$V = V_u + V_b \Rightarrow \frac{dV}{d\theta} = \frac{dV_u}{d\theta} + \frac{dV_b}{d\theta} \tag{3.3}$$

The total volume of the engine cylinder and the rate of its change can be expressed respectively as:

$$V = \frac{1}{2}S(\frac{\pi D^2}{4})[\frac{2}{CR-1} + 1 - \cos\theta + \frac{R}{4L}(1 - cos2\theta)] \tag{3.4}$$

and

$$\frac{dV}{d\theta} = \frac{1}{2}S(\frac{\pi D^2}{4})(\sin\theta + \frac{R}{2L}\sin 2\theta) \tag{3.5}$$

where

- D= The internal diameter of the cylinder
- S= Stroke
- CR= Compression ratio
- R= Crank radius
- L= Length of the connecting rod

Indicated Work of the Engine: The incremental work done by the whole charge considered to be the system can be further expressed by the mean cylinder pressure and the corresponding change of the system volume.

$$\frac{dW}{d\theta} = P\frac{dV}{d\theta} \tag{3.6}$$

Energy Conservation: The energy equation for the whole charge at any instant of time, corresponding to a crank angle, θ, is:

$$\frac{dQ}{d\theta} = \frac{dU}{d\theta} + \frac{dW}{d\theta} \tag{3.7}$$

where

$$U = m_u u_u + m_b u_b \Rightarrow \frac{dU}{d\theta} = m_u\frac{du_u}{d\theta} + u_u\frac{dm_u}{d\theta} + m_b\frac{du_b}{d\theta} + u_b\frac{dm_b}{d\theta} \tag{3.8}$$

and

- $dQ/d\theta$= the rate of heat transfer of the charge.
- $dW/d\theta$= the rate of work done by the charge.
- $dU/d\theta$= the rate of change in internal energy of the charge due to the change in temperature and chemical reaction of the mixture.

Calculating the amount of residual gas: At the end of the exhaust stroke residual gas fills the whole clearance volume at the exhaust pressure and temperature. The amount of residual gas is given as:

$$n_r = \frac{P_e V_c}{\overline{R} T_e} \tag{3.9}$$

where n_r is the number of moles of residuals, $\overline{R}$ is the universal gas constant, V_c is clearance volume, P_e and T_e are exhaust pressure and temperature.

Intake stroke: At the beginning of the intake stroke, the residual gas expands from exhaust pressure to the intake pressure. Assuming an isentropic expansion for this stage, if number of mole of residuals, n_r, exhaust and intake pressures, etc. are known, the cylinder volume at point (1) in Figure 3.1 which is the starting point for entering fresh charge into the cylinder can be estimated. Note that at the beginning of the intake stroke, because the pressure of residuals is higher than that of intake manifold, the fresh charge cannot enter into the cylinder.

The fresh charge is assumed to mix homogeneously with the residual gas. The resulting charge temperature and the amount of fresh charge can be estimated by applying the energy and mass conservation equations. Since the intake valve does not close exactly at the bottom dead center and does not open at the top dead center and because of pressure loss through the intake valve and scavenging process, a correction factor, called volumetric efficiency, for the amount of fresh charge is needed. It is defined as the volume flow rate of air into the intake system divided by the rate at which volume is displaced by the piston.

$$\eta_v = \frac{m_a}{\rho_{a,i} V_d} \tag{3.10}$$

where m_a is the mass of fresh charge into the cylinder per cycle, $\rho_{a,i}$ is the air density and V_d is the swept volume.

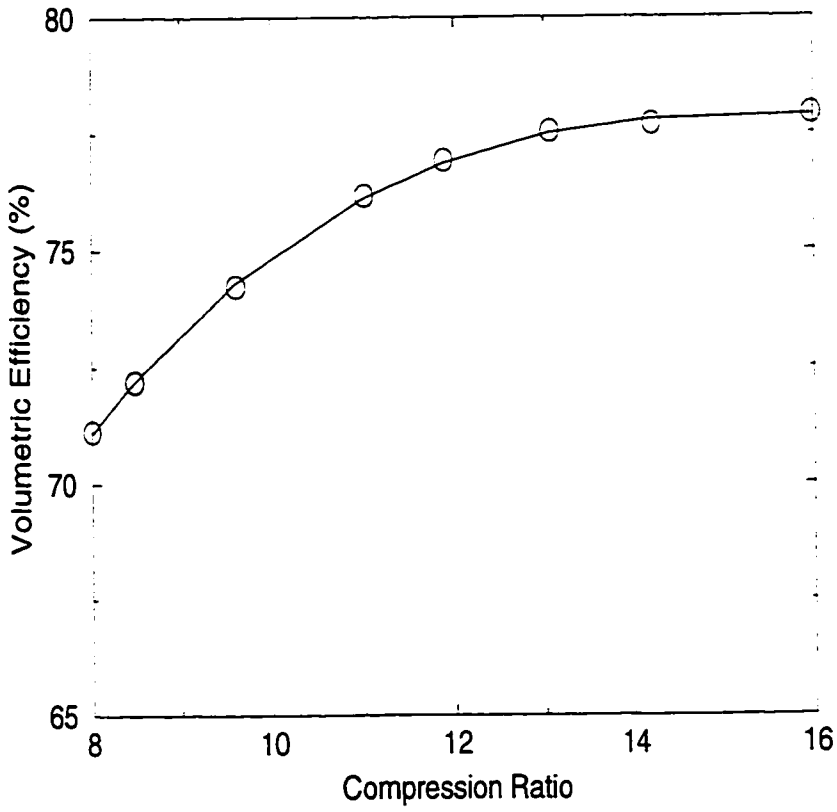

Figure 3.3: Variations of the volumetric efficiency with compression ratio for a naturally aspirated CFR engine at atmospheric temperature of 300 K.

From a set of tests with a CFR engine for constant temperature, the volumetric efficiency was found to be mainly a function of compression ratio. Its variations with compression ratio for the CFR engine available to us is shown in Figure 3.3. It was fitted to a cubic function as of:

$$\eta_v = 26.684 + 9.369CR - 0.570CR^2 + 0.0115CR^3 \tag{3.11}$$

Compression and Expansion Strokes: The compression process is assumed to start at the bottom dead center (BDC). The state of the gas at this point is derived by using a perfect mixing model for fresh charge and residual from the previous cycle. During compression, the gaseous fuels reactions are neglected for simplicity. However, they can be accounted for, when considered to be necessary. Then, the charge is ignited by a spark discharged before top dead center (TDC) and expanded after TDC.

The First Law of Thermodynamics, during the compression stroke before flame initiation and expansion stroke after flame consumption of the mixture, can be simplified for a single zone as follows:

$$\frac{dQ}{d\theta} = mCv\frac{dT}{d\theta} + P\frac{dV}{d\theta} \tag{3.12}$$

A combination of Equations 3.1 and 3.12 after rearrangement gives:

$$\frac{dP}{d\theta} = [-(1 + \frac{R}{Cv})P\frac{dV}{d\theta} + (\frac{R}{Cv})\frac{dQ}{d\theta}]/V \tag{3.13}$$

$$\frac{dT}{d\theta} = T(\frac{1}{V}\frac{dV}{d\theta} + \frac{1}{P}\frac{dP}{d\theta}) \tag{3.14}$$

Combustion Period: During flame propagation, when the volume charge is assumed to be divided into two zones, burned and unburned zone, the energy equation can be written as:

$$(u_b - u_u)\frac{dm_b}{d\theta} + m_u Cv_u\frac{dT_u}{d\theta} + m_b Cv_b\frac{dT_b}{d\theta} + P\frac{dV}{d\theta} - \frac{dQ}{d\theta} = 0 \tag{3.15}$$

Differentiating the equation of state , $PV = mRT$, with respect to crank angle θ:

$$\frac{dV}{d\theta} = (\frac{V_b}{m_b} - \frac{V_u}{m_u})\frac{dm_b}{d\theta} + \frac{m_u R_u}{P}\frac{dT_u}{d\theta} + \frac{m_b R_b}{P}\frac{dT_b}{d\theta} - \frac{V}{P}\frac{dP}{d\theta} \tag{3.16}$$

Applying the first law to a unit of mass of m_u:

$$\frac{du_u}{d\theta} = \frac{1}{m_u}\frac{dQ_u}{d\theta} - P\frac{dv_u}{d\theta} \tag{3.17}$$

where Q_u is heat transfer to the unburned mixture and v_u is the specific volume of the unburned mixture. Equation 3.17 can be rewritten as:

$$Cv_u\frac{dT_u}{d\theta} = \frac{1}{m_u}\frac{dQ_u}{d\theta} - Pv_u(\frac{1}{T_u}\frac{dT_u}{d\theta} - \frac{1}{P}\frac{dP}{d\theta}) \tag{3.18}$$

Using $Pv = RT$ and $R = Cp - Cv$, the above equation can be reduced to:

$$m_u Cp_u\frac{dT_u}{d\theta} = V_u\frac{dP}{d\theta} + \frac{dQ_u}{d\theta} \tag{3.19}$$

From Equations 3.15, 3.16 and 3.19, the equations for $dT_u/d\theta$, $dT_b/d\theta$ and $dP/d\theta$ are:

$$\frac{dT_u}{d\theta} = \frac{V_u}{m_u Cp_u}\frac{dP}{d\theta} + \frac{1}{m_u Cp_u}\frac{dQ_u}{d\theta} \tag{3.20}$$

$$\frac{dT_b}{d\theta} = \frac{P}{m_b R_b}[\frac{dV}{d\theta} - \frac{(R_b T_b - R_u T_u)}{P}\frac{dm_b}{d\theta} - \frac{R_u V_u}{PCp_u}\frac{dP}{d\theta} - \frac{R_u}{PCp_u}\frac{dQ_u}{d\theta} + \frac{V}{P}\frac{dP}{d\theta}] \tag{3.21}$$

$$\begin{aligned} &- \frac{dP}{d\theta}(\frac{Cv_u}{Cp_u}V_u - \frac{Cv_b R_u}{R_b Cp_u}V_u + \frac{Cv_b}{R_b}V) = (1 + \frac{Cv_b}{R_b})P\frac{dV}{d\theta} - \frac{dQ}{d\theta} \\ &+[(u_b - u_u) - Cv_b(T_b - \frac{R_u}{R_b}T_u)]\frac{dm_b}{d\theta} + (\frac{Cv_u}{Cp_u} - \frac{Cv_b}{R_b}\frac{R_u}{Cp_u})\frac{dQ_u}{d\theta} \end{aligned} \tag{3.22}$$

As stated earlier, in this work the heat transfer from the two zones to the outside wall was estimated, using formulations recommended by Woschni [43]. Alternative formulations of course could be used if necessary.

$$\frac{dQ}{dt} = \lambda A(T - T_w) \tag{3.23}$$

where T is the mean temperature of the charge, estimating by the following equation:

$$T = \frac{m_u\overline{Cp_u}T_u + m_b\overline{Cp_b}T_b}{m_u\overline{Cp_u} + m_b\overline{Cp_b}} \tag{3.24}$$

and λ is the heat transfer coefficient in $(\frac{\mathrm{W}}{\mathrm{m^2K}})$:

$$\lambda = 3.26 D^{-0.2} P^{0.8} T^{-0.55} [C_1 S_p + C_2 \frac{V T_1}{P_1 V_1} (P - P_{\mathrm{mt}})]^{0.8} \tag{3.25}$$

A is the area of the cylinder wall. According to the recommendation of Woschni, in this equation, C_1 equals to 6.18 must be applied to the scavenging period. For compression and expansion stroke, C_1 is equal to 2.28. C_2 is 3.24×10^{-3} (m/s°K) for the whole cycle. D is cylinder diameter in (m). V_1, T_1 and P_1 represent the known state of working gas related to the inlet valve closure. P_{mt} is the gas pressure in the cylinder of the corresponding motored engine in the absence of combustion. V, T and P represent the instantaneous known state of the working gas in real engine in m^3, K and kPa. S_p is the average piston speed.

The total heat transfer through the cylinder walls equals to the sum of the heat transfers from the burned and unburned zones.

$$\frac{dQ}{dt} = \frac{dQ_{\mathrm{u}}}{dt} + \frac{dQ_{\mathrm{b}}}{dt} \tag{3.26}$$

This equation may be written as follows:

$$\lambda A(T - T_w) = \lambda_{\mathrm{u}} A_{\mathrm{u}} (T_{\mathrm{u}} - T_w) + \lambda_{\mathrm{b}} A_{\mathrm{b}} (T_{\mathrm{b}} - T_w) \tag{3.27}$$

where

$$A = A_{\mathrm{u}} + A_{\mathrm{b}} \tag{3.28}$$

Combining Equations 3.27 and 3.28, burned and unburned zone heat transfer areas, A_{b} and A_{u}, may be found.

$$A_{\mathrm{b}} = \frac{A[\lambda(T - T_w) - \lambda_{\mathrm{u}}(T_{\mathrm{u}} - T_w)]}{\lambda_{\mathrm{b}}(T_{\mathrm{b}} - T_w) - \lambda_{\mathrm{u}}(T_{\mathrm{u}} - T_w)} \tag{3.29}$$

$$A_u = \frac{A[\lambda(T - T_w) - \lambda_b(T_b - T_w)]}{\lambda_u(T_u - T_w) - \lambda_b(T_b - T_w)} \tag{3.30}$$

Thus, the heat transfer through the burned and unburned zones are:

$$\frac{dQ_b}{dt} = \lambda_b A_b(T_b - T_w) \tag{3.31}$$

$$\frac{dQ_u}{dt} = \lambda_u A_u(T_u - T_w) \tag{3.32}$$

3.4 Multi-Species Equilibrium Calculation

It is consistent with experimental evidence to assume that over the entire possible ranges for operating variables, solids (such as soot) are not formed, while the products of combustion due to flame propagation are in equilibrium at the local temperature and pressure. The problem of calculating the products composition during combustion by flame propagation, then reduces to the calculation of the gas phase equilibrium composition of a general C-H-O-N-I system, where 'I' could be an inert and 'C', 'H', 'O' and 'N' are carbon, hydrogen, oxygen and nitrogen respectively. This approach was based on that suggested by Strehlow [115].

The species composition of the initial mixture allows the calculation of the atomic ratios $\overline{N}_{C/O}, \overline{N}_{H/O}, \overline{N}_{N/O}$, and $\overline{N}_{I/O}$. This information, the specified equilibrium pressure and temperature and the list of the species present at equilibrium plus the assumption that the gas is an ideal gas, are all that is required to perform an equilibrium product composition calculation. A very general case is assumed in which the 14 species, oxygen, O_2, nitrogen, N_2, hydrogen, H_2, carbon dioxide, CO_2, carbon monoxide, CO, water vapor, H_2O, hydroxyl radical, OH, nitric oxide, NO, nitrogen dioxide, NO_2, oxygen atoms, O, nitrogen atoms, N, hydrogen atoms, H,

methane, CH_4, and an inert, I, are present at equilibrium.

The atomic ratios which specify the fixed atomic composition can be written in terms of partial pressures as follows:

$$\overline{N}_{C/O} = \frac{B_C}{B_O} \qquad \overline{N}_{H/O} = \frac{B_H}{B_O} \qquad \overline{N}_{N/O} = \frac{B_N}{B_O} \qquad \overline{N}_{I/O} = \frac{B_I}{B_O} \tag{3.33}$$

where

$$\begin{aligned} B_C &= P_{CO_2} + P_{CO} + P_{CH_4} \\ B_O &= 2P_{O_2} + 2P_{CO_2} + P_{CO} + P_{H_2O} + P_{OH} + P_{NO} + 2P_{NO_2} + P_O \\ B_H &= 2P_{H_2} + 2P_{H_2O} + P_{OH} + P_H + 4P_{CH_4} \\ B_N &= 2P_{N_2} + P_{NO} + P_{NO_2} + P_N \\ B_I &= P_I \end{aligned} \tag{3.34}$$

with the added equation that the specified pressure of the system is the sum of the partial pressures:

$$P = \sum_{i=1}^{s} P_i \tag{3.35}$$

At this point, there are 14 unknowns (the P_i's) and only five equations [Eqs. 3.33 and 3.35]. Thus additional nine independent equilibrium equations are needed to solve for the equilibrium composition. As stated by Strehlow [115], the choice is arbitrary and the following independent equations are used:

1. Carbon dioxide dissociation: $CO_2 \rightleftharpoons CO + \frac{1}{2}O_2$

$$K_{p1} = \frac{P_{CO} P_{O_2}{}^{\frac{1}{2}}}{P_{CO_2}} \tag{3.36}$$

2. The dissociation of water: $H_2O \rightleftharpoons H_2 + \frac{1}{2}O_2$

$$K_{p2} = \frac{P_{H_2} P_{O_2}{}^{\frac{1}{2}}}{P_{H_2O}} \tag{3.37}$$

3. The formation of hydroxyl radical: $H_2O \rightleftharpoons \frac{1}{2}H_2 + OH$

$$K_{p3} = \frac{P_{H_2}^{1/2} P_{OH}}{P_{H_2O}} \tag{3.38}$$

4. The dissociation of hydrogen: $\frac{1}{2}H_2 \rightleftharpoons H$

$$K_{p4} = \frac{P_H}{P_{H_2}^{1/2}} \tag{3.39}$$

5. The dissociation of oxygen: $\frac{1}{2}O_2 \rightleftharpoons O$

$$K_{p5} = \frac{P_O}{P_{O_2}^{1/2}} \tag{3.40}$$

6. The formation of methane: $4H_2 + CO_2 \rightleftharpoons CH_4 + 2H_2O$

$$K_{p6} = \frac{P_{CH_4} {P^2}_{H_2O}}{{P_{H_2}}^4 P_{CO_2}} \tag{3.41}$$

7. The formation of nitrogen atoms: $\frac{1}{2}N_2 \rightleftharpoons N$

$$K_{p7} = \frac{P_N}{P_{N_2}^{1/2}} \tag{3.42}$$

8. The formation of nitric oxide: $\frac{1}{2}N_2 + \frac{1}{2}O_2 \rightleftharpoons NO$

$$K_{p8} = \frac{P_{NO}}{{P_{N_2}}^{1/2} {P_{O_2}}^{1/2}} \tag{3.43}$$

9. The formation of nitrogen dioxide: $\frac{1}{2}N_2 + O_2 \rightleftharpoons NO_2$

$$K_{p9} = \frac{P_{NO_2}}{{P_{N_2}}^{1/2} P_{O_2}} \tag{3.44}$$

Based on the Strehlow [115], the solution of this set of equations can be reduced by noting that the partial pressures of the species N, NO and NO_2 will always be

rather small and that they can be calculated by an *add-on technique*. This reduces the main calculation to the determination of the composition of a system containing only the three active components 'C', 'H' and 'O'.

To do this, one only needs to assume the partial pressures of three species that independently contain the component elements. Any set that satisfies this requirement may be chosen, such as $P'_{CO_2}, P'_{O_2}, P'_{H_2}$ or $P'_{CO_2}, P'_{H_2O}, P'_{O_2}$, etc., where the primes indicate that the partial pressure is a guessed value. Using this guess the (incorrect) partial pressures of the remaining species, P'_i, may be calculated using the equilibrium constants. The three mass-conservation equations [from using Eqs. 3.33, 3.34, and 3.35] are then written by substituting $P_i = P'_i + \delta_i$ where δ_i is the correction to the partial pressure which is unknown. However, the equilibrium relations written in terms of $P_i = P'_i + \delta_i$ can be differentiated to yield an expression for each of the remaining δ_i's in terms of the three guessed correction factors δ_i's for the three pre-selected species. When these are substituted into the mass-balance set, three equations are obtained for the three unknown correction factors, one for each of the three guessed species. Since these equations are linear they are easily solved in determinant form. The calculation converges rapidly when the initial guesses for partial pressures are reasonable and the guessed species have a relatively large partial pressure at equilibrium.

The nitrogen-containing species and the inert are included in the calculation as *add-on* species at each step by writing:

$$P_{calc} = P - P_N - P_{NO} - P_{NO_2} - P_I \tag{3.45}$$

where P_I is calculated from $\overline{N}_{I/O}$ and the properly weighted partial pressures of

the oxygen containing species (Eq. 3.34) and the P_N, P_{NO}, P_{NO_2} are calculated from the values of P_{N_2} and P_{O_2} and the appropriate equilibrium constants. The main calculation is then performed using P_{calc} as a fictitious total pressure for the C-H-O system.

3.5 Energy Release Pattern

As stated earlier, for knock modeling, the reactions in the end-gas need monitoring and flame propagation merely dictates the pressure time development which fixes the temperature level in the end-gas. Hence, a gross simulation such as the one being put forward is both adequate and accurate.

The combustion energy release rate due to the burning of the fuel can be derived from an energy release pattern which needs to be defined. From the mass analysis of experimental data using mainly methane as the fuel an effective formulation for the mass burning rate can be made that is adequate for modeling knock [32].

The combustion energy release takes place over a certain combustion period $\Delta\theta_c$ that starts just beyond the instant of spark timing after an ignition lag time when energy begins to be released due to flame kernel development and ends as a result of the end of flame propagation having consumed the entire mixture. The area enclosed by the resulting energy release rate diagram with time would represent the total effective energy release by combustion. The examination of a very large number of such diagrams for a wide range of operating conditions indicated that the shape of these diagrams tends to be essentially similar [32, 112]. A simple approach may consider to approximate such diagrams to triangles with a base that is the

corresponding combustion period and the area is the known total energy release. Alternative modification to such a shape will contribute very little to changing the pressure development with time.

3.5.1 Combustion Duration

The combustion duration in a spark ignited engine can be estimated for the purpose of knock modeling using a simple experimentally based approach which is adequate for the purpose. The variation of combustion duration with equivalence ratio is found to have a similar trend to that shown typically in Figure 3.4, which is consistent with the typical variations of the turbulent flame speed with equivalence ratio, since the duration is proportional to the inverse of the average flame speed. Moreover, the combustion failure limits, as encountered in a typical spark ignition engine, correspond to extremely long combustion periods and can be established experimentally or estimated for any specific engine [116]. The minimum combustion period which occurs around the stoichiometric ratio, also can either be estimated or measured experimentally [75]. Therefore, an appropriate combustion period correlation can be formulated for any engine operating condition. As an example, the following formula, proposed by Gao [112], was used:

$$\Delta\theta_c = Ae^x + Be^z \tag{3.46}$$

where

$$z = -(\phi_{min} - \phi)/(\phi_r - \phi) \tag{3.47}$$

and

$$x = (\phi_{min} - \phi)/(\phi - \phi_l) \tag{3.48}$$

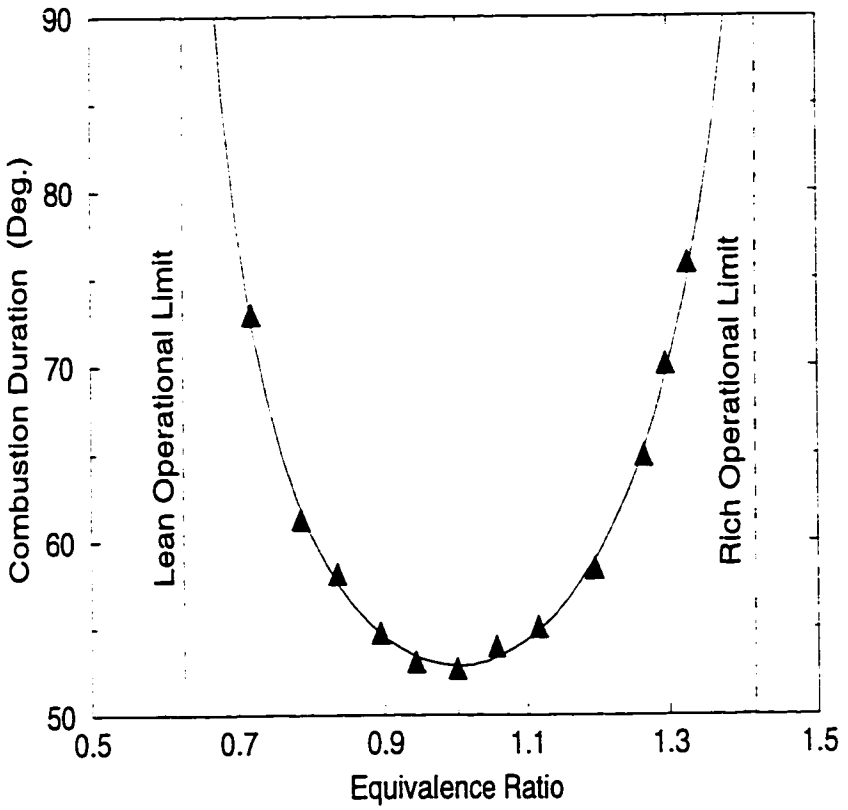

Figure 3.4: Typical variation of experimentally derived combustion duration versus equivalence ratio in a CFR spark ignition engine with methane at 900 RPM, $\theta_{st} = 10$ BTDC, CR =8.5:1, $T_o = 300$ K and $P_o = 87$ kPa.

$\Delta\theta_c$ is the combustion duration in degrees for an equivalence ratio of ϕ. The lean and rich operational limits of equivalence ratios are ϕ_l and ϕ_r, respectively. The equivalence ratio for minimum combustion time is ϕ_{min} which is usually around stoichiometric. A and B are constants that can be derived for the engine and conditions employed. ϕ_l and ϕ_r can be found or estimated for any operating conditions. Karim et. al. [57, 116] measured the apparent lean and rich operational limits for several fuels in a CFR spark ignition engine for different operating conditions. The

lean limit, for methane, was found to be approximately a linear function of the mean mixture temperature at the moment of spark discharge by Karim and Wierzba [117]. The lean operational limit can then be represented by:

$$\phi_l = A_1 T_{st} + B_1 \tag{3.49}$$

where A_1 and B_1 are constants, which were found to be $-1/50000$ and 0.071, respectively, by fitting the relevant experimental data in a CFR engine. T_{st} is the average mixture temperature (K) at the moment of spark discharge.

Karim and Wierzba [117] also found that the rich flammability limit is a linear function of the difference of the mixture temperature at the moment of spark discharge (T_{st}) and the mixture temperature at intake conditions (T_o).

$$\phi_r = A_2(T_{st} - T_o) + B_2 \tag{3.50}$$

where A_2 and B_2 are constants. These were found from fitting the relevant experimental data in a CFR engine to be 1/10000 and 0.1, respectively.

The lean and rich flammability limits for hydrogen in air, at atmospheric temperature and pressure, are 4% and 75% by volume, respectively [115]. These values will be modified at higher temperatures and pressures such as those existing in the cylinder at the time of spark passage.

For a mixture of fuels the accepted Le'Chatelier's rule can be applied to estimate the corresponding limits of the mixture [115] by using the values of the known limits of the individual fuel components under the same operating condition.

$$\frac{100}{L_{mix}} = \sum \frac{c_i}{L_i} \tag{3.51}$$

where c_i is the concentration of the species i in the mixture, L_i is the flammability limit of that species at that specified temperature and pressure and L_{mix} is the flammability limit of the mixture.

Since the combustion period reaches a minimum for a mixture with an equivalence ratio of ϕ_{min}, around the stoichiometric mixture, then the following simplified equations which establish the values of A and B in terms of ϕ_l, ϕ_r, ϕ_{min} and $\Delta\theta_{c,min}$ can be derived by substituting $\phi = \phi_{min}$ in Equation 3.46 and taking $d\Delta\theta_c/d\phi|_{\phi_{min}} = 0$:

$$A + B = \Delta\theta_{c,min} \tag{3.52}$$

$$\frac{A}{B} = (\phi_{min} - \phi_l)/(\phi_r - \phi_{min}) \tag{3.53}$$

where $\Delta\theta_{c,min}$ is the minimum combustion duration.

As stated by Gao [112], there are basically two main factors affecting the combustion duration in degrees. The first factor is the cylinder geometry and size, which decide the effective flame propagation distance. The other factor is the flame propagation speed, which determines how fast the flame covers that distance.

$$\Delta\theta_{c,min} = f(d_{ef}, S_f) \tag{3.54}$$

where d_{ef} is the effective flame propagation distance and S_f is the flame propagation speed. In a spark ignition engine, due to the motion of the piston and the changing with time of temperature and pressure, both d_{ef} and S_f are varying during combustion. Some simplifications need to be introduced to find a simple correlation for estimating the minimum combustion duration for a certain engine and operating condition. Assuming that the flame propagation distance d_{ef} is proportional to $V_{st}^{1/3}$ is a reasonable approximation during combustion, where V_{st} is the combustion

chamber volume at the time of spark discharge and depends on the spark timing and the compression ratio. Advanced spark timing and low compression ratio will lead to a longer flame propagation path. Correlating experimental data obtained from a CFR engine leads to the following equation [118]:

$$\Delta\theta_{c,\min} = C\frac{{V_{st}}^{1/3}}{CR^{1/2}}f(S_f) \tag{3.55}$$

where V_{st} is the cylinder volume at the instant of spark discharge and CR is the compression ratio. The flame propagation speed is the other important factor influencing combustion duration. It is known that the flame propagation speed for any equivalence ratio and engine speed depends on mixture temperature and pressure. Since the flow in a spark ignition engine is strongly turbulent, the flame propagation is also turbulent and it is affected by the nature of the turbulence intensity and scale. Numerous research investigations have been carried out on premixed laminar flame propagation in constant volume cells. Some correlations for laminar flame propagation have been developed. However, these correlations cannot be applied directly to the engine modeling mainly because of the variable geometry of the combustion chamber and the intense turbulent nature of the flow in a running engine. A general approach that proved to be effective is to use the correlations for laminar flame propagation after incorporating some appropriate corrections to fit the experimental engine data [29, 32].

Al-Himyary [32] developed a generalized expression for the maximum flame propagation speed for methane based on extensive experimental data obtained by others under different operating conditions. He found that the maximum burning speed occurs at an equivalence ratio of 1.036, corresponding to the minimum combustion

duration, and that:

$$S_{f,max} = P^{-0.457} \exp(-746.8/T + 6.193) \tag{3.56}$$

where P and T are instantaneous mixture pressure (atm) and temperature (K), respectively, and $S_{f,max}$ is the maximum flame propagation speed in (m/s).

For a fixed engine speed, it is reasonable to assume that the maximum turbulent flame speed is proportional to the $S_{f,max}$. Thus, with the maximum burning speed according to Equation 3.56, the minimum combustion duration of Equation 3.55 may be expressed as:

$$\Delta\theta_{c,min} \propto \frac{d_{ef}}{S_{f,max}} \propto \frac{V_{st}^{1/3}}{CR^{1/2}} P^{0.457} e^{(746.8/T)} \tag{3.57}$$

In this formula, P and T are the instantaneous mean pressure and temperature of the mixture during combustion. They are unknown before the combustion process calculation in a predictive model. But, what is known are the P and T values at the moment of spark discharge. Thus, some corrections are needed for this formula to make it usable for predicting combustion duration. The exponential index for pressure and the term $746.8/T$ may need to be modified to match the considerable increase of the cylinder pressure later on during combustion. Thus, the following formula was found to be a good approximation for the minimum combustion duration for methane operation as found experimentally.

$$\Delta\theta_{c,min} = C \frac{V_{st}^{1/3}}{CR^{1/2}} P^{0.457} e^{(746.8/T)} \tag{3.58}$$

The effects of turbulence on the combustion duration are still to be discussed. It is known that the turbulent characteristic velocity is usually a function of piston speed S_p [21] and it can be used to represent turbulence effects. Hirst et. al. [119] found

that:

$$\Delta\theta_{c,min} \propto {S_p}^{1/3} \tag{3.59}$$

Utilizing this simple relationship will yield the following expression for the final form of minimum combustion duration correlation.

$$\Delta\theta_{c,min} = C' \frac{V_{st}^{1/3}}{C R^{1/2}} P^{0.457} e^{(746.8/T)} {S_p}^{1/3} \tag{3.60}$$

where C' is a constant which depends on the cylinder geometry and the spark plug location and S_p is piston speed. Other correlations of experimentally observed data can be derived in similar form. In any case, the value of $\Delta\theta_{c,min}$ in the key relationship of Equation 3.52 does not necessarily require high accuracy. Moreover, for lean operation even an assumed negligibly small value for $\Delta\theta_{c,min}$ at stoichiometric can produce a reasonably workable approximation for the value of $\Delta\theta_c$ as a function of ϕ.

For any given operating conditions, from the computations during the compression stroke, the pressure and temperature at the moment of spark discharge can be estimated. Equation 3.60 gives the minimum combustion duration, while the lean and rich operational limits can be found using the procedure described in Section 3.5.1. The constants A and B then can be calculated. By substituting these into Equation 3.46, the combustion duration can be predicted. This method for estimating the combustion duration may be applied for various operating conditions. Only one constant C' needs to be determined by measuring the combustion duration once for the engine of interest. A typical comparison between the estimated combustion duration and experimental data is shown in Fig. 3.5. Figure 3.6 shows the corresponding predicted values when the spark timing is changed for two compression ratios. It can be seen, from these typical cases, that the combustion duration

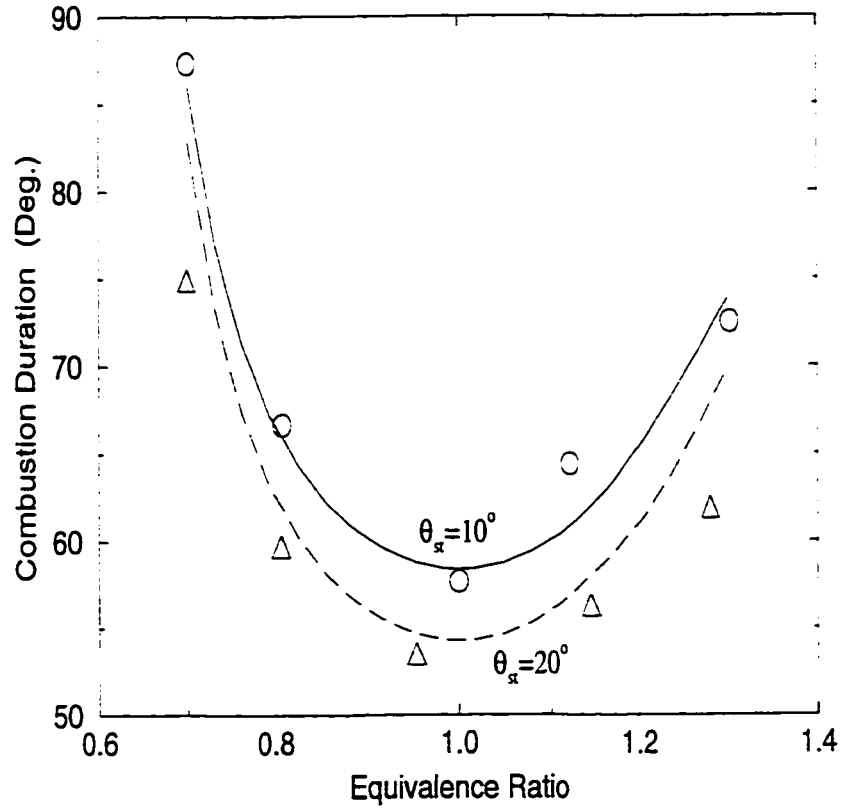

Figure 3.5: A comparison between estimated combustion duration versus equivalence ratio and the corresponding experimental data from a CFR spark ignition engine with methane at 900 RPM, CR =8.5:1 and T_o = 300 K for two spark timings.

can be estimated and that the proposed predictive model produces good agreement with experimentally derived data.

3.5.2 Ignition Lag

The combustion process in a spark ignition engine can be conceived to progress by two primary stages, the ignition lag and the effective combustion duration. When the spark is discharged, no significant combustion energy release appears immediately.

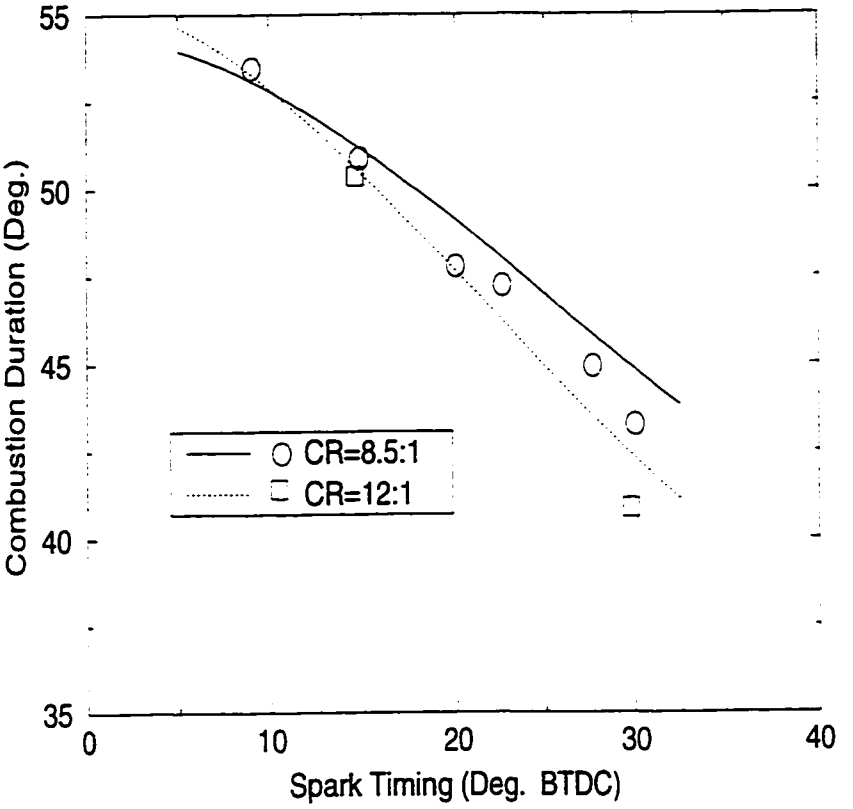

Figure 3.6: The variations of combustion duration with different spark timing for a CFR spark ignition engine with methane at 900 RPM, $\phi = 1.0$ and $T_o = 300$ K for two compression ratios. Corresponding experimental data are shown.

The period for the ignition lag starts at the moment of spark discharge and ends at the time when a significant flame development takes place involving a certain amount of burned mass and some energy release is detected. The definition of this ignition delay, termed ignition lag for spark ignition engines to distinguish it from that of the ignition delay in diesel engines, is somewhat arbitrary. Usually, the amount of the burned gas mass during the ignition lag is taken for convenience as the criterion for the ignition lag length. The amount ranges from 1% to 5% of total charge. Hires [34]

took 1% of total mass as the end of the ignition lag, while Hong [30] considered 2% at the end point. Al-Himyary [32] suggested 5% mass consumption at the end of ignition lag. In the present work, Al-Himyary's criterion for ignition lag is used so that the model predictive results can be compared with the mass of his diagnostic results.

In a spark ignition engine, the length of the ignition lag is governed mainly by the chemical reaction activity and the diffusive transport processes. Although most of the details concerning the chemistry and fluid mechanics of the initial flame kernel growth in a spark ignition engine are yet unclear, the effects of several operational parameters on the ignition lag have been investigated [32, 72]. It was found, among the many important operational parameters influencing ignition lag length are the equivalence ratio, piston speed, mixture temperature and pressure. To find a correlation for the variations of the ignition lag with operating conditions, a similar procedure as that used for estimating the combustion duration was adopted. Figure 3.7 shows a typical plot of experimentally derived values of the ignition lag with equivalence ratio [31] displaying excessively long lags at the lean and rich limits. There is also a minimum ignition lag that corresponds to the fastest flame propagation for any operational conditions. Accordingly, the variations of the ignition lag with equivalence ratio can also be represented by a similar exponential function as that of Equation 3.46 obtained for the combustion duration:

$$\Delta\theta_{ig} = A_i \exp\left(\frac{\phi_{min} - \phi}{\phi - \phi_l}\right) + B_i \exp\left(\frac{\phi - \phi_{min}}{\phi_r - \phi}\right) \tag{3.61}$$

where

- $\Delta\theta_{ig}$ ignition lag length, crank angle (Deg).

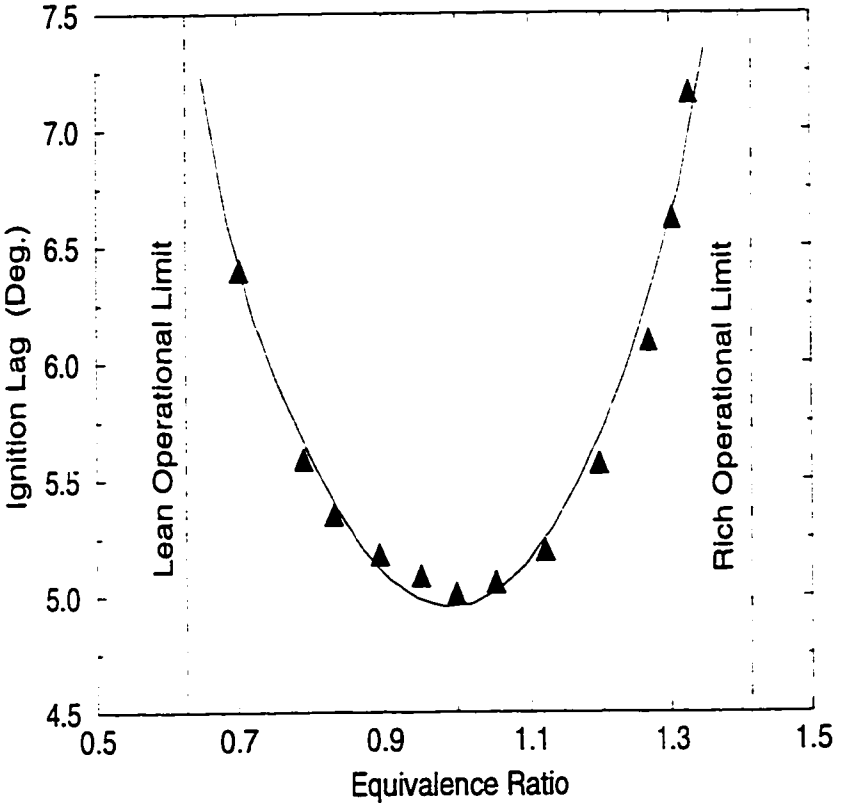

Figure 3.7: Typical Variations of experimentally derived ignition lag with equivalence ratio in a CFR spark ignition engine with methane at 900 RPM, $CR = 8.5 : 1$, $P_o = 87$ kPa and $T_o = 300$ K.

- ϕ equivalence ratio.
- ϕ_{min} equivalence ratio where the combustion duration is the shortest.
- ϕ_l lean operational limit.
- ϕ_r rich operational limit.
- A_i, B_i constants.

and similar to the model for combustion period:

$$\frac{A_i}{B_i} = (\phi_{min} - \phi_l)/(\phi_r - \phi_{min}) \tag{3.62}$$

and

$$A_i + B_i = \Delta\theta_{ig,min} \tag{3.63}$$

The value of the minimum ignition lag, $\Delta\theta_{ig,min}$, can be found also by fitting experimental data to the following expression to produce acceptable agreement with the corresponding experimental observations.

$$\Delta\theta_{ig,min} = C'' \frac{T_{st}^{1/2} S_p^{1/3}}{C R^{1/2}} \tag{3.64}$$

where $\Delta\theta_{ig,min}$ is the minimum ignition delay and C'' is a constant. A_i and B_i may be derived from Equations 3.62 and 3.63. Hence, the ignition lag can be found using Equation 3.61. Figure 3.8 is a typical comparison between the estimated ignition lag using the approach described and the corresponding results of experimental analysis [31]. It is to be remembered that since the value of the ignition lag tends to be always small relative to the length of the combustion duration, a less precise estimate of the length of the ignition lag would not produce significant errors in estimating engine output parameters.

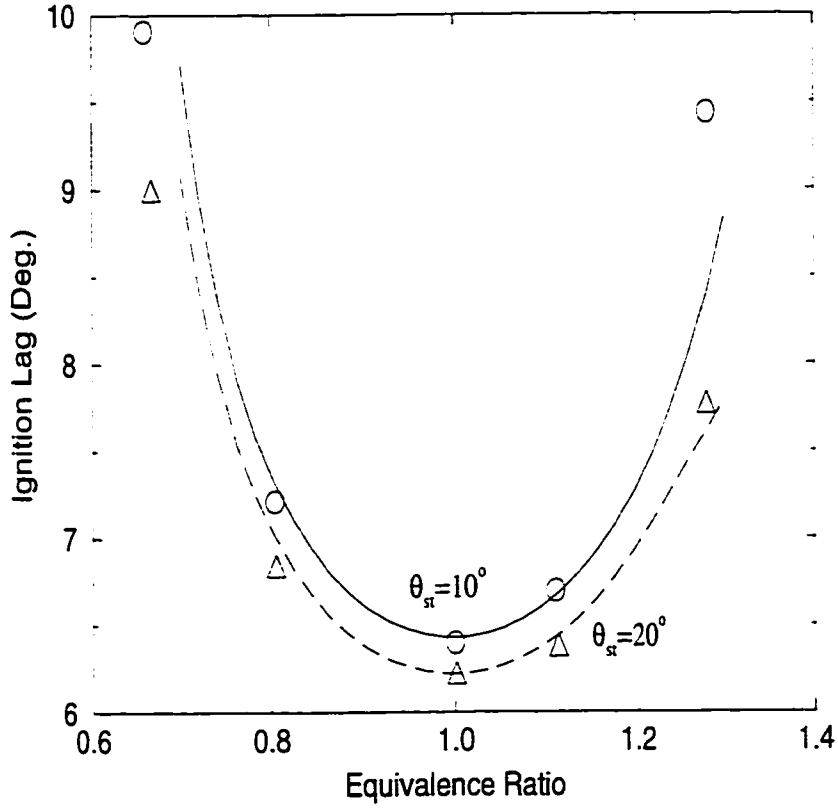

Figure 3.8: A comparison between the estimated ignition lag and the corresponding experimental data from a CFR spark ignited engine for methane operation at 900 RPM, CR =8.5:1, T_o = 300 K and P_o = 87 kPa for two spark timings.

3.5.3 Combustion Duration and Ignition Lag for Fuel Mixtures

Many researchers investigated the effect of hydrogen addition to methane on the effective flame burning velocity [2, 12, 120]. Generally, there appears to be no reliable model capable of predicting the burning velocity of the hydrogen-methane mixture within a wide range of temperatures, pressures and the concentrations of hydrogen in the mixture, especially in relation to the spark ignition engine, where fully turbulent conditions prevail. Hence, any correlation for the combustion duration and ignition delay, for methane-hydrogen mixtures, must be based on experimental data obtained directly for the measurement of the combustion period and ignition lag in the engine. Consequently, an expression for the combustion duration of a fuel mixture based on experimental data from a CFR engine can be given approximately as:

$$\frac{1}{\Delta\theta_{c,m}} = \frac{y_1}{\Delta\theta_{c1}} + \frac{y_2}{\Delta\theta_{c2}} + \frac{y_3}{\Delta\theta_{c3}} + \ldots \tag{3.65}$$

where y_i is the molar fraction of the fuel i in the fuel mixture and $\Delta\theta_{ci}$ is the corresponding combustion period or ignition lag for the engine when operating with the fuel component i on its own under the same conditions. $\Delta\theta_{c,m}$ is the combustion period or ignition lag for the mixture. Typical comparisons between such estimated combustion duration and ignition lag with experimentally derived data for mixtures of hydrogen and methane in the CFR engine are shown in Figures 3.9 and 3.10.

Thus, the complete model developed to estimate the mean effective combustion duration and ignition lag for methane operation can be extended for applications involving other gaseous fuels and their mixtures. Due to the nature of the strong turbulent flow encountered within a running spark ignition engine and the associated

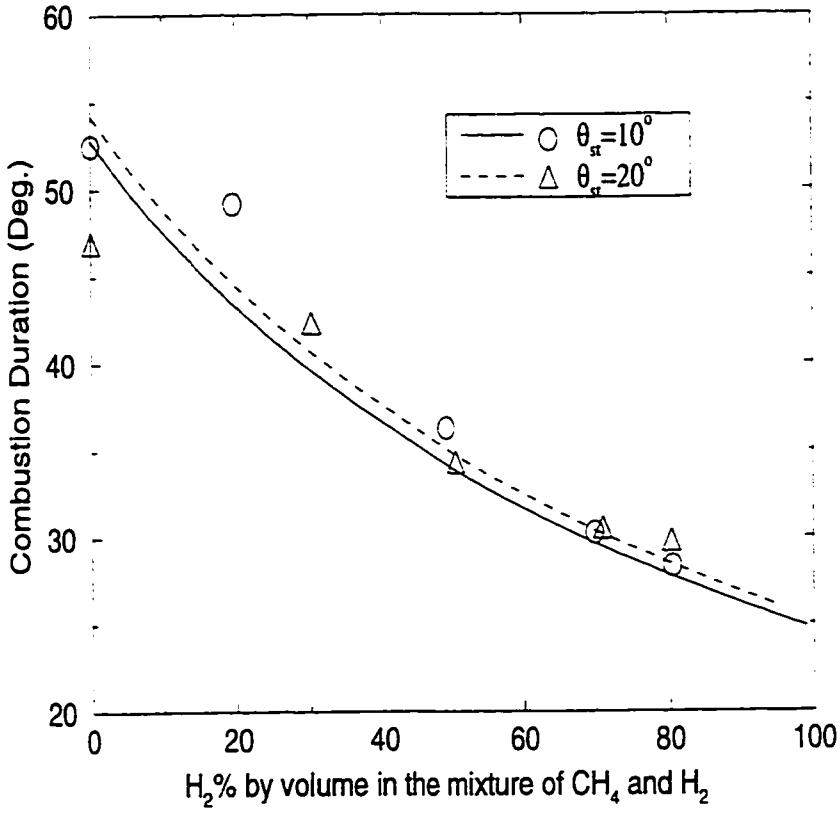

Figure 3.9: Calculated combustion duration variations for mixtures of CH_4 and H_2 at 900 RPM, CR =8.5:1, $\phi = 1.0$, $P_o = 87$ kPa, $T_o = 300$ K. Our own experimental points are shown.

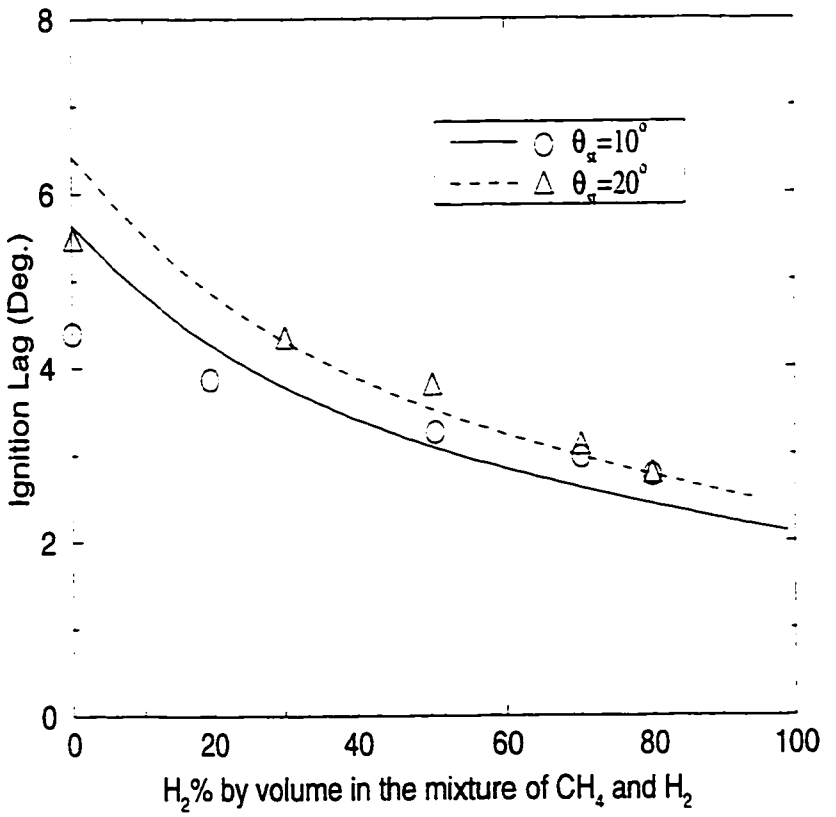

Figure 3.10: Comparison of the calculated ignition lag with experimental data for mixtures of CH_4 and H_2 at 900 RPM, CR =8.5:1, $\phi = 1.0$, $P_o = 87$ kPa, $T_o = 300$ K.

cylic variations, the real value of the combustion duration tends to be statistical in nature and necessarily fluctuating. Hence, the accurate prediction of the combustion duration in a theoretical model is difficult, if not unavailable at present and in any case as will be shown is strictly unnecessary.

3.5.4 Mass Burning Rate Profile

Several functions have been suggested in the literature to represent the mass burning rate in spark ignition engines. For example, triangular, sine and Weibe type functions have been used [21]. The mass of data obtained experimentally when methane is the fuel over a very wide range of operating conditions, as shown typically in Figure 3.11, can be viewed to approximately follow a triangular format [32, 112] for the mass burning rate. Therefore, it can be represented by:

$$\frac{dm}{d\theta} = \frac{2m_o}{\Delta\theta_c}\sigma \tag{3.66}$$

where

$$\sigma = \frac{\theta - \theta_{\text{e.i.}}}{\theta_{\max} - \theta_{\text{e.i.}}} \qquad \text{when} \qquad \theta_{\text{e.i.}} \leq \theta \leq \theta_{\max} \tag{3.67}$$

$$\sigma = \frac{\theta_{\text{e.c.}} - \theta}{\theta_{\text{e.c.}} - \theta_{\max}} \qquad \text{when} \qquad \theta_{\max} \leq \theta \leq \theta_{\text{e.c.}} \tag{3.68}$$

where $\theta_{\text{e.i.}}$, $\theta_{\text{e.c.}}$ and $\theta_{\max}$ are the crank angles at the end of ignition lag, the end of combustion period and at a location associated with maximum mass burning rate assumed to be at 2/3 of the combustion period for the CFR engine at specified operating conditions.

The solution of the set of relevant simultaneous equations employing numerical methods yields values of the main properties of the two zones and their variations with time. From a knowledge of the calculated cylinder pressure variations with

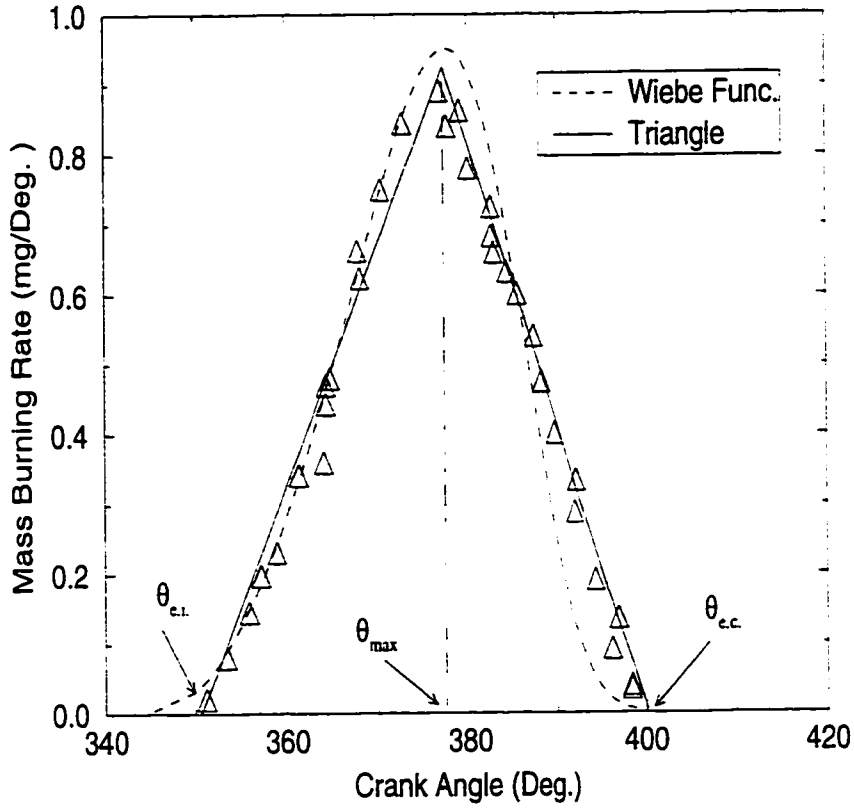

Figure 3.11: Comparison between calculated and experimentally derived mass burning rates. Operating parameters 900 RPM, CR =8.5:1, θ_{st} = 15 BTDC, ϕ = 1.0, T_o = 300 K.

volume changes, the corresponding indicated power output and thermal efficiency could be evaluated by simple integration of PdV over the working cycle. No reliable estimates however can be made at this stage of the nature and extent of emissions.

3.6 Knock Prediction

The current model described considers knock to take place when the energy released due to preignition reaction activity within the end-gas becomes sufficiently significant and intense. The knock criterion developed by Karim and Gao [112] was used. It is based on the calculated accumulated amount of energy release due to end-gas preignition reactions per unit of the instantaneous charge volume, relative to the total energy to be released normally through flame propagation over the whole cycle per unit of cylinder swept volume, i.e.

$$Knock \quad Criterion(K) = \frac{\frac{Energy \quad Released \quad by \quad End \quad Gas \quad Reactions}{Volume}|_t}{\frac{Energy \quad Released \quad By \quad Combustion}{Volume}|_{t0}} \tag{3.69}$$

The energy released by end-gas self reaction is defined as:

$$H_{u_t} = \int_{t_{st}}^{t} dE_u = (h_{st} - h_t)m_u \tag{3.70}$$

where h is the enthalpy of the mixture per unit of mass ($h = \sum c_i h_i$) and m_u is the instantaneous end-gas mass. Subscripts st and t indicate the values at the spark discharge and at any instant of time, respectively.

The energy released due to normal combustion can be simplified as:

$$H_o = h_o m_o \tag{3.71}$$

where h_o is the effective heating value of the fuel and m_o is the initial or total mass. Consequently, Equation 3.69 may be rewritten as:

$$K = \frac{(h_{st} - h_t)m_u/V_t}{h_o m_o/V_o} \tag{3.72}$$

In order to predict the energy release by end-gas reactions, a detailed chemical kinetic model including 155 reaction steps and 39 species is used. A chemical reaction

scheme involving i species and j reaction steps can be represented by the following set of reaction equations:

$$\sum_{i=1}^{n} \alpha_{ijf} X_i \underset{K_{jb}}{\overset{K_{jf}}{\rightleftharpoons}} \sum_{i=1}^{n} \alpha_{ijb} X_i \qquad j = 1, 2, ..., n \tag{3.73}$$

where α_{ijf} and α_{ijb} are stoichiometric coefficients of the i^{th} species appearing in the reactants and products of the j^{th} reaction, respectively. X_i is the chemical formula for a species i taking part in the reaction.

The net rate of production and consumption of each species (i) of a reactive end-gas charge depends on the rates of all the reaction steps involved [107, 121] in the detailed chemical kinetic scheme for the oxidation of fuel. Therefore, the change of chemical species concentration over a certain element of time can be calculated from the following set of equations:

$$\frac{dc_i}{dt} = \frac{1}{\rho} \sum_{j=1}^{n} (R_{jb} - R_{jf}) \tag{3.74}$$

where c_i is the concentration of i^{th} species, ρ is the mixture density, R_{jf} and R_{jb} are forward and backward reaction rates of the j^{th} reaction, respectively, which can be calculated by:

$$\begin{aligned} R_{jf} &= K_{jf} \prod_{i=1}^{n} (\rho c_i)^{\alpha_{ijf}} \\ R_{jb} &= K_{jb} \prod_{i=1}^{n} (\rho c_i)^{\alpha_{ijb}} \end{aligned} \tag{3.75}$$

K_{jf} and K_{jb} are the forward and backward rate constants for the j^{th} reaction and

can be calculated according to the following:

$$\begin{aligned} K_{jf} &= A_{jf} T^{B_{jf}} \exp(-\frac{E_{jf}}{RT}) \\ K_{jb} &= A_{jb} T^{B_{jb}} \exp(-\frac{E_{jb}}{RT}) \\ or \qquad K_{jb} &= \frac{K_{jf}}{K_{jc}} \end{aligned} \tag{3.76}$$

K_{jc} is the equilibrium constant and A_{jf}, A_{jb}, B_{jf} and B_{jb} are constants for the forward and backward rate constants of the j^{th} reaction equation. E_{jf} and E_{jb} are the activation energies of the j^{th} forward and backward reactions, respectively. K_{jf} and K_{jb} are related through the corresponding equilibrium constant.

When the above set of simultaneous equations is solved numerically, the concentration of each species in the unburned zone at any instant of time can be found. The physical properties of the species, the reaction scheme used and its corresponding constants for methane, propane and hydrogen are listed in Appendix (A).

The knock modeling thus proceeds to monitor the reaction activity and the concentrations of each of the reacting species using the above group of equations right from the time of spark discharge, or even earlier, if it is necessary. This is carried out for each time increment while accounting for the local temperature, pressure and volume of the end-gas throughout, right up to the point of the total consumption of the unburned charge by the propagating flame at the end of the combustion period. Due to the end-gas chemical reaction activity, the associated energy release may also cause some further temperature and pressure rise.

The effect of the unburned gas reaction on the whole cylinder pressure is relatively small compared with that due to normal combustion, prior to the onset of knocking. However, the situation for the unburned zone temperature maybe different. The

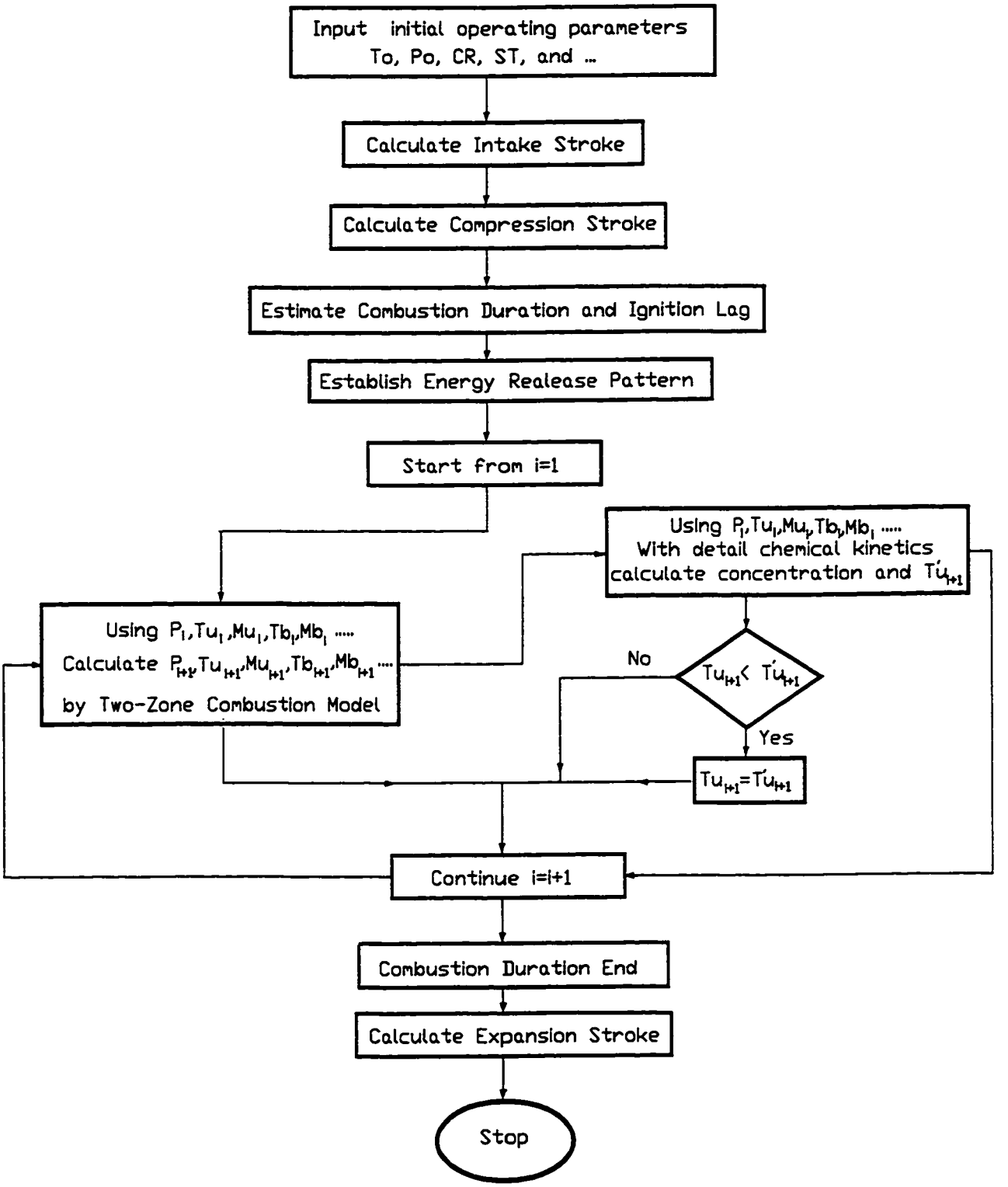

Figure 3.12: Flow-chart of the two-zone knock modeling.

effect of the end-gas reaction on temperature is assumed to be limited to the end-gas zone itself. Since the end-gas reaction rate is very sensitive to temperature, the effect of the end-gas reaction on the end-gas temperature should be accounted for. These influences, clearly, cannot be predicted from the thermodynamic two-zone combustion model alone. Accordingly, a modified procedure was employed to consider the effects of the thermal contribution of the end-gas reactions. At each time interval, the reaction rates of the end-gas were calculated at the predicted T_{ub} and P from the two-zone model. Then, the resulting temperature change dT'_{ub} of the end-gas zone due to these reactions over the short time interval was evaluated at constant cylinder pressure. If the resulting calculated temperature change dT'_{ub} is larger than the temperature change dT_{ub}, due to only flame propagation, then it was used as the new dT_{ub} for the next interval of considering the chemical reaction rate instead of the value derived from the two-zone combustion progression model. The flow chart of knock modeling is shown schematically in Figure 3.12.

Figure 3.13 compares the variations of the calculated unburned gas mean cylinder charge temperature with crank angle for methane operation based on the normal flame propagation model and reactive end-gas model for a typical knocking operating condition. Since the combustion process in the engine involves a significant end-gas reaction activity, T_{ub} increases quickly, which speeds up the preignition reactions and causes advanced autoignition with greater intensity. The effect of the end-gas reaction on the unburned zone temperature is made through the addition of the temperature rise due to end-gas reaction to the normal unburned zone temperature obtained from the two zone combustion model. This modified unburned zone temperature is used to estimate the end-gas chemical reactivity. If operating conditions

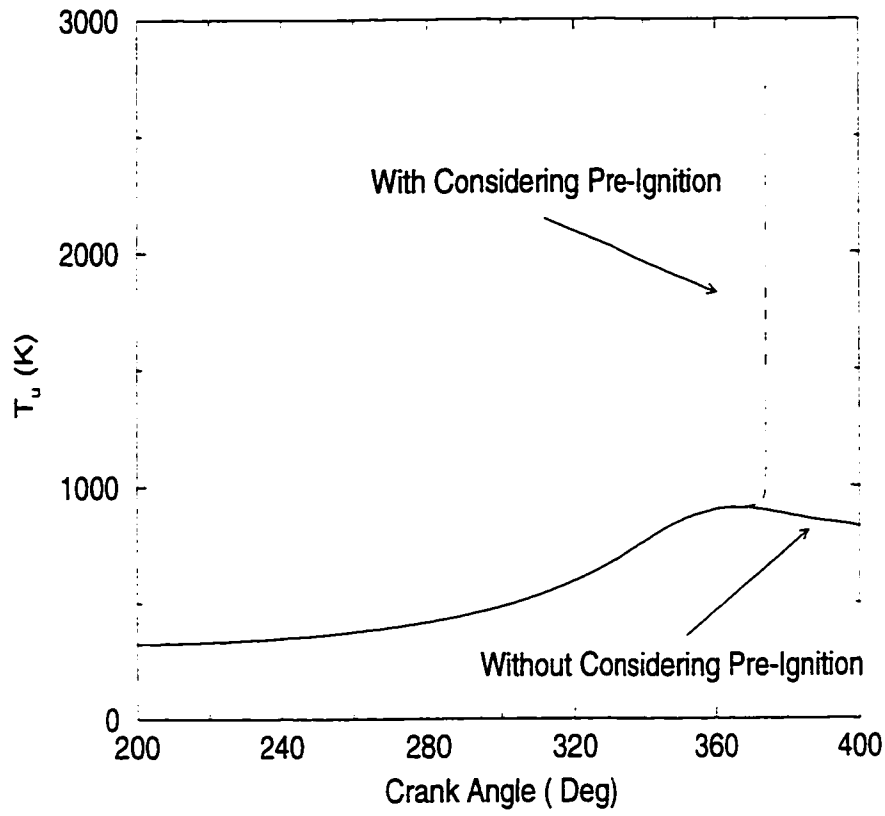

Figure 3.13: Variations of the calculated unburned zone temperature versus crank angle for methane operation at 900 RPM, $CR = 16$, $\phi = 0.88$, $\theta_{st} = 10$ BTDC and $T_o = 311$ K at experimentally knocking state for a CFR engine.

were far from those producing knock, the changes in the T_{ub} due to reaction activity were negligible and the unburned zone temperature obtained from the modified model, including the effect of the chemical reaction, were the same as the two-zone progression model.

3.7 Discussions

The model described has been shown to be capable of predicting engine performance parameters such as the temporal variations in cylinder pressure and the two zone temperatures for different speeds, intake temperatures, intake pressures and spark timings, as well as the effects of changes in some design parameters such as bore diameter and compression ratio [112]. Good agreement with available corresponding experimental data was evident, as shown typically in Figures 3.14 and 3.15.

The model appears to be capable also of predicting satisfactorily the onset of autoignition which is responsible for engine knock. An important feature of the approach followed is that the model can be used without requiring direct cylinder pressure-time data beforehand, correlations for the level of turbulence of the charge nor direct modeling of flame propagation.

The knock criterion of Equation 3.72 can be used to test for the onset of knock and to represent effectively engine knock intensity in gas fueled spark ignition engines. Since the spark timing is set so that most combustion takes place around top dead center to produce the largest power output from the engine, V_o/V_t is approximately equal to $(CR-1)$. Hence, to understand the effect of physical processes on the value of knock criterion, Equation 3.72 may be simplified as:

$$K = (\frac{h_{st} - h_t}{h_o})\frac{m_u}{m_o}(CR-1) \tag{3.77}$$

Figures 3.16 and 3.17 show two typical variations with time of end-gas relative energy release, dimensionless mass and knock criterion K for a knock free and a borderline knock operations. At the beginning of the combustion process in the engine, since the reaction rate of the end-gas is very slow, K values tend to be small.

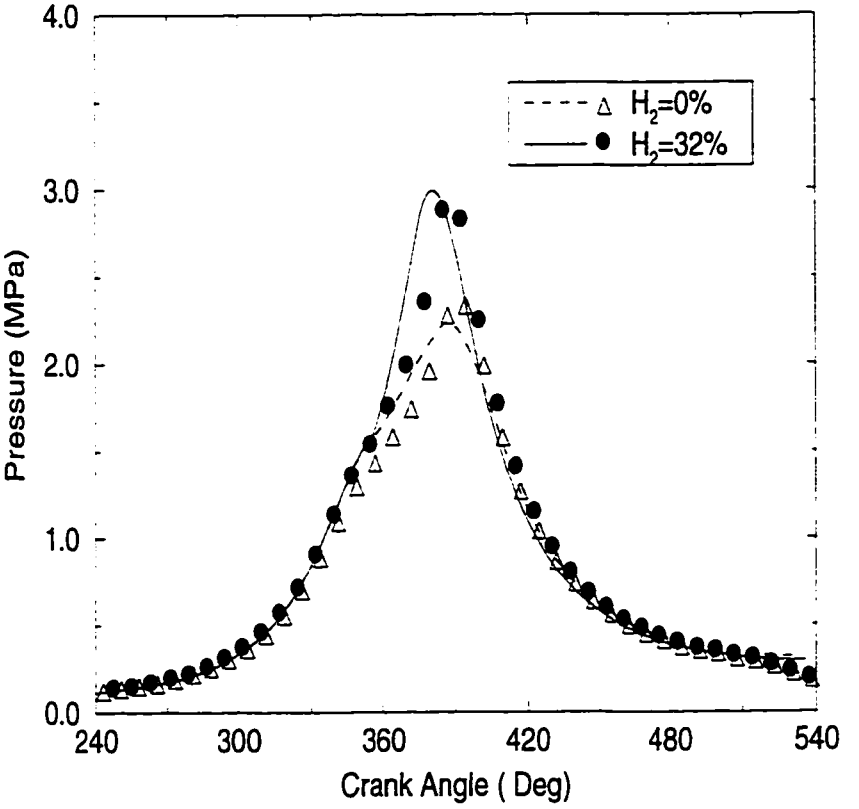

Figure 3.14: Variations of the calculated pressure with crank angle for methane and hydrogen mixtures at 900 RPM, $\phi = 0.9$, CR =8.5:1, $\theta_{st} = 10$ BTDC, $P_o = 87$ kPa and $T_o = 300$ K. The corresponding experimental points are shown.

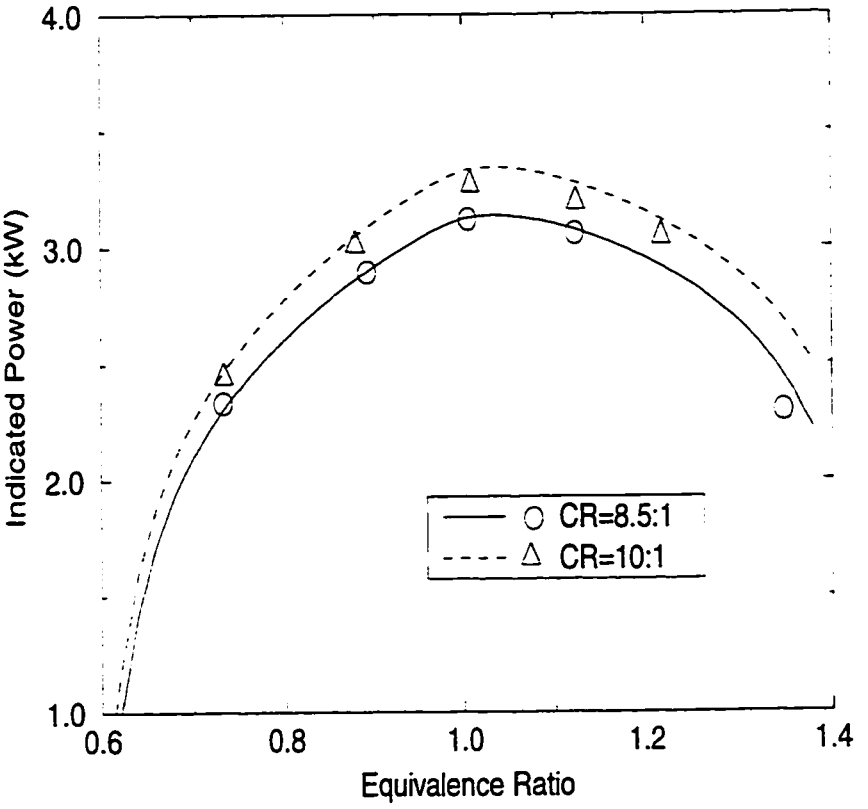

Figure 3.15: Variations of the indicated work output with changes in equivalence ratio for methane operation at 900 RPM, $\theta_{st} = 15$ BTDC, $P_o = 87$ kPa, $T_o = 300$ K. The corresponding experimental points are shown.

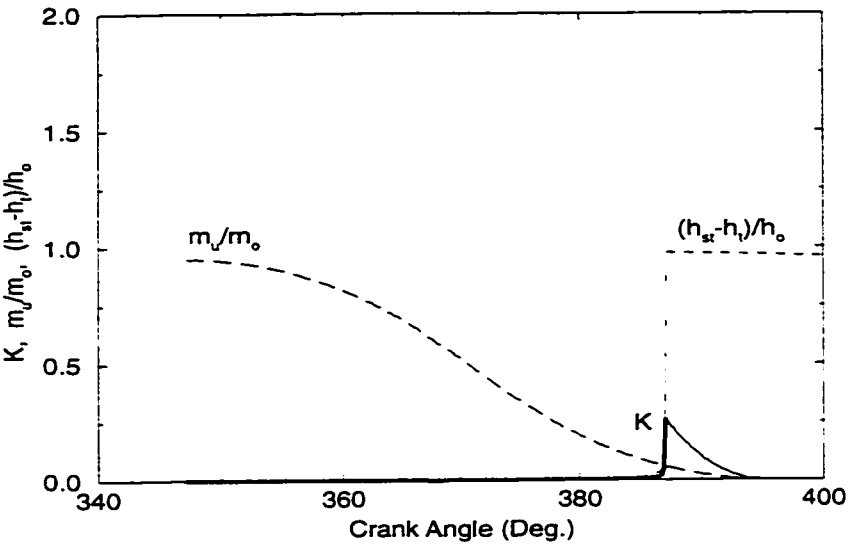

Figure 3.16: Typical variations of K, m_u/m_o and $(h_{st} - h_t)/h_o$ with crank angle for a knock free operation with methane at 900 RPM, CR =11:1, ϕ = 1.0, $\theta_{st} = 18°$ BTDC, $P_o = 87$ kPa, $T_o = 308$ K. The thick line shows the variation of K before autoignition of the end-gas.

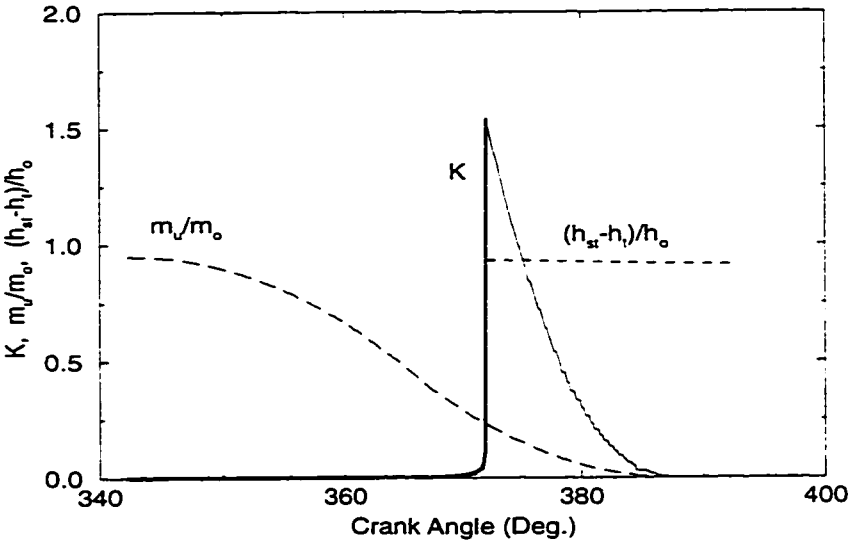

Figure 3.17: Typical variations of K, m_u/m_o and $(h_{st} - h_t)/h_o$ with crank angle for borderline knock operation with methane at 900 RPM, CR =11:1, ϕ = 1.0, $\theta_{st} = 23°$ BTDC, $P_o = 87$ kPa, $T_o = 308$ K. The thick line shows the variation of K before autoignition of the end-gas.

As the combustion process progresses, the end-gas temperature and pressure are increased, causing an increase in the reactivity of the end-gas and therefore end-gas energy release due to autoignition. On the other hand, the consumption of the charge by flame propagation decreases the ratio of m_u/m_o according to the mass burning rate function of Equation 3.66. As a result, the K value increases to a maximum and then drops to zero as the end-gas is consumed by the flame propagation. A rapid rise in the value of K is associated with the onset of autoignition in the mixture. The maximum value of K depends on the amount of self reacted energy released, which is a function of the size of the end-gas at the time of autoignition. If autoignition takes place at virtually the end of the combustion duration, the amount of energy released will be too small to produce a detectable knock. But, if under more severe operating conditions a large portion of the charge participated in the autoignition well ahead of flame arrival, a detectable knock can be observed (see Figures 3.16 and 3.17).

Through comparison with experimental data, it was found that whenever the value of the knock criterion exceeded a certain threshold value, then the operating conditions were associated with a knocking behavior. The bigger the difference, the greater is the intensity of knock, as shown typically in Figure 3.18. For knock free operation, the value of this criterion remains throughout below the threshold value. This represents perhaps for the first time a relatively simple criterion for computational testing of the incidence of knock through following the preignition reaction activity of the end-gas. It appears to work well enough to establish whether knock is to be encountered and its relative intensity for any set of operating conditions.

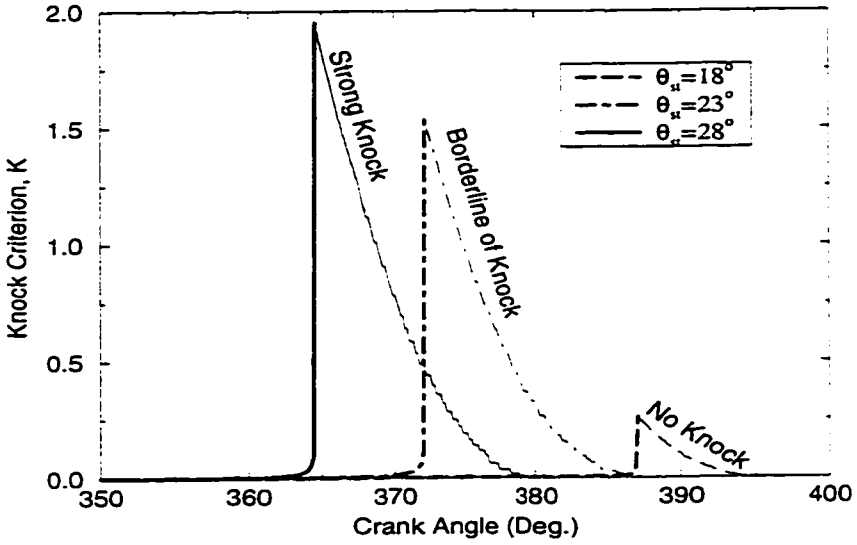

Figure 3.18: Variations of the knock criterion K with crank angle for methane operation at 900 RPM, $CR = 11 : 1$, $\phi = 1.0$, $T_o = 308$ K, and $P_o = 87$ kPa at three experimentally conditions showing no knock, borderline knock and strong knock operations. The thick lines indicate the variations before autoignition of the end-gas.

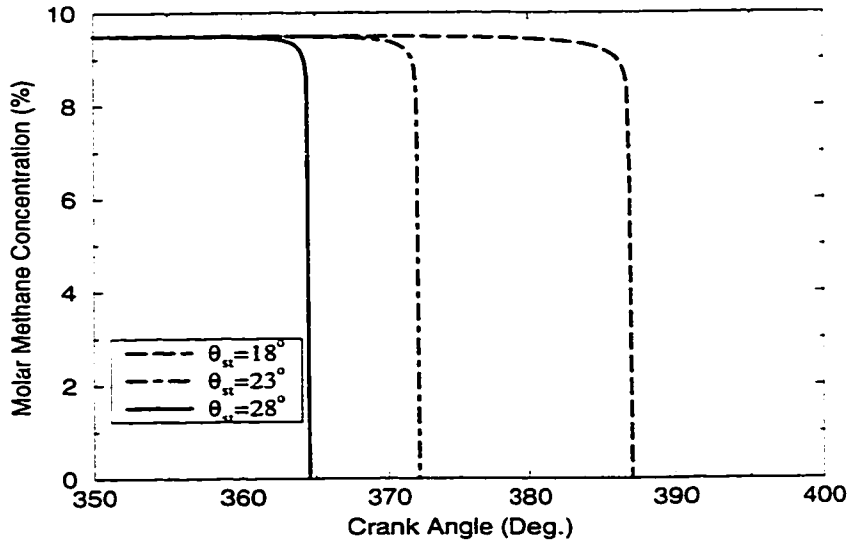

Figure 3.19: Variations of the volumetric methane concentration in the end-gas with crank angle for methane operation at 900 RPM, $CR = 11 : 1$, $\phi = 1.0$, $T_o = 308$ K, and $P_o = 87$ kPa at three experimentally conditions showing no knock, borderline knock and strong knock operations.

The variations of the corresponding end-gas methane concentration are plotted in Figure 3.19. For knock free operation, the end-gas self reaction is low throughout and only a small part of the unburned gas undergoes changes due to reaction before the arrival of the normal flame propagation. It is clearly evident when there is negligible end-gas reaction activity, no autoignition will take place. In the case of no autoignition or if the autoignition takes place at the end of the combustion period, (see Figure 3.19 for $\theta_{st} = 18°$ BTDC), the value of the K factor will remain negligibly small. However, when autoignition occurs at a time such that a significant size of the end-gas will be involved, the value of K becomes unacceptably large (see Figure 3.18 for spark timing 23 and 28 degrees BTDC). Accordingly, through the continuous evaluation of the value of this K criterion during cycle modeling it can be established whether knock will take place or not. The value of K for any operating conditions reaches a maximum value before the end of combustion. This maximum value can be used to establish whether knock is to take place or not and its likely intensity.

The model was applied to some operating conditions (that were established experimentally to produce light knock in a CFR engine in our lab) to investigate the threshold value for knock criterion at borderline knock. The variations of K values with crank angle for some of these typical examples, for methane-hydrogen operations at 900 RPM, are shown in Figure 3.20. The maximum values of the knock criterion was found to be approximately 1.50 for these borderline knock operations. These typical examples and other similar results show that the operating condition for the knock limit may be determined theoretically by assuming a value of 1.5 for maximum knock criterion value at borderline knock operation.

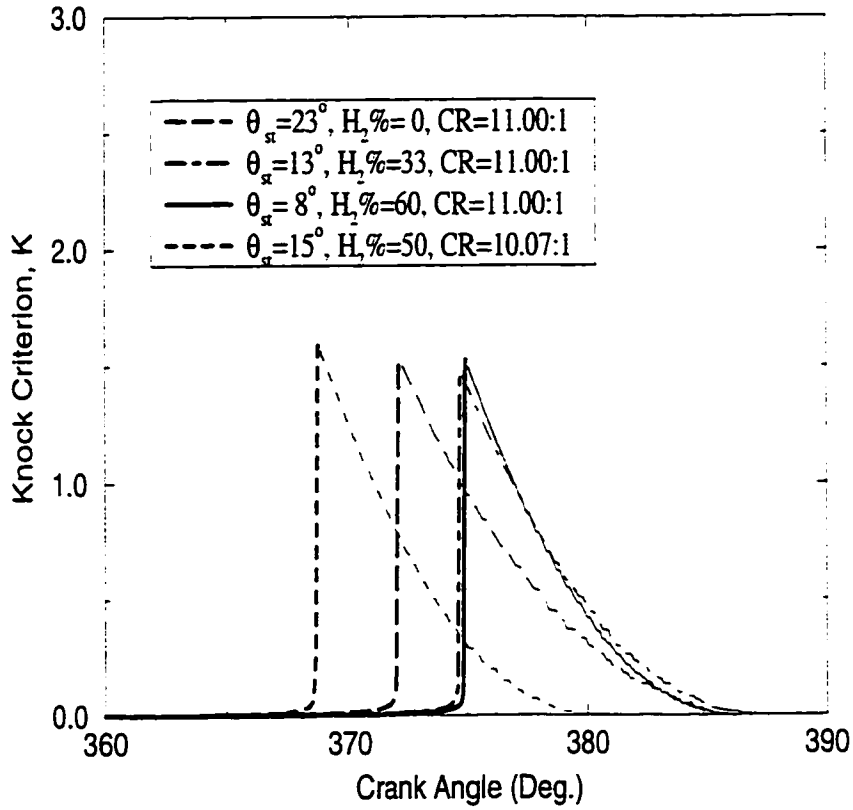

Figure 3.20: Variations of the calculated K with crank angle for some operating conditions associated with knock limit operations in a CFR engine using methane-hydrogen mixtures at 900 RPM, ϕ = 1.0, P_o = 87 kPa, T_o = 305 K. The thick lines show the variations of K before autoignition of the end-gas.

The origin of the size of this critical value is uncertain, but probably represents a slight excess (e.g. of 50%) of energy release due to autoignition at knock relative to the normal total energy release that can be released in the swept volume which the engine can cope with adequately. Also, K represents a pressure ratio of the pressure increase due to preignition reactions in the end gas relative to the mean effective combustion pressure rise over the whole cycle.

Chapter 4

Apparatus and Experimental Procedure

In order to establish and validate the empirical correlations developed for the combustion duration, ignition lag and the volumetric efficiency of the engine needed in the two-zone model described in Chapter 3 and investigate borderline knock operations, a reliable measurement of the cylinder pressure-time records needed to be made throughout the cycle. The corresponding crank angle-time records had to be also measured for calculation of the cylinder volume at every point in the cycle. The model, like all engine diagnostic models, needs to be applied under a variety of engine operating conditions. Therefore, it was necessary that the effects of variations in key operating parameters such as equivalence ratio, fuel composition, spark timing, mixture intake temperature and compression ratio be investigated experimentally. Of particular interest is the validation of the correlation for the effective combustion period developed for methane operation and presented in Chapter 3.

This chapter describes the experimental set up and the procedure of collecting and analyzing data.

4.1 Apparatus

4.1.1 Engine

A single cylinder, four stroke, spark ignition, ASTM-CFR engine of continuously variable compression ratio and spark timing (up to 40° before top dead center) was

used. The engine has the following dimensions as specified for model CFR-48 by the relevant ASTM manual [122]:

- Pancake shape combustion chamber
- Crankshaft Radius = 57.15 mm
- Stroke = 114.3 mm
- Connecting Rod Length = 254.0 mm
- Cylinder Bore = 82.55 mm
- Displacement = 611.73 cm^3
- Shrouded Intake Valve opens at 10° ATDC and closes at 34° ABDC.
- Plain Exhaust Valve opens at 40° BTDC and closes at 15° ATDC.
- Cylinder Water Jacket maintained constant (approximately 373 K).

The engine was coupled to an induction motor dynamometer that maintains an engine speed of 900 RPM. The intake system of the existing facility allows operation on gaseous fuels and provides control and metering of the fuel/air ratio. Further modifications to the original engine set-up and instrumentation, as will be explained later, allow continuous recording of the pressure-crank angle data. Figure 4.1 shows a schematic diagram of the experimental set-up.

The instrumentation available can be categorized into two systems, Engine Instrumentation and a Data Acquisition System. The former is intimately associated with the running of the engine while the latter is primarily intended for actual data collection and storage activities.

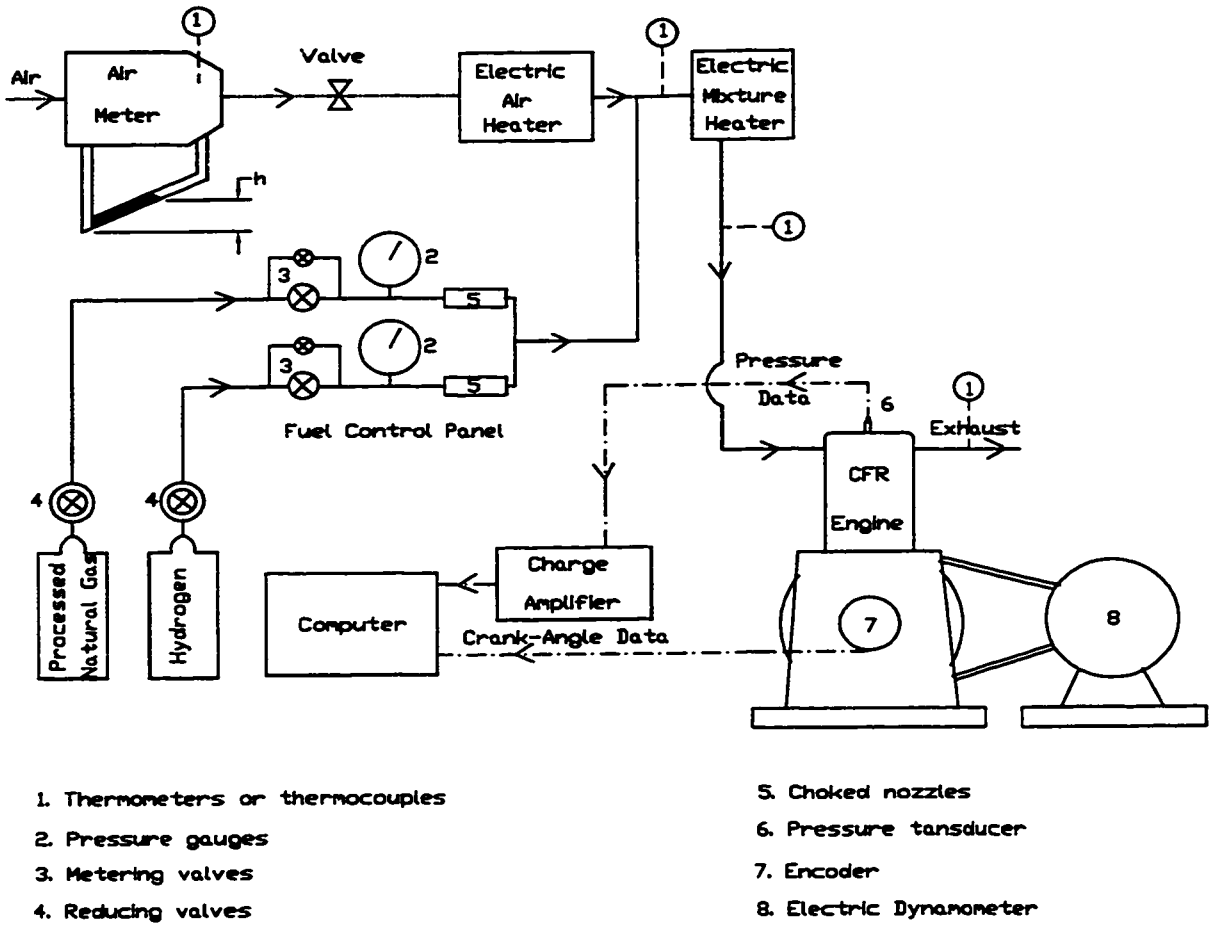

Figure 4.1: Schematic diagram of the experimental set-up.

4.1.2 Engine Instrumentation

The engine tested had been modified from the standard ASTM setup to include air and fuel metering systems. The spark timing control system and the mechanisms for varying the compression ratio were part of the engine as supplied by the manufacturer. Spark timing can be varied from -40 to +40 degrees before top dead center, while compression ratio can be changed from 4.46:1 to 16:1.

Gaseous Fuels, as shown in Figure 4.1, were drawn from high pressure bottles. Samples of the composition of the processed natural gas and other fuels used during

the work appear in Appendix (C). The fuels flow rates were metered by calibrated choked nozzles, while the air mass flow rate was measured by a laminar viscous flow meter. The system provides the capability to measure and control the fuel composition accurately for a wide range of Air/Fuel ratios. The details of air and fuel metering systems and the procedure for their calibration plus the final calibration graphs are discussed in Appendix (B).

4.1.3 Data Acquisition System

A water cooled piezoelectric *Kistler* pressure transducer (model 609 with sensitivity of 0.285 mC/psi) for pressure measurement was mounted flush with the cylinder surface through an opening in the top of the pancake shaped cylinder head such that the axis of the transducer was parallel to the cylinder axis. The transducer was connected to a *Kistler* charge amplifier and the resultant signal was routed to the data acquisition system computer for sampling.

The other instrumentation system is the crank angle and real time measurement system which is an electric encoder fitted to the end of the crank shaft that can recognize 1000 points in each 360°, with the first one at TDC. The timing system and the corresponding time data (2000 points for each thermodynamic cycle) were then written to a binary file on hard disk of the computer.

4.1.4 Main Computer for Data Processing

The instrumentation systems listed above provide timing and pressure data in binary form for a chosen number of cycles. These data had to be processed and converted to decimal values before further processing could be undertaken. This operation was

carried out on the same computer system on which the program for the diagnostic model was run. The mainframe computer used was IBM 486 and a Sun Computer System. Both supported a graphics package that was extensively used in all stages of data manipulation and processing. A detailed description of the use of the graphics capabilities of the system will be included in the section on experimental procedure. Final plots were produced on a laser printer attached to a Sun Computer System.

4.1.5 Phasing the Cylinder Pressure to the Crank Angle

In order to fix the TDC position initially accurately, the single cylinder CFR spark ignition engine fueled with natural gas was started and operated until the cylinder water jacket temperature reached the boiling temperature of water. A computer program was used to calculate the rate of pressure rise $dP/d\theta$ and display it in the graphic terminal. Four sets of data for four different compression ratios from 8.5:1 to 12:1 were recorded at motoring condition. From these data it was noted that the point at which $dP/d\theta$ was equal to zero did not coincide with the declared TDC position of the engine. As can be seen in Figure 4.2, the point at which $dP/d\theta$ was zero occurred at approximately two degrees before the TDC. Thus, the phasing of the timing needed to be adjusted to correct for the incorrectly declared marking of the TDC. The necessary adjustment was carried out until the $dP/d\theta$ curves for the four typical compression ratios appeared to intercept at zero at the modified location of the TDC, as shown in Figure 4.3.

It was deduced subsequently that the phasing of the cylinder pressure to the crank angle had a probable error of less than 0.1 degree, which was considered to be negligible.

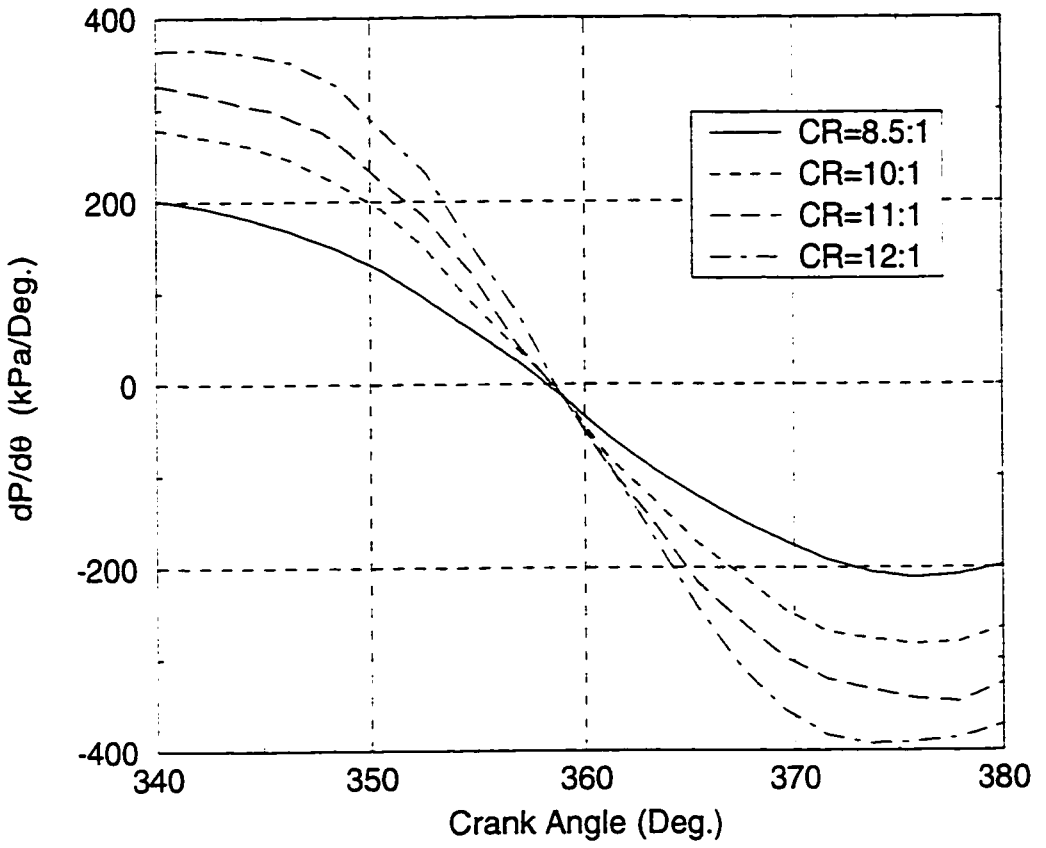

Figure 4.2: Variations of $dP/d\theta$ with crank angle.

Lancaster et. al. [123] considered the effect of errors in defining the TDC on the $P-V$ diagram. They suggested that since the compression and expansion strokes at motoring condition may be approximated by a polytropic function, the variation of $log(p)$ with $log(V)$ should have a linear relationship. Deviation from a straight line at TDC indicates the existence of an error in evaluating the clearance volume. A logarithmic $P-V$ and the corresponding $P-V$ diagrams for the CFR engine are shown in Figures 4.4 and 4.5. A linear relationship between $log(P)$ and $log(V)$ can be seen, confirming the suitable adjustment for TDC.

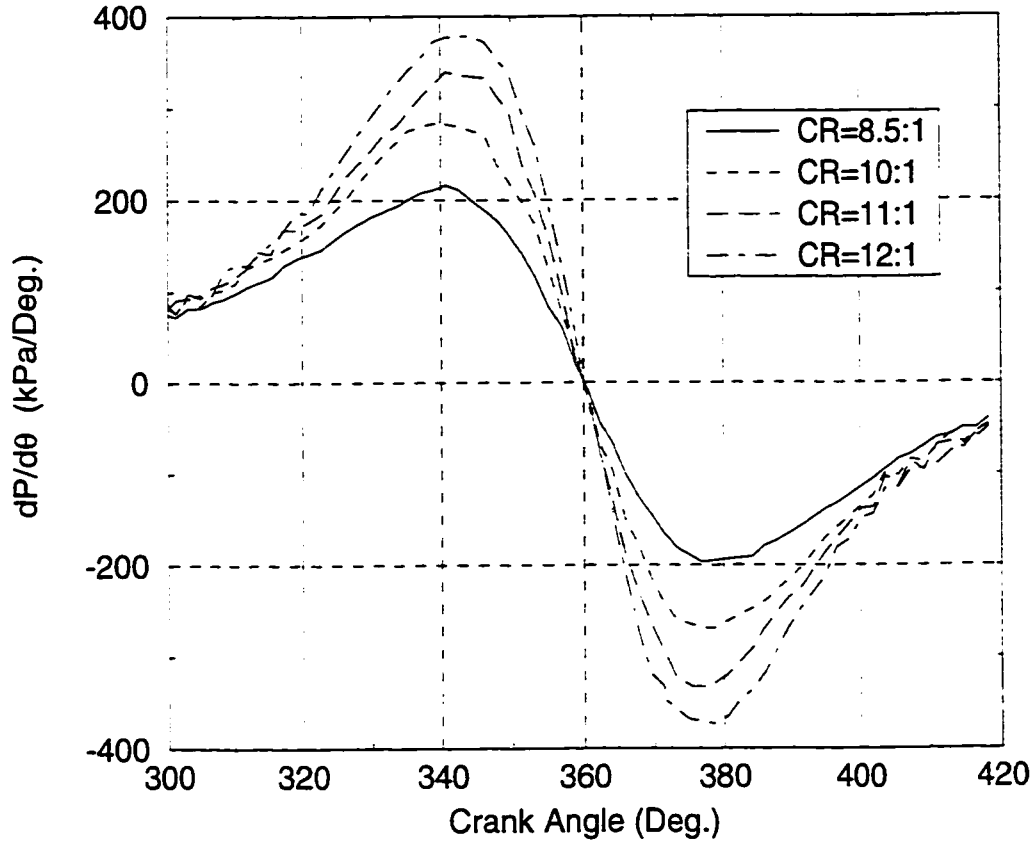

Figure 4.3: Variations of $dP/d\theta$ with crank angle after adjustment.

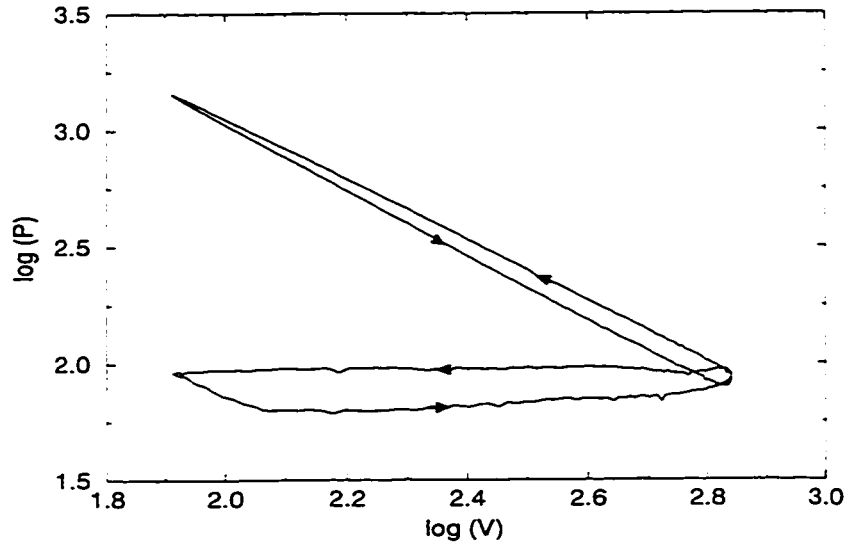

Figure 4.4: The log(P) versus log(V) graph at motoring condition.

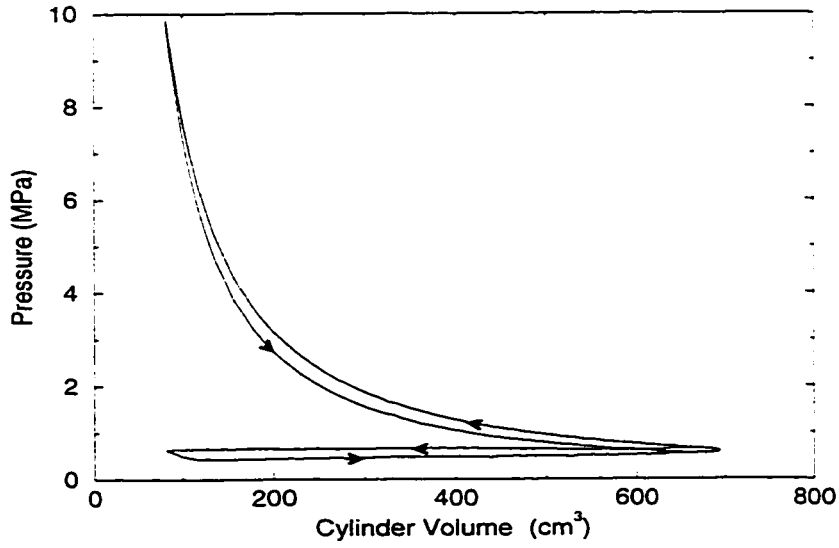

Figure 4.5: The variations of pressure versus cylinder volume at motoring condition.

4.2 Experimental Procedure

The experimental procedure was designed to obtain data such that the effects of changes to the main operational parameters of the engine could be examined with minor modification and adjustment to the engine setup.

Generally, a set of operating conditions was chosen and the data from the engine collected and stored for later processing. Following are the different parameters that were varied and the values chosen for them.

Most of the data were collected with spark timings of 10, 15, 20 and 30 degrees of crank angle before top dead center. These values were chosen since they represent a wide range of conditions as well as to limit the amount of data to be collected without a significant loss in the capability to analyze results. In some cases only three values of the spark timing were used because of either misfiring or knock occurrence.

Four values of compression ratio were used , namely 8.5:1, 10:1, 11:1 and 12:1. There were also cases when it was not possible to use all these values of compression ratios due to the onset of knock. Some tests for compression ratios of up to 16:1 were also carried out.

The equivalence ratio was varied from 0.65 to 1.20 approximately with all other operating conditions kept constant. This range was repeated for each change in spark timing and compression ratio for a constant intake mixture temperature. Data were also collected for conditions when it was possible to run the engine at a leaner equivalence ratio without detecting misfire. The calculation of the equivalence ratio was based on the volumetric composition of the fuels as described in Appendix (C).

The effects of the addition of hydrogen, butane, propane or ethane to the mixtures

of processed natural gas and air were investigated. These additives were added to the processed natural gas from 0% to 100% by volume of the resulting additive-natural gas mixture. The intake mixture temperature was maintained constant at 21° C for all the experiments carried out.

4.3 Data Collection and Processing Procedure

A three hour warming up period was provided for the stabilization of the charge amplifier of the pressure transducer. The data acquisition system would then be prepared for data collection by feeding in the necessary program. The engine was then started and allowed to run until the water coolant jacket reached the steady state temperature of 373 K. After all the operating conditions were established, the data collection would begin. The pressure signal was frequently affected by the excessive magnetic field generated by the spark as well as the spark system capacitor recharged cycle. This could not be avoided, and sometimes it resulted in very steep pressure trace spikes appearing at spark time. It was decided to deal with this problem at the data processing stage since very little could be done to solve it at the hardware level with the resources available.

When operating with fuel mixtures a computer program was used to determine the settings on the additive control panel such that the percentage of additive with respect to the fuel was kept constant even as the fuel-air ratio was varied. The independent addition of hydrogen, butane, propane or ethane did not affect the independently preset mass flow rate of the methane but it affected obviously the mass flow rate of air intake to the cylinder.

Each run consisted of collecting data for 20 consecutive cycles at a sampling rate of 66.7 microseconds (which corresponds to 0.36° at the 900 RPM used). This produced 2000 pressure-time sample points per thermodynamic cycle. At the same time the crank angle was recorded from the encoder to produce a pressure-crank angle data on a computer file. The processing of the data file was carried out by a computer program which performed the following operations.

(a) Conversion

All of the pressure data were converted to the decimal system from the binary numbers provided by the analogue to digital (A/D) system. The range as well as the gain factor settings of the A/D were taken into consideration while doing this conversion.

(b) Establishing a Reference Point

The voltages generated by the pressure transducer were not indicative of the absolute values of pressure. It was therefore important that a fixed absolute value of pressure was associated with one point of the cycle such that a correlation between voltage and pressure could be established for each cycle. The absolute value of the cylinder pressure at the first sampled point of each cycle (TDC of the intake stroke) was assumed to have a value similar to the local atmospheric value. This assumption allowed the processing of the data to yield a pressure-time record for each cycle.

(c) Data Examination

The data collected were first examined to check for any irregularities caused by the magnetic fields generated when the spark was passed. The affected points were smoothed by the program and a corrected data file would be recorded.

(d) Correction for Spark-Induced Spikes

When the spark-induced spikes occurred, they typically involved a single sample point that was affected by the spark passage to register a high value of voltage. The magnitude of spikes varied between prominent values where the rate of pressure rise was thousands of times higher than expected to that where it was twice the expected rate. They were all characterized by a sudden rise then drop in pressure value. The computer graphics capabilities were utilized to plot each cycle in a run separately for visual inspection, as well as to calculate and examine the rate of change of pressure around spark time. Corrections were made by adjusting the value of the affected sample point such that it would lie on the straight line through the two points on either side of this spike.

(e) Average Cycle Data Calculation

Arithmetic averaging of the pressure-time data of 20 cycles for each run was carried out after all of the above corrections to the recorded data. In order to examine the magnitude of error in the final results, the errors in determining the combustion period and ignition delay were plotted in Figures 4.6 and 4.7, using the following equations:

$$E_{CD} = \| \frac{\Delta\theta_{CD,av} - \Delta\theta_{CD}}{\Delta\theta_{CD,av}} \| \tag{4.1}$$

and

$$E_{ig} = \| \frac{\Delta\theta_{ig,av} - \Delta\theta_{ig}}{\Delta\theta_{ig,av}} \| \tag{4.2}$$

where $\Delta\theta_{CD,av}$ and $\Delta\theta_{ig,av}$ are the average of combustion period and ignition delay, respectively, of twenty individual cycles in each run, and $\Delta\theta_{CD}$ and $\Delta\theta_{ig}$ are the combustion period and ignition delay according to the average pressure crank angle

file. It can be seen that the maximum error for combustion period, even at lean

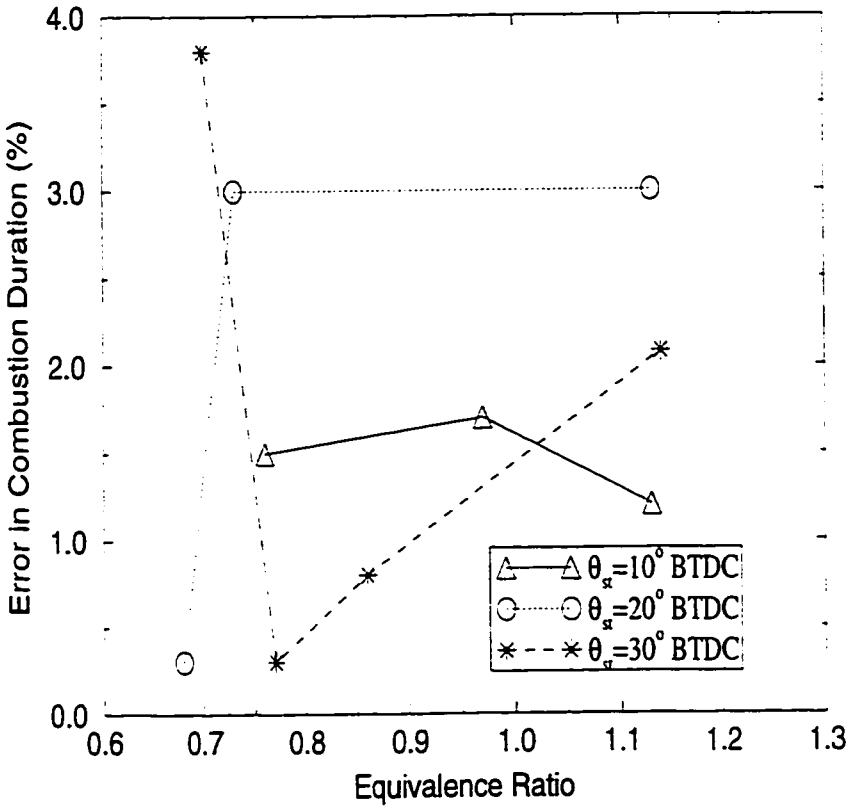

Figure 4.6: The error in determining the combustion period for 20% hydrogen in the mixture.

mixtures which are suffering from misfiring and cyclic variation, is less than 4%, while for the ignition delay, it is less than 20%. Since the order and magnitude of ignition delay is about 5 to 10 degrees of crank angle, such error cannot affect our results seriously, if the average pressure-crank angle data file of each run is used instead of the pressure-crank angle data file of each individual cycle. As a result, a single average pressure-time record was produced and used to estimate the combustion

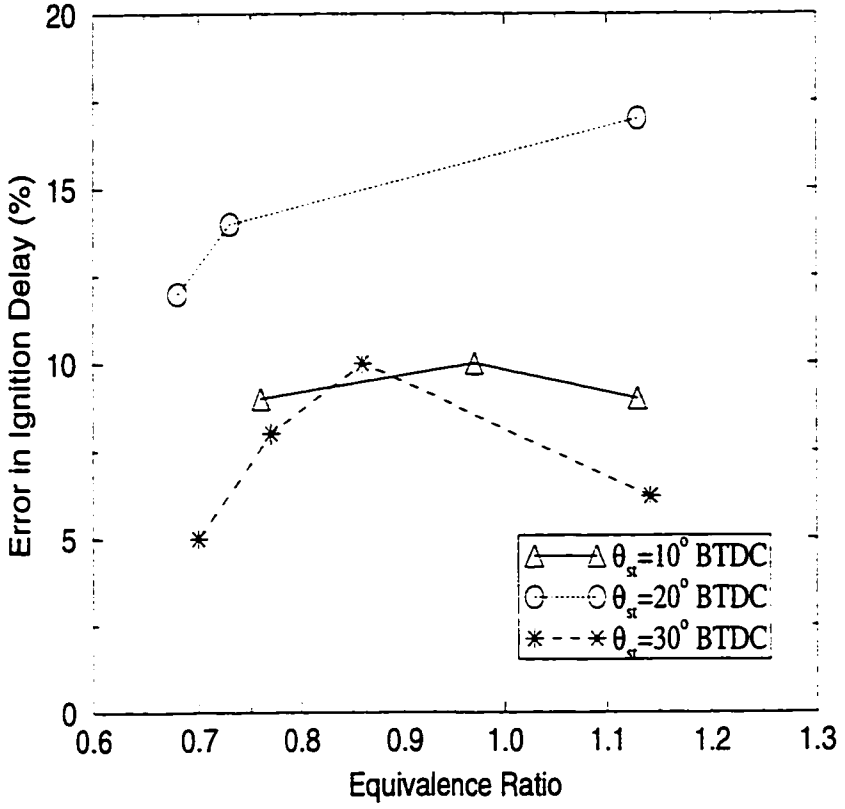

Figure 4.7: The error in determining the ignition delay for 20% hydrogen in the mixture.

duration and ignition delay. This record contained 2000 points of average cylinder pressure and corresponding crank angle of that run. The data resulting from the above treatment were used by the program embodying the model for calculating power output, combustion duration, ignition lag, etc. without further modification.

4.4 Mathematical Approach

The thermodynamic processes during the compression and expansion strokes may be approximated by a polytropic process. The polytropic index, n_θ, changes during flame propagation and it is approximately constant in compression of the fresh charge and expansion of the products. Hence, the evaluation of the ignition lag and combustion duration for spark ignition engine is simplified merely by evaluating the instantaneous polytropic index n_θ for both compression and expansion for the observed values of pressure and the corresponding cylinder volume, i.e.:

$$PV^{n_\theta} = Constant \tag{4.3}$$

Differentiating and re-arranging for polytropic index n_θ:

$$n_\theta PV^{n_\theta - 1}dV + V^{n_\theta}dP = 0 \Rightarrow n_\theta = -\frac{VdP}{PdV} \tag{4.4}$$

where V and P are the instantaneous cylinder volume and pressure. For discrete pressure and volume readings, Equation 4.4 can be reduced to:

$$n_\theta = -\frac{V_m(P_j - P_{j-1})}{P_m(V_j - V_{j-1})} \tag{4.5}$$

where

$$\begin{aligned} V_m &= \frac{V_j - V_{j-1}}{2} \\ P_m &= \frac{P_j - P_{j-1}}{2} \end{aligned} \tag{4.6}$$

$j-1$ and j represent the initial and final conditions of each sampling time.

For any operating condition, the crank angle at which the spark takes place is fixed at a constant value of θ_{st}. Usually the spark causes only a small kink in the

apparent value of n_θ. Moreover, this crank angle, θ_{st}, indicates the beginning of the ignition lag, while its end ($\theta_{e.i.}$) is associated with a rapid increase in the value of the index n_θ (see Figure 4.8). $\theta_{e.i.}$ also indicates at the same time the start of the

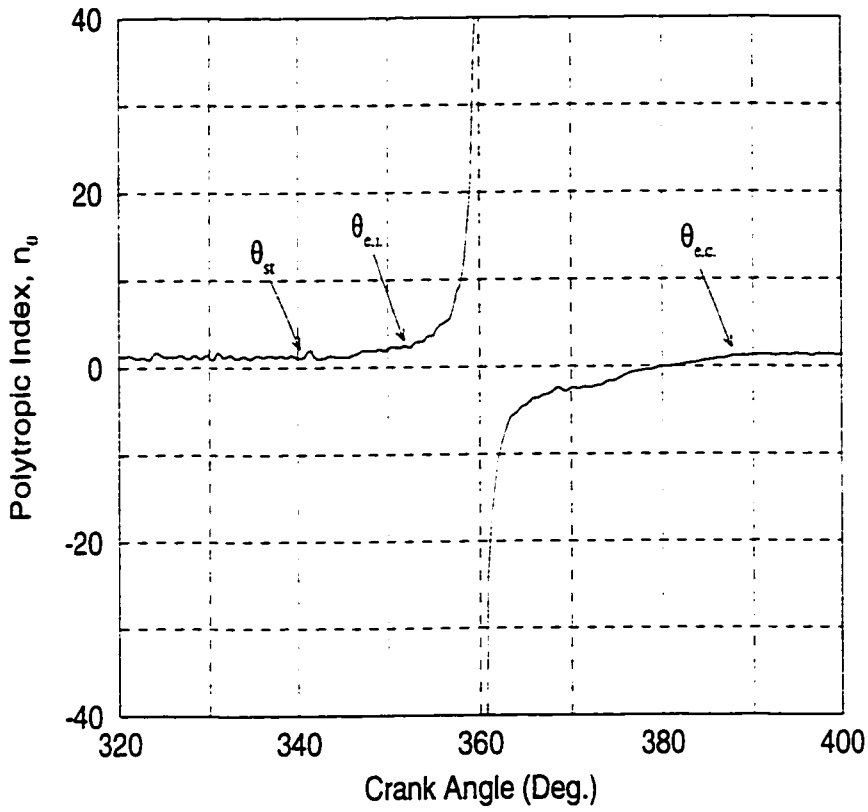

Figure 4.8: The typical variation of polytropic index with crank angle.

significant energy release and the beginning of combustion, i.e.:

$$Ignition \quad Lag = \theta_{e.i.} - \theta_{st} \tag{4.7}$$

The end of energy release by combustion will be associated with the first occasion of the effective polytropic index n_θ approaching a relative constant value that of

polytropic expansion index involving the products of combustion (see Figure 4.8). This crank angle will be called $\theta_{e.c.}$, i.e.:

$$Combustion \quad Duration = \theta_{e.c.} - \theta_{e.i} \tag{4.8}$$

The indicated power output can merely be calculated by integration of PdV over the whole cycle. Hence, it is:

$$Power = \sum P(V_j - V_{j-1}) \tag{4.9}$$

Chapter 5

Methane and Hydrogen Mixtures as a Fuel for a Spark Ignition Engine

5.1 Introduction

Lean mixture combustion is one of the most promising approaches for the reduction of NO_x emissions without much sacrifice in thermal efficiency as long as the possibility of partial burn or misfire under lean operation can be safely eliminated [6]. The main drawback of natural gas operation is an increase in the combustion duration because of its low flame speed, particularly for lean operation, causing an increase in the unburned hydrocarbon in the exhaust. Hydrogen can be used to increase the flame speed and improve the combustion of methane and other fuels [124, 125].

This chapter presents calculated results using the model developed and described earlier in Chapter 3 to provide typical examples of usage and further insight mainly into the following questions:

- How do operational variables affect engine performance parameters such as indicated power, thermal efficiency and the onset of knock and its intensity?
- How does hydrogen addition to methane affect the brake power output, thermal efficiency and knock intensity of the engine?

5.2 Some Calculated Features of Methane Operation

The variations of the indicated power output with changes in equivalence ratio for different compression ratios, CR, for methane operation in a naturally aspirated single cylinder of the CFR type when operating under full throttle conditions at 900 RPM and spark timing of 17 degrees BTDC, are shown in Figure 5.1. The

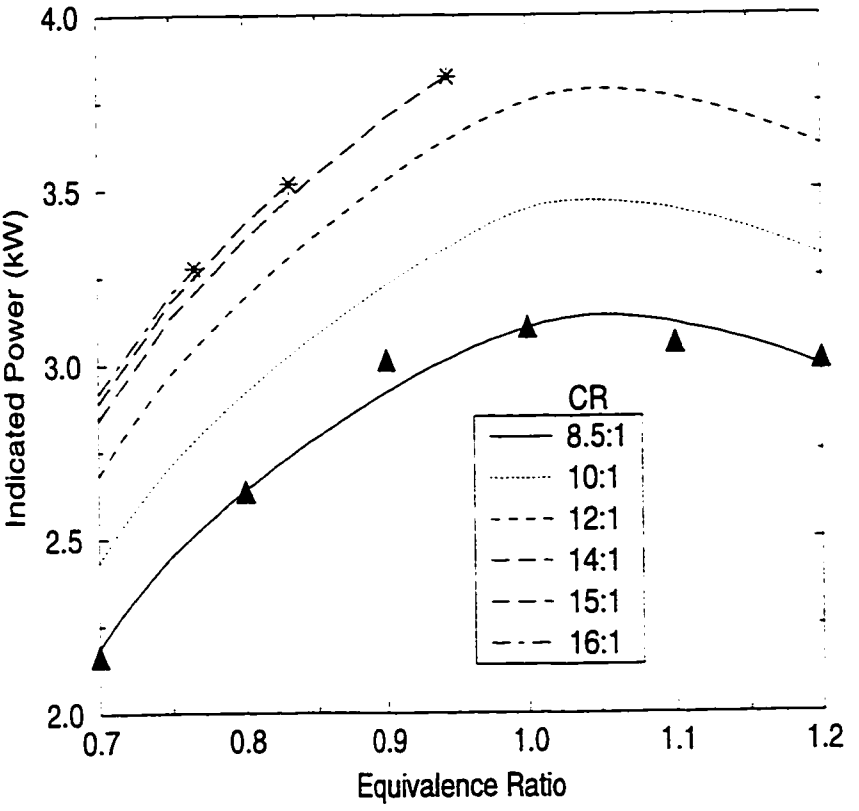

Figure 5.1: Variations of the calculated indicated power output with changes in equivalence ratio with methane at 900 RPM, θ_{st} = 17° BTDC, P_o = 87 kPa, T_o = 300 K. Experimental data for CR =8.5:1 are also shown by triangles and borderline knock operation by stars.

stars show the borderline knock operation for any specified operating conditions

associated with $K_{max} = 1.5$, while the triangles are experimental points obtained in this investigation for compression ratio 8.5:1. These symbols will consistently have the same meaning in all the graphs displayed in this chapter. The maximum value of engine power output, if not restricted by the onset of knock such as the data for $CR = 8.5 : 1$, is achieved with slightly richer mixtures than chemically correct, around $\phi = 1.05$, as expected from our experimental data and those of the references [31, 32]. Reducing the equivalence ratio, ϕ, towards leaner mixtures decreases the power output dramatically due to the reduced energy release and the longer combustion period. The influence of changes in compression ratio on the indicated power output at a constant equivalence ratio is more significant at low compression ratio values, e.g. changes in the compression ratio, CR, from 10:1 to 12:1 at $\phi = 0.75$, increase the indicated power output by 8% while changes from 12:1 to 14:1 under the same conditions produce a 6% change in power output. This is expected thermodynamically and by the relative increase in friction and heat transfer from the engine at high compression ratios.

Figure 5.2 shows the corresponding variations of the thermal efficiency with changes in equivalence ratio for different compression ratios. As expected from the experimental data [31] for wide open throttle operation, the maximum efficiency occurs somewhere between an equivalence ratio of 0.8 and 0.85, depending on the compression ratio and spark timing and whether it is optimized.

Variations of the calculated maximum values of the knock criterion, K_{max}, with changes in equivalence ratio for different compression ratios are shown in Figure 5.3. The biggest value of the criterion is associated with a stoichiometric mixture condition, as long as the maximum allowable value for equivalence ratio is not limited by

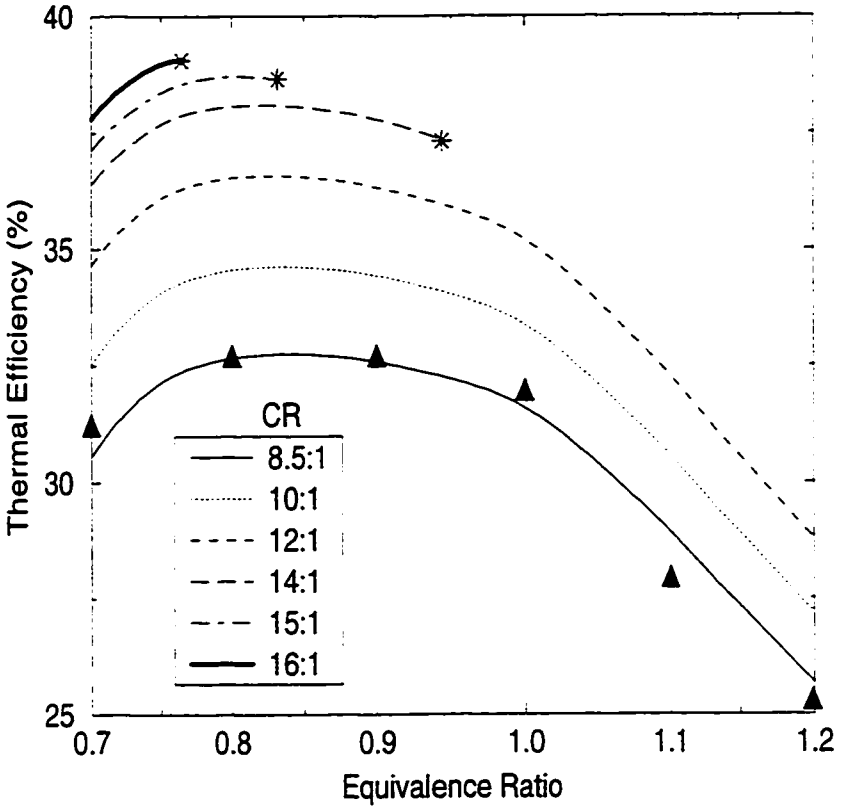

Figure 5.2: Variations of the calculated thermal efficiency with changes in equivalence ratio with methane at 900 RPM, $\theta_{st} = 17°$ BTDC, $P_o = 87$ kPa, $T_o = 300$ K. Stars and triangles are borderline knock operation and experimental points at CR =8.5:1.

the onset of knock. This is in agreement with the experimental data for similar conditions [57], showing that the knock intensity is highest at a stoichiometric condition. As can be seen, the equivalence ratio has a very substantial effect on the value of knock criterion ($K_{\mathbf{max}}$) at borderline knock operations assumed to be associated with a value around 1.5 for knock criterion $K_{\mathbf{max}}$, as shown previously in Chapter 3. A small increase of equivalence ratio, especially at high compression ratio, can increase the value of the knock criterion significantly. It indicates that the engine may knock

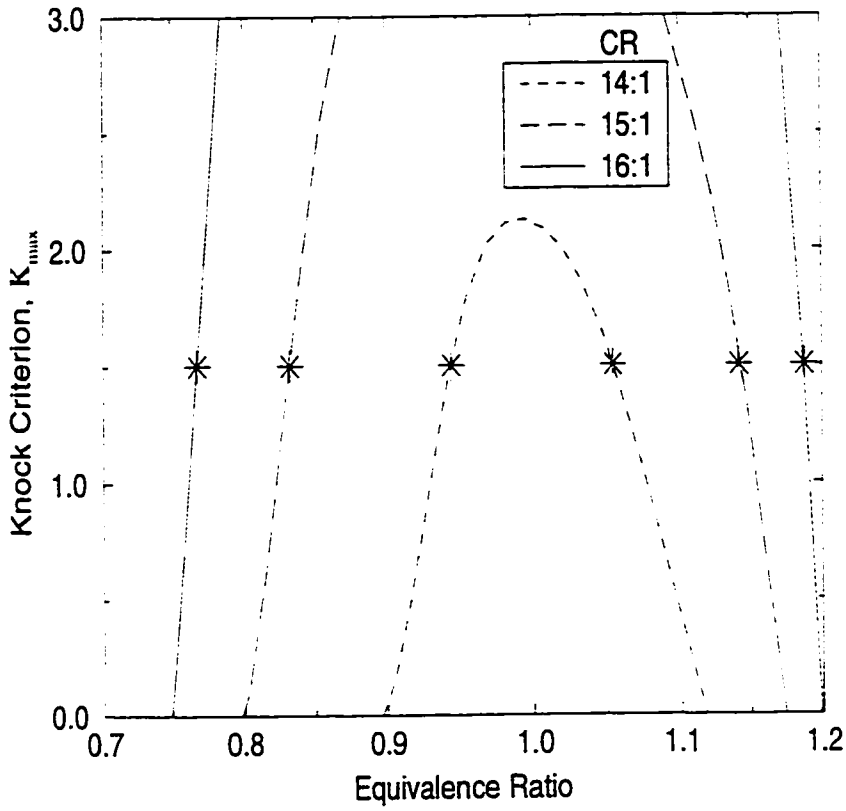

Figure 5.3: Variations of the calculated K_{max} with equivalence ratio for different compression ratio with methane at 900 RPM, θ_{st} = 17° BTDC, P_o = 87 kPa, T_o = 300 K. Stars indicate borderline knock operation.

heavily from a knock free operation close to the knock limit with a small change of equivalence ratio.

Figure 5.4 shows the variations of the equivalence ratio for maximum knock free indicated power and maximum knock free thermal efficiency with compression ratio for methane operation at 900 RPM, θ_{st} = 17° BTDC and T_o = 300 K. The thick line indicates the engine operations at borderline knock. The maximum power output at compression ratios less than 12:1 (away from borderline knock) is produced with

slightly richer mixture than stoichiometric, while for compression ratios greater than 13:1 which is associated with the knock limited operations, the equivalence ratio for maximum power, ϕ_{max}, decreases rapidly. Increasing the compression ratio from 14:1 to 16:1 requires a drop in equivalence ratio from 0.95 to 0.76 to keep the engine out of knocking region, while keeping the other operational variables unchanged. The decreasing rate of ϕ_{max} accelerates once the engine starts knocking at high compression ratios. A similar trend can be observed for the variations of equivalence ratio for knock free maximum efficiency operation. As expected, this equivalence ratio is associated with lean mixture operation and is between 0.8 to 0.85 for low compression ratios, but its value can drop to 0.75 at high compression ratios to stay out of the knocking region.

The corresponding maximum efficiency and maximum power versus compression ratio at the constant spark timing of 17° BTDC and T_o = 300 K are shown in Figure 5.5. Bold lines indicate the variations of power output and its corresponding efficiency for maximum power operation. Maximum indicated power increases by raising the compression ratio up to an optimum value, ($CR = 13.2 : 1$ and $\phi = 0.99$), then it drops due to a reduction in the knock free equivalence ratio and consequently less energy release by the charge, while the corresponding thermal efficiency increases all the way from a compression ratio 8.5:1 to 16:1.

The curves with the less bold regular lines show the changes of maximum efficiency that can be achieved by this typical engine and its corresponding power output with variable equivalence ratios at 900 RPM, θ_{st} = 17° BTDC and $T_o = 300$ K. Because of lean mixture operation ($\phi \leq 0.85$), the thermal efficiency is higher than that for maximum power operation, but the power is much less. Again, the thermal

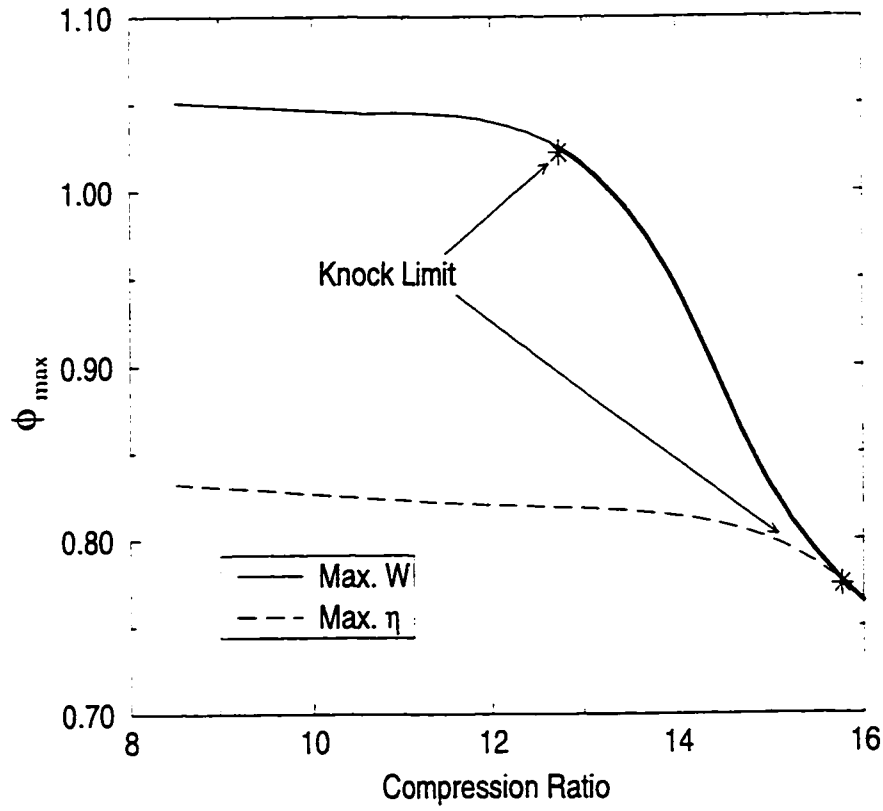

Figure 5.4: Variations of the equivalence ratio for maximum indicated power and maximum thermal efficiency with compression ratio with methane at 900 RPM, $\theta_{st} = 17°$ BTDC, $P_o = 87$ kPa, $T_o = 300$ K. Thick line show the borderline knock operation.

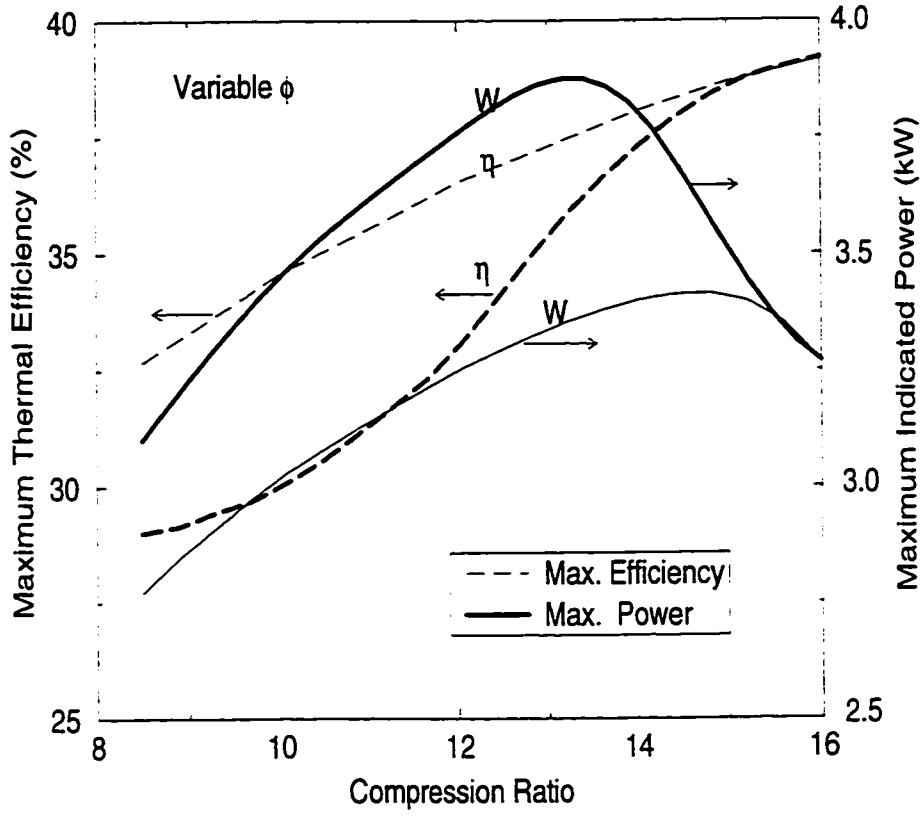

Figure 5.5: The bold lines show the variations of maximum indicated power with the corresponding thermal efficiency, while the thin lines show maximum thermal efficiency and the corresponding power output with compression ratio for methane operation with varying equivalence ratio at 900 RPM, $\theta_{st} = 17°$ BTDC, $P_o = 87$ kPa, $T_o = 300$ K.

efficiency increases with increasing compression ratio and approaches that for maximum power operation at $CR = 16 : 1$, due to having the same knock limit operation for both maximum power and maximum efficiency operation. The peak power for maximum thermal efficiency operation occurs at CR equals to 14.8:1, which is associated with a $\phi = 0.81$.

Figure 5.6 shows the variations of the indicated power with changes in spark timing for different compression ratios. The trends emphasize the existence of an optimum spark timing for maximum power output for any compression ratio. The corresponding variations of the thermal efficiency with changes in spark timing are shown in Figure 5.7. A similar trend as that of the indicated power output can be seen. The influence of the changes in compression ratio is more pronounced at low compression ratios as expected from a simple fuel air cycle analysis [126]. The optimum spark timing for maximum thermal efficiency is less advanced as the compression ratio increases due to a lower combustion duration and the onset of knock.

The variations of $K_{\mathbf{max}}$ with changes in spark timing at a constant equivalence ratio of $\phi = 0.9$, as shown in Figure 5.8, indicate that there is a maximum value for the knock criterion with respect to changes in the spark timing. When the spark timing is sufficiently delayed to be very close to TDC, then there would be insignificantly low reaction activity within the unburned zone during the period of flame propagation, keeping the value of $K_{\mathbf{max}}$ small. When the spark timing is increasingly advanced, auto-ignition can occur and $K_{\mathbf{max}}$ increases rapidly at a rate which depends also on the other operational variables. Advancing the spark timing yet further, reduces the value of the knock criterion $K_{\mathbf{max}}$ due to the consumption of

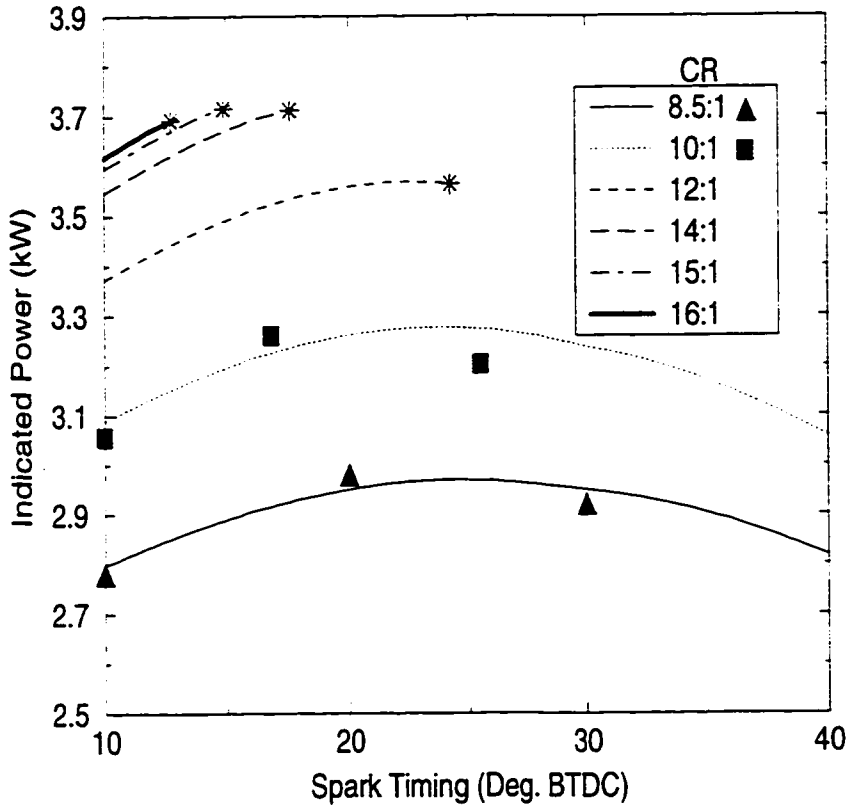

Figure 5.6: Variations of the calculated indicated work output with changes in spark timing and compression ratio with methane at 900 RPM, $\phi = 0.9$, $T_o = 300$ K, $P_o = 87$ kPa. Stars indicate borderline knock operation. Triangles and squares show the experimental points.

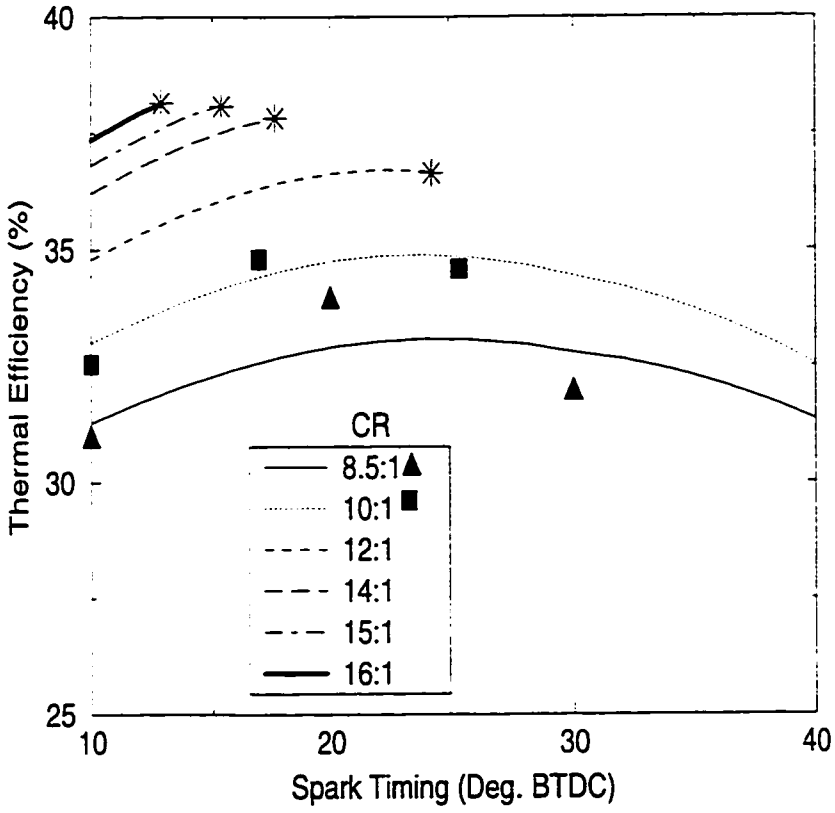

Figure 5.7: Variations of the calculated thermal efficiency with changes in spark timing and compression ratio with methane at 900 RPM, $\phi = 0.9$, $T_o = 300$ K, $P_o = 87$ kPa. Stars indicate borderline knock operation. Triangles and squares show the experimental points.

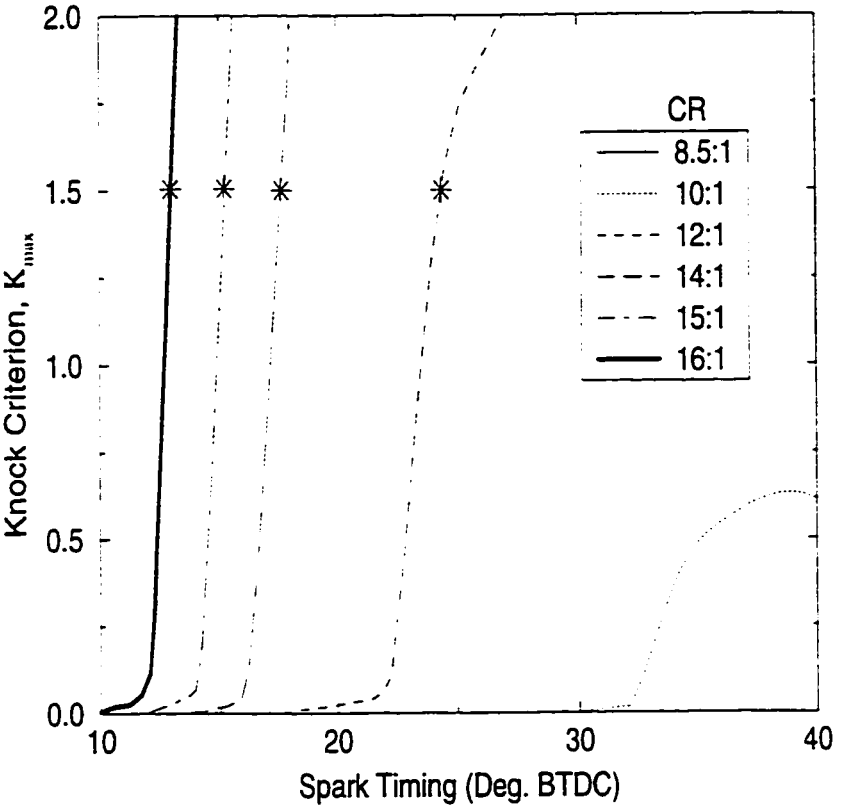

Figure 5.8: Variation of the calculated K_{max} with compression ratio for different spark timings and compression ratios with methane at 900 RPM, $\phi = 0.9$, $T_o = 300$ K, $P_o = 87$ kPa. Stars indicate borderline knock operation.

much of the charge through flame propagation before the piston reaches the top dead center. Meanwhile, advancing excessively the spark timing increases the negative work due to compression and reduces the power output significantly.

Figure 5.9 shows the minimum spark timing for knock free maximum power output when operating at a constant equivalence ratio of $\phi = 0.9$ for three different intake mixture temperatures. The thick lines show knock limited operation while the thin lines are for engine operation far from borderline knock. For borderline

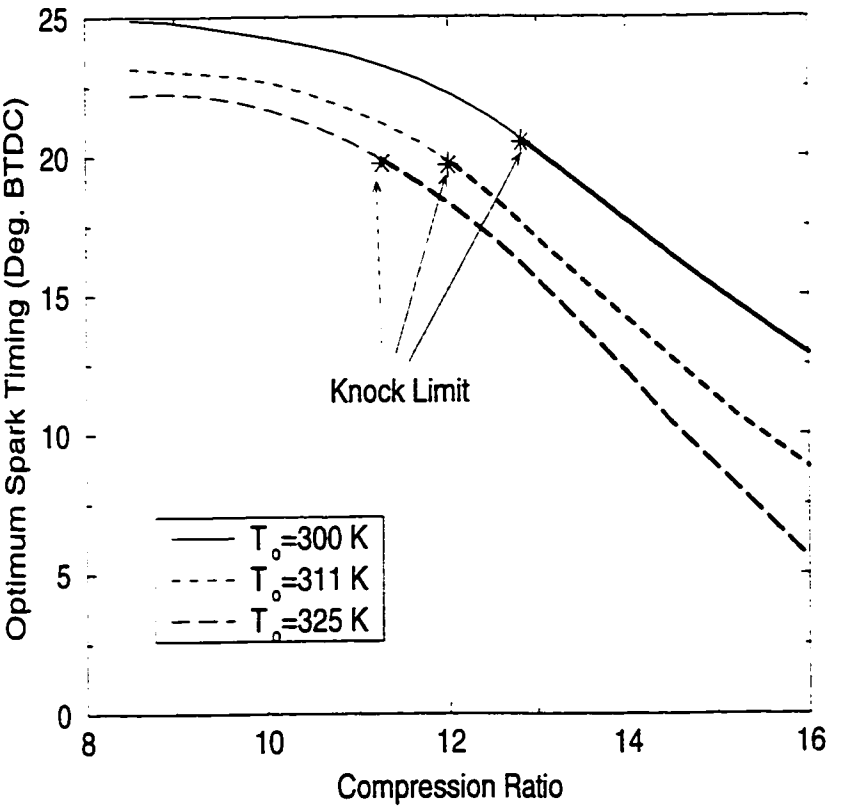

Figure 5.9: Variation of the optimum spark timing for maximum power with compression ratio for different intake temperatures with methane at 900 RPM, $\phi = 0.9$, $P_o = 87$ kPa. Thick lines show knock limited operation.

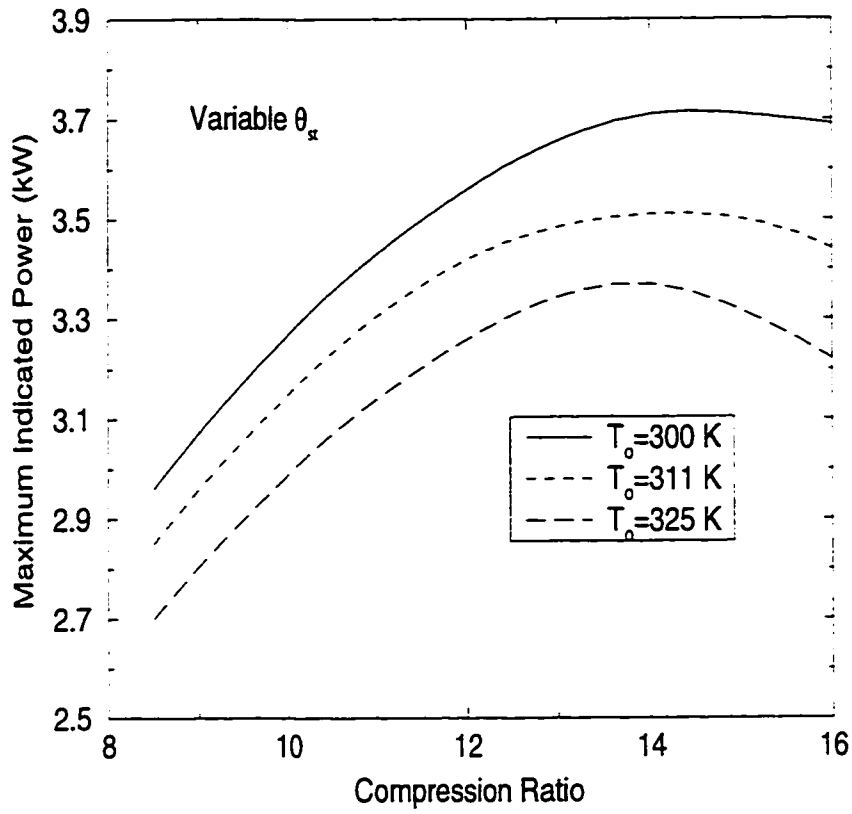

Figure 5.10: Variation of the maximum indicated power with compression ratio for different intake temperature and MBT timing with methane at 900 RPM, $\phi = 0.9$, $P_o = 87$ kPa.

knock operation, e.g. at $T_o = 311$ K and $CR \geq 12:1$, the MBT timing variations with compression ratio can be approximated by a straight line. An increase of one unit in compression ratio, for $T_o = 311$ K, requires a 3° crank angle retard in the spark timing. For low compression ratios and for the low intake temperatures shown, the minimum spark timing for maximum power has almost the same value of around 23° BTDC. The corresponding variations of maximum indicated power are shown in Figure 5.10, which indicate also the existence of an optimum compression ratio for

any intake temperature, e.g. around 14:1 for an intake temperature of 300 K. The power output decreases for compression ratios higher than this optimum value due to the retarded spark timing for maintaining knock free operation. The changes in the corresponding thermal efficiency are shown in Figure 5.11. Increasing the intake temperature moves the location of this optimum compression ratio to a lower value, mainly because of more retarded spark timing at high intake temperature for knock free operation.

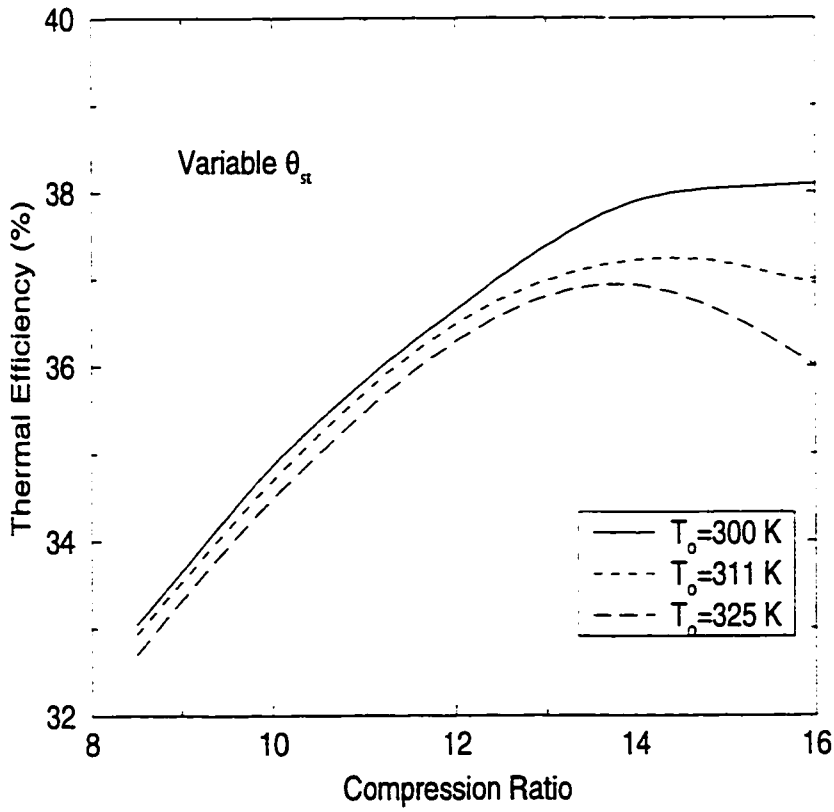

Figure 5.11: Variation of the thermal efficiency corresponding to maximum indicated power with compression ratio for different intake temperature and MBT timing with methane at 900 RPM, $\phi = 0.9$, $P_o = 87$ kPa.

When the intake temperature is changed independently of other operating variables while maintaining knock free operation, then the power output will change mainly due to the resulting change in the mass charge, while thermal efficiency improves with an increase in temperature mainly because of the associated faster flame propagation (see Figures 5.12 and 5.13). The change in power output shows almost

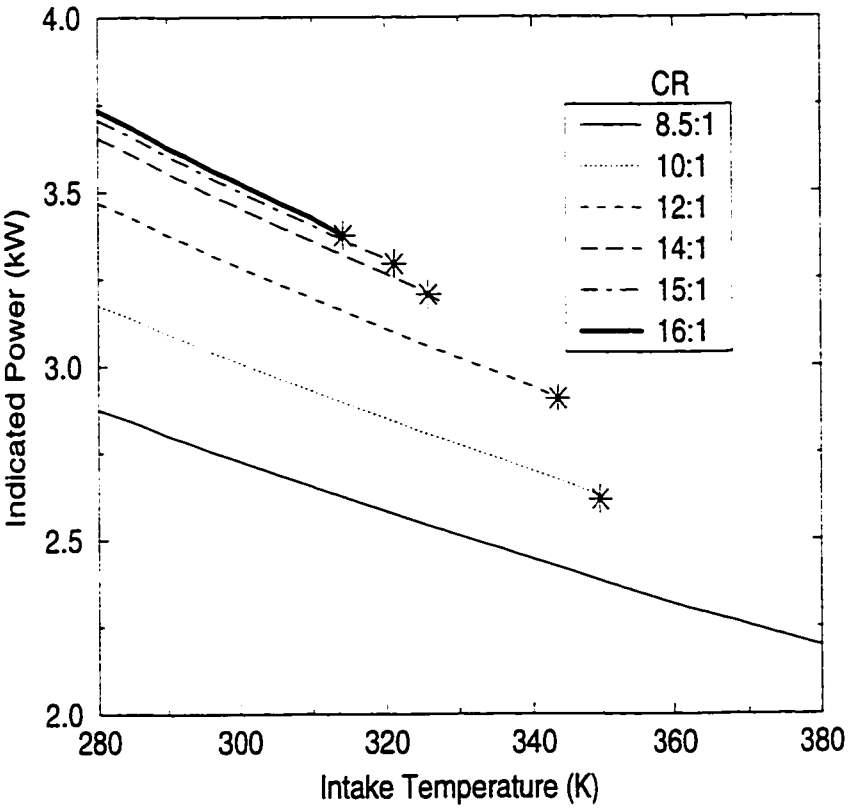

Figure 5.12: Variation of the calculated work output with changes in intake temperature with methane at 900 RPM, $P_o = 87$ kPa, $\phi = 0.9$, $\theta_{st} = 10$ BTDC. Stars indicate borderline knock operation.

a linear relationship with changes in the intake temperature. The corresponding variation of $\partial W/\partial T_o$ with compression ratio, shown in Figure 5.14, indicates that

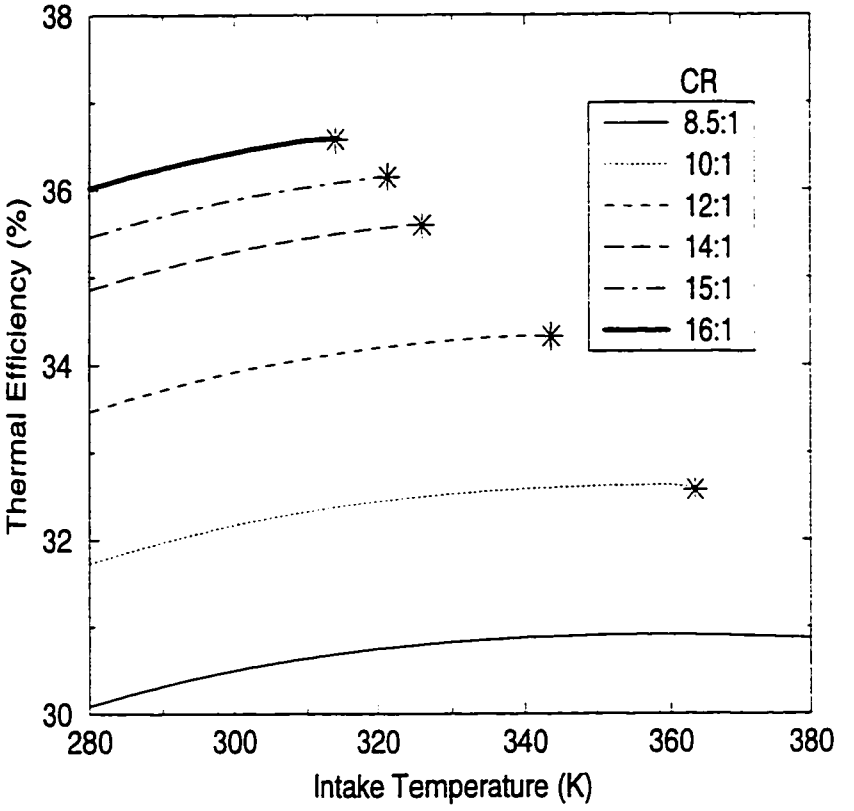

Figure 5.13: Variation of the calculated thermal efficiency with changes in intake temperature with methane at 900 RPM, P_o = 87 kPa, ϕ = 0.9, θ_{st} = 10 BTDC. Stars indicate borderline knock operation.

increasing the compression ratio increases the rate of the reduction in power output due to an increase in the intake temperature, probably due to the relative increase in heat transfer with increasing compression ratio and intake temperature.

Figure 5.15 shows the variation of the knock criterion $K_{\max}$ with changes in the intake temperature. The intake temperature has a very strong effect on the knock intensity as expected by the exponential dependence of reaction rates on temperature, while the combustion period varies virtually linearly with temperature. The general

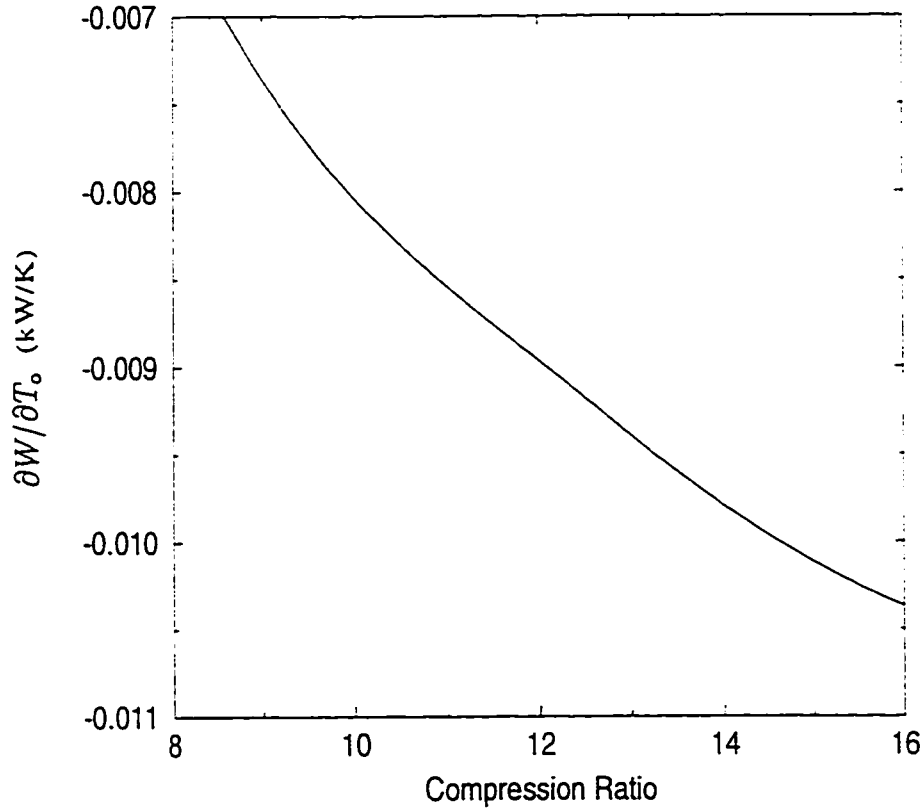

Figure 5.14: Variation of the calculated $\partial W/\partial T_o$ versus compression ratio with methane at 900 RPM, $P_o = 87$ kPa, $\phi = 0.9$, $\theta_{st} = 10$ BTDC.

trend for K_{max} with an increase in temperature is to have a small value up to a certain intake temperature, then it increases rapidly and virtually linearly leading the engine quickly to the onset of severe knocking.

Figure 5.16 shows a linear variation of the critical intake temperature for producing borderline knock with compression ratio for the operating conditions indicated. For example, increasing the compression ratio from 13:1 to 14:1, requires the lowering of the intake temperature from 335 down to 327 K, a drop of 8 K to retain knock free operation. The corresponding variations in the power output and thermal

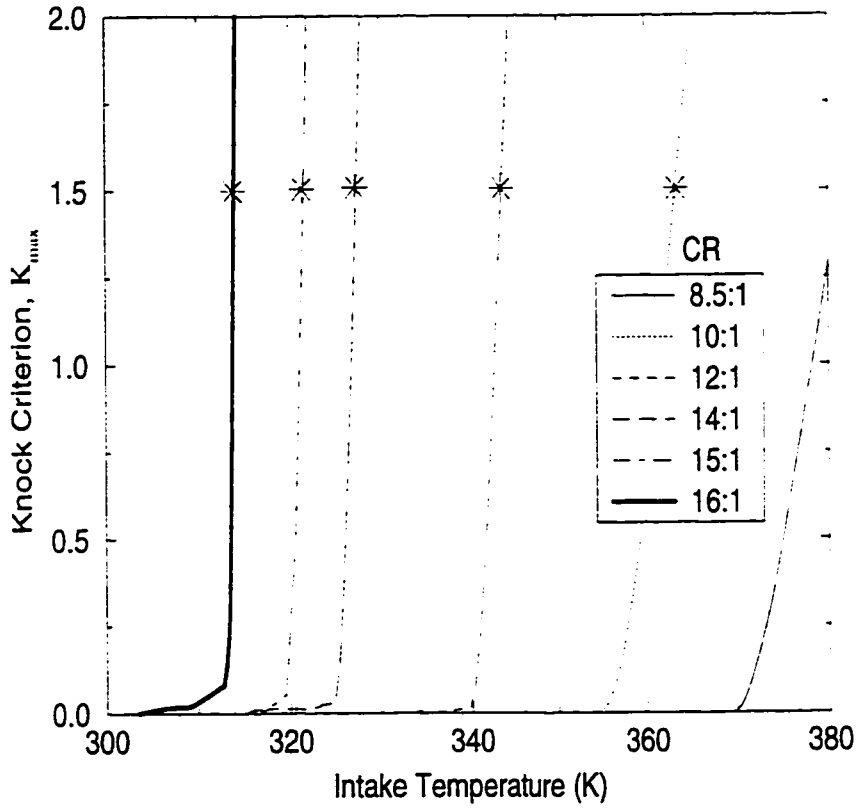

Figure 5.15: Variation of the calculated K_{max} with intake temperature for different compression ratios with methane at 900 RPM, $P_o = 87$ kPa, $\phi = 0.9$, $\theta_{st} = 10$ BTDC. Stars indicate the borderline knock operation.

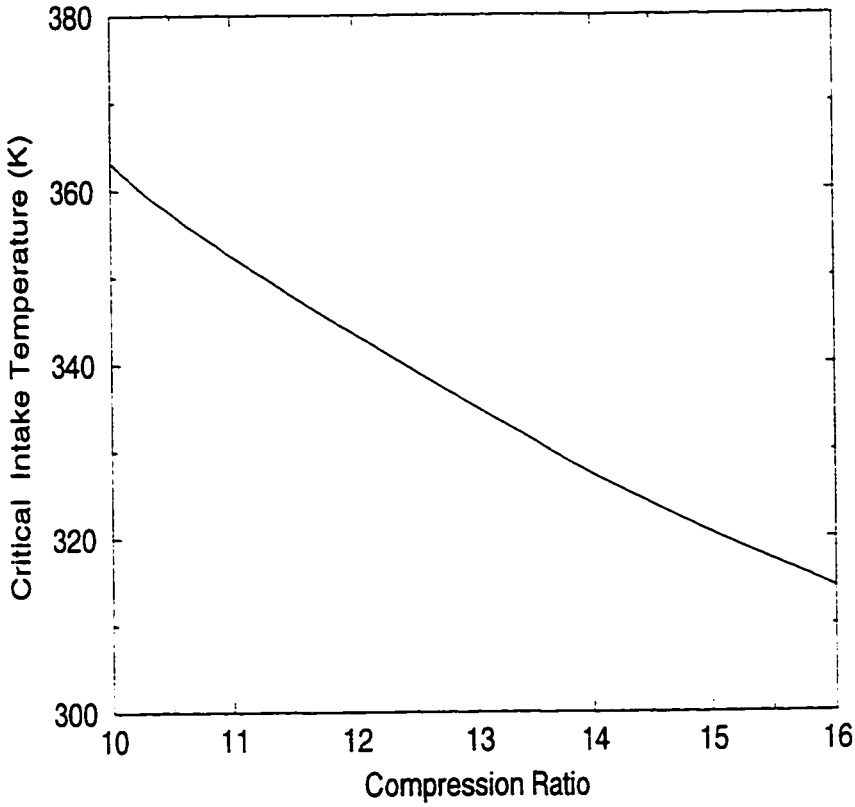

Figure 5.16: Variation of the critical intake temperature with compression ratio for borderline knock for methane operation at 900 RPM, P_o = 87 kPa, ϕ = 0.9, θ_{st} = 10 BTDC.

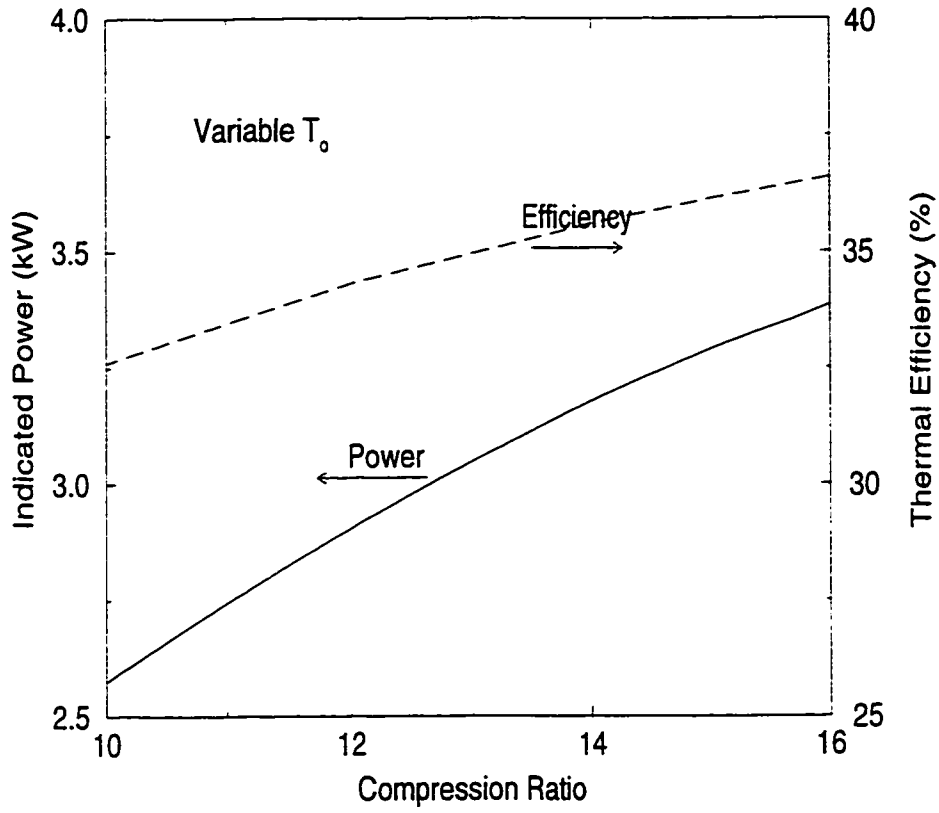

Figure 5.17: The corresponding values of the knock limited power output and thermal efficiency for critical intake temperature varying with compression ratio, shown in Fig. 5.16 for methane operation at 900 RPM, $P_o = 87$ kPa, $\phi = 0.9$, $\theta_{st} = 10$ BTDC.

efficiency are plotted in Figure 5.17 showing increasing trends with compression ratio. If the intake temperature is set sufficiently low to be far from knock limit operation (say 280 K), then the power output will be higher as shown in Figure 5.12. Thus, regarding intake temperature, the knock limit operation is not necessarily associated with maximum power operation. However, the thermal efficiency may increase with knock limit operation (see Figure 5.13).

5.3 Methane-Hydrogen Operation

Changes in the calculated indicated power output and the corresponding variations in thermal efficiency with changes in the hydrogen concentration in a binary fuel mixture of methane and hydrogen are shown in Figures 5.18 and 5.19, respectively. These results can be seen to be consistent with the experimental trends reported in reference [127]. Increasing the concentration of hydrogen in the methane increases the engine power output slightly and reduces cyclic variation [128] due to the resulting faster flame propagation, especially with very lean mixtures. When the concentrations of the hydrogen added to the methane becomes relatively large, then the inevitable reduction in the total amount of energy released begins to affect engine performance and power output adversely. Maximum power output normally is associated with hydrogen concentrations of 30% to 50% in the mixture for the specified operating conditions. As an example, the power output for a compression ratio of 8.5:1 and 40% hydrogen in the fuel mixture (see Figure 5.18) is 2.97 kW, while for pure methane it is 2.85, showing an increase of 3.4%. Similar trends can be observed for the thermal efficiency in Figure 5.19.

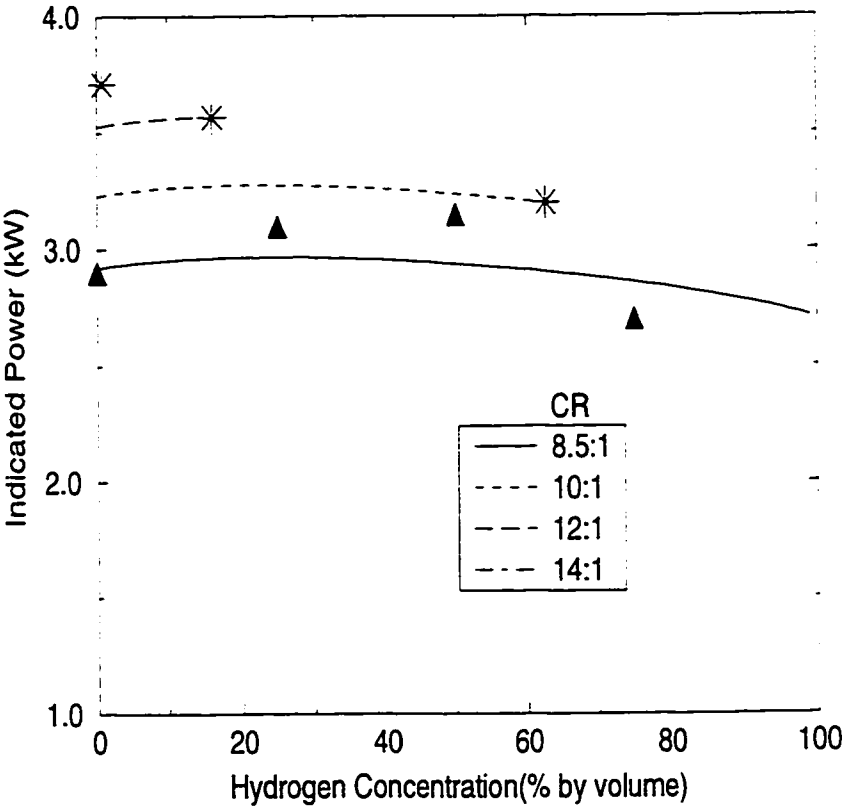

Figure 5.18: Variation of the calculated indicated power with changes in hydrogen concentration for methane-hydrogen mixtures at 900 RPM, $\phi = 0.9$, $\theta_{st} = 17°$ BTDC, $P_o = 87$ kPa, $T_o = 300$ K. Stars and triangles show borderline knock operation and experimental points with CR =8.5:1.

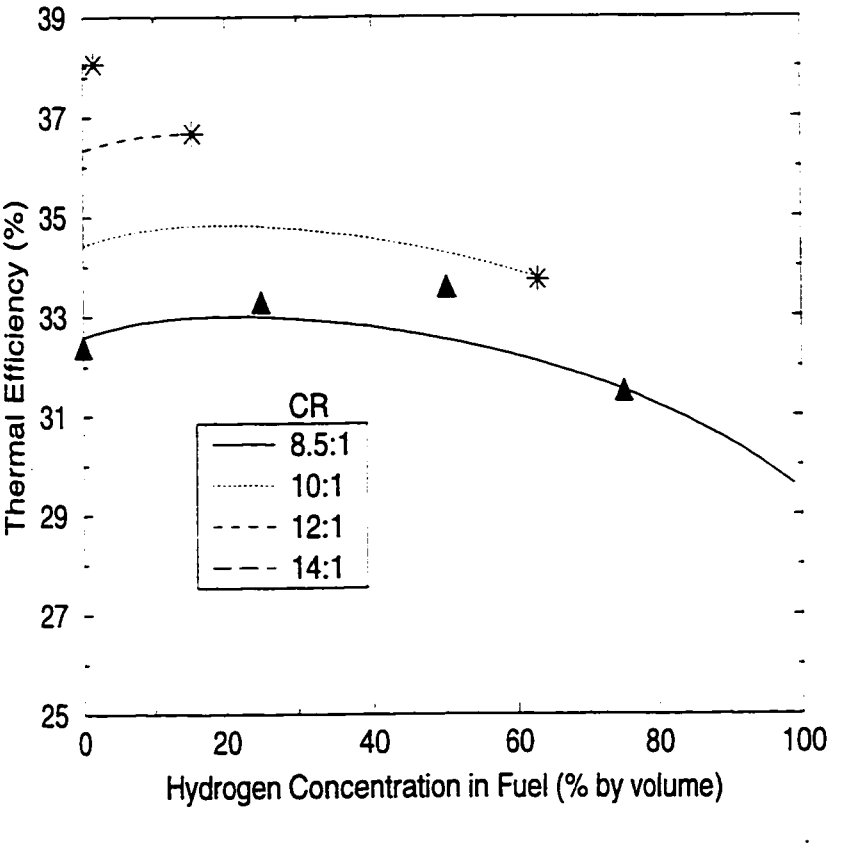

Figure 5.19: Variation of the calculated thermal efficiency with changes in hydrogen concentration in methane-hydrogen mixtures at 900 RPM, $\phi = 0.9$, $\theta_{st} = 17°$ BTDC, $P_o = 87$ kPa, $T_o = 300$ K. Stars and triangles show borderline knock operation and experimental points with CR =8.5:1.

Figure 5.20 shows the value of the knock criterion K_{max} for the same conditions. At low compression ratios, adding some hydrogen to methane does not change K_{max}

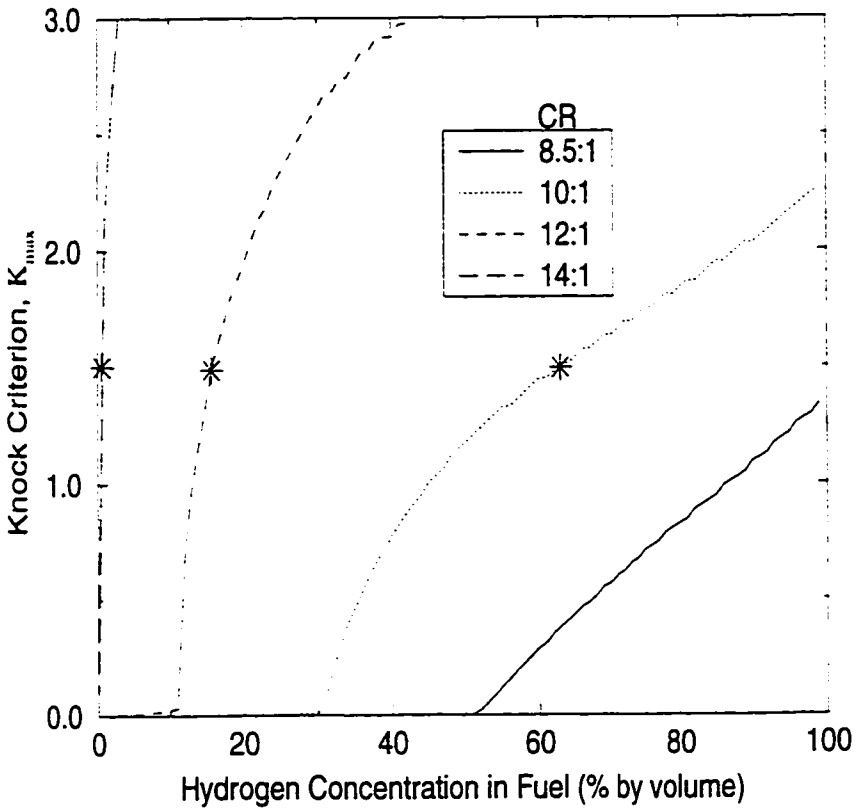

Figure 5.20: Variation of the calculated K_{max} with changes in hydrogen concentration in methane-hydrogen mixtures at 900 RPM, $\phi = 0.9$, $\theta_{st} = 17°$ BTDC, $P_o = 87$ kPa, $T_o = 300$ K. Stars indicate the borderline knock operation.

significantly up to a certain hydrogen concentration in the methane that depends on operational parameters. Beyond this value, K_{max} increases almost linearly at a rate dependent on compression ratio and other operational parameters. For example at a compression ratio of 14:1 the addition of a very small amount of hydrogen to the methane can produce knock, while at a compression ratio of 8.5:1 the engine

can be run on up to 95% hydrogen in the mixture of methane-hydrogen without encountering knock. This indicates decreasing tolerance to the presence of hydrogen in the methane as the compression ratio is increased.

The maximum hydrogen concentration in a methane-hydrogen mixture that produces a maximum indicated power is plotted in Figure 5.21. Increasing the compression ratio decreases the tolerance to hydrogen in the fuel mixture for maximum power production. At low compression ratios, far from borderline knock operation, the hydrogen concentration has a value of around 20%, while for high compression ratios which are associated with knock limited operation, the allowable volumetric hydrogen concentration in the fuel drops rapidly until, at around 14:1 compression ratio, no hydrogen can be present with the methane.

Figure 5.22 shows the maximum power and the corresponding thermal efficiency that can be produced by the CFR engine by the addition of some hydrogen to methane at a spark timing of 17° BTDC, equivalence ratio of 0.9 and T_o of 300 K. The rate of relative increase in power output with increasing compression ratio is higher than that of thermal efficiency. Typically, increasing the compression ratio from 10:1 to 12:1 for $T_o = 300$ K, while adjusting the hydrogen concentration based on Figure 5.21 can make an increase of 4.6% in thermal efficiency and 7.6% in power output.

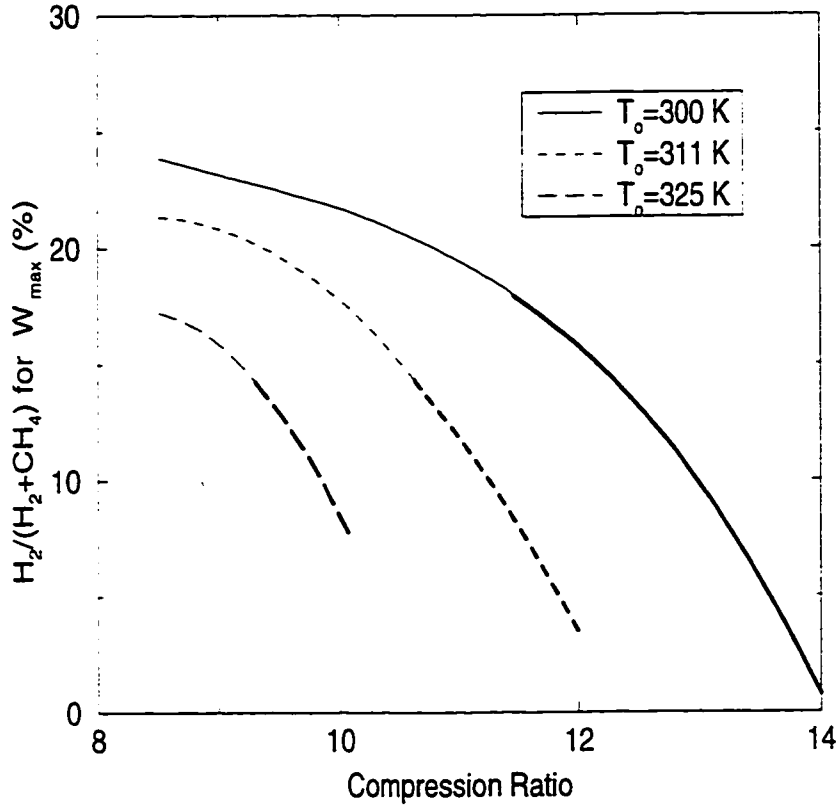

Figure 5.21: Variation of the volumetric H_2 concentration in methane-hydrogen mixtures with compression ratio for maximum indicated power at 900 RPM, $\phi = 0.9$, $\theta_{st} = 17°$ BTDC, $P_o = 87$ kPa and different intake temperatures.

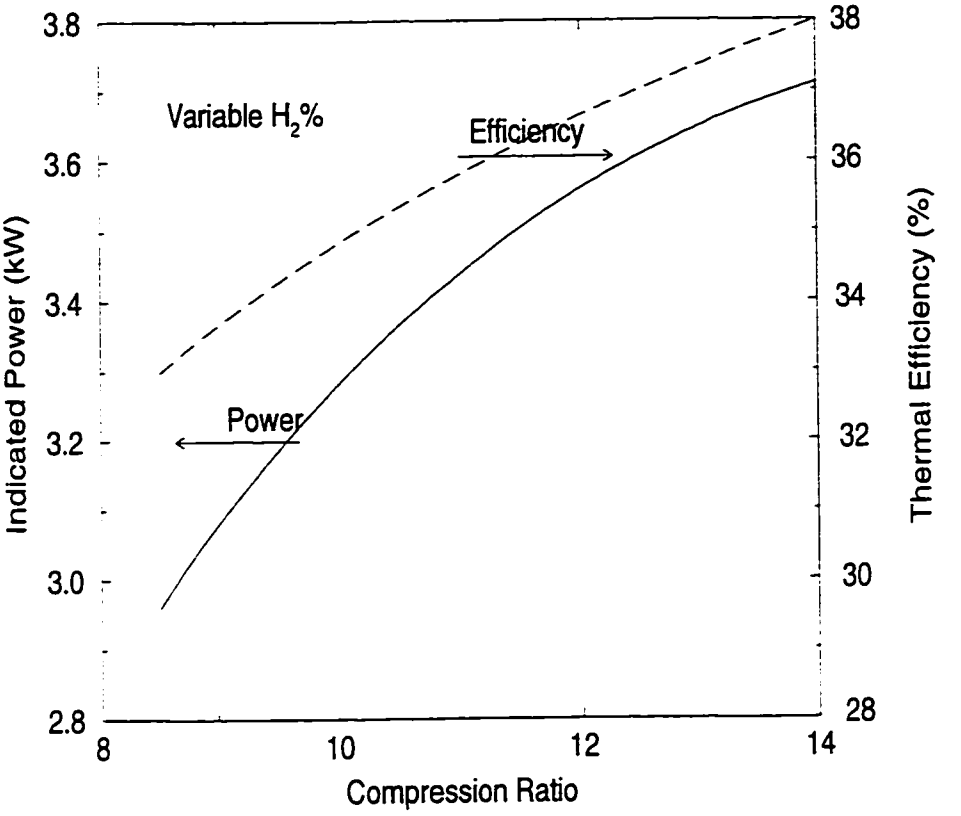

Figure 5.22: Variation of the maximum indicated power and the associated thermal efficiency with compression ratio for different intake temperatures at 900 RPM, $\phi = 0.9$, $\theta_{st} = 17°$ BTDC, $T_o = 300$ K, $P_o = 87$ kPa. H_2 concentration set either at borderline knock or at a value to produce maximum power.

5.4 Minimum Spark Advance Timing for Best Power

The modeling procedure can be used in principle also to establish the minimum spark advance timing for best knock free power output (MBT) for any set of operating conditions instead of resorting to lengthy testing procedures. MBT timing is a function of the operational variables such as equivalence ratio, fuel composition, etc. [31], and engine design parameters such as compression ratio, combustion chamber shape, bore, type, number and location of spark plugs, etc. The timing is varied as a function of compression ratio also in the ASTM standard for octane rating of liquid fuels [122]. This is mainly because the values of the flame speed (and hence combustion duration) and heating values of different liquid fuels tend to be broadly similar and also the fact that knock in engines is associated with full load operation with essentially stoichiometric mixtures. In the case when using blends of methane and hydrogen as a fuel, assuming that the timing is only a function of compression ratio is quite unrealistic due to a substantial decrease in the combustion duration as a result of the faster burning with the addition of hydrogen to methane. For simplicity, based on the preset range of variations in the different operational variables, the MBT may be assumed to be mainly a function of compression ratio and the hydrogen concentration in a blend of hydrogen-methane at the following reference operating condition:

$$900 \text{ RPM}, \phi = 0.9, \ T_o = 300 \text{ K and } P_o = 87 \text{ kPa}$$

The variation of the calculated knock free MBT timing with volumetric hydrogen concentration in the mixture of hydrogen-methane for different compression ratios is plotted in Figure 5.23. Experimental points are shown for compression ratios 8.5:1

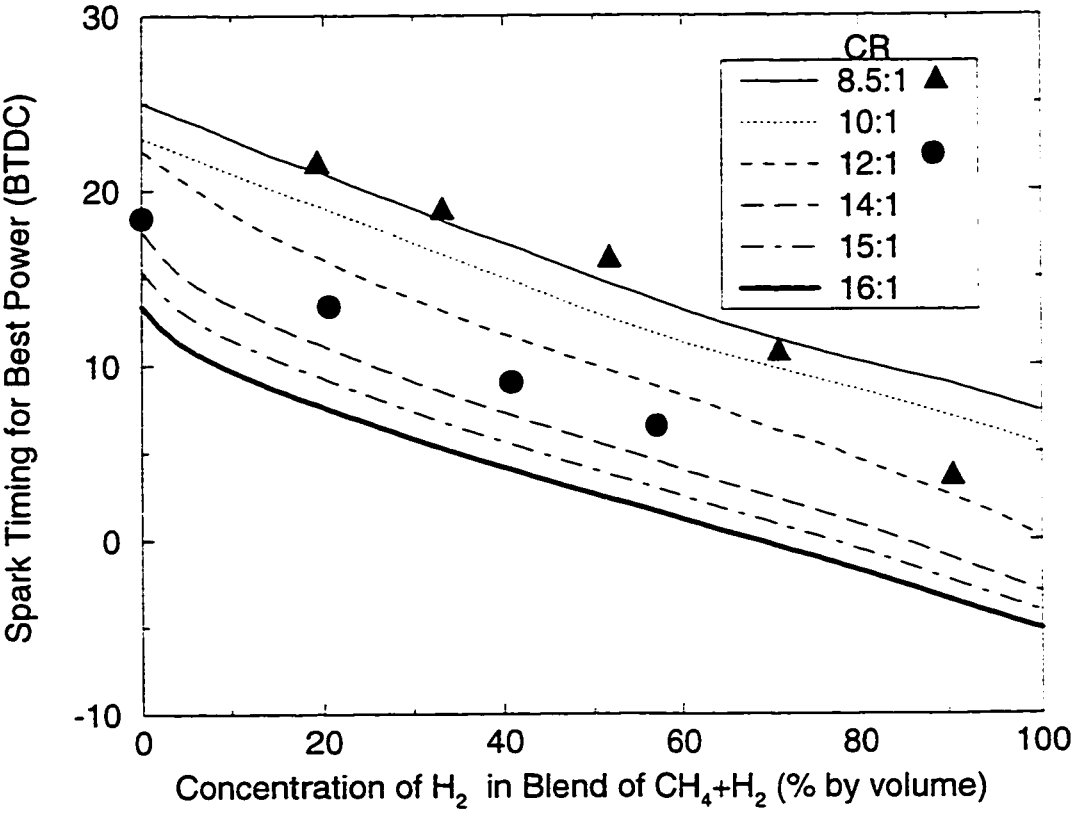

Figure 5.23: Variation of the knock free MBT timing for different compression ratios and hydrogen concentration in blends of methane and hydrogen at 900 RPM, $\phi = 0.9$, $P_o = 87$ kPa, $T_o = 300$ K. Experimental data are shown.

and 12:1 by triangles and circles, respectively. Good agreement can be seen between the model values and the corresponding experimental values. It can be seen that the MBT decreases almost linearly with the increase in the hydrogen concentration in the fuel for the set of typical operating conditions and the range of compression ratios considered. The corresponding variations in the indicated power for these MBT timings with hydrogen concentrations, which are shown in Figure 5.24, are higher than those of Figure 5.18 due to the use of MBT timing. It can be seen that

for these operating conditions, the employment of MBT timing, makes the maximum power output at each compression ratio occurs with pure methane operation, while increasing the hydrogen concentration decreases power output. It is also to be noted

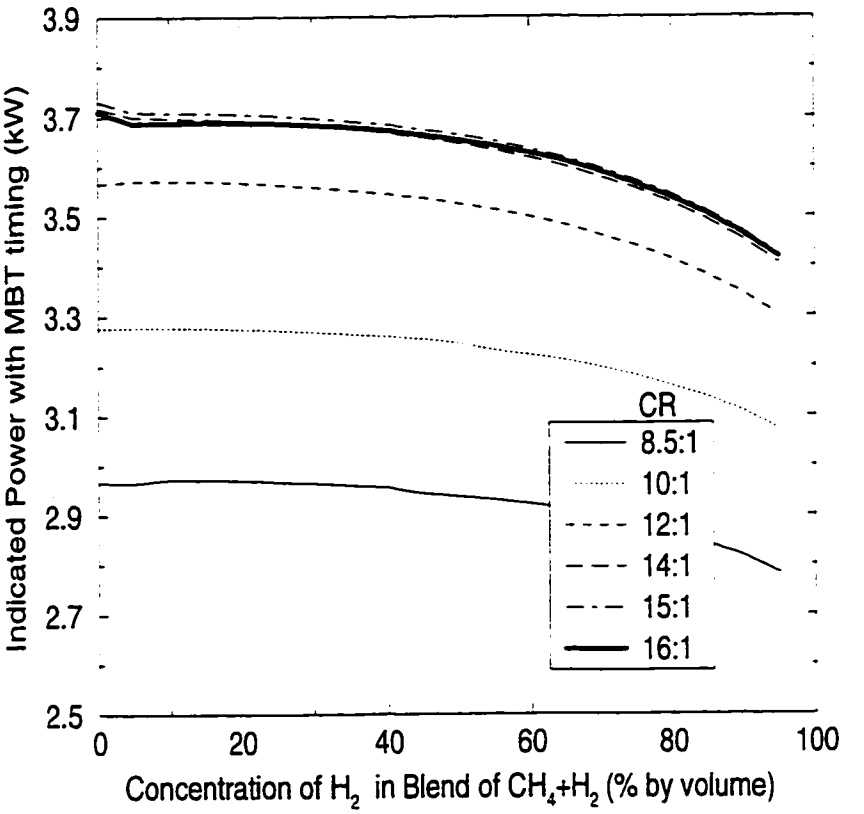

Figure 5.24: Variation of indicated power output at MBT timing for different compression ratios and hydrogen concentration in blends of methane and hydrogen at 900 RPM, $\phi = 0.9$, $P_o = 87$ kPa, $T_o = 300$ K.

that a compression ratio of 15:1 can produce more power than that of 16:1. This is mainly due to the relative increase in heat transfer and the employment of somewhat a retarded spark timing for the higher compression ratio to avoid the onset of knock.

The corresponding variation of the thermal efficiency is shown in Figure 5.25. It

can be seen that the thermal efficiency using MBT timing increases with compression ratio, but tends to decrease with the addition of hydrogen to methane because of less advanced spark timing, causing a delay in the location of peak pressure in the engine cycle.

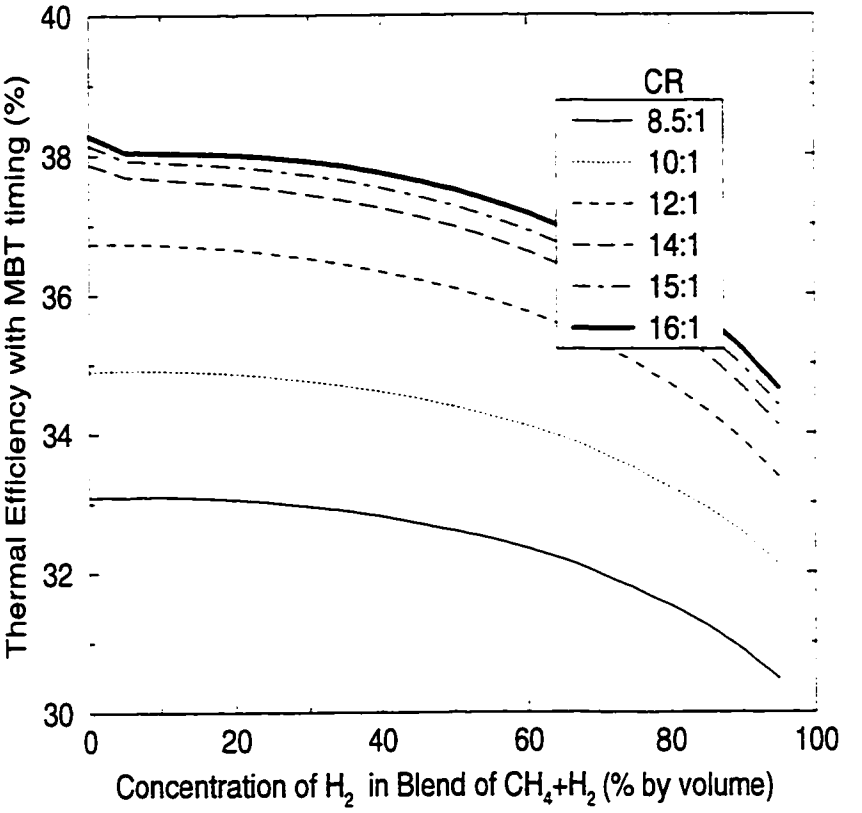

Figure 5.25: Variation of thermal efficiency at MBT timing for different compression ratios and hydrogen concentration in blends of methane and hydrogen at 900 RPM, $\phi = 0.9$, $P_o = 87$ kPa, $T_o = 300$ K.

The time for auto-ignition of the end-gas for MBT spark timing as a fraction of the corresponding combustion period is plotted in Figure 5.26 and the corresponding values of the knock criterion is shown in Figure 5.27. The intensity of knock depends

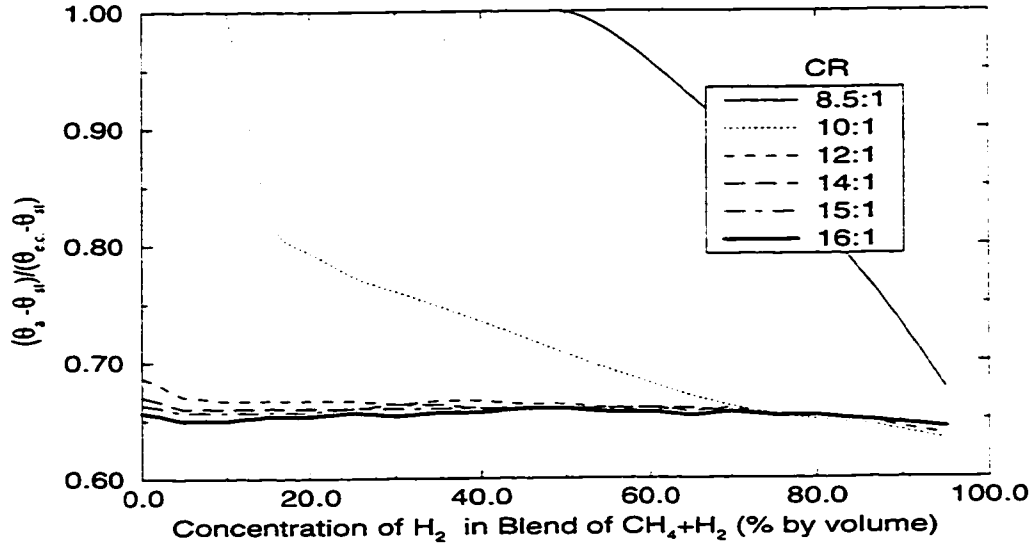

Figure 5.26: Auto-ignition time fraction at MBT timing with hydrogen concentration in blends of methane and hydrogen for different compression ratios and at 900 RPM, $\phi = 0.9$, $P_o = 87$ kPa, $T_o = 300$ K.

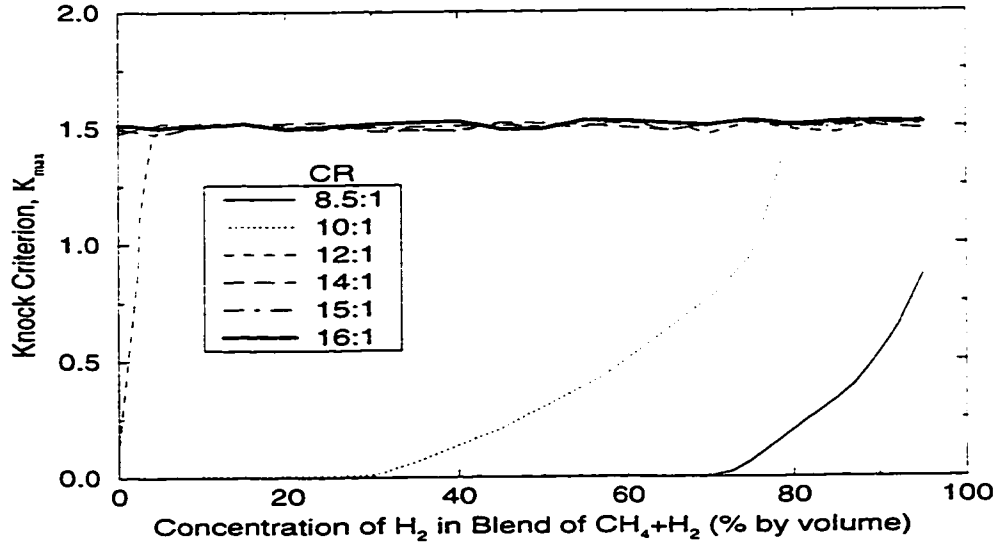

Figure 5.27: The variation of knock criterion with hydrogen concentration in blends of methane and hydrogen for different compression ratios and MBT timing at 900 RPM, $\phi = 0.9$, $P_o = 87$ kPa, $T_o = 300$ K.

on the total energy released due to the end-gas autoignition and therefore it is related to the amount of unburned zone mass at the time of end-gas self ignition. These figures show that, for compression ratios 8.5:1 and 10:1, end-gas autoignition may occur but since it is at the end of combustion duration, the amount of energy released is insufficient to produce detectable knock and the value of the knock criterion is less than 1.5. Auto-ignition of the end-gas at the borderline knock (associated with $K_{\max} = 1.5$) tends to occur later on during flame propagation (somewhere between 0.6 to 0.7 of the combustion duration).

5.5 Conclusions and Summary

The effects of changes in operational variables on engine performance tend not to be straight forward. Some parameters have significant influence on engine performance, while others may improve the engine performance at a specific condition, but undermine it at another set of conditions. The model has been shown capable of predicting engine performance for different operating conditions such as intake temperature and spark timing, as well as the effects of changes in some design parameters such as compression ratio. Hence, it reduces the time and effort for the design, modification and testing of engines. It also enables a better understanding of the influence of the different parameters on engine performance and knock intensity. The following general trends, well established in the literature, can be pointed out by the application of the model to a relatively limited typical cases:

1. Increasing the compression ratio increases power output, efficiency and the tendency to knock and its intensity.

2. Increasing the equivalence ratio up to a stoichiometric value increases power output and the tendency to knock. Maximum thermal efficiency is achieved with leaner mixtures of equivalence ratio between 0.7 and 0.8.

3. Increasing the intake temperature decreases the power output, but increases the thermal efficiency and the tendency to knock.

4. Advancing the spark timing up to a point increases power output, efficiency and the tendency to knock and its intensity. An optimum spark timing for maximum power (MBT) may be found for any operating condition.

5. MBT spark timing is approximately linearly correlated with the volumetric concentration of hydrogen in methane-hydrogen mixtures for compression ratios considered.

6. An optimum compression ratio may be found to produce maximum power.

7. For each compression ratio when employing MBT timing, over a normal range of engine operating conditions, maximum power corresponds to pure methane for methane-hydrogen fuel mixtures.

8. At a fixed spark timing, the addition of hydrogen to methane may increase power output up to a certain value of hydrogen in the blend of hydrogen and methane.

9. The thermal efficiency at high compression ratio and MBT timing decreases with hydrogen addition to methane.

Chapter 6

Borderline Knock Operation

6.1 Introduction

The recent interest in the application of natural gas as an alternative fuel for internal combustion engines focuses attention on the high-compression ratio piston engine as a means for the efficient utilization of gaseous fuels for power production. The power output of these engines is severely limited by the onset of knock. Knock, which is defined as the abnormal rapid combustion of the end-gas before the arrival of the turbulent flame front, can impose a serious limit to the overall performance of a spark ignition engine. There is a need to provide effective guidelines for predicting the highest limit for acceptable performance output for any spark ignition engine just before the onset of knock when operating on gaseous fuels. Investigating the effects of the different operational variables on the performance of a spark ignition engine at the borderline of knock will help engine designers, developers and operators to provide a more suitable set of operating conditions for optimum yields from the engine.

This chapter provides some information about engine operation close to the borderline of knock. A simple procedure will be described to select a suitable set of operating conditions for a knocking engine to get it out of knock without degrading engine performance unnecessarily.

6.2 The Effects of Engine Controlling Parameters on the Performance at Borderline Knock

The literature indicates that generally, for gasoline operated engines, the highest tendency to knock and hence the octane number requirement peaks at around 5% rich of the stoichiometric [129, 130, 131]. A similar trend could be observed for a methane fueled engine from the results of Chapter 5.

Figure 6.1 shows how the calculated critical equivalence ratio (ϕ_{cr}) for borderline knock varies with compression ratio for a constant spark timing of 17° BTDC and three intake temperatures for the CFR engine. The squares show the limit for bor-

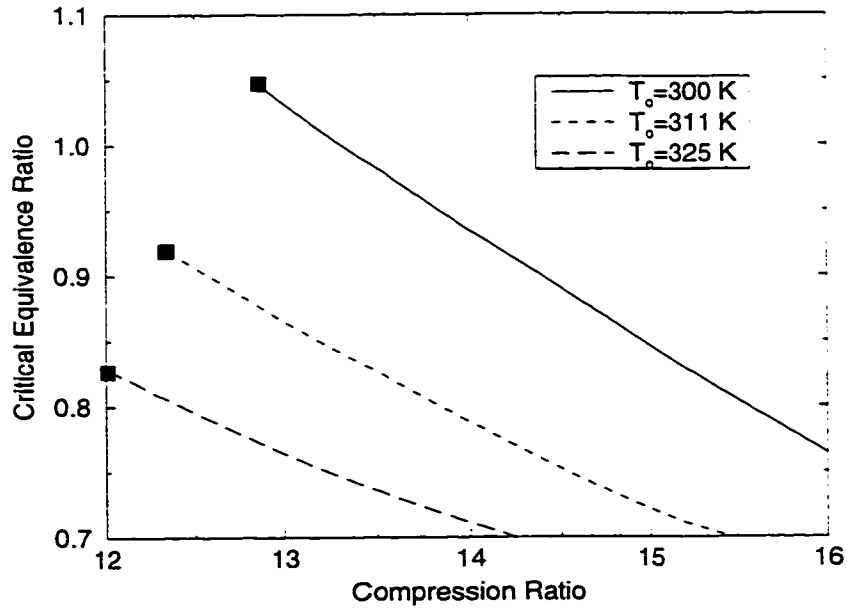

Figure 6.1: Variation of the critical equivalence ratio with compression ratio at borderline knock for different intake temperatures with methane at $\theta_{st} = 17°$ BTDC, 900 RPM, $P_o = 87$ kPa. The squares show the limit for borderline knock operation.

derline knock operation. Increasing the compression ratio and intake temperature

decreases the critical value for the equivalence ratio. ϕ_{cr} changes almost linearly with compression ratio. As a reference for comparison between the influence of different operational parameters at knock limit operation, the case of $T_o = 311$ K will be considered. A drop of 0.1 in the equivalence ratio (almost 11%) is needed for a unit increase in the compression ratio to maintain borderline knocking state.

The changes in the partial derivative of the knock criterion with respect to equivalence ratio, $(\frac{\partial K}{\partial \phi})_{cr}$, at borderline knock is plotted in Figure 6.2. The equivalence ratio is varied as in Figure 6.1. $(\frac{\partial K}{\partial \phi})_{cr}$ increases with increasing compression ratio

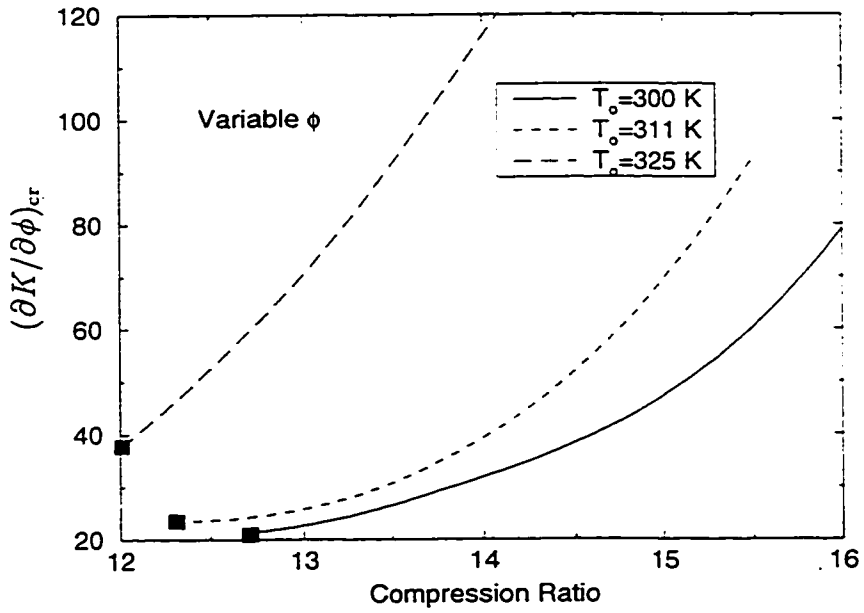

Figure 6.2: Variation of $(\partial K/\partial \phi)_{cr}$ with compression ratio for different intake temperatures with methane operation at 900 RPM, $\theta_{st} = 17°$ BTDC, $P_o = 87$ kPa. The squares show the limit for borderline knock operation.

and temperature, indicating that changing the equivalence ratio has a greater influence on the tendency to knock at high compression ratios and temperatures, as expected, due to the associated higher gas pressure and temperature.

Spark timing has a very strong influence on knock. Advancing the spark timing produces a higher cylinder pressure and temperature which occur closer to top dead center. The increased temperature of the unburned zone increases the tendency for autoignition and knock. The spark timing for maximum power at borderline knock with methane operation at 900 RPM and $\phi = 0.9$ is shown in Figure 6.3. It shows

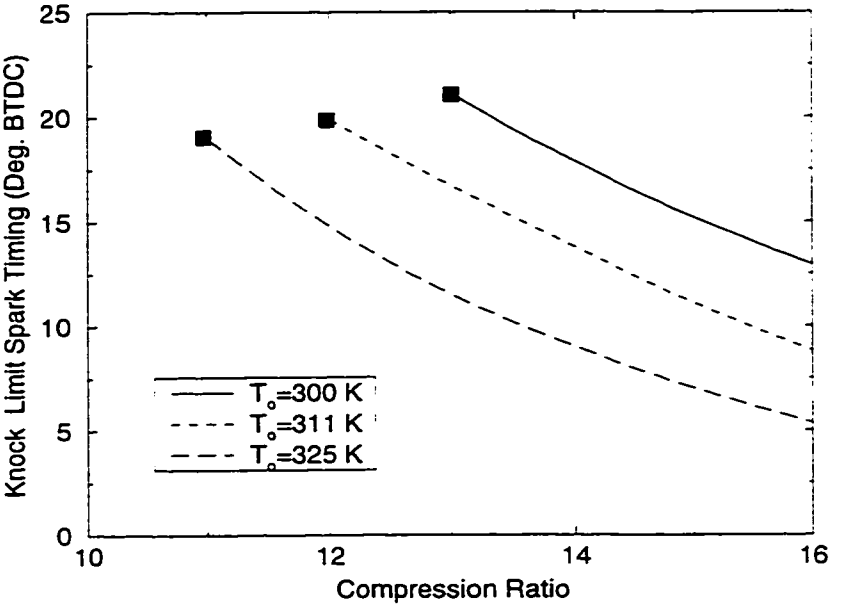

Figure 6.3: Variation of the knock limit spark timing for maximum power with compression ratio with methane operation at 900 RPM, $\phi = 0.9$, $P_o = 87$ kPa. The squares show the limit for borderline knock operation.

almost a linear variations of the spark timing with compression ratio for any intake temperature with higher intake temperatures tolerating less advance. Increasing one unit in compression ratio requires retarding the spark timing by 2 to 5 degrees of crank angle depending on the intake temperature, e.g. increasing the compression ratio from 13:1 to 14:1 at $T_o = 311$ K, requires retarding spark timing by 3 degrees.

Figure 6.4 shows the changes in the partial derivative of knock criterion with

respect to spark timing with changes in compression ratio at the knock limit. The spark timing is chosen from the results of Figure 6.3. The increased sensitivity of the knock intensity to the variations of the spark timing at high compression ratio and high intake temperatures can be seen.

The type of fuel being used has a well known profound effect on the knocking tendency of any engine. The behavior of an equivalent blend of methane and hydrogen under specified operating conditions has been used as a criterion for describing the effective knock rating of a gaseous fuel in a manner similar to that employed for the knock rating of liquid fuels through the octane number [13]. The percentage of methane by volume in the equivalent mixture of methane and hydrogen is described as the Methane Number (MN) of the test fuel.

The variation of the knock limited hydrogen concentration by volume in the mixture of methane-hydrogen with compression ratio is shown in Figure 6.5. Increasing the compression ratio and/or the intake temperature decreases significantly the maximum allowable hydrogen concentration in the mixture. At T_o=311 K, changing the compression ratio from 10:1 to 11:1 reduces the maximum hydrogen concentration from 33% down to 18%, indicating a 45 percent decrease in the hydrogen concentration for a unit increase in compression ratio. Comparing these curves with those of Figure 5.21 indicates that, for low compression ratios, the onset of knock occurs at higher hydrogen concentrations than those producing maximum power; but for high compression ratios, the hydrogen concentration for maximum power is that associated with the knock limited operation.

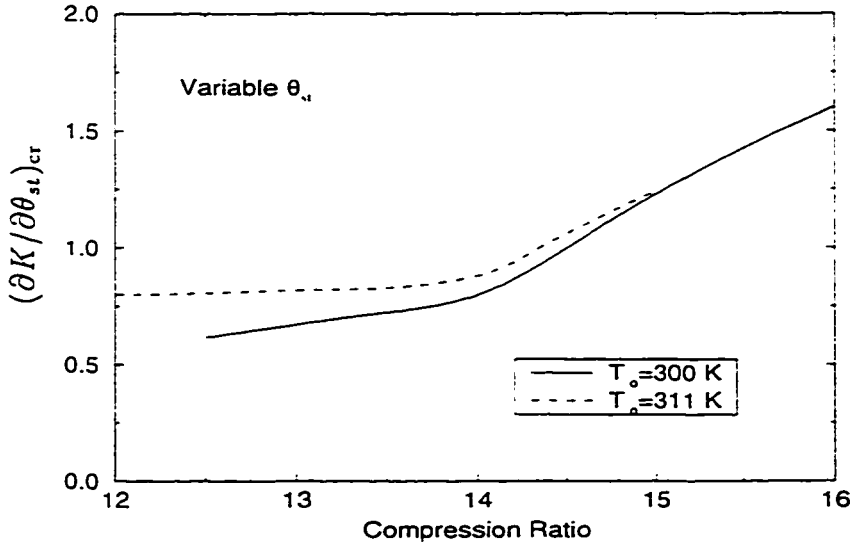

Figure 6.4: Variation of $(\partial K/\partial\theta_{st})_{cr}$ with compression ratio with different intake temperatures for methane operation at 900 RPM, $\phi = 0.9$, $P_o = 87$ kPa.

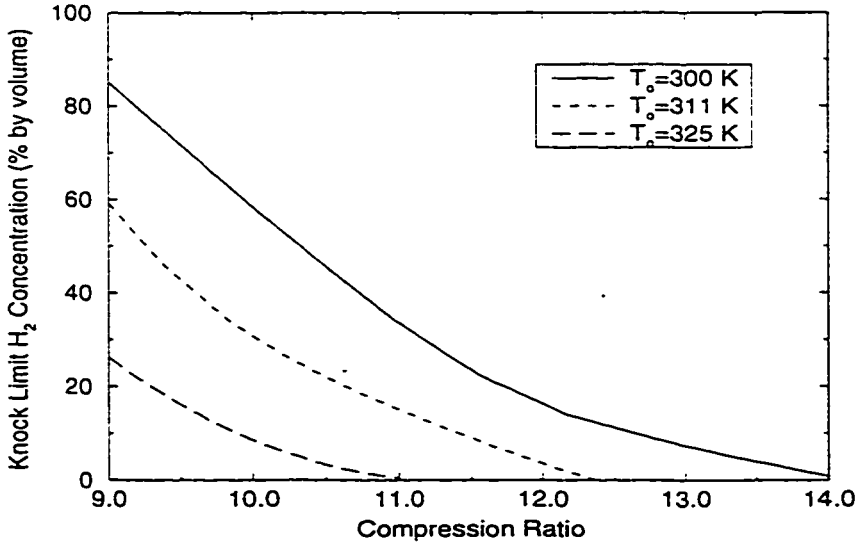

Figure 6.5: Variation of the knock limit H_2 concentration in methane-hydrogen mixtures with compression ratio for different intake temperatures at 900 RPM, $\phi = 0.9$, $\theta_{st} = 17°$ BTDC, $P_o = 87$ kPa.

Figure 6.6 shows the corresponding variations of the partial derivative of the knock criterion K_{max} with respect to the volumetric hydrogen concentration in the blend of methane-hydrogen at the knock limit ($K_{max} = 1.5$) with varying compression ratio. It indicates that the engine, when operating at high compression ratios, cannot

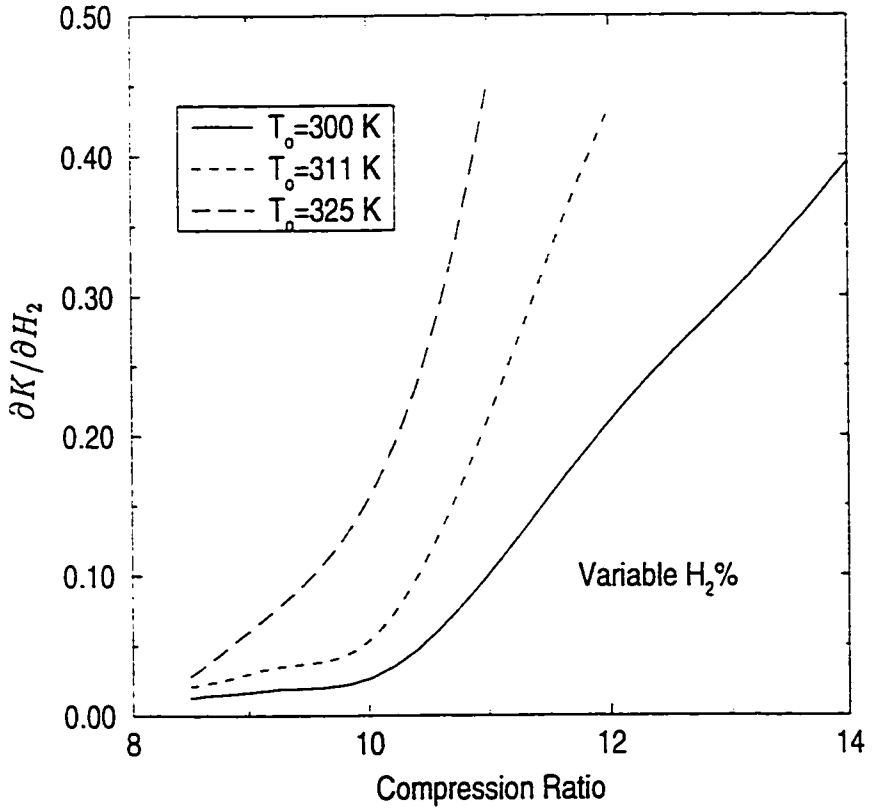

Figure 6.6: Variation of the partial derivative of knock criterion with respect to H_2 concentration in methane-hydrogen mixtures with compression ratio for different intake temperatures at 900 RPM, $\phi = 0.9$, $\theta_{st} = 17°$ BTDC, $P_o = 87$ kPa.

tolerate well the presence of hydrogen in the methane. As confirmed experimentally, at low compression ratios it tolerates it better. Also, at any compression ratio, higher intake temperatures increase this intolerance to hydrogen addition.

The temperature history of the end-gas, as explained earlier, has a strong effect on the incidence of knock due to its exponential relationship to autoignition. The value of the intake temperature which represents the initial condition of the end-gas has a magnifying effect on the temperature-time history. At a compression ratio of 10:1 in Figure 6.5, changing the intake temperature from 300 to 311 K, decreases the knock limited hydrogen concentration from 63% to 33%, emphasizing a drop of 30% in the hydrogen concentration for an eleven degrees increase of the intake temperature, which corresponds for this typical case, to having the same effect as increasing the compression ratio by a unit. Figure 5.16 showed also a linear relationship between the critical intake temperature and compression ratio for borderline knock for methane operation. This also confirms an 11 degrees reduction in the critical intake temperature for a unit increase in compression ratio.

To summarize the results, for the above set of operating conditions, reducing equivalence ratio by around 0.1 has a similar effect on the critical compression ratio at borderline knock as retarding the spark timing by 3 degrees of crank angle or decreasing the hydrogen volumetric concentration in the fuel by 15% or reducing the intake temperature at a compression ratio 10:1 by 11 K. On the other hand, in terms of the methane number, increasing the compression ratio by a unit or any of these mentioned changes in the operational variables requires an increase in the methane number of the fuel by 15 units.

6.3 A Simple Approach for Choosing a Set of Operating Conditions for a SI Engine to Get it Out of Knock

To get an engine out of a knocking state, changes in the operating conditions should be chosen in the direction of the negative gradient of K_{max}. It can be confirmed mathematically that the negative gradient of K_{max} represents a direction of the maximum rate of decreasing K_{max} [87], which is necessary for eliminating knock with a minimum reduction in power output. Consequently, the following equation is applied to choose the necessary changes in operating conditions when the engine is knocking to get out of such a condition:

$$K_{max} - K_{cr} \leq \sum_{i=1}^{n} -\frac{\partial K_{max}}{\partial x_i} \Delta x_i \tag{6.1}$$

where K_{max} is the value of the knock criterion under the initial knocking conditions, K_{cr} is the value of the criterion at the onset of mild knock (assumed on the basis of experiments when using a CFR engine to be ≈ 1.50) and x_i is the value of the operating variable to be adjusted. Obviously, there are a large number of possible scenarios that can be followed in adjusting the values of operating parameters to get the engine out of knock. However, Equation 6.1 can be employed analytically in the selection of the optimum changes without degrading significantly power output (W) nor efficiency (η). Meanwhile, the partial derivative of indicated power and thermal efficiency must be considered to make sure that the engine performance is not degraded unnecessarily.

The partial derivative of the knock criterion, power output and thermal efficiency with respect to the operational variables for some typical cases from knock free up to severe knocking operation were calculated and are shown in Table 6.1.

Table 6.1: The gradient of different operational parameters on engine performance.

Number	x_i		W (kW)	η (%)	K_{max}	$\frac{\partial W}{\partial x_i}$ (kW/x_i)	$\frac{\partial \eta}{\partial x_i}$ (% /x_i)	$\frac{\partial K_{max}}{\partial x_i}$ (per x_i)
1	ϕ	0.9	3.477	36.902	0.018	2.406	-9.838	0.354
	θ_{st}	10.0				0.027	0.277	0.036
	T_o	311.15				-0.010	0.004	0.524
	CR	15.0				0.032	0.557	0.059
	$H_2\%$	0.0				0.769	7.568	73.357
2	ϕ	0.9	3.382	36.021	0.805	2.048	-11.578	9.505
	θ_{st}	10.0				0.013	0.128	0.827
	T_o	311.15				-0.011	-0.008	0.226
	CR	12.0				0.109	0.783	2.316
	$H_2\%$	25.0				0.148	1.034	17.224
3	ϕ	0.9	3.109	34.126	0.841	1.679	-11.854	4.471
	θ_{st}	10.0				0.005	0.045	0.293
	T_o	311.15				-0.011	-0.014	0.116
	CR	10.0				0.166	1.028	1.039
	$H_2\%$	50.0				-0.128	-2.044	6.163
4	ϕ	0.90	3.420	36.479	1.021	2.073	-12.454	8.294
	θ_{st}	19.00				0.006	0.054	0.600
	T_o	311.15				-0.012	-0.011	0.189
	CR	12.0				0.109	0.790	2.308
	$H_2\%$	0.0				0.181	1.426	36.982
5	ϕ	0.9	3.529	37.434	2.482	2.373	-10.666	13.333
	θ_{st}	12.0				0.023	0.230	1.512
	T_o	311.15				-0.011	0.000	0.419
	CR	15.0				0.031	0.562	4.597
	$H_2\%$	0.0				0.635	6.148	67.370

Operating condition number (1) indicates a knock free operation far from borderline knock. Numbers (2), (3) and (4) are three knock free operating conditions close to the knock limit and number (5) is a knocking operation. The influence of a unit change in the different operational variables (e.g. spark timing, compression ratio and equivalence ratio) on engine performance, as expected, is different and varies depending on engine operating conditions. As was explained earlier, increasing the hydrogen volumetric concentration in the blend of methane-hydrogen increases the power output up to a specific amount of hydrogen in the mixture, usually between 40 to 50 percent, then a further addition of hydrogen may result in deteriorating engine performance (e.g. number (3) in Table 6.1 which has a negative value for $\partial W/\partial H_2\%$). As can be seen, the influence of equivalence ratio on the power output is strong and relatively small changes would affect the power output significantly. Hence, it would be desirable to keep the equivalence ratio fixed for maximum power and try to get out of knock, if the engine was knocking, by changing the other operating variables, to avoid a substantial drop in power. In contrast, the equivalence ratio has less influence on the thermal efficiency near maximum efficiency operation (see Figure 5.2). Also, changes in the hydrogen concentration in the fuel may change the thermal efficiency significantly as explained earlier due to the effect on combustion duration.

In order to compare the influence of the different operational parameters on the engine performance, a unique assessment procedure was needed. The value of the knock criterion $K_{\mathbf{max}}$ was used for this purpose. It is unsuitable to compare the influence of each operational variable on the performance by comparing the partial derivative of indicated power, efficiency and knock criterion with respect to the op-

Table 6.2: The influence of changing different operational parameters for one unit increase in K_{max} at knock limit, on engine performance for Example (4) in Table 6.1.

x_i	$\frac{\partial x_i}{\partial K_{max}}$	ΔW (kW)	$\Delta\eta$ (%)	$\frac{\Delta W}{W}$ (%)	$\frac{\Delta\eta}{\eta}$ (%)
ϕ	0.121	0.250	-1.502	7.3	-4.1
θ_{st}(Deg. BTDC)	1.667	0.010	0.090	0.29	0.25
T_o (K)	5.291	-0.063	-0.058	-1.84	-0.16
CR	0.433	0.047	0.342	1.37	0.94
H_2% (by volume)	0.027	0.005	0.039	0.14	0.11

erational variables because of the significant changes in the power output, efficiency and knock criterion due to a unit change in some of the operational variables such as equivalence ratio. The evaluation was based on how much each operational parameter needs to be changed to produce a unit increase in the value of the knock criterion and how these changes can affect power output and thermal efficiency. The results are presented in Table 6.2 for the condition of number (4) in Table 6.1. Increasing the equivalence ratio by 0.121 can increase the value of K_{max} as much as advancing the spark timing by 1.667°, or increasing the intake temperature by 5.29 K, or the compression ratio by 0.433 or the hydrogen concentration by 0.027. This illustrates how some operational variables are more influential in changing the engine performance and knock intensity than others. At a lean Fuel/Air ratio such as in this example, any change in the operating parameters, except that of the intake temperature, to produce higher power would increase the tendency to knock and its intensity. In contrast, for a naturally aspirated engine, decreasing T_o increases the power output and decreases the knock intensity. Hence, the lowering of intake temperature is probably one of the best and most effective factors that can help

to reduce the tendency to knock while increasing power output. The intake temperature however normally cannot be changed easily, promptly and independently of other engine variables and cannot be used for transient operation, e.g. for a knocking engine during acceleration. Note that if a mixture is too lean, decreasing the intake temperature can reduce the power output due to the long resulting combustion periods. Hence, its practical use to control the incidence of knock needs to be considered carefully, especially when turbo-charged operation is considered. Equivalence ratio has a significant effect on power output, with a lesser effectiveness in changing the knock criterion value. Therefore, it is less effective to change the equivalence ratio to get the engine out of knock. Consequently, it is suggested to keep the equivalence ratio at an optimum acceptable value, e.g. stoichiometric, and try to get the engine out of knock by changing some of the other operating parameters. Spark timing is normally the most convenient way, up to a point, to take an engine out of a knocking state and can be used over a wide range of engine operations, transient or steady. Changing any of these parameters to improve the engine performance somewhat increases $K_{\mathbf{max}}$. Hence, their applicability for knock control is also limited and must be applied cautiously.

From the above discussion, the operational variables may be ranked as follows in the order of their suitability for getting an engine out of knock in relation to retaining

high values of indicated power output and thermal efficiency:

Operational Variable	Power Output	Thermal Efficiency
ΔT_o	1	2
$H_2\%$	2	3
θ_{st}	3	4
CR	4	5
ϕ	5	1

These results demonstrate that to get an engine out of knock while producing maximum power, the best operational parameter to be adjusted is the intake temperature and the worst is equivalence ratio. For maximum knock free efficiency, the best parameter for adjustment is the equivalence ratio and the worst is the compression ratio.

Now consider the operating condition number (5) in Table 6.1, which is a knocking condition. To modify operating conditions for a knock free operation, using Equation 6.1, the following procedure must be carried out. The initial condition is pure methane operation at 900 RPM, $\phi = 0.9$, $\theta_{st} = 12°$ BTDC, $CR = 15.0 : 1$ and T_o=311.15 K with intake pressure of 87 kPa. The negative partial derivative of $K_{\max}$ indicates that some hydrogen must be taken out of the fuel to get out of knock. Since the initial conditions chosen in this case involve pure methane operation, this point has been satisfied to its limit and the hydrogen concentration has already been taken out from the set of controlling operational variables. Because of the strong influence of equivalence ratio on power output, it is kept constant at 0.9. Since decreasing T_o increases power output and decreases knock intensity, making all the necessary reduction in $K_{\max}$ through reducing intake temperature is desirable. Hence, the in-

take temperature should be kept constant at the minimum acceptable value. In this example, it is assumed that the intake temperature is mainly dependent on the ambient condition and cannot be changed. Therefore, the modified negative gradient vector of the knock criterion $K_{\max}$ may be written as:

$$\vec{S} = -\nabla K_{\max} = -1.512\vec{e_{\theta_{st}}} - 4.597\vec{e_{CR}} \tag{6.2}$$

where $\vec{e_{\theta_{st}}}$ and $\vec{e_{CR}}$ are the unit vectors in the direction of spark timing and compression ratio, respectively. $\vec{S}$ has the maximum rate for decreasing the value of knock criterion [87]. Consequently, to have a knock free operation, the following equation must be satisfied.

$$K_{\max} - K_{cr} = 2.482 - 1.5 = \lambda \|\vec{S}\| \tag{6.3}$$

where λ is a scalar multiplier and $\|\vec{S}\|$ is the norm of vector $\vec{S}$ with values equal to 0.203 and 4.84 for this specific example. The modified values for operational or design variables can be estimated by the following equation:

$$\vec{x_{i+1}} = \vec{x_i} + \lambda \vec{S} \tag{6.4}$$

where $\vec{x_i}$ stands for initial set of operational variables and $\vec{x_{i+1}}$ is modified operational variables. Using Equation 6.4, the modified set of operating conditions is estimated as $\phi = 0.9$, $\theta_{st} = 11.69°$ BTDC, $T_o = 311.15$ K, $CR = 14.07 : 1$ and $H_2\%$=0.0 which corresponds to $K_{\max} = 0.01$, $W = 3.48$ kW and $\eta = 36.8\%$. Due to the sensitivity of the knock criterion at borderline knock to changes in operational parameters, this answer is good enough for practical purposes and may be used for initial evaluation.

If Equation 6.1 is applied without considering the advantage and disadvantage of changes in the different operational variables, the performance of the engine may

be degraded unnecessarily, or would not be physically viable. Having an automated model to optimize the engine performance without a need for considering these compromises is desirable. Such automated optimization models will be introduced in Chapter 7.

6.4 Conclusions and Summary

A review of the effect of the engine operating conditions on knock limit operation was presented. The results of this study compared closely with those found in the literature even though the engine and/or operating conditions were quite different in certain cases. The following may be pointed out as a guideline on the effect of various parameters on the knock tendency of a gas fueled spark ignition:

1. Changes in the operational variables have a stronger effect on the engine knock intensity at high compression ratio and high intake temperature, as confirmed experimentally.

2. The gradient of $K_{\mathbf{max}}$ with respect to various operational variable can be used as a tool for getting a knocking engine out of knock without degrading engine performance unnecessarily.

3. Changes in variables that have strong effects on both $K_{\mathbf{max}}$ and power output should be considered carefully when trying to get out of a knocking situation. Accordingly it is recommended that the equivalence ratio may be kept constant at an acceptable value while other parameters are adjusted to get out of knock, so that the power output would not decrease significantly.

4. Based on the results, guidelines on the effect of various parameters on the apparent methane number requirement of the engine are:

Operational Variable	Gas Fueled Engine
T_o	1.36 MN/K
θ_{st}	5 MN/degree
CR	15 MN/CR
ϕ	1.5 MN/1%

Chapter 7

Optimization Algorithms for Engine Performance

7.1 Introduction

Optimization is concerned with achieving the best outcome of a given operation while satisfying certain restrictions. Human beings, guided and influenced by their natural surroundings, almost instinctively perform all functions in a manner that economizes energy or minimizes discomfort and pain. The motivation is to exploit the available limited resources in a manner that maximizes output or profit. For example, engine designers seek always to maximize power output and/or efficiency. Douglas Wilde [132] provides an account of the origin of the word optimum and the definition of an optimum design. He offers the definition of an optimum design as being "the best feasible design according to a pre-selected quantitative measure of effectiveness."

The modern internal combustion engine is expected to satisfy simultaneously a large number of performance requirements that are dependent in a very complex, and sometimes uncertain manner, on numerous design and operating variables. Accordingly, engine designers, developers and operators spend much resources, time and effort in experimentation and control to bring about a satisfactory compromise to achieve optimum operation with any fuel.

The phenomenon of knock represents a serious constraint on engine performance which imposes an operational barrier to the limits of power output and efficiency

of common engines. In the necessary efforts to avoid knock, empirical procedures based on experience and trial and error are presently followed. These often lead to engines operating under conditions that are far from those that yield optimum performance. Clearly, it would be desirable to formulate analytical procedures that would ensure the achievement of optimum performance features while maintaining throughout knock free operation.

This chapter describes two analytical approaches for optimization procedures that can be used together with the analytical model described earlier that models engine performance and can predict the onset of knock and its intensity. One of the major difficulties in most of the engineering problems is the existence of some local optimum design configurations comparable to those giving the global optimum solution. Furthermore, the capability of the instrumentation to control operational parameters in engines is discontinuous and discrete. A suitable technique for considering the discrete design space with some local optimum configurations is that described as a 'genetic' algorithm [93]. Genetic algorithms are very successful in searching for a set of operating conditions that are close to the global optimum solution, but they may have difficulty in converging to the optimum solution itself. To avoid this difficulty, the genetic algorithm can be combined with a deterministic procedure such as a Gradient-Based Algorithm. These algorithms are among the most important methods in the deterministic category, which are very successful in searching for a local optimum configuration. Therefore, they may be employed to find the best set of engine operating conditions that are close to an initial setting.

It is shown that such procedures may be employed to indicate the optimum changes to engine and operating variables for producing maximum power and/or

efficiency of a gas fueled spark ignition engine in the absence of knock.

7.2 Penalty Function and Optimization

An analytical procedure for optimization can be converted to that of a minimization approach which may be written in general as:

$$\begin{aligned} \text{Minimizing} \qquad & f(\vec{x}) \qquad && \text{such that:} \\ & \overline{g}_k(\vec{x}) = 0.0 \quad , && k = 1, ..., n_e \\ & g_j(\vec{x}) \leq 0.0 \quad , && j = 1, ..., n_g \end{aligned} \tag{7.1}$$

$\vec{x}$ denotes a set of design variables or operational parameters in case of engine control, with components x_i where $i = 1, ..., n$. $\overline{g}_k(\vec{x})$ and $g_j(\vec{x})$ are equality and inequality constraints, respectively [87].

The constraint requirements divide the domain of design and operating variables into two regions, one that is feasible where the constraints are satisfied and the other that is unfeasible where at least one of the constraints is violated. Often in most practical problems, the minimum value of the desired function occurs at the boundary between the feasible and unfeasible regions [133]. In a constrained optimization, the constraints can be replaced by *penalties* depended on the extent or degree of violations of the constraints. This approach replaces a constrained optimization problem by an unconstrained one, which makes it easier to be formulated. The penalties associated with the constraint violation have to be sufficiently high that the constraints are only slightly violated [133]. This method is sometimes referred to as the *exterior penalty function* [87, 88, 133], since penalties are applied only in

the exterior of the feasible region. The most common penalties function is one which associates a penalty to be proportional to the square of a violation, which replaces Equation 7.1 with the following equation as objective function $\Psi(\vec{x}, r)$:

$$\text{Minimize} \qquad \Psi(\vec{x}, r) = f(\vec{x}) + r \sum_{k=1}^{n_e} \overline{g}_k^2(\vec{x}) + r \sum_{j=1}^{n_g} \prec g_j \succ^2 \tag{7.2}$$

where $r = r_1, r_2, \ldots\ldots$ $r_i \rightarrow \infty$ and $\prec g \succ$ denotes $\max(g(\vec{x}), 0)$. The positive multiplier r controls the magnitude of the penalty terms. The minimization must be started with a relatively small value of r, which is gradually increased [133]. A typical plot of $\Psi(\vec{x}, r)$ as a function of r is shown in Figure 7.1 for the linear function chosen as a simple example, $f(x) = 4x + 1$ with the constraint of $x \geq 3.0$. It can be

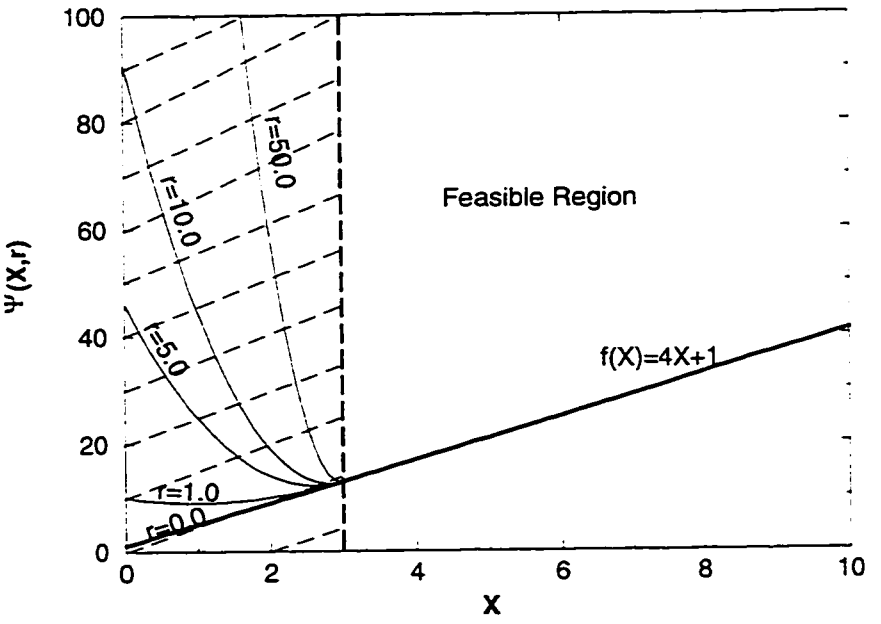

Figure 7.1: Exterior penalty function for $f(x) = 4x + 1$ subject to $x \geq 3.0$.

seen that as r is increased, the minimum of $\Psi(\vec{x}, r)$ moves closer to the constraint

boundary. The curvature of Ψ near the minimum also increases. The high values of the curvature associated with large values of r may lead to numerical difficulties, particularly for gradient-based algorithms. By using a sequence of increasing values of r, the minimum value of the objective function, Ψ, obtained for small values of r is used as starting point for the search to evaluate the minimum with higher r values which can help in eliminating the associated numerical problems [87, 88, 133, 134]. Also, by this gradual increase of the penalty multiplier r, initially, the constraints are not penalized severely to permit the algorithm perform a more efficient overall search to find the global optimum solution [103].

7.3 Genetic Algorithm

Genetic algorithms [93, 135] which are among the most promising optimization techniques are based on the principle of selecting the most appropriate optimum values. They work with a population of *individuals*, each representing a possible solution to a given problem. Each such individual is assigned a fitness score according to how well it solves the given problem. To translate a problem into a suitable form, a potential solution should be represented as a set of operational and design parameters (for instance in a spark ignition engine application: compression ratio, equivalence ratio, spark timing, etc.). These parameters are then linked in a binary string of values:

$$(\phi, CR, \theta_{st}) = (1, 8, 15) \rightarrow \underline{0001} \quad \underline{1000} \quad \underline{1111}$$

The algorithm is composed of an evaluation procedure, an initializing step and three operators. These operators work on a population pool of individuals which is

made up of a number of binary strings of sets of engine operational variables.

Evaluation

The first step in every iteration is to determine how well each set of operational variables can solve the problem. An external penalty function, as of that explained in Section 7.2, consisting of the engine performance and violation of the constraints is used to formulate the constrained optimization problems [87] called the objective function.

Initiation

In the initiation step, an initial *population* including N sets of operating conditions in the form of binary strings is generated by random selection of the individual bits in a binary string of given length to compose families of strings. Each string represents a single set of the independent variables such as compression ratio, spark timing, equivalence ratio, etc. The appropriateness or fitness of each string is then evaluated and assessed against the objective function (Eq. 7.2), which is to be optimized. The strings in the best families are given favorable weighting in a selection process whereby pairs of strings are chosen and combined by genetic algorithm operators selection, crossover and mutation to produce a more suitable set of operational variables.

Selection

The selection is based on retaining the most successful and fittest solution. The standard procedure for maximizing the objective function is to define the probability

of a particular solution survival to be:

$$P_{sj} = F_j / \sum_{j=1}^{N} F_j \tag{7.3}$$

where F_j is the scaled fitness of solution j calculated using the following equation:

$$F_j = 1/(A + \Psi_j(\vec{x_j}, r)) \tag{7.4}$$

A is a constant defined such that F_j always gets a positive value [136].

These probability factors (P_{sj}) are calculated for any individual string and used to determine which member can exist in a new generation. For example, if the target is to maximize a function, the strings or operating conditions having higher values of P_{sj} represent better selections for the following generation. Normally, half of the population of any generation belong to the previous one and the rest are evaluated based on the crossover and mutation processes.

Crossover

In the crossover operator, some couples of strings are selected randomly and by swapping parts of the strings with each other, members of a new generation are formed. As an example, a simple one-point crossover is shown as follow:

$$01001\underline{101} \rightarrow 01001\underline{110}$$

$$01100\underline{110} \rightarrow 01100\underline{101}$$

The swapping portion is determined also randomly. Although, the members created by the crossover are different from their parents, some of their characteristics are inherited.

Mutation

To provide insurance against the irrevocable loss of information and hence to maintain diversity within the population, a mutation stage is needed. For instance, if every solution in the population has a "0" as the value of a particular bit, then no amount of crossover will produce a solution with a "1" there instead. A few strings are selected randomly and then a bit character is switched to zero or one at a location which is selected also randomly, e.g.:

$$01001101 \rightarrow 01000101$$

Obviously, although it is possible to produce improvement in fitting with such mutation which cannot be produced by crossover, it is also possible to produce a sudden deterioration. Therefore, the occurrence of this mutation should be kept at a small probability (2% in our work).

A new population of possible solutions is thus produced by selecting the best individuals from the current generation and combining them to produce an improved new set of individuals using crossover and mutation. In essence, by mixing and exchanging components of better individuals over many generations, good characteristics are spread out through the population. With the view of an optimization perspective, by randomly generating the initial population, a broad area of search space can be investigated, and then by retaining and using the more suitable individuals, the most promising area of this space may be explored and it is in this sense that the genetic algorithms may more likely come up with the global optimum, when designed well. After each cycle of selection, the fitness of each family is again assessed by evaluating the objective function. The cycle then continues into the

next generation. The process is terminated when convergence is detected or when the specified maximum number of generations is reached.

7.3.1 Controlling Parameters

An efficient genetic algorithm is considered to be that which has a fast converging rate to the optimum solution and a high possibility to find the global optimum in a pre-defined domain. The efficiency of a GA is highly dependent on the values of the algorithm control parameters. These parameters are:

- the population size N
- the crossover probability P_c
- the mutation probability P_m

De Jong [137] made some recommendations based on his observations of the performance of genetic algorithms on five optimization problems included examples with difficult characteristics such as discontinuities, high dimensionality, and noise. His work suggested that setting of:

$$(N, P_c, P_m) = (50, 0.60, 0.001)$$

would give satisfactory performance over a wide range of problems.

Grefenstette [138] went one stage further and used a genetic algorithm to optimize these parameters for a test bed of problems. He concluded that:

$$(N, P_c, P_m) = (30, 0.95, 0.01)$$

resulted in the best performance when the average fitness of each generation was used as the indicator of optimum solution, while:

$$(N, P_c, P_m) = (80, 0.45, 0.001)$$

gave rise to the best performance when the fitness of the best individual member in each population was monitored. The first one is used when it is meant to search for a generation with good performance spread all over its members, while the second one is for finding an optimum individual solution with the best performance. Of course, the later is the more usual performance measure for optimization routines.

In general, the population size should be no smaller than 20 or 30 whatever the problem being tackled and for problems of high dimensionality larger population size (of the order of hundreds) is more appropriate. Since the controlling parameters are problem dependent, it is recommended that the code developer should check and find suitable values for GA parameters based on the nature of his problem and computational facilities available to him.

In order to find a suitable set of controlling parameters for genetic algorithm to optimize the engine power output and/or efficiency with a reasonable computational time, some runs of the computer program were carried out with different operating conditions for different values of GAs controlling parameters. Figure 7.2 shows the progress in reducing the objective function of the best individual within each population and the average fitness of each generation for one of these typical examples. The difference between these two measures is indicative of the degree of convergence in the population. As explained earlier, in many applications GAs locate the neighborhood of the global optimum efficiently yet they may have problems, sometimes,

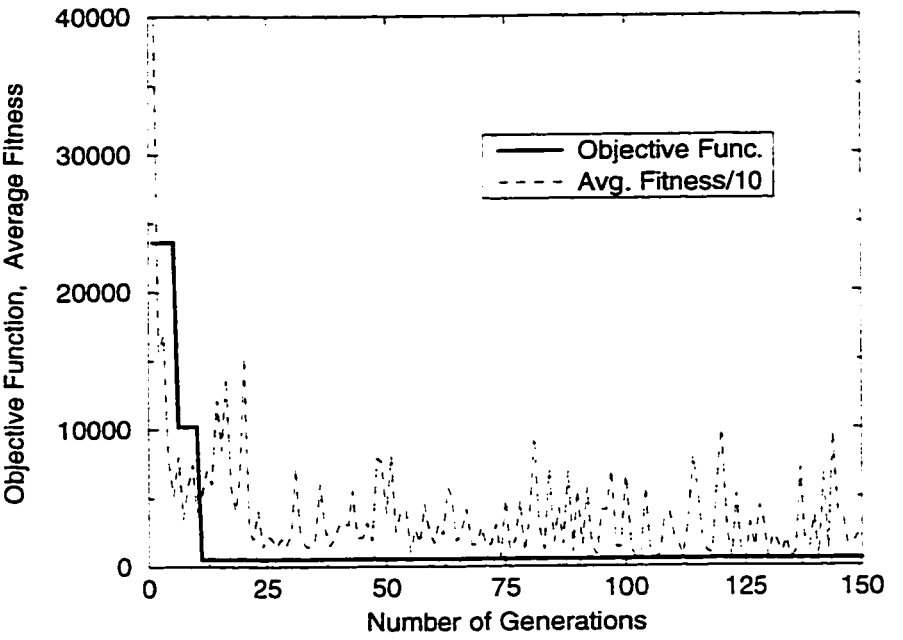

Figure 7.2: Variations of the objective function and the average fitness in each population with the number of generations.

converging onto the optimum itself.

Increasing the population size N increases the possibility of finding the global optimum solution, but with a drawback of increasing the computational time. A typical variation of the minimum objective function, for a similar optimization problem, with generation number for two different population sizes are plotted in Figure 7.3. As can be seen, changing the population size from 20 to 40 cannot make a significant improvement in the GA algorithm performance for our engine problem. The same calculations were carried out for different values of N, P_c and P_m to find suitable values for these parameters with a reasonable calculation time. At last, from the results, the following set is chosen as the controlling parameters for the application of the

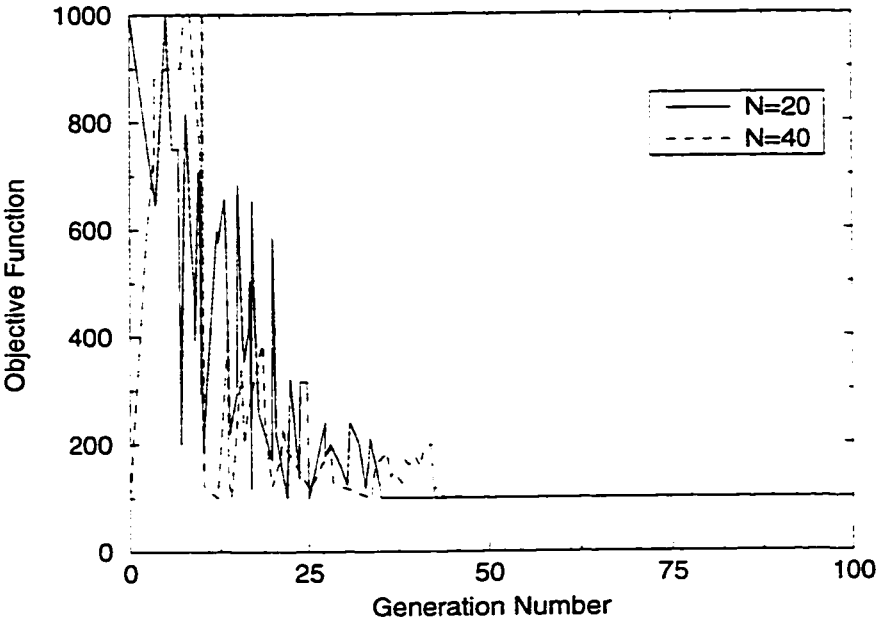

Figure 7.3: Variation of the objective function with the number of generations for two different population size.

GA algorithm to the optimization of spark ignition engine performance problems.

$$(N, P_c, P_m) = (20, 0.5, 0.02)$$

7.3.2 Formulation of the GA Procedure for Engine Application

Since there is no experimentally formulated relationship that can link all the major operating and design parameters, optimization of engine performance is only possible, if applied to an analytical model such as the one described earlier. The objective of the procedure is to search for an operating condition of maximum power or efficiency without the onset of knock. There are many factors that control the power output of a spark ignited engine. However, it can be assumed that the main variables controlling the engine power output with some hydrogen present in the fuel are

equivalence ratio ϕ, compression ratio CR, spark timing θ_{st}, intake temperature T_o and the concentration of hydrogen in the binary fuel mixture $H_2\%$. The optimization problem can be defined as minimizing the following function of optimum power output:

$$f(\vec{x}) = f(\phi, CR, \theta_{st}, T_o, H_2\%) = 1/W \tag{7.5}$$

or in relation to optimum thermal efficiency:

$$f(\vec{x}) = f(\phi, CR, \theta_{st}, T_o, H_2\%) = 1/\eta \tag{7.6}$$

where W and η are the indicated power output and thermal efficiency at any operating condition, which can be derived from the two-zone model described in Chapter 3.

The knock free operating condition brings a constraint to the optimization problem on the value of the knock criterion, assumed to have a value at the knock limit around 1.5, i.e.:

$$K_{\min} \leq K_{\max}(\phi, CR, \theta_{st}, T_o, H_2\%) \leq 1.5 \tag{7.7}$$

Since the values of these chosen variables cannot be varied in practice indiscriminately, permitted ranges for these operating variables are assigned based on experience and the specific requirements of the situation. These will represent the additional constraints to be considered.

$$\begin{aligned}
\phi_{\min} \leq \quad & \phi \quad \leq \phi_{\max} \\
CR_{\min} \leq \quad & CR \quad \leq CR_{\max} \\
\theta_{st_{\min}} \leq \quad & \theta_{st} \quad < \theta_{st_{\max}} \\
T_{o_{\min}} \leq \quad & T_o \quad \leq T_{o_{\max}} \\
H_{2_{\min}} \leq \quad & H_2\% \quad \leq H_{2_{\max}}
\end{aligned} \tag{7.8}$$

The approach described in Section 7.2 is used with the optimization problem converted to that of minimization of the unconstrained objective function shown in Eq. 7.2. Since all these operational constraints are inequality constraints, the term $\sum \overline{g}_k^2(\vec{x})$ in the equation becomes zero and the objective function is reduced to the minimization of:

$$\Psi(\vec{x}, r) = f(\vec{x}) + r \sum_{j=1}^{n_g} \prec g_j \succ^2 \tag{7.9}$$

where $\vec{x} = \vec{x}(\phi, CR, \theta_{st}, T_o, H_2\%)$ is the vector of operating condition. The penalty multiplier; $r = r_1, r_2, ..., r_i \rightarrow \infty$ and $\prec g_j \succ = \max(0, g_j)$ when $j = 1, 2, ...$

7.3.3 Results of the Application of Genetic Algorithm Only

The lower limit for $K_{\max}$ is chosen 1.3 to make sure the algorithm search for the maximum power on the verge of knock, i.e.:

$$1.3 \leq K_{\max}(\theta_{st}, \phi, H_2\%, CR) \leq 1.5 \tag{7.10}$$

The permitted range of the operation condition, for the variables chosen, were assumed to be as:

$$\begin{aligned} 0.0 \leq \quad & \theta_{st} \quad \leq 30.0 \qquad \text{(degrees BTDC)} \\ 0.6 \leq \quad & \phi \quad \leq 1.0 \\ 0.0 \leq \quad & H_2\% \quad \leq 20.0 \\ 12 \leq \quad & CR \quad \leq 17 \end{aligned} \tag{7.11}$$

The results of applying the above genetic algorithm to some typical examples involving a single cylinder spark ignited CFR engine when operating at full throttle on methane and hydrogen under ambient pressure are presented in the following.

Engine speed and intake temperature are assumed to be constant at 900 RPM and 311 K.

Example 1: In this example, the operating variables are assumed to be spark timing, equivalence ratio, compression ratio and hydrogen concentration in the fuel that can be varied within the ranges specified in Eq. 7.11. Maximum power output was predicted to be produced at $\theta_{st} = 20°$ BTDC, $\phi = 1.0$, $H_2\%$=0 and $CR = 13.4:1$, associated with $K_{\max} = 1.449$, $W = 3.69$ kW and $\eta = 42.7\%$ through the employment of this procedure, just before the onset of knock. Any further changes to these operating conditions will result either in a loss of power or a violation of the imposed constraints, in the form of an unacceptable value for $K_{\max}$, indicating an onset of knock, or an unacceptable value for the set of operating parameters. Maximum efficiency can be achieved when operating parameters are chosen such that $\theta_{st} = 23°$ BTDC, $\phi = 0.64$, $H_2\%$=18 and $CR = 13.75:1$, corresponding to calculated values of $K_{\max} = 1.375$, $W = 2.68$ kW and $\eta = 46.5\%$. It indicates that maximum power is associated with pure methane operation at a stoichiometric condition mainly as a result of the higher volumetric energy content of methane compared to that of fuel mixtures of hydrogen-methane. As expected, a lean hydrogen-methane mixture can provide a superior efficiency due to a faster flame speed and less fuel consumption in comparison to that of pure methane with stoichiometric mixture.

Figure 7.4 shows the variations of maximum power output with changes in the molar hydrogen concentration in the fuel mixture for a range of compression ratios and MBT spark timing shown in Figure 7.5. Hydrogen addition to methane at MBT timing for compression ratios less than 14.5:1 decreases power output, indicating that maximum power at a low compression ratio is associated with pure methane

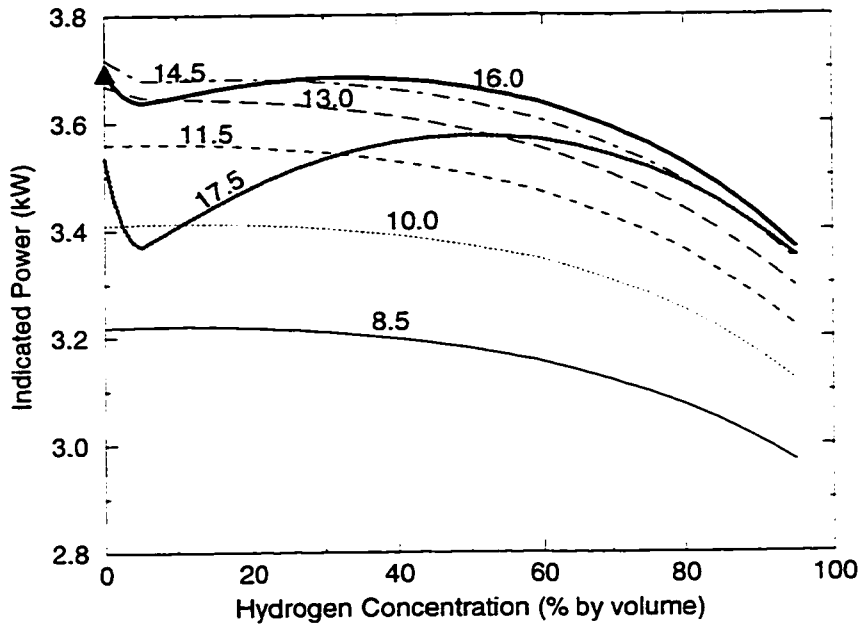

Figure 7.4: Variation of the maximum power output with compression ratio and hydrogen concentration in the blend of hydrogen and methane at 900 RPM with MBT spark timing, $\phi = 1.0$, $P_o = 87$ kPa, $T_o = 311$ K.

operation, which is confirmed by the results of Example (1). Adding a small amount of hydrogen to methane at high compression ratios (higher than 14.5:1) causes auto-ignition and knock in the engine. To avoid this, the spark timing has to be retarded. Hence, a decrease in power output can be observed. Increasing the hydrogen concentration in the fuel to higher than 20% by volume may improve power output as a result of faster flame speed. The maximum power for optimum operating conditions of Example (1), shown in Figure 7.4 by a triangle, emphasizes the success of the GA algorithm in finding an operating condition close enough to optimum solution while satisfying all the required constraints.

Example 2: In this example pure methane operation is investigated. The acceptable

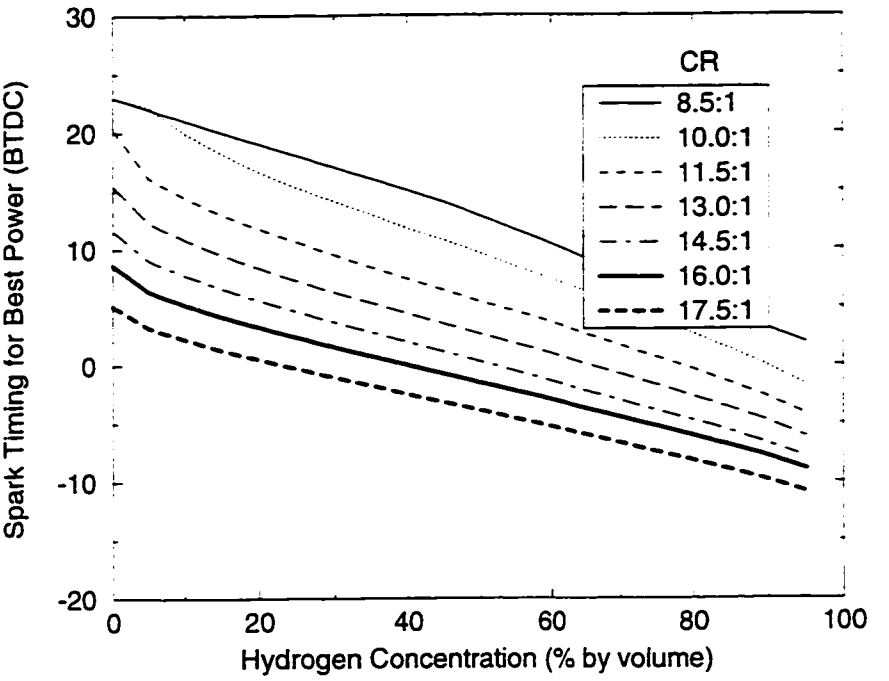

Figure 7.5: Variations of the MBT timing for different compression ratios and hydrogen concentration in blends of methane and hydrogen at 900 RPM, $\phi = 1.0$, $P_o = 87$ kPa, $T_o = 311$ K.

values for compression ratio, equivalence ratio and spark timing are assumed to be as of Eqs. 7.11. The power output and efficiency are to be maximized. The results of the optimization procedure for the power and efficiency are the following:

$$\begin{pmatrix} & \theta_{st} & \phi & CR & K_{\max} & W(\text{kW}) & \eta(\%) \\ Max.\ Power & : & 18 & 0.98 & 14.10:1 & 1.497 & 3.68 & 43.3 \\ Max.\ Effi. & : & 23 & 0.76 & 14.45:1 & 1.353 & 3.09 & 45.7 \end{pmatrix}$$

Comparing the results of Examples (1) and (2) shows that although the operating parameters for maximum power are slightly different, the maximum power output

has almost the same value. The results for maximum thermal efficiency show that running an engine on only methane, instead of hydrogen and methane required for attaining maximum efficiency, changed the equivalence ratio from 0.64 to 0.76 and increased the compression ratio from 13.75:1 to 14.45:1. Note that the maximum efficiency decreased with pure methane operation compared to that of hydrogen-methane for the conditions defined for these typical examples.

Example 3: The objective of this typical example is to maximize the power output for methane operation while introducing two constraints for the values of the knock criterion and thermal efficiency such as:

$$\begin{aligned} 1.3 \leq \quad K_{\mathbf{max}} \quad &\leq 1.5 \\ \eta \quad &\geq 45 \end{aligned}$$

The permitted ranges for the operating parameters are assumed to be those of Eqs. 7.11. The optimum set of operating parameters to maximize power output while satisfying both the constraints on knock criterion $K_{\mathbf{max}}$ and efficiency is found to be as $\theta_{st} = 22°$ BTDC, $\phi = 0.84$ and $CR = 13.75:1$, which is associated with $K_{\mathbf{max}} = 1.47$, $W = 3.33$ kW and $\eta = 45.13\%$, indicating that the algorithm was successful in finding an optimum operating condition within the acceptable range of operating parameters and satisfying the imposed constraints, if it is physically possible. Of course, any other set of operating parameters will produce either less power or unacceptable values for the required knock criterion and/or thermal efficiency. If it is not possible to have some of the pre-selected constraints, for example if thermal efficiency is chosen to be greater than 60%, then the algorithm will not be able to find a set of operating condition satisfying all the impose constraints and converge

to a proper solution.

7.4 Gradient-Based Optimization

One of the simplest methods to minimize the objective function $\Psi(\vec{x}, r)$, with a deterministic algorithm, is to use the negative value of its gradient in calculating the direction for minimizing the function [87, 133]. This gradient-based algorithm has two-phases, search direction and step size determination. After determining the search direction, the step length can be determined in a one-dimensional minimization problem. To search for the minimum, *Cauchy's Steepest Descent Method* [139] for solving a system of linear equations, can be used. To improve the convergence speed, it may be combined with quadratic programming [87]. The following is a short and brief description of these two search methods. The reader is referred to references [90, 91] for more details.

7.4.1 Search Direction(First Order Methods)

First order methods for unconstrained minimization of a function $Y(\vec{x})$ uses the gradient of the function as well as its value in calculating the move direction for the function minimization. These methods possess a linear or a superlinear rate of convergence [133].

Perhaps the oldest known method for minimizing a function of n variables is the steepest descent method first proposed by Cauchy [139] for solving a system of linear equations. It is described by the following steps:

1. Set the iteration number i equal to zero and start with an initial value for

design operation vector $\vec{x}$.

2. Calculate the gradient of $Y(\vec{x})$.

3. Calculate $\vec{S} = -\nabla Y(\vec{x})$ as search direction toward the minimum of $Y(\vec{x})$. It is needed, because the negative of the gradient of any function has the maximum rate toward decreasing that function [87]. If the norm of $\vec{S}$, $\|\vec{S}\|$, is less than a termination criterion ϵ, then stop.

4. Calculate $\vec{s} = \frac{\vec{S}}{\|\vec{S}\|}$.

5. Calculate the new design operational variables as $\vec{x_{i+1}} = \vec{x_i} + \lambda \vec{s}$, where λ is a step size such that $Y(\vec{x})$ is minimized along the chosen direction by using any one of the one-dimensional techniques.

6. Set $i = i+1$ and repeat from step 2 until reaching the minimum of the function $Y(\vec{x})$ by satisfying the termination criteria in step 3.

Figure 7.6 shows the procedure of finding the minimum of a one-dimensional problem, using the above method. A similar procedure can be followed for a multi-dimensional problem.

7.4.2 Quadratic Programming

The steepest descent methods described in the previous section, needs a small value for λ, therefore it needs a long computational time for finding the minimum of the function $Y(\vec{x})$. In order to reduce the number of iterations required for finding the minimum of the function $Y(\vec{x})$, a quadratic procedure is added to the model. In this procedure, instead of trying to find the minimum of a function only by line

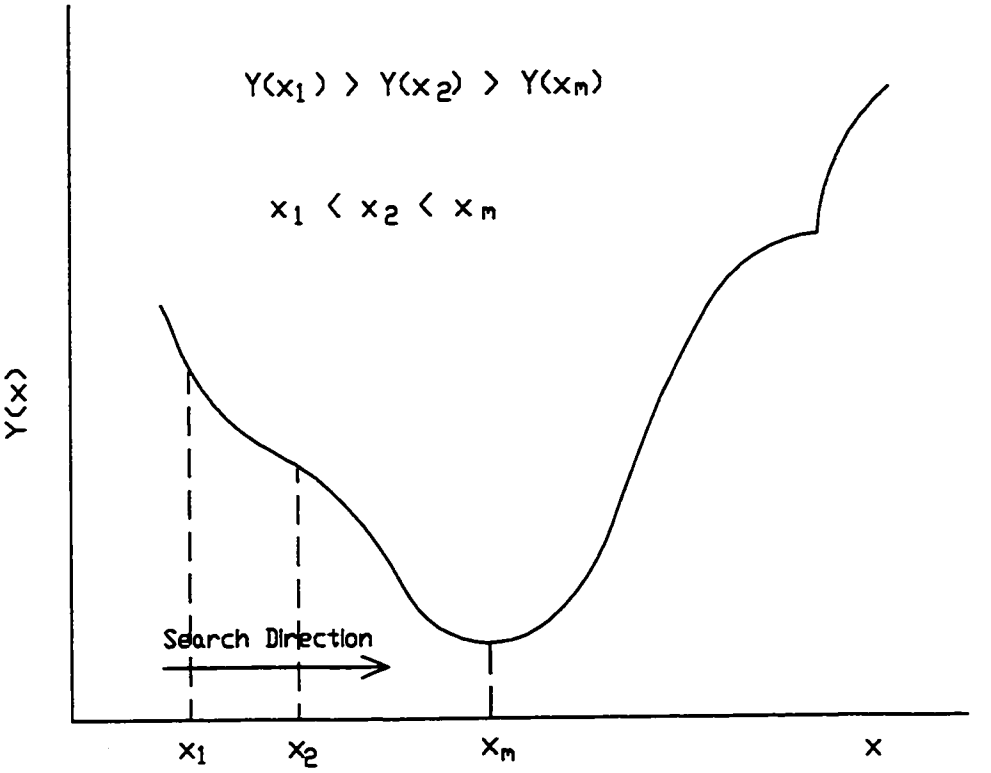

Figure 7.6: Line search method in a one-dimensional problem.

search, three points in the acceptable interval will be found by using the line search method (Section 7.4.1) in such a way that a minimum is located between them. Then a quadratic function is fitted to these three points. The minimum of this quadratic function, which can be found analytically, is accepted as the minimum of $Y(\vec{x})$.

A quadratic interpolation procedure starts with an interval of uncertainty $[x_1, x_3]$ and a point x_2 such that $x_1 \leq x_2 \leq x_3$ and $Y(x_2) < Y(x_1)$, $Y(x_2) < Y(x_3)$ (see Figure 7.7). The quadratic approximation $q(x) = ax^2 + bx + c$ is constructed so that it coincides with $Y(x)$ at the three points, that is $q(x_i) = Y(x_i)$, $i = 1, 2, 3$. Thus, a uniquely defined parabola is fitted in the bracket $[x_1, x_3]$ that is guaranteed to have

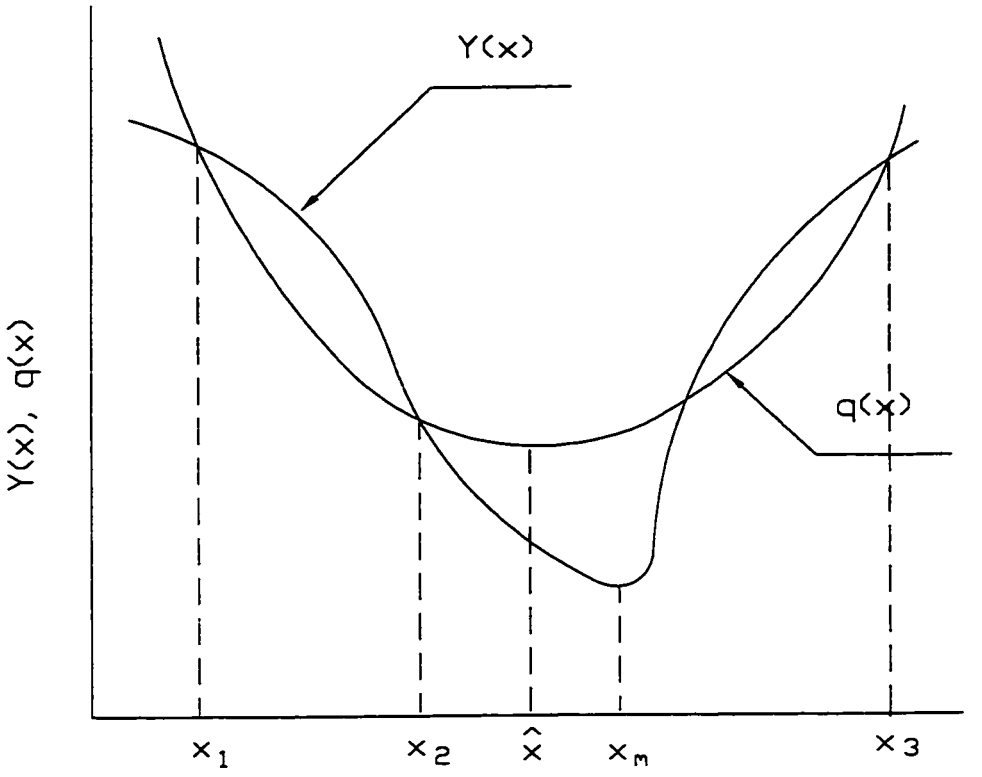

Figure 7.7: Quadratic interpolation.

a minimum at the point.

$$\hat{x} = \frac{1}{2}\frac{(x_2^2 - x_3^2)Y(x_1) + (x_3^2 - x_1^2)Y(x_2) + (x_1^2 - x_2^2)Y(x_3)}{(x_2 - x_3)Y(x_1) + (x_3 - x_1)Y(x_2) + (x_1 - x_2)Y(x_3)} \tag{7.12}$$

The point $\hat{x}$ will be used instead of x_1, x_2 or x_3 for a new bracket and a new interpolation. This procedure will be repeated until the value of $\hat{x}$ converges and its consequence change becomes smaller than a termination criterion.

7.4.3 Application of Gradient-Based Algorithm

As explained earlier, the objective was to find the best performance output of the engine without encountering knock which often is associated with being on the verge of knock. That is to search for an operating condition for maximum power or efficiency just before the onset of knock. The procedure can be used not only to choose a suitable operating condition for a knocking engine to get out of knock, but also to modify operating conditions for a knock free engine to produce better performance.

For example, it can be assumed that the main variables controlling the power output of a spark ignited methane fueled engine with some hydrogen addition which can be varied independently of each other are equivalence ratio ϕ, compression ratio CR, spark timing θ_{st}, intake temperature T_o, and the concentration of hydrogen in the mixture of hydrogen and methane $H_2\%$. The optimization problem can be defined as minimizing the following function:

$$f_1(\vec{x}) = f_1(\phi, CR, \theta_{st}, T_o, H_2\%) = W_o - W \tag{7.13}$$

where W_o is the initial indicated power output at the initial engine operating condition, which can be estimated by the genetic algorithm described in Section 7.3 or can be set by the engine designer/developer based on his experience, and W is the indicated power output at any operating condition. The constraints are assumed to be as of Equations 7.7 and 7.8. Therefore, by minimizing $f_1(\vec{x})$, the maximum possible power out close to the initial setting can be derived.

Accordingly, to obtain the desired solution, the following steps were carried out:

1. An initial value for $\vec{x_1} = \vec{x}(\phi, CR, \theta_{st}, T_o, H_2\%)$ and a relatively small value for the penalty multiplier r_1, e.g. 10, were chosen. This initial setting can be the

outcome of the application of the genetic algorithm described earlier.

2. $g_j(\vec{x_1})$ and $f_1(\vec{x_1})$ were calculated from Eqs. 7.7, 7.8 and 7.13. Then $\Psi(\vec{x_1}, r_1)$ was calculated from Eq. 7.9.

3. The gradient of $\Psi(\vec{x}, r)$ with respect to the specified variables $\vec{x}$ was calculated by changing just one parameter at a time and keeping the others constant and repeating step (2).

4. The direction of the search for a minimum value of the objective function Ψ was calculated by using $\vec{s} = -\frac{\nabla\Psi(\vec{x},r)}{\|\nabla\Psi(\vec{x},r)\|}$.

5. A new operating condition associated with $\vec{x}$ could be evaluated by $\vec{x} = \vec{x_1} + \lambda\vec{s}$. A value for λ to minimize $\Psi(\vec{x}, r)$, called λ^*, was found using the steepest descent method and a quadratic algorithm. Then, a new set of operating variables was calculated by $\vec{x_2} = \vec{x_1} + \lambda^*\vec{s}$.

6. Steps (2) to (5) were repeated until $\|\nabla\Psi\| \leq \epsilon$, where ϵ is a small number considered an acceptable termination parameter.

7. If the penalty multiplier r was not large enough, it was changed to a larger value and steps were repeated, until the results converge to the required accuracy.

It is evident that this approach involving the combustion and knock engine model together with the optimization algorithms requires extremely large computational time even for local optimization. For example, each run on an IBM RS 6000 R30 computer operating under AIX system, which was available to us, took 1 to 2 weeks to reach the results! Accordingly, this approach at this stage, can be applied to engines at the design or operational modification stages only.

7.4.4 Results and Discussion of the Application of Gradient-Based Algorithm Only

Gradient-Based Algorithm may be applied alone to search for an optimum operating condition close to an initial setting, e.g. finding a knock free operating condition close to a knocking state. The results of applying this procedure to five typical examples involving a single cylinder spark ignited CFR engine, when operating at full throttle on methane at constant speed under ambient pressure, are summarized in Table 7.1. The permitted operating conditions, for the variables chosen, were assumed to be in the following ranges:

$$\begin{aligned} 0.6 \leq \quad & \phi \quad \leq 1.0 \\ 8:1 \leq \quad & CR \quad \leq 16:1 \\ 0.0 \leq \quad & \theta_{st} \quad \leq 30.0 \qquad \text{(degrees BTDC)} \\ 280 \leq \quad & T_o \quad \leq 330 \qquad \text{(kelvin)} \end{aligned} \tag{7.14}$$

In Examples (1) and (2) the power output of the engine was to be improved by modifying only the equivalence ratio and spark timing while maintaining the compression ratio and intake temperature constant. Example (1) shows for a typical knock free engine condition, that advancing the spark timing by 10 degrees for a stoichiometric mixture, the power output can be increased by 10.6% just before the onset of knock. Example (2) relates to a knocking engine. If the spark timing is retarded by 4.75 degrees (from 23° to 18.25° BTDC) and the equivalence ratio increased from 0.8 to stoichiometric operation, the engine not only can get out of knock but also can produce an increase of 15% in its power output. The corresponding variations with the number of iterations of the objective function, Ψ, for these

Table 7.1: Some Typical Results for Methane Operation Showing Initial and Optimized Conditions. I.O.C. stands for Initial Operating Condition and M.O.C. is for Improved Operating Condition.

No.		ϕ	CR	θ_{st} (BTDC)	T_o (K)	K_{max}	W (kW)
1	I.O.C.	1.0	15.0:1	5.00	300.0	0.001	3.36
	M.O.C.	1.0	15.0:1	15.36	300.0	1.488	3.72
2*	I.O.C.	0.8	14.0:1	23.00	300.0	1.697	3.22
	M.O.C.	1.0	14.0:1	18.25	300.0	1.480	3.71
3	I.O.C.	1.0	15.5:1	10.00	300.0	0.003	3.56
	M.O.C.	1.0	16.0:1	12.68	299.1	1.397	3.70
4*	I.O.C.	1.0	17.5:1	10.00	300.0	5.910	3.68
	M.O.C.	1.0	15.9:1	13.11	298.9	1.500	3.72
5*	I.O.C.	1.0	16.0:1	27.00	280.0	5.078	4.15
	M.O.C.	1.0	14.1:1	26.24	280.1	1.500	4.04

$*$: a knocking condition

two examples, are shown in Figure 7.8.

Since the initial operating condition for Example (1) was a knock free condition in a feasible region, the objective function had a low value at the beginning. It then increased to some high value due to the violation of the constraints, and then decreased to some lower value as compared to the initial one and finally ended up with a knock free operating condition with better performance than the initial operating condition. But, in case of Example (2), which involved a knocking engine, the objective function had a high value at the beginning and after some fluctuation it decreased to a low value with a knock free operating condition within the acceptable ranges of operational parameters.

Figure 7.9 shows the calculated variation of indicated power with spark timing for stoichiometric methane operation at two compression ratios of 14:1 and 15:1. The circles show the indicated power output of the initial operating condition (I.O.C.)

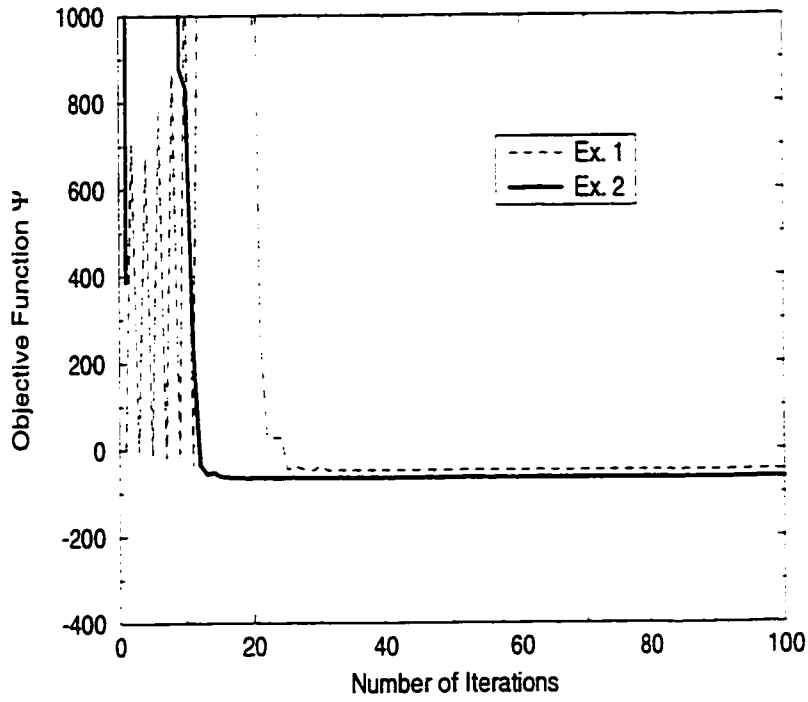

Figure 7.8: Variations of the objective function with iteration number for Examples 1 and 2.

and the modified operating condition (M.O.C.) of Example (1) in Table 7.1. The corresponding data of Example (2) are shown with triangles. This figure indicates clearly how well the described algorithm can find an operating condition that is close enough to the optimum solution while satisfying all the required constraints.

In Examples (3), (4) and (5) of Table 7.1, the operational variables were varied subject to the limiting values of Equation 7.14. Example (3) relates to a non-knocking engine. The results of the optimization calculation show that the compression ratio can be increased by 0.5 and the spark timing can be advanced by 2.7 degrees, without encountering knock to improve the power output by 3.4%. Example (4) relates to a case involving a knocking condition. The application of the optimization procedure

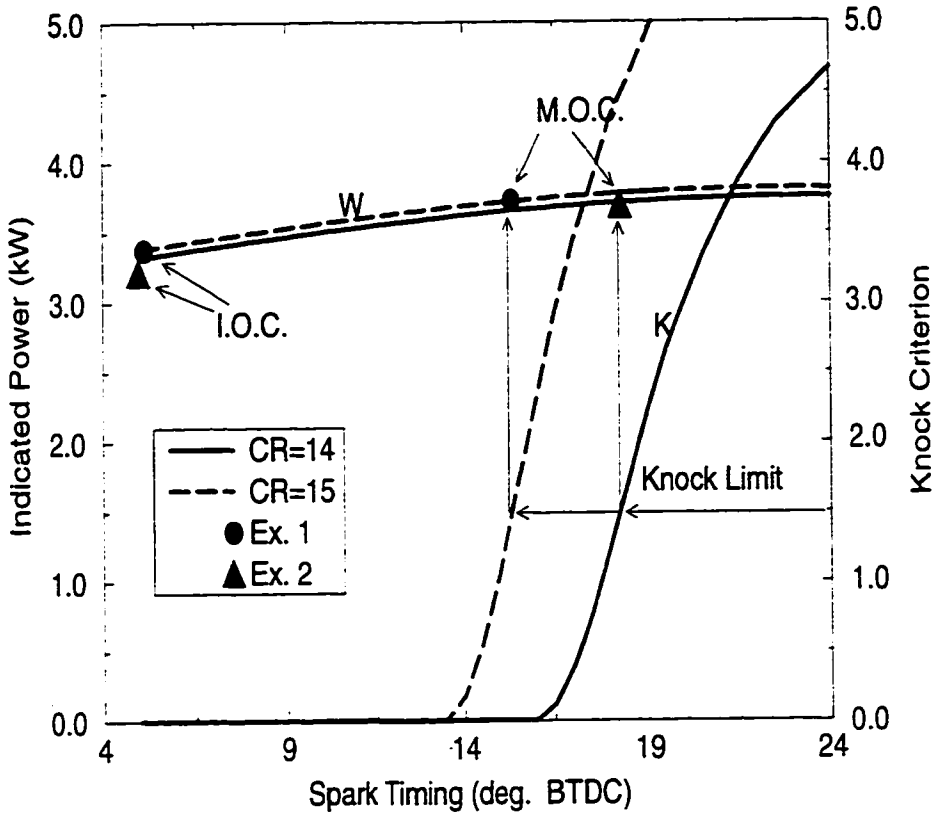

Figure 7.9: Variations of the indicated power and knock criterion with spark timing and compression ratio for methane operation at 900 RPM, $T_o = 300$ K and $\phi = 1.0$.

produces a further improvement in power output while getting out of the knocking situation. In this case, the reason that the algorithm did not select the lowering of T_o to the minimum possible assigned value, 280 K, which would have obtained yet higher power output, is that convergence usually takes place towards the closest local optimum point and not necessarily to the global one. To overcome this feature, it is suggested that the initial value for each of the main variables chosen such that maximum indicated power is produced by each of them individually. In Example (5),

the initial value for compression ratio was chosen at the maximum acceptable one, 16, spark timing around 27° BTDC which is close to the optimum spark timing for power output when only spark timing is changed, and the intake temperature at its minimum acceptable value of 280 K which would represent a strongly knocking situation. After applying the optimization procedure, the resulting optimum operating conditions for a non-knocking condition are $CR = 14.12$, $\theta_{st} = 26.24°$ BTDC and $T_o = 280.14$ K, which produce a reduction in power output down to $W = 4.04$ kW. Any further changes to these operating conditions will result in an unacceptable value for $K_{\max}$, indicating an onset of knock, and/or loss in power output.

In normally aspirated engines, the intake temperature is usually dictated by atmospheric conditions and its value cannot be varied readily. Moreover, changes in the compression ratio can be made at the design stage but normally for operational engines they are limited to relatively small changes such as those resulting from changes in thickness of the cylinder head gasket. Variations in equivalence ratio, spark timing and fuel composition (the percentage of hydrogen in this case) can be accomplished normally more easily. Hence, in another set of examples for the application of this optimization procedure, the following variables and limits were assumed:

$$\begin{aligned} 0.6 \leq \quad & \phi \quad \leq 1.0 \\ 0.0 \leq \quad & \theta_{st} \quad \leq 25.0 \qquad \text{(deg. BTDC)} \\ 0.0 \leq \quad & H_2\% \quad \leq 20.0 \\ CR - 0.3 \leq \quad & CR \quad \leq CR + 0.3 \end{aligned}$$

Table 7.2 shows the results for two typical examples. In the first example, a

Table 7.2: Some Typical Results of the Optimization Procedure for Mixtures of CH_4 and H_2 at 900 RPM and $T_o = 300$ K. I.O.C. and M.O.C. stand for Initial Operating Condition and Improved Operating Condition, respectively.

No.		ϕ	CR	θ_{st} (BTDC)	$H_2\%$	K_{max}	W (kW)
1*	I.O.C.	0.80	14.00:1	23.00	10.0	5.596	3.26
	M.O.C.	0.71	14.06:1	21.82	7.43	1.496	2.90
2	I.O.C.	1.00	14.00:1	18.00	0.00	1.332	3.71
	M.O.C.	1.00	14.25:1	18.00	0.00	1.485	3.73

* denotes a knocking condition.

severely knocking engine is taken out of knock by a combination of reducing the equivalence ratio, a small increase in its initial compression ratio, retarding slightly the spark timing and adding 7.4% hydrogen to the methane, while reducing the power output. The second example indicates an initially non-knocking situation when its power output is further increased slightly through a small increase in the compression ratio while retaining the non-knocking status of the engine.

7.5 Modifying the Results of Genetic Algorithm with a Gradient-Based Algorithms

As explained earlier, the genetic algorithm is efficient in finding an optimum solution close to the global optimum one, but may have difficulty to converge to the optimum value itself, while the gradient-based algorithm is successful in searching for the closest optimum solution for an initial setting. Hence, if these two algorithms are linked together, the searching for a global optimum solution will be more efficient.

In the following example, the operating variables are again assumed to be spark

timing, equivalence ratio, compression ratio and hydrogen concentration in the fuel. Except for that of hydrogen concentration, the acceptable ranges of the operational variables are as of Eq. 7.11, except for the hydrogen concentration which can be varied between 0% to 80% by volume. The constraint for the knock criterion is assumed to be $1.3 \leq K_{\max} \leq 1.5$ (Eq. 7.10). The intake temperature is assumed to be 300 K. The maximum power output is predicted to be produced at $\theta_{st} = 4°$ BTDC, $\phi = 1.0$, H_2%=31 and $CR = 15.5 : 1$, associated with values of $K_{\max} = 1.35$, $W = 3.91$ kW and $\eta = 36.20\%$ through the employment of the genetic algorithm after more than 200 generations.

Having the output of the application of genetic algorithm as an initial guess for the gradient-based algorithm, the optimum operating condition for the engine is estimated as $\theta_{st} = 4.1°$ BTDC, $\phi = 1.0$, H_2%=31.25 and $CR = 15.50 : 1$, which is corresponding to $K_{\max} = 1.49$, $W = 3.912$ kW and $\eta = 36.23\%$. This shows a little further increase in power output and thermal efficiency and shows how the genetic algorithm is successful in searching for global optimum operating conditions. Since the genetic algorithm was allowed to perform many iterations and get closer to the global optimum, the application of the gradient-based procedure did not produce a big change in the estimated optimum operating condition.

The real benefit from combining the two optimization algorithms is reducing the computation time. The gradient-based algorithm is faster than the genetic algorithm in converging to the optimum solution. In the following example, there are three constraints on the knock criterion, minimum acceptable thermal efficiency and maximum peak pressure in the cylinder. It was tried to find the maximum power output from the engine in the same acceptable operational variables as of the previous

example, with the following constraints:

$$\begin{aligned} 1.3 \leq \quad & K_{\max} \quad \leq 1.5 \\ 38\% \quad \leq \quad & \eta \\ P_{\max} \quad \leq \quad & 6 \text{ (MPa)} \end{aligned}$$

To reduce the computational time to almost half, the optimum operating condition found by the genetic algorithm after 80 generations is used in the gradient-based algorithm approach. These initial and modified operating conditions by the gradient-based algorithm are shown in the following:

	ϕ	CR	θ_{st} (BTDC)	H_2 (%)	$K_{\max}$	W (kW)	η (%)	$P_{\max}$ (MPa)
I.O.C. from GA	0.760	15.00 : 1	8.00	24	0.12	3.25	38.23	4.10
M.O.C. by GB	0.814	15.52 : 1	8.01	20	1.50	3.45	38.23	4.34

This indicates the success of the above optimization procedures in finding an optimum solution in a reasonable computational time, while satisfying all the imposed constraints.

7.6 Conclusions

The optimization algorithms developed in association with the simple two-zone model, describing the combustion processes in a spark ignition engine fueled with methane and capable of generating important performance parameters and testing for the occurrence of knock and its intensity, appear to be powerful tools for selecting

the optimum operating conditions of a spark ignition engine while satisfying some imposed requirements. The specific examples considered, showed that maximum power can be achieved with pure methane operation at compression ratios around 14:1 when operating at MBT timing and chemically correct mixtures, while maximum efficiency is associated with lean hydrogen-methane operation. The addition of some hydrogen to methane allows for higher efficiency but with a lower compression ratio compared to that of pure methane. Furthermore, a solution that is closer to the global optimum can be obtained by selecting initial operating conditions for a gradient-based algorithm either from the output of the genetic algorithm or such that maximum power is produced by each of the operational variables individually followed by application of the gradient-based algorithm.

Chapter 8

Knock Rating of Gaseous Fuels

8.1 Introduction

Knock which is encountered usually with high load operation of spark ignition engines, is one of the main acknowledged barriers to the improvement of engine efficiency and power. It is believed to be caused mainly by autoignition of the unburned mixture in the end gas. The onset of knock involves exceedingly rapid combustion of the gaseous fuel-air mixture. It is associated with increased heat transfer to the cylinder walls, excessively high cylinder pressure and temperature levels, which can be destructive when persisting to engine components, particularly the piston.

One of the most important factors is the fuel resistance to knock. The terms 'knock limit' and 'knock rating' need to refer to a specified engine and defined engine operating conditions. There have been a number of attempts to establish standard procedures for knock rating of fuels in the past such as through the use of the "octane number" and "methane number" [13, 61, 140]. However, these tend to be entirely empirical and there is still a need to develop more reliable and more widely applicable procedures for knock rating of fuels, especially of the gaseous type.

This chapter provides a comparison between two different knock rating procedures proposed for gaseous fuels in the past. One procedure is based on the use of mixtures of hydrogen and methane and the other involves the use of normal butane and methane as reference fuels for knock rating in a CFR engine. Blends of ethane-

methane and propane-methane are also considered.

8.2 Background

The motor *octane number* (ON) is defined primarily by the standard ASTM procedure for knock rating of liquid fuels. It uses iso-octane (2, 2, 4 trimethyl pentane) and n-heptane as the reference fuels, where a 100 percent iso-octane equals "100 ON" and 100 percent n-heptane equals "zero ON". The lesser known *methane number* (MN) scale [61] is based on the molar percentage of methane in a methane-hydrogen fuel mixture, with a "100 MN" being given for neat methane and "zero MN" for pure hydrogen. A *methane number* is usually assigned to a gaseous fuel on the basis of the percentage by volume of methane in a blend of hydrogen and methane that exactly matches the knock intensity of the unknown gas mixture under a specified set of operating conditions in a knock testing engine. In contrast, the *butane number* (BN) method [13] is based on molar blends of methane and butane with neat methane equal to "zero BN" and "100 for pure butane". Table 8.1 is a listing of the corresponding knock rating according to these differing methods for C_1 to C_4 normal paraffins, which make up most of natural gases and represent the major contributors to the combustion characteristics of the natural gas.

Leiker et. al. [61] developed the methane number experimentally and provided a correlation to predict the methane number of a gaseous fuel from a knowledge of its composition. Ryan et. al. [13] examined different knock rating methods, such as the methane, butane and octane numbers and indicated the existence of a linear relationship between octane number and methane number. They suggested that "The

Table 8.1: Knock rating for C_1 to C_4 normal paraffins.
Data from reference [13].

Gas	Formula	Motor Octane No.	Methane No.	Butane No.
Methane	CH_4	122	100	0.0
Ethane	C_2H_6	101	44	7.5
Propane	C_3H_8	97	34	10
Butane	C_4H_{10}	89	10	100

Table 8.2: CFR/RDH engine operating conditions for methane number rating.
Data from references [13, 61].

Engine Parameter	Set Point
Equivalence Ratio	1.0
Speed	900 RPM
Spark Timing	15° BTDC
Intake Temperature	21° C

methane number appears to be the *the best choice* for rating the knock sensitivity of natural gases". Their tests were carried out at a constant spark timing and their results were based on the critical compression ratio for the knock limit. Their test conditions for the methane number rating procedures are listed in Table 8.2 for a naturally aspirated engine. A linear relationship was found between the methane number and the compression ratio for the specified test procedure.

Another procedure, which is used widely by researchers, is to use variable spark timing and to present the results based on either the knock limited spark timing (KLST) for each compression ratio [60] or the knock limited compression ratio (KLCR) for a preset variable spark timing as a function of compression ratio [57]. These types of procedures are closer to the real engine operations, since usually operating conditions are chosen such that the engine produces maximum power.

8.3 Test Procedure

For the variable spark timing procedure followed in this investigation, the tests were carried out with constant values of compression ratio of 8.5:1 and 11:1 for equivalence ratios of 0.8 and 1.0. After setting the fuel composition and mixture strength, the spark timing was changed to the point of borderline knock. The results, therefore, can be presented in the form of knock limited spark timing against volumetric concentration of the additives (hydrogen, ethane, propane and butane) in a binary mixture with methane for different compression ratios and equivalence ratios. This method has been used also by other researchers such as in reference [60].

To compare our results with those of others [13, 61], the test conditions for knock rating with constant spark timing were chosen as listed in Table 8.2. All the data were collected at 900 RPM. In order to consider the effect of equivalence ratio, the tests were carried out with equivalence ratios 0.8 and 1.0. In this procedure, the variations of knock limited compression ratio with changes in the fuel composition were investigated.

8.3.1 Observation of Knock

Examination of several methods of observation of knock led to the adoption of direct visual assessment of an oscilloscope display of the cylinder-pressure variations with time. As the spark timing was advanced (or the compression ratio was increased) from a knock free setting, the onset of knock could be identified by the appearance of high frequency pressure oscillations near the beginning of the expansion stroke. Because of the cyclic variability of combustion, the knock oscillations would appear

at first only on a small proportion of cycles. Increasing the advance of spark timing (or compression ratio) would increase the proportion of knocking cycles and the intensity of oscillations. The knock boundary was taken to be the ignition timing (or compression ratio) at which clearly perceptible oscillations occurred on 10 to 20 percent of the cycles. After detecting the knock limit operation, the variations of pressure with crank angle, for 100 consecutive cycles, were recorded by computer to confirm and check the above condition for knock limit with sufficient accuracy.

8.4 An Examination of the Methane Number

Figure 8.1 shows the variations of the calculated compression ratio for different values of the knock criterion, $K_{\mathbf{max}}$, plotted against methane number at the conditions described in Table 8.2. The experimental points for the knock limit obtained in our laboratory are shown too. For high methane numbers, which are associated with high compression ratios, the range of compression ratio from light knock to heavy knock operations (corresponding to a $K_{\mathbf{max}}$ between 0.5 to 2.0) is narrow; while at low methane number (i.e. with high concentrations of hydrogen), this range is wider due to the corresponding low compression ratios. Good agreement with experiment for the knock limit can be observed for high methane numbers. For low methane numbers, the test data show some deviation from the values predicted by the two-zone model. This is believed to be due to the difficulty in recognizing the borderline of knock experimentally for a mixture with high concentration of hydrogen, because of the fast flame speed and the associated high rates of combustion heat release.

The corresponding power output is plotted in Figure 8.2. The associated com-

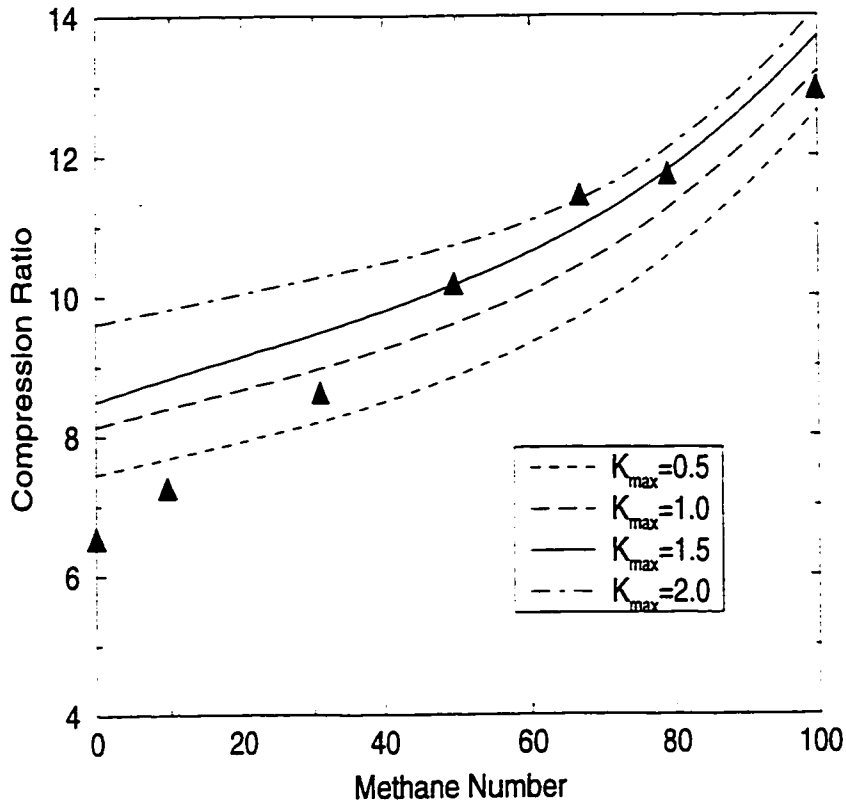

Figure 8.1: Compression ratio variations with the methane number for different values of the knock criterion at 900 RPM, $\phi = 1.0$, $\theta_{st} = 15°$ BTDC, $T_o = 300$ K, $P_o = 87$ kPa. Experimental points for borderline knock are shown by triangles.

pression ratio with any operating condition is shown by a number beside that point. Indicated power increases with increasing methane number due to the higher associated compression ratio and energy content of the charge mixture. It shows that, at high compression ratios, the indicated power is not sensitive to the values of the knock criterion and the associated methane number of the mixture. This is believed to be due to an increase in the rate of change in the value of knock criterion at high compression ratios, causing its value to increase from 0.5 to 2.0 for a small change

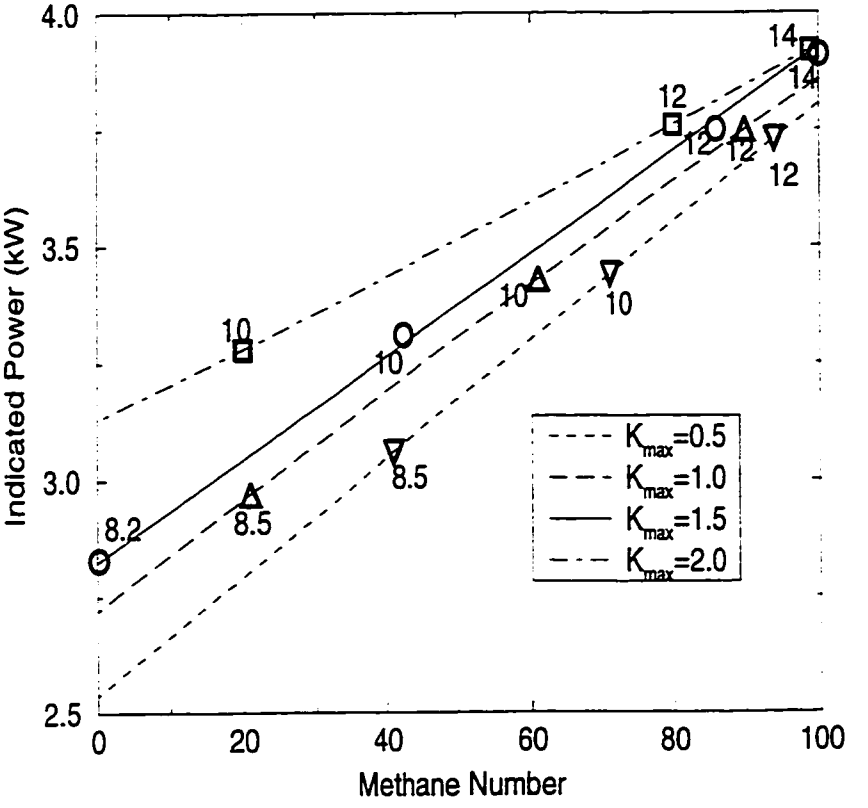

Figure 8.2: Knock limited power output versus methane number for different values of the knock criterion and compression ratios, shown by numbers beside the associated points, at 900 RPM, $\phi = 1.0$, $\theta_{st} = 15°$ BTDC, $T_o = 300$ K, $P_o = 87$ kPa.

in the operating condition.

8.5 KLCR with MBT Spark Timing

The calculated MBT timing based on the two-zone combustion model, shown in Figure 5.23, has been used for this purpose. The variations of knock limited compression ratio (KLCR), associated with $K_{max} = 1.5$, and the corresponding spark timing

versus hydrogen molar concentration in blends of methane-hydrogen are plotted in Figures 8.3 and 8.4. The KLCR decreases slightly when the fuel composition is

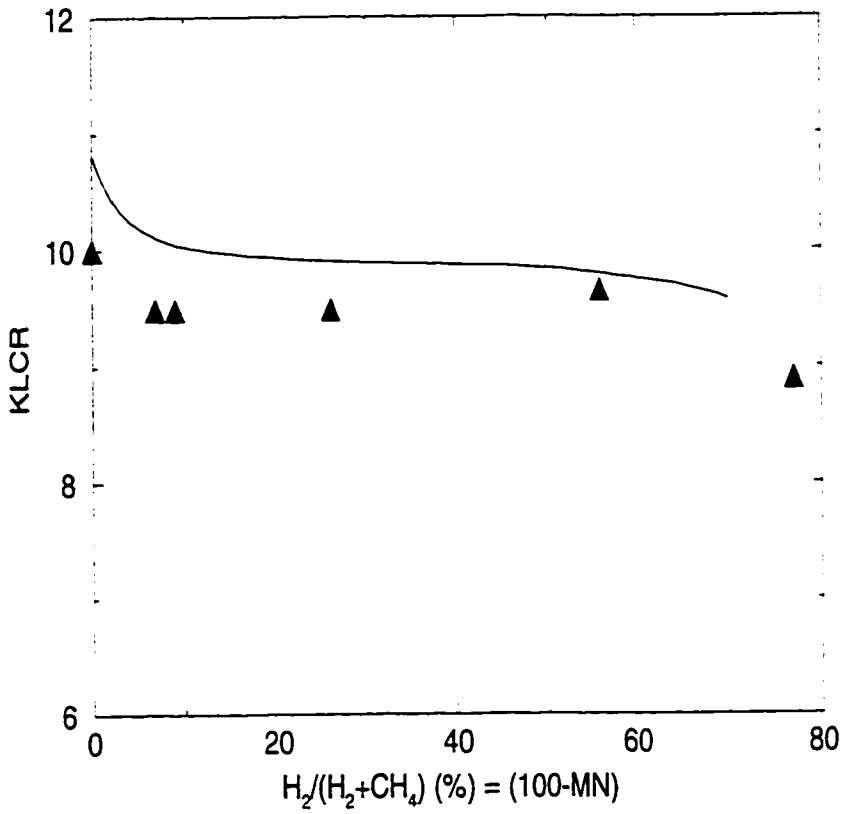

Figure 8.3: Variation of the knock limited compression ratio with hydrogen molar concentration in methane-hydrogen mixtures (i.e. 100-MN) with MBT timing at 900 RPM, $\phi = 1$, $P_o = 87$ kPa, $T_o = 300$ K. The experimental points are also shown.

changed from pure methane to a mixture of 20% hydrogen-80% methane. Then, it becomes almost constant for a mixture with more than a 20% volumetric concentration of hydrogen. The occurrence of knock and its intensity is related to the times required for flame propagation and self-reaction. The addition of a small amount of hydrogen to methane, as shown in Chapter 3, does not change significantly the com-

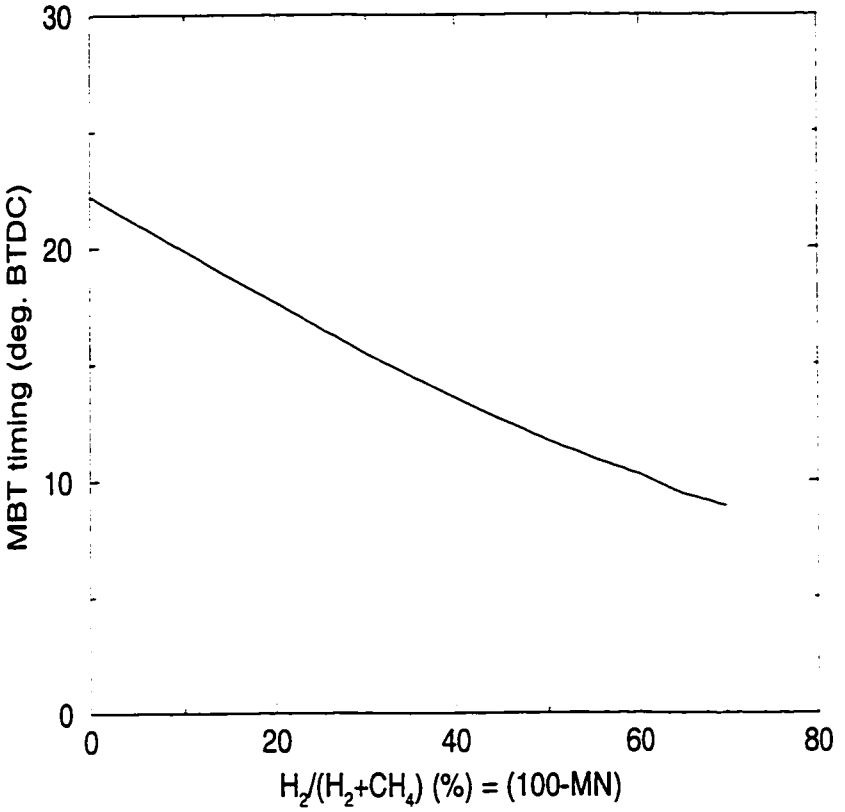

Figure 8.4: Variation of the MBT timing at knock limited compression ratio with hydrogen molar concentration in methane-hydrogen mixtures at 900 RPM, $\phi = 1$, $P_o = 87$ kPa, $T_o = 300$ K.

bustion duration, but it tends to improve the reactivity of the mixture and reduces the self-reaction time, mainly due to an increase of hydrogen based radicals in the mixture. Therefore, the KLCR decreases slowly with the addition of some hydrogen to pure methane. For a mixture with a high concentration of hydrogen, the effective flame speed increases markedly, and the reduction in the combustion duration becomes the dominant phenomenon, leading to some reduction in the knock intensity of the mixture. Thus, the KLCR does not change significantly for methane-hydrogen

mixtures having more than 20% hydrogen.

The knock limited power output with MBT timing and MBT-5° are shown in Figure 8.5. The triangles show experimental data for MBT-5° spark timing. It shows a slight decrease with increasing the relative concentration of hydrogen in the mixture, mainly because of the reduction in the energy input with a small lowering of the knock limited compression ratio.

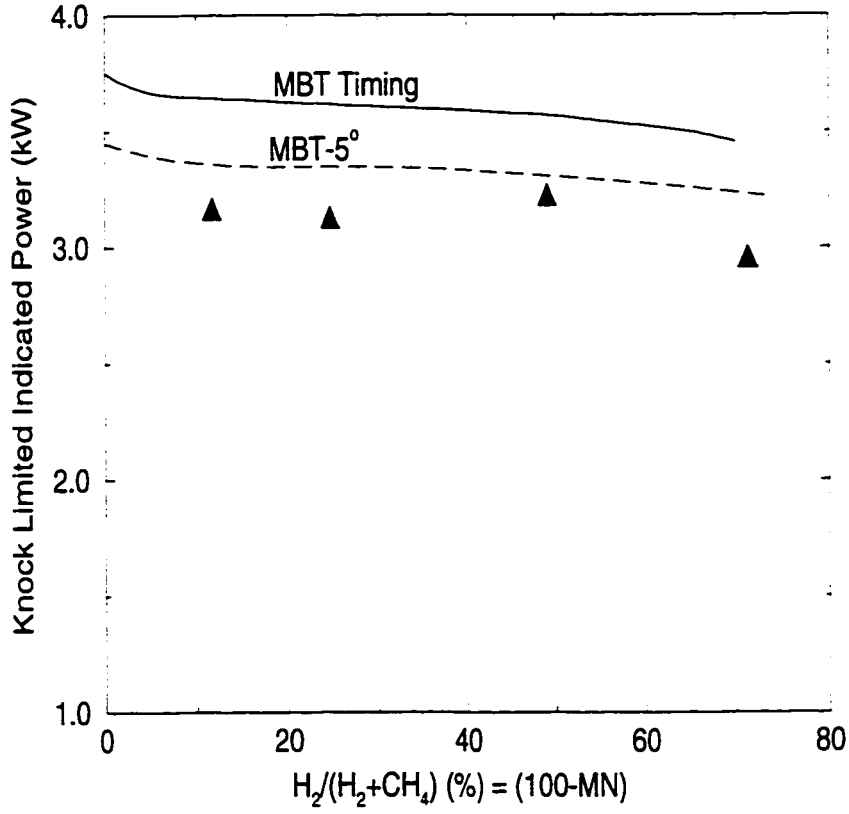

Figure 8.5: Variation of the indicated power at knock limited compression ratio with hydrogen volumetric concentration in methane-hydrogen mixtures and MBT timing at 900 RPM, $\phi = 1$, $P_o = 87$ kPa, $T_o = 300$ K. The experimental points for spark timing equal MBT-5° are shown.

8.6 Knock Limited Spark Timing (KLST)

The analytical consideration of the engine performance and the incidence of knock when using the fuels ethane, propane and butane requires further modifications in the chemical kinetic model and the combustion duration correlation. This was judged to require very significant additional computational and experimental efforts beyond this project, particularly when high reliability in such a prediction is to be maintained. Accordingly, it was decided to approach this extension to the original objectives of the project only experimentally. For the sake of consistency, the data for the methane-hydrogen mixture, when compared to those of methane and other gaseous mixtures, were also those derived from experiments carried out similarly in the CFR engine.

The knock limited spark timing (KLST) at different compression ratios and equivalence ratios of 0.8 and 1.0 are plotted in Figure 8.6 against volumetric hydrogen concentration in blends of methane and hydrogen. The thin and bold lines show the data for compression ratio 8.5:1 and 11:1, respectively. The KLST decreases almost linearly with increasing the volumetric concentration of hydrogen in the mixture, then begins to drop significantly when the volumetric concentration of hydrogen increases beyond 80%. The linear relationship shown is due to an almost linear reduction in the combustion duration with increasing hydrogen concentration in the mixture while affecting the reactivity rate only slightly. The equivalence ratio does not affect the KLST significantly, specially for the high compression ratio of 11:1 shown. For a stoichiometric mixture of 50% methane and 50% hydrogen, the KLST is retarded from 19° to 9° before top dead center when the compression ratio

is changed from 8.5:1 to 11:1, while it changes only from 19° to 16° BTDC for a $CR = 8.5 : 1$ when the equivalence ratio is varied from 0.8 to 1.0. The rate of change in the KLST increases with increasing hydrogen concentration in the mixture, particularly for more than 80% hydrogen by volume in the mixture. Retarding the spark timing somewhat to avoid knock increases the charge temperature during flame initiation and propagation and speeds up the reactivity of the mixture when it contains a high concentration of hydrogen, producing a rapid drop in the KLST value for mixtures with more than 80% hydrogen.

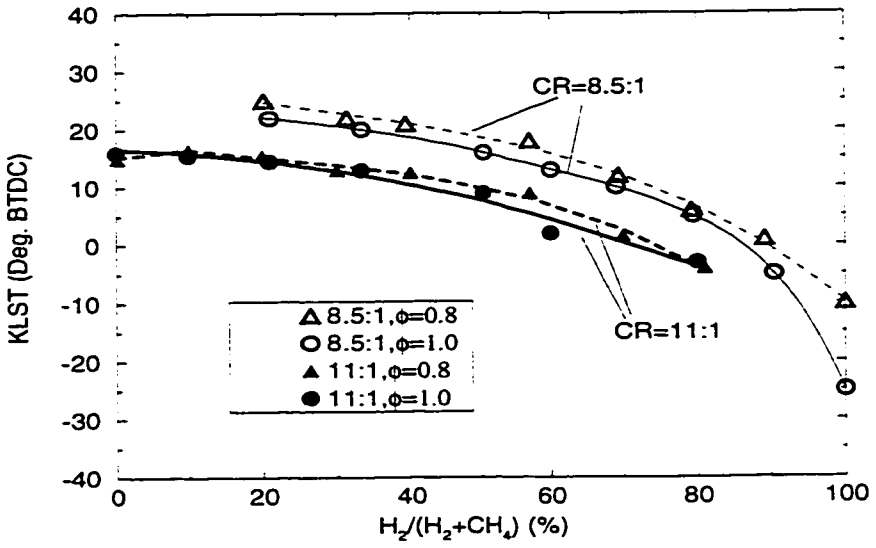

Figure 8.6: Variation of the KLST with volumetric hydrogen concentration in methane-hydrogen mixtures at 900 RPM, $P_o = 87$ kPa, $T_o = 300$ K.

Changes in the KLST with changes in the volumetric concentration of ethane, propane or butane in their binary mixtures with methane are shown in Figures 8.7, 8.8 and 8.9. The effect of equivalence ratio on the KLST remained similar when the hydrogen concentration in hydrogen-methane mixtures increases, while it becomes

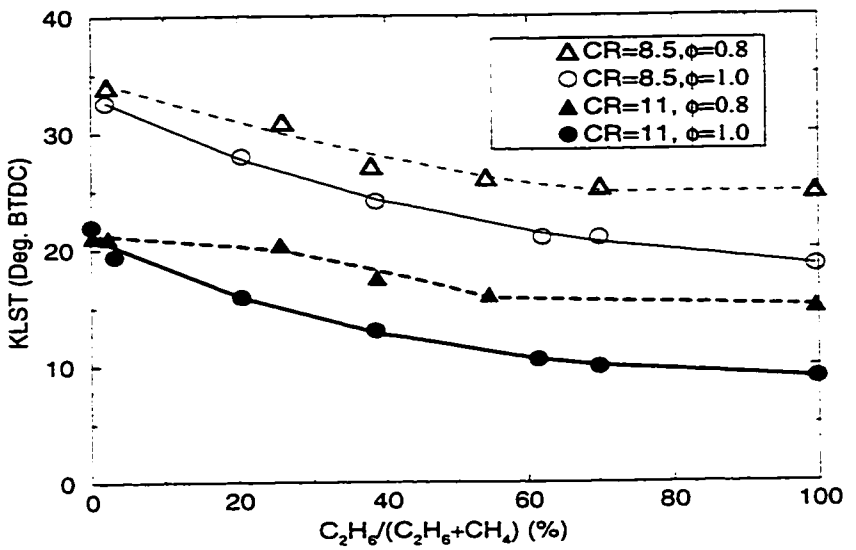

Figure 8.7: Variation of the KLST with volumetric concentration of ethane in a mixture with methane at 900 RPM, $P_o = 87$ kPa, $T_o = 300$ K.

larger when the concentrations of ethane, propane and butane increase in their binary fuel mixtures with methane. This is believed to be due to the higher energy content of the mixture, causing higher temperature and pressure in the end gas. This is more pronounced for butane-methane mixtures. The addition of ethane, propane or butane to methane decreases the KLST throughout. In contrast to the addition of hydrogen to methane, the rate of drop in the KLST decreases with increasing the additive concentration in the mixture. It can be due to the lowering of the cylinder charge temperature during flame initiation and propagation compared to that obtained with pure methane operation, because of the lowering of the effective polytropic index as high concentrations of the ethane, propane or butane are employed.

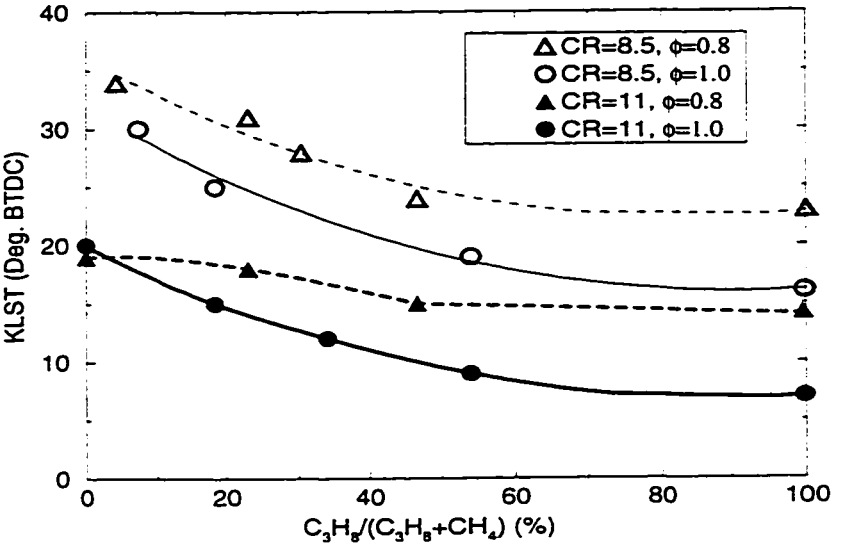

Figure 8.8: Variation of the KLST with volumetric concentration of propane in a mixture with methane at 900 RPM, $P_o = 87$ kPa, $T_o = 300$ K.

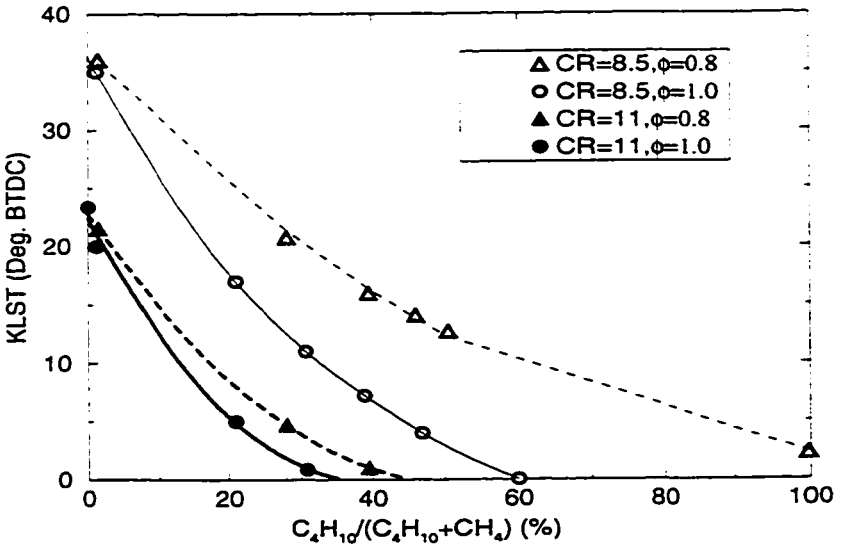

Figure 8.9: Variation of the KLST with volumetric concentration of butane in a mixture with methane at 900 RPM, $P_o = 87$ kPa, $T_o = 300$ K.

Figure 8.10 shows the calculated variation of the polytropic index with changes in the volumetric concentration of the fuel additive to methane in a stoichiometric methane-additive mixture. The addition of ethane, propane or butane to the methane decreases the effective polytropic index. Therefore, the charge tempera-

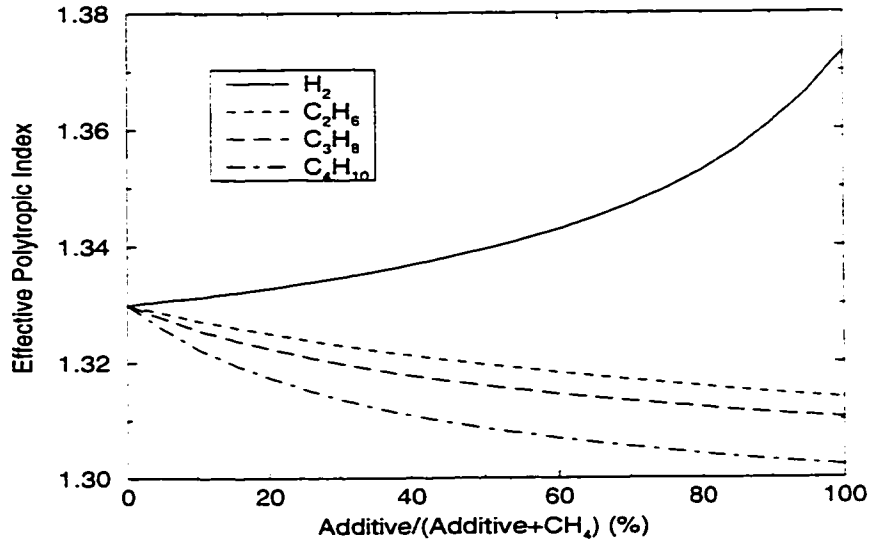

Figure 8.10: Variation of the effective polytropic index with volumetric concentration of the additives in a mixture with methane at 900 RPM, CR =8.5:1, P_o = 87 kPa, T_o = 300 K.

ture at top dead center, for constant compression ratio operation, decreases with increasing concentration of ethane, propane or butane in the charge. In view of the exponential dependence of the reaction rate on temperature, this will reduce the auto-ignition reactions of the end gas and will bring about a reduction in the intensity of knock in the engine. In the case of hydrogen-methane, the charge temperature increases a little due to the increasing effective polytropic index with the addition of hydrogen to methane.

The KLST for pure methane operation with an equivalence ratio 0.8 is less than

that of a stoichiometric mixture at a compression ratio of 11:1, mainly because of the longer combustion duration at an equivalence ratio of 0.8 (see Figures 8.7 and 8.8). At high compression ratios, the temperature is high and is not strongly dependent on the equivalence ratio. Therefore, the time required for self-ignition of the mixture does not change significantly with changing mixture strength. Since combustion duration increases for lean mixtures, the intensity of knock increases and consequently, the KLST decreases.

To compare the influence of different gases on KLST, the data are replotted in Figures 8.11 to 8.14. The thin lines show the data for a compression ratio of 8.5:1, while the bold lines are for 11:1. Ethane has the most advanced KLST, while butane has the most retarded one. The KLST for propane is less than that of ethane and higher than that of hydrogen. At high concentrations of additives in the fuel, the rate of decrease in KLST tends to decrease in comparison to that for low concentrations of the additives, except for the hydrogen-methane mixture. This, as stated earlier, is probably due to the effect of the lower polytropic index, producing a lower charge temperature. The KLST for ethane and propane has the lowest sensitivity to their volumetric concentration in the mixture. Changes in the composition of blends of hydrogen-methane do not show a strong effect on the KLST, particularly for the high compression ratio (CR =11:1); while the concentration of butane in butane-methane mixtures has significant influence on the KLST throughout and can distinguish the knock intensity of the engine for the whole range of butane concentration in the mixture. Consequently, a butane-methane mixture looks to be a better reference mixture for the knock rating of gaseous fuels, compared to the other mixtures examined.

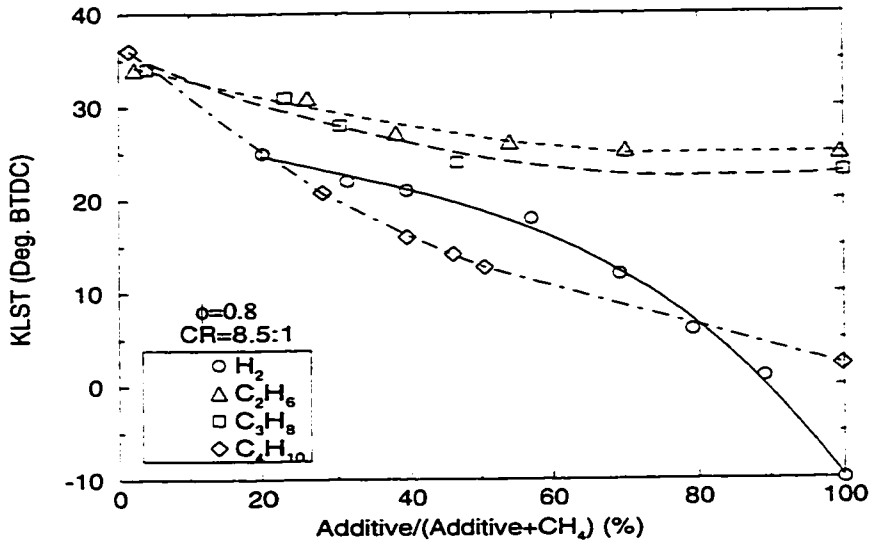

Figure 8.11: Variation of the KLST with volumetric concentration of additive to methane at 900 RPM, $\phi = 0.80$, CR =8.5:1, $P_o = 87$ kPa, $T_o = 300$ K.

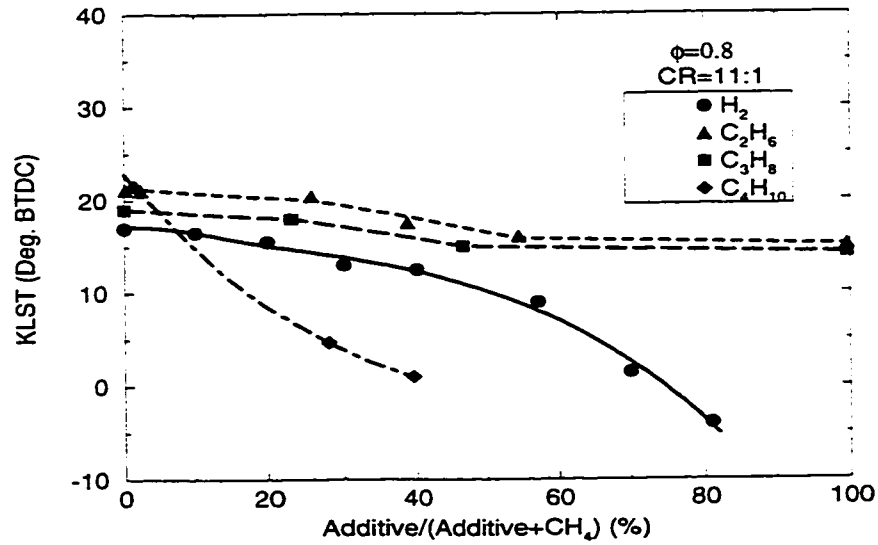

Figure 8.12: Variation of the KLST with volumetric concentration of additive to methane at 900 RPM, $\phi = 0.80$, CR =11:1, $P_o = 87$ kPa, $T_o = 300$ K.

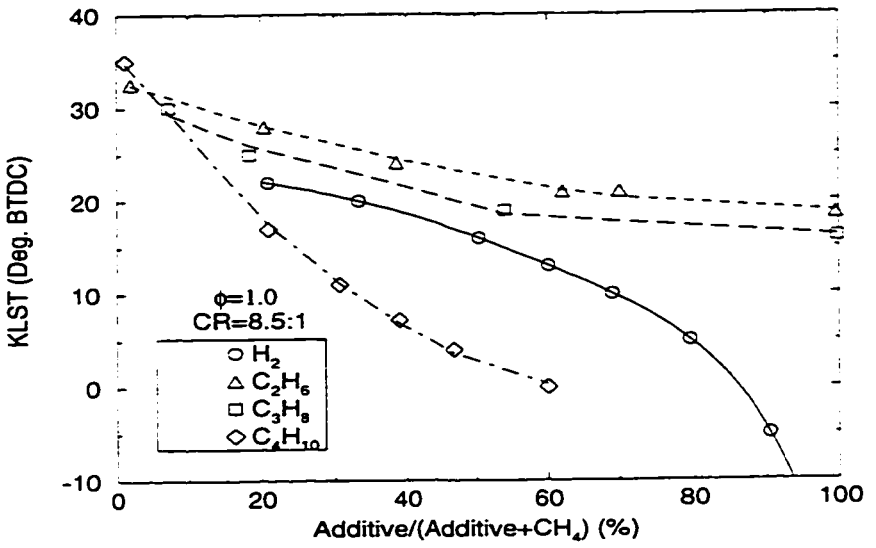

Figure 8.13: Variation of the KLST with volumetric concentration of additive to methane at 900 RPM, $\phi = 1.0$, CR =8.5:1, $P_o = 87$ kPa, $T_o = 300$ K.

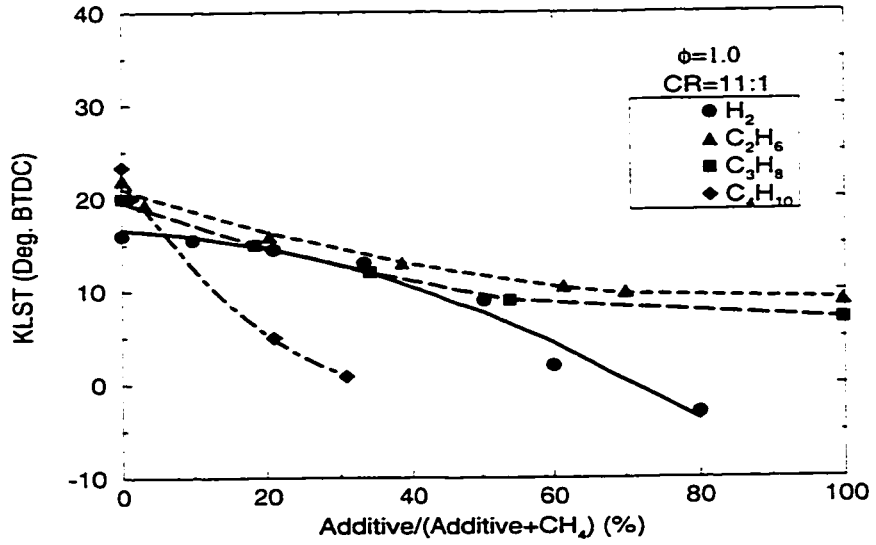

Figure 8.14: Variation of the KLST with volumetric concentration of additive to methane at 900 RPM, $\phi = 1.0$, CR =11:1, $P_o = 87$ kPa, $T_o = 300$ K.

An ideal procedure for knock rating of gaseous fuels should provide a similar effective temperature for different fuel compositions during flame propagation to be able to compare better their reactivity as well as the effective rate of flame propagation. Therefore, keeping the compression ratio constant while changing the fuel composition may not be a suitable approach to investigate changes in the KLST. An improvement in the comparative aspects of the results can be achieved, if the compression ratio is modified for any composition according to the following relationship:

$$\frac{T_{\mathrm{TDC}}}{T_{\mathrm{o}}} = CR_m{}^{\gamma_m - 1} = CR_{ref}{}^{\gamma_{ref} - 1} \tag{8.1}$$

where $\gamma = Cp/Cv$ and CR is compression ratio. T_{o} and T_{TDC} are the initial temperature and the charge temperature at TDC. Subscript 'm' stands for the mixture of the additive-methane-air and subscript 'ref' is for methane-air mixture.

Figure 8.15 shows the required modified compression ratio with the volumetric concentration of the additives in their stoichiometric mixtures with methane for CR_{ref} equals to 8.5:1 and 11:1. It can be seen that the compression ratio needs to be reduced as the hydrogen concentration in its blend with methane is increased, while the compression ratio needs to be increased for binary mixtures of ethane, propane or butane with methane.

On this basis, the variations of the KLST with the volumetric concentration of the additives to methane with the compression ratios modified in accordance with Equation 8.1 are plotted in Figures 8.16 and 8.17. Thin and bold lines show the data for the original geometrical compression ratio 8.5:1 and 11:1, respectively. As expected, hydrogen has the highest KLST, while butane has the lowest. The KLST for ethane is higher than that of propane. A similar trend to that of constant compres-

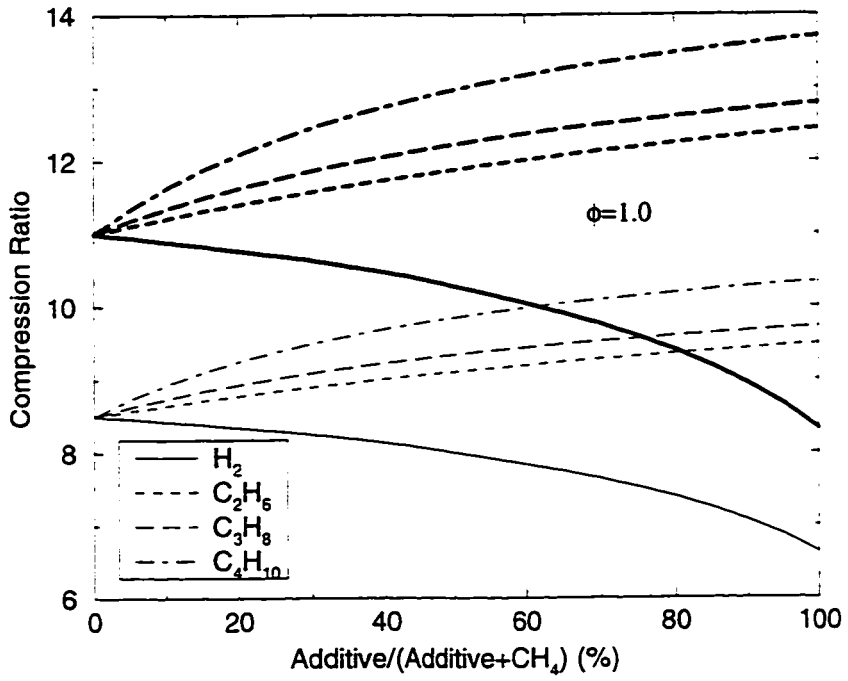

Figure 8.15: Variation of the modified compression ratio with volumetric concentration of additive to methane at 900 RPM, $\phi = 1.0$, $CR = 8.5:1$ and 11:1.

sion ratio can be observed, except for hydrogen-methane mixtures with compression ratio 8.5:1. For the modified compression ratios and a CR_{ref} =8.5:1, the KLST decreases for hydrogen-methane mixture with increasing concentration of hydrogen in the mixture and then increases due to the associated low compression ratio. The KLST does not change significantly with changes in the volumetric concentration of the additive in the mixture for a blend of more than 40% of ethane and propane. A butane-methane mixture has the strongest effect on the KLST, which should make it a suitable fuel combination for the knock rating of gaseous fuels.

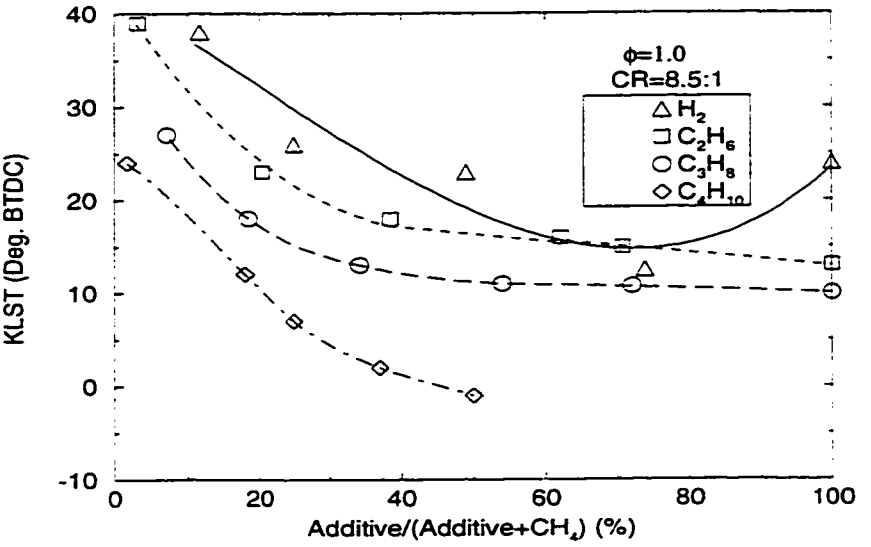

Figure 8.16: Variation of the KLST with volumetric concentration of additive to methane with modified compression ratio at 900 RPM, $\phi = 1.0$, $CR = 8.5 : 1$, $P_o = 87$ kPa, $T_o = 300$ K.

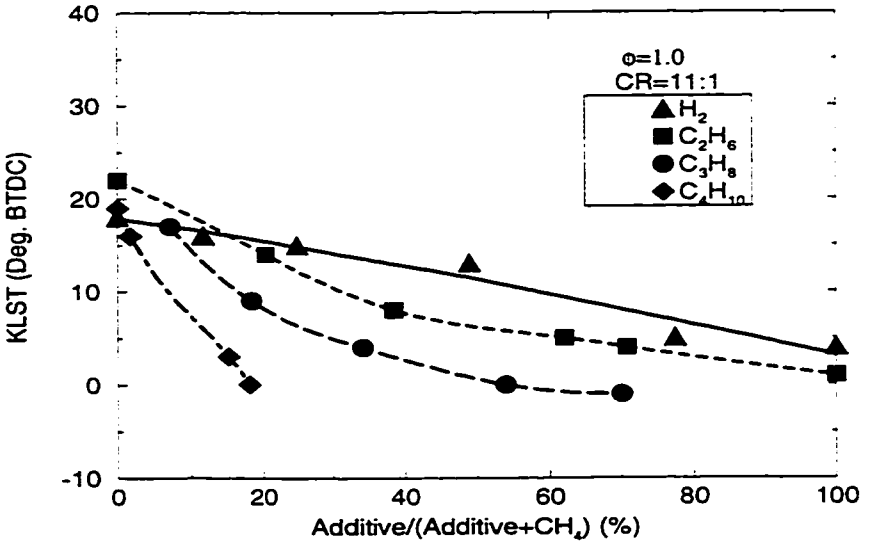

Figure 8.17: Variation of the KLST with volumetric concentration of additive to methane with modified compression ratio at 900 RPM, $\phi = 1.0$, $CR = 11 : 1$, $P_o = 87$ kPa, $T_o = 300$ K.

8.7 KLCR with Constant Spark Timing

The variations of the knock limited compression ratio (KLCR) at a constant spark timing of 15 degrees BTDC with the volumetric concentration of the fuel additive in a binary mixture with methane are plotted in Figures 8.18 and 8.19. The knock limited compression ratio decreases with increasing concentration of the additives in their blends with methane. The linear relationship, reported in reference [61], for hydrogen-methane mixtures is confirmed, while ethane, propane and butane blends with methane did not produce a linear variation of the knock limited compression ratio. The linearity of the KLCR with hydrogen-methane mixtures is mainly due to the almost linear variation in the associated combustion duration. The corresponding combustion duration variation for mixtures of other fuel additives with methane tends to be in comparison relatively small while the corresponding variations in the auto-ignition reaction rates are very much more substantial.

Changes in the concentration of ethane and propane in their blends with methane do not show a significant effect on the KLCR for lean mixtures ($\phi = 0.8$), while for hydrogen and butane a similar and significant effect on the KLCR for different equivalence ratios can be seen. Therefore, for a constant spark timing procedure, it appears that a mixture of either hydrogen-methane or butane-methane can better represent the knock rating of a gaseous fuel than an ethane-methane or propane-methane mixture.

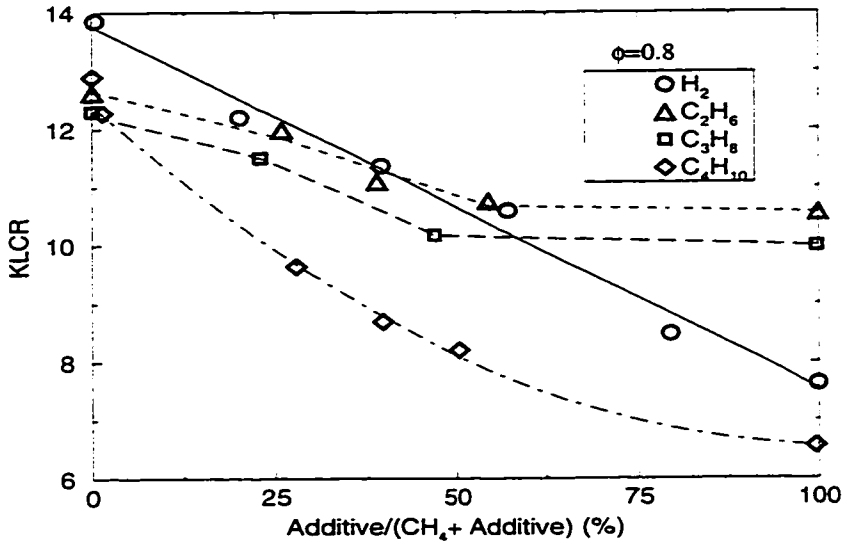

Figure 8.18: Variation of the knock limited compression ratio with volumetric concentration of additive to methane at 900 RPM, $\theta_{st} = 15°$ BTDC, $\phi = 0.8$, $P_o = 87$ kPa, $T_o = 300$ K.

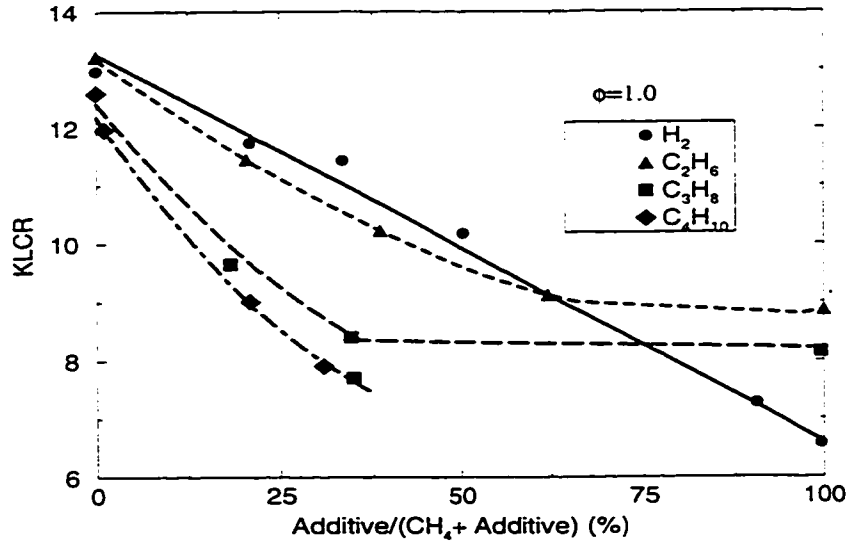

Figure 8.19: Variation of the knock limited compression ratio with volumetric concentration of additive to methane at 900 RPM, $\theta_{st} = 15°$ BTDC, $\phi = 1.0$, $P_o = 87$ kPa, $T_o = 300$ K.

To compare the effect of equivalence ratio for butane-methane and hydrogen-methane mixtures on knock limited compression ratio, the data from the previous figures for these two mixtures with θ_{st} = 15° BTDC are re-plotted in Figure 8.20. In the case of hydrogen-methane, the equivalence ratio has almost a similar effect

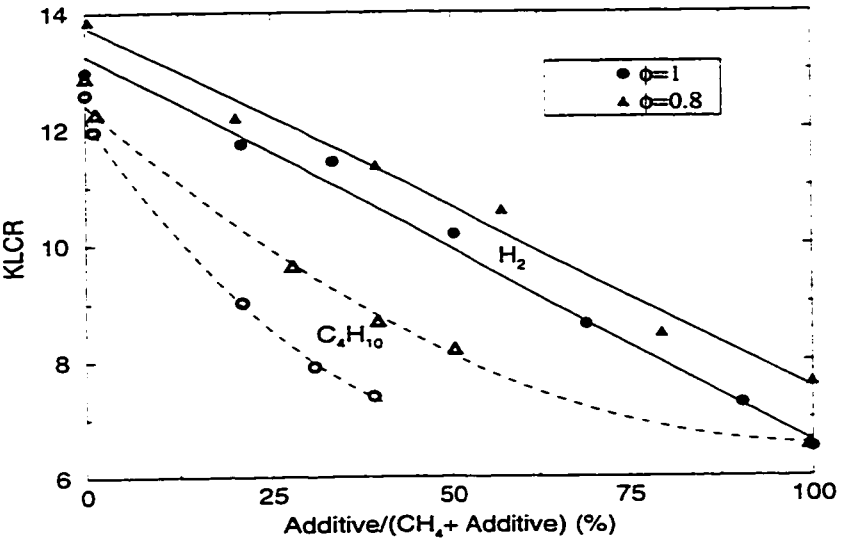

Figure 8.20: Variation of the knock limited compression ratio with volumetric concentration of the additives to methane for different equivalence ratios at 900 RPM, θ_{st} = 15° BTDC, P_o = 87 kPa, T_o = 300 K.

throughout, while its influence on KLCR is changed, becoming greater when the concentration of butane in its mixture with methane increases.

8.8 Summary and Conclusions

The KLCR and KLST decrease with increasing concentration of the additives with methane and increasing equivalence ratio. The corresponding changes for ethane and propane additions have a relatively small effect on the KLCR or KLST, which make

them less suitable for the knock rating of gaseous fuels. Hydrogen-methane mixtures show different influence on KLCR and KLST based on the chosen knock rating procedure and the concentration of the hydrogen in the mixture. For a constant spark timing, the variation of the KLCR with changes in the volumetric concentration of hydrogen in the mixture is linear, while the changes of KLST at constant compression ratio is not. Hence, the results of knock rating a fuel with methane and hydrogen is related to the procedure employed.

A mixture of butane and methane may be considered to be a superior choice for knock rating of gaseous fuels, since the variations of KLCR and KLST with butane concentration in the mixture show a similar trend with sufficient sensitivity to the mixture composition.

Chapter 9

Conclusions and Recommendations

9.1 Introduction

The primary objectives of the present work, as indicated earlier, were the investigation of the effect of different operational variables on the performance and knock intensity of a spark ignition engine fueled with gaseous fuels such as methane, proposing some analytical approaches for optimizing the engine power output and/or efficiency while considering the occurrence of knock and evaluating different knock rating methods for gaseous fuels, used by others.

Most of the knock prediction models, reported in the literature, require experimentally based data, such as the pressure-time history. However, during knocking combustion, the unstable variations of the state parameters make the experimental data unstable and consequently inaccurate, producing unacceptable uncertainties in the predicted results. Moreover, such models cannot be used to predict knock under operating conditions where no experimental data are available.

The two-zone model described in this work is a total predictive model except for emissions. It does not require direct experimental data and in principle it can be applied to any operating conditions. The model not only establishes whether the engine is to knock or not, but can also provide quantitative information about how far the engine is from the onset of knock for any given set of operating conditions. With the established energy based knock criterion, the operating conditions for borderline

knock and the extent of the knock free region can be explored without expensive and time consuming experiments. The computer program developed is generally easy to use and does not need to deal with elaborate computations for predicting turbulent flame propagation.

Two comprehensive automated procedures for optimizing the engine performance with some pre-defined constraints were also presented. It was shown that these procedures can be linked to the two-zone combustion model to search efficiently for either local or global optimum operating conditions for the engine.

The ability to predict engine knock quantitatively without direct experimental data, and the relative ease and universality of application over a range of engine operating conditions makes this model a useful and attractive tool for engine designers, operators and researches. In particular, it would enable specific guidelines to be drafted for the effective conversion of existing engines to gaseous fuel operation.

Some of the limitations of this model, which come largely from the theoretical basis and the associated assumptions of the model are the following:

- In the two-zone model, the combustion chamber is divided into two sections, and it is assumed that each section has uniform temperature and pressure. The unburned zone chemical reaction activities were predicted with de-coupled calculated uniform unburned gas temperature and pressure. This assumption ignores the turbulent nature of the flow in the cylinder and the fact that the flame front is uneven due to turbulence and the end-gas temperature is not necessarily uniform. Some regions that have higher temperatures may lead to an earlier autoignition and knock than when predicted on the basis of a

uniform temperature assumption. Moreover, instead of somehow calculating directly turbulent flame propagation rates and the associated flame front area, an effective energy release pattern was used. This approximation of the real combustion process in the spark ignition engine, though it facilitates the modeling process, has its obvious limitations.

- It was assumed that the cylinder wall temperature is constant and equal to the coolant temperature for lack of better and more realistic representation. In reality, the cylinder wall temperature not only is varying but also may differ from one location to another which affects the amount of heat transfer from the unburned zone to outside. Moreover, when the engine begins to knock the excessive heat transfer to the wall in the region of the end-gas cannot be modeled realistically. These assumptions affect the unburned gas temperature and the accuracy of prediction.

- In simulating the end-gas chemical reactivity, the end-gas temperature was modified when its calculated temperature rise due to the chemical energy release was significant in comparison to that due to the normal combustion. No modification was considered necessary for the cylinder pressure. Furthermore, the normal combustion process was assumed not to be affected directly by the end-gas reaction activity. Since, in a real engine, the combustion and autoignition are inevitably interactive, this approach brings in some unknown errors in the predicted results, particularly when knock is encountered.

- The reaction scheme used in this model has been developed to describe the end-gas autoignition reactions of methane and hydrogen mixtures with air.

However, for other higher hydrocarbons, further experimental data are needed to validate better the combustion period correlations and to use a more comprehensive kinetic scheme [108]. Hence, the application of the model to higher hydrocarbon fuels has its limitations and needs to be carried out more carefully.

Despite these limitations the provision of a generalized model such as the one described can be viewed as a very effective tool in lieu of direct experimentation for projecting and optimizing the performance of a wide range of engines when operating on natural gas and some other common gaseous fuels.

9.2 Conclusions

The simple two-zone model describing the combustion processes in a spark ignition engine can generate important performance parameters, such as the temporal variations in cylinder pressure, the two zone temperatures, power output and efficiency for different values of intake temperature, intake pressure, spark timing and speed, as well as the effects of changes in some design parameters, such as compression ratio, for a spark ignited engine. The results calculated according to this model showed good agreement with the relevant experimental data. The model can also be used to test for the occurrence of knock for any set of operating conditions while employing detailed reaction kinetics for the reactions of the end-gas region. When knocking is encountered, the value of the knock criterion, K, builds up to a sufficiently high value that exceeds an acceptable limit. Under normal operating conditions, the value of K remains at a comparatively low level throughout the combustion period. Its corresponding calculated value can provide an indication of the intensity of the resulting

knock when it occurs. For the CFR engine tested, the knock free limit operation was found to be associated with a maximum value of K that is less than 1.5. The larger the value of K, the bigger the potential intensity of knock.

Procedures were extended to consider operation with fuel mixtures and also to select optimum changes to key operational parameters to get the engine out of a knocking situation with a minimum degradation of engine power and efficiency. The gradient of the knock criterion K_{max} was found to be a proper tool for this purpose. Parametric considerations show that some variables, e.g. equivalence ratio, have significant effects on both the onset of knock and power output. Therefore, changes in their values should be considered carefully when needed to get the engine out of knock. Accordingly, to avoid a significant drop in the power output, it is recommended that equivalence ratio must be kept constant at a maximum acceptable value while other parameters are adjusted to get out of knock.

Some important engine operational parameters (e.g. MBT timing) can be estimated by the two-zone model. It was found that the MBT spark timing can be correlated approximately linearly with the volumetric concentration of hydrogen in methane-hydrogen mixtures for any compression ratio.

The optimization algorithms developed in association with this two-zone combustion model, may be considered as a powerful tool for predicting optimum operating conditions of a spark ignition engine while satisfying a set of imposed requirements. The specific examples considered showed that maximum power can be achieved with pure methane operation at compression ratios around 14:1 and a chemically correct mixture, while maximum efficiency is associated with lean hydrogen-methane operation. The addition of some hydrogen to methane produces a higher efficiency with a

lower compression ratio compared to that for pure methane. A solution that is closer to the global optimum can be obtained from a gradient-based algorithm by selecting initial operating conditions either through the application of the genetic algorithm to a similar problem, or such that maximum power is produced by each of the operational variables individually followed by application of the gradient-based algorithm. An insight into the nature of the problem shows the genetic algorithm is the most appropriate search technique for the global optimum solution, while a gradient-based method can be applied successfully to search for an optimum operating condition close to an initial setting.

The incidence of knock is strongly dependent on the type of the gaseous fuel being used. The effect of various parameters on the apparent methane number requirement of the engine were also investigated and compared with experimental data. Good agreement was observed throughout. The knock region for methane operation is the narrowest among various gaseous fuel-air mixtures investigated and does not change substantially with moderate changes in the intake temperature or the concentration of methane in the mixture. The disagreement between the experimental and analytical results for a blend of methane and hydrogen with a high volumetric concentration of hydrogen is believed to be due to the very high rate of energy release resulting from rapid flame propagation, which makes it difficult to recognize the borderline of knock experimentally. A comparison between methane number procedure and other knock rating procedures was outlined. In contrast to methane-hydrogen mixtures, the concentration of butane in methane-butane mixtures has a strong effect on the knock limited operating conditions; which perhaps indicates that methane and butane can be a more suitable mixture for knock rating of the gaseous fuels.

9.3 Recommendation for Future Work

The present research has made some contributions towards improving our understanding of the combustion process in a spark ignition engine and its influence on the engine performance and its knock intensity. But, there is still much need to continue with similar attempts to improve the present model.

There is a need for further analytical and experimental work to investigate the combustion process and the occurrence of knock especially due to cyclic variations in spark ignition engines. Experimental verification needs to be made of important parameters such as the charge temperature, pressure, fuel composition, etc. The application of the model shall be extended beyond the present four stroke and single cylinder engine. It needs to consider a wider range of engines that would include different sizes and applications of both four and two stroke engines as well as turbocharging.

The present two-zone model was developed mainly for methane-hydrogen mixtures. However, the model can be applied to more complex fuels and their mixtures, such as propane, butane, etc., when the appropriate kinetic schemes and data are made available. Thus, the knock performance can be investigated for the gaseous fuels of different composition.

The effect of the end-gas reaction activity on the whole combustion process is not fully considered. The interaction effect between the end-gas reaction and normal combustion in the two-zone model can be investigated more by considering its effect on the cylinder pressure.

The knock model described did not consider in detail the intake and exhaust

processes (e.g. the effect of scavenging process, turbocharging, intercooling, etc.). Further work is needed to include a more comprehensive modeling of these processes. Also, it needs to have more detailed accounting for the variations in gas motion (e.g. swirl and squish).

In the present work, the intake temperature was assumed to be equal to the lab temperature. Actually, due to the heat transfer from the engine block to the intake manifold, the mixture temperature increases a few degrees. A simple calculation showed that this temperature rise can be up to 10 degrees kelvin. The model needs to be modified to consider the influence of manifold processes including heat transfer on the charge temperature.

References

[1] Karim G.A., Wierzba I., and Al-Alusi Y., "Methane-Hydrogen Mixtures as a Fuel", *Int. J. of Hydrogen and Energy*, Vol. 21, pp. 625–633, 1996.

[2] Kido H., Huang S., Tanoue K., and Nitta T., "Improving the Combustion Performance of Lean Hydrocarbon Mixtures by Hydrogen Addition", *SAE of Japan*, No. 9430653, 1994.

[3] Das A., *Optimization of a Natural Gas Spark Ignition Engine*, PhD thesis, Department of Mechanical and Manufacturing Engineering, University of Melbourne, September 1995.

[4] Weaver C.S., "Natural Gas Vehicle- A Review of the State of Art", *SAE*, No. 892133, 1989.

[5] Klimstra J., "Performance of Lean-Burn Natural-Gas-Fueled Engines on Specific Fuel Consumption, Power Capacity and Emissions", *SAE*, No. 901495, 1990.

[6] Jacob K., "Performance of Lean-Burn Natural Gas Fueled Engine- on Specific Fuel Consumption, Power Capacity and Emissions", *SAE*, No. 901495, 1990.

[7] Dulger M. and Sher E., "Experimental Study on Spark Ignition of Flowing Combustible Mixtures", *SAE*, No. 951004, 1995.

[8] Gatowski J.A. and Heywood J.B., "Effects of Valve-Shrouding and Squish in Combustion in a Spark Ignition Engine", *SAE*, No. 852093, 1985.

[9] Seong-Soo Kim and Sung-Soo Kim, "Effects of Swirl and Spark Plug Shape on Combustion Characteristic in a High Speed Single-Shot Visualized SI Engine", *SAE*, No. 951003, Feb. 1995.

[10] Kesler M. and Rychter T.J., " A Jet Dispersed Combustion (JDC) Method to Stimulate Lean Burning in SI Piston Engines", *SAE*, No. 951006, Feb. 1995.

[11] Olsson K. and Johansson B., "Combustion Chambers for Natural Gas SI Engines, Part 2: Combustion and Emissions", *SAE*, No. 950517, Feb. 1995.

[12] Milton B.G. and Keck J.C., "Laminar Burning Velocity in Stoichiometric Hydrogen and Hydrogen-Hydrocarbon Gas Mixtures ", *Comb. and Flame*, Vol. 58, pp. 13–22, 1984.

[13] Ryan T.W., Callahan T.J., and King S.R., "Engine Knock Rating of Natural Gases-Methane Number ", *Trans. of ASME, J. of Engineering for Gas Turbines and Power*, Vol. 115, pp. 769, October 1993.

[14] Cornetti F., De Cristofaro G.M., and Gozzelino R., "Engine Failure and High Speed Knock", *SAE*, No. 770147, 1977.

[15] Nates R.J. and Yates A.D.B., "Knock Damage Mechanisms in Spark-Ignition Engines", *SAE*, No. 942064, October 1994.

[16] Renault F., "A New Technique to Detect and Control Knock Damage", *SAE*, No. 820073, 1982.

[17] Hirshfeld C.F. and Barnard W.N, *Elements of Heat-Power Engineering*, John Wiley and Sons, 1915.

[18] Ricardo H.R., *The High Speed Internal Combustion Engine*, Blackie and Son Limited, UK, 1923.

[19] Withrow L. and Rassweiler G.M., "Engine Knock", *Automobile Engineer*, Vol. 24, pp. 281–284, 1934.

[20] Withrow L. and Rassweiler G.M., "Slow-Motion Shows Knocking and Non-Knocking Explosions", *SAE*, Vol. 39-2, pp. 297–303, 1936.

[21] Heywood J.B., *Internal Combustion Engine Fundamentals*, McGraw Hill Book Co., 1988.

[22] Warnatz J. and Stahl G., "Numerical Investigation of Time-Dependent Properties and Extinction of Strained Methane and Propane-Air Flamelets", *Combustion and Flame*, Vol. 85, pp. 285–299, 1991.

[23] Westbrook C.K. and Pitz W.J., "A Comprehensive Chemical Kinetics Reaction Mechanism for Oxidation and Pyrolysis of Propane ", *Combustion Science and Technology*, Vol. 37, pp. 117–152, 1984.

[24] Westbrook C.K. and Pitz W.J., "Detailed Kinetic Modeling of Autoignition Chemistry", *SAE*, No. 872107, 1987.

[25] Westbrook C.K., Wartnatz J., and Pitz W.J., "A Detailed Chemical Kinetic Mechanism for the Oxidation of Iso-Octane and n-Heptane over an Extended Temperature Range and its application to Analysis of Engine Knock", 22^{nd} *Symposium (Int.) on Combustion, The Combustion Institute*, 1988, pp. 893–901.

[26] Westenberg A.A. and Fristrom R.M., "H and O Atoms Profile Measure by ESR in C_2 Hydrocarbon-O_2 Flames", 20^{nd} *Symposium (Int.) on Combustion, The Combustion Institute*, 1985, pp. 473.

[27] Krieger R.B. and Borman G.L., "The Computation of Apparent Heat Release for Internal Combustion Engines", *ASME*, No. 66-WA/DGP-4, 1966.

[28] Peters B.D. and Borman G.L., "Cyclic Variations and Average Burning Rates in a SI Engine", *SAE*, No. 700064, 1970.

[29] Benson R.S., Annand W.J.D., and Baruah P.C., "A Simulation Model Including Intake and Exhaust Systems for a Single Cylinder Four Stroke Spark Ignition Engine", *Int. J. Mech. Sci.*, Vol. 17, pp. 97–124, 1975.

[30] Hong C.W., "A Combustion Correlation for Spark Ignition Engines Simulation Under Steady and Transient Conditions", *SAE*, No. 901602, 1990.

[31] Al-Alousi Y., *Examination of the Combustion Processes and the Performance of a Spark Ignition Engine, Using a Data-Acquisition System*, PhD thesis, Department of Mechanical Engineering, University of Calgary, 1982.

[32] Al-Himyary T.J., *A Diagnostic Two-Zone Combustion Model for Spark Ignition Engines Based on Pressure Time Data*, PhD thesis, Department of Mechanical Engineering, University of Calgary, 1988.

[33] Karim G.A. and Gao J., "A Predictive Model for Knock in Gas Fueled Spark Ignition Engine", *Proceeding of the International Congress on Computational Methods in Engineering (ICCME)*, May, Iran 1993, Vol. 2, pp. 429–437.

[34] Hires S.D., Tabaczyinski R.J., and Novak J.M., "The Prediction of Ignition Delay and Combustion Intervals for a Homogeneous Charge Spark Ignition Engine", *SAE*, No. 780232, 1978.

[35] Tabaczynski R.J., Ferguson C.R., and Radhakrishnar K., "A Turbulent Entrainment Model for Spark Ignition Engine Combustion", *SAE*, No. 770647, 1977.

[36] Blumberg P.N. and Kummer J.T., "Prediction of NO Formation in Spark Ignited Engines- An Analysis of Methods of Control", *Combustion Sci. and Tech.*, 1971, Vol. 4, pp. 73–95.

[37] Borgnakke C. and Arpaci V.S., "A Model for the Instantaneous Heat Transfer and Turbulence in a Spark Ignition Engine", *SAE*, No. 800287, 1980.

[38] Davis G.C, Mikulec A., Kent J.C., and Tabaczynski R.J., "Modeling the Effect of Swirl on Turbulence Intensity and Burn Rate in S.I. Engines and Comparison with Experiment", *SAE*, No. 860325, 1986.

[39] Assanis D.N. and Heywood J.B., "Development and Use of Computer Simulation of the Turbocompounded Deisel System for Engine Performance and Component Heat Transfer Studies", *SAE*, No. 860329, 1986.

[40] Watson N. and Janota M.S., *Turbocharging the Internal Combustion Engine*, John Wiley and Sons, New York, 1982.

[41] Kentfield J.A.C., *Nonsteady, One-Dimensional, Internal, Compressible Flows: Theory and Application*, Oxford University Press, 1993.

[42] Bulaty T. and Niessner H., "Calculation of 1-D unsteady flows in pipe systems of I.C. Engines", *ASME*, No. ASME-WA7, 1984.

[43] Woschni G., " A Universally Applicable Equation for the Instantaneous Heat Transfer Coefficient in the Internal Combustion Engines", *SAE Trans.*, Vol. 76, No. 670931, pp. 3065–3083, 1967.

[44] Woschni G. and Fieger J., "Experimental Investigation of the Heat Transfer at Normal and Knocking Combustion in Spark Ignition Engines ", *MTZ*, Vol. 43-2(1982-2), pp. 63–87, 1982.

[45] Syrimis M., Shigahara K., and Assanis D.N., "Correlation Between Knock Intensity and Heat Transfer Under Light and Heavy Knocking Conditions in a Spark Ignition Engine", *SAE*, No. 960495, 1996.

[46] Shayler P.J., May S.A., and Ma T., "Heat Transfer to the Combustion Chamber walls in Spark Ignition Engines", *SAE*, No. 950686, 1995.

[47] Annand W.J.D., "Heat Transfer in the Cylinders of Reciprocating Internal Combustion Engines", *Proc. of IMechE*, Vol. 177, No. 36, 1963.

[48] Eichelburg G., "Some New Investigations of Old Combustion Engine Problems", *Engineering*, Vol. 149, pp. 547, 1939.

[49] Shayler P.J., May S.A., and Ma T., "The Determination of Heat Transfer from the Combustion Chambers of SI Engines", *SAE*, No. 931131, 1993.

[50] Lu J.H., Ezekoye D., Iiyama A., Greif R., and Sawyer R.F., "Effect of Knock on Time-Resolved Engine Heat Transfer", *SAE*, No. 890258, 1989.

[51] Harigaya Y., Fujio T., Ohyagi S., and Tsuji H., "Surface Temperature and Wall Heat-Flux in a Spark Ignition Engine under Knocking and Non-Knocking Conditions", *SAE*, No. 891795, 1989.

[52] Morell T., Rachmil C.I., Kerobar R., and Jennings M.J., "Model for Heat Transfer and Combustion in Spark Ignited Engines and Its Comparison with Experiments", *SAE*, No. 880198, 1988.

[53] Checkel M.D. and Dale J.D., "Testing a Third Derivative Indicator on a Production Engine", *SAE*, No. 861216, 1986.

[54] Checkel M.D. and Dale J.D., "Computerized Knock Detection From Engine Pressure Records", *SAE*, No. 860023, 1986.

[55] Checkel M.D. and Dale J.D., "Pressure Trace Knock Measurement in a Current SI Production Engine", *SAE*, No. 890243, 1989.

[56] Haghgooie M., "Effects of Fuel Octane Number and Inlet Air Temperature on Knock Characteristics of a Single Cylinder Engine", *SAE*, No. 902134, 1990.

[57] Karim G.A. and Klat S.R., "Knock and Autoignition Characteristics of Some Gaseous Fuels and Their Mixtures", *J. of the Institute of Fuel*, Vol. 39, pp. 109–119, March 1966.

[58] Lovell W.G., "Knocking Characteristics of Hydrocarbons", *Ind. Engng. Chem.*, 1948, Vol. 40, pp. 2388–2438.

[59] Boyd T.A., "Pathfinding in Fuels and Engines", *SAE Trans.*, Vol. 4, pp. 182, 1950.

[60] Annand W.J.D. and Sulaiman S.J., "Knock Limits and Performance of Some Gaseous Fuels in a Supercharged Spark Ignition Engine", *Proc. Inst.. Mech. Enggrs*, 1970, Vol. 185-62/71, pp. 857–867.

[61] Leiker M., Christoph K., Rankl M., Cartellieri W., and Pfeifer U., "Evaluation of Anti-Knock Property of Gaseous Fuels by means of the Methane Number and its Practical Application to Gas Engines", *ASME*, No. 72-DGP-4, pp. 1–15, 1973.

[62] Nakagawa Y., Takagi Y., Itoh T., and Iijima T., "Laser Shadow graphic Analysis of Knocking in SI Engine", *SAE*, No. 845001, 1984.

[63] Nakajima Y., Nagai T., Iijima T., Yokoyama J., and Nakamura K., "Analysis of Combustion Patterns Effective in Improving Anti-Knock Performance of a SI Engine", *JSAE Review*, Vol. 13, pp. 9–17, 1984.

[64] Konig G. and Sheppard C.G.W., "End Gas Autoignition and Knock in a Spark Ignition Engine", *SAE*, No. 902135, 1990.

[65] Spicher U. and Kollmeier H.P., "Detection of Flame Propagation During Knocking Combustion by Optical Fiber Diagnostics", *SAE*, No. 861532, 1986.

[66] Spicher U. and Krebs R., "Optical Fiber Technique as a Tool to Improve Combustion Efficiency", *SAE*, No. 902138, 1990.

[67] Spicher U., Kroger H., and Ganser J., "Detection of Knocking Combustion Using Simultaneously High-Speed Schlieren Cinematography and Multi Optical

Fiber Technique", *SAE*, No. 912312, 1991.

[68] Cuttler D.H. and Girgis N.S., "Photography of Combustion During Knocking Cycles in Disc and Compact Chambers", *SAE*, No. 880195, 1988.

[69] Karim G.A., "An Analytical Approach to Auto-Ignition and Knock in Internal Combustion Engines", *J. Mech. Eng. Sci.*, Vol. 6, No. 4, pp. 353, 1964.

[70] Livengood J.C. and Wu P.C., "Correlation of Autoignition Phenomena in Internal Combustion Engines and Rapid Compression Machines", *Fifth Symposium(International) on Combustion*, 1955, pp. 347–356.

[71] Westbrook C.K. and Dryer F.L., "Chemical Kinetic Modeling of Hydrocarbon Combustion", *Prog. Energy Combustion Sci.*, Vol. 10, pp. 1–56, 1984.

[72] Dimpelfeld P.M. and Foster D.E., "The Prediction of Autoignition in a Spark Ignition Engine", *SAE*, No. 841337, 1984.

[73] Zhou G. and Karim G.A., "The Uncatalyzed Partial Oxidation of Methane for the Production of Hydrogen with Recirculation", *ASME, Fossil Fuel Combustion,* PD, Vol. 39, pp. 77–84, 1992.

[74] Karim G.A. and Liu Z., "A prediction Model for Knock in Dual Fuel Engines", *SAE Trans.*, Vol. 101, No. SP 927, 1992.

[75] Karim G.A. and Gao J., "Prediction of the Performance of Spark Ignition Engine Including Knock", *SAE*, No. 932823, 1993.

[76] Cowart J.S., Keck J.B., Heywood C.K., Westbrook, and Pitz W.J., "Engine Knock Predictions Using a Fully-Detailed and Reduced Chemical Kinetic

Mechanism", *Twenty-Third Symposium (International) on Combustion, The Combustion Institute*, pp. 1055, 1990.

[77] Schreiber M., Sadat Sakak A., Poppe C., Griffiths J.F., and Rose D.J., "Spatial Structure in End-Gas Autoignition", *SAE*, No. 932758, 1993.

[78] Pan J. and Sheppard C.W., "A Theoretical and Experimental Study of the Modes of End Gas Autoignition Leading to Knock in SI Engines", *SAE*, No. 942060, 1994.

[79] Blunsdon C.A. and Dent J.C., "The Simulation of Autoignition and Knock in a Spark Ignition Engine with Disk Geometry", *SAE*, No. 940524, 1994.

[80] Bazari Z. and French B.A., "Performance and Emissions Trade-Offs for a HSDI Diesel Engine- An Optimization Study", *SAE*, No. 930592, 1993.

[81] Gardner T.P., "Investigation of the Effects of Engine Design Parameters on Diesel Combustion and Emissions Using Taguchi Methods", *SAE*, No. 920116, 1992.

[82] Hunter C.E., Gardner T.P., and Zakrajsek C.E., "Simultaneous Optimization of Diesel Engine Parameters for Low Emissions Using Taguchi Methods", *SAE*, No. 902075, 1990.

[83] Yan J., Rogalla R., and Kramer T., "Diesel Combustion and Transient Emissions Optimization Using Taguchi Methods", *SAE*, No. 930600, 1993.

[84] Taguchi G., *System of Experimental design: Engineering Methods to Optimize Quality and Minimize Cost*, American Supplier Institute Inc., Dearborn,

Michigan, 1987.

[85] Sobol I., *The Monte-Carlo Method*, The University of Chicago Press, Chicago, 1974.

[86] Shroff H.D. and Hodgetts D., "Simulation and Optimization of Thermodynamic Processes of Diesel Engine", *SAE*, No. 740194, Feb. 1974.

[87] Arora J.S., *Introduction to Optimum Design*, Mc.Graw Hill, 1989.

[88] Rao S.S., *Optimization- Theory and Application*, Wiley Eastern, New Delhi, India, 1979.

[89] Fletcher R., *Practical Methods of Optimization*, John Wiley and Sons, Great Britain, 1987.

[90] Luenberger D.G., *Linear and Nonlinear Programming*, Addison-Wesley, Masschusetts, 1984.

[91] Dennis J.E. and Schnabel R.B., *Numerical Methods for Unconstrained Optimization and Nonlinear Equation*, Prentice-Hall, Englewood Cliffs, New Jersey, 1983.

[92] Mu H., Sun M., Wang R., and Chen J., "The Investigation of Calculation Methods for Optimization of the Performance of the Diesel Engine", *SAE*, No. 930606, 1993.

[93] Holland J. H., *Adaptation in Natural and Artificial Systems*, Univ. of Michigan Presss, Ann Arbor, MI, 1975.

[94] Stadnyk I., "Schema Recombination in Pattern Recognition Problems", *Proc. of the 2nd International Conference on Genetic Algorithm*, Cambridge, MA, July 1987.

[95] Sannier H.A.V. and Goodman E.D., "Genetic Learning Procedures in Distributed Environments", *Proc. of the 2nd International Conference on Genetic Algorithms*, July 1987.

[96] Glover D.E., *Solving a Complex Keyboard Configuration Problem Through Generalized Adaptive Search, Genetic Algorithms and Simulated Annealing*, Lawrence Davis and Morgan Kauffman publishers, Los Altos, CA, 1987.

[97] Davis L. and Steenstrup M., *Genetic Algorithms and Simulated Annealing: An Overview*, Lawrence Davis and Morgan Kauffman publishers, Los Altos, CA, 1987.

[98] Sinnott E.W., Dunn L.C., and Dobhansky T., *Principles of Genetics*, McGraw Hill, NY, 1950.

[99] Hajela P. and Lin C.Y., "Genetic Search Strategies in Large Scale Optimization", *American Institute of Aeronautics and Astronautics (AIAA)*, Vol. 93-CP, pp. 2437–2447, 1993.

[100] Esat I.I. and Pillai R., "Genetic Algorithm Based Vibration Synthesis", *J. of Structural Dynamics and Vibration, ASME*, Vol. PD-52, pp. 21–26, 1993.

[101] Rajeev S. and Krishnamoorthy C.S., "Discrete Optimization of Structures Using Genetic Algorithms", *J. of Structural Engineering*, Vol. 118, No. 5, May

1992.

[102] Jenkins W.M., "Towards Structural Optimization via the Genetic Algorithm", *Computer and Structures*, Vol. 40, No. 5, pp. 1321–1327, 1991.

[103] Androulakis I.P. and Venkatasubramanian V., "A Genetic Algorithmic Framework for Process Design and Optimization", *Computer Chem. Eng.*, Vol. 15, No. 4, pp. 217–228, 1991.

[104] Hopfield J.J., "Neural Networks and Physical Systems with Emergent Collective Computational Abilities", *Proc. of Natl. Acad. Sci.*, 1979, pp. 2554–2558.

[105] Ashrafzadeh F., Nowicki E.P., and Salmon J.C., "The Automatic Design and Optimization of Fuzzy Logic Controllers Based on the Genetic Algorithm", *Proc. of American Neural Network Inst. Of Engineering (ANNIE) Conference*, 1995, pp. 537–542.

[106] Edwards S.P., Pilley A.D., Michon S., and Fournier G., "The Optimization of Common Rail FIF Equipped Engines Through the Use of Statistical Experimental Design, Mathematical Modeling and Genetic Algorithms", *SAE*, No. 970346, pp. 143–161, 1997.

[107] Karim G.A. and Zhou G., "An Analytical Examination of Various Criteria for Defining Autoignition within Heated Methane-Air Mixtures", *Trans. of the ASME, J. of Energy Resources Technology*, September 1994, Vol. 116-3, pp. 175–180.

[108] Liu Z., *Combustion in Gas Fueled C.I. Engines.*, PhD thesis, Department of Mechanical Engineering, University of Calgary, 1995.

[109] Rassweiler G.M. and Withrow L., "Motion Pictures of Engine Flames Correlated with Pressure Cards", *SAE Trans.*, Vol. 42, pp. 185–204, 1938.

[110] Hu H. and Kech J., "Autoignition of Adiabatically Compressed Combustible Gas Mixture", *SAE*, No. 872110, 1987.

[111] Dimpelfeld P.M. and Foster D.E., "The Prediction of Auto-Ignition in a Spark Ignited Engine", *SAE*, No. 841337, 1984.

[112] Gao J., *Knock Modeling in S.I. Engines*, PhD thesis, Department of Mechanical Engineering, University of Calgary, 1993.

[113] Karim G.A. and Al-Himyary T.J., "A Diagnostic Two-Zone Combustion Model for Spark Ignition Engines Based on Pressure-Time Data", *SAE*, No. 880199, 1988.

[114] JANAF, *Thermochemical Tables*, National Bureau of Standards, Washington D.C., USA, 1985.

[115] Strehlow R., *Fundamentals of Combustion*, McGraw Hill Co., 1988.

[116] Badr O., Elsayed N., and Karim G.A., "An Investigation of the Lean Operational Limits of Gas Fueled Spark Ignition Engines", *Trans. of the ASME, J. of Energy Resources Technology*, Vol. 118, pp. 159–163, 1996.

[117] Karim G.A and Wierzba I., "Experimental and Analytical Studies of the Lean Operational Limits in Methane Fueled Spark Ignition and Compression Ignition Engines", *SAE*, No. 891637, 1989.

[118] Al-Himyary T.J., *CFR Engine Operation*, Research Report, The University of Calgary, 1988.

[119] Hirst S.L. and Kirsch L.J., *The Application of a Hydrocarbon Autoignition Model in Simulating Knock and other Engine Combustion Phenomena*, Plenum Press, 1980.

[120] Yu G., Law C.K. , and Wuck, "Laminar Flame Speeds of Hydrocarbon-Air Mixtures with Hydrogen Addition", *Combustion and Flame*, Vol. 63, pp. 339, 1986.

[121] Westbrook C.K. and Pitz W.J., *Complex Chemical Reaction Systems Mathematical Modeling and Simulation*, J. Warnatz and W. Jager(eds.) Springer-Verlag, Heidelberg,West Germany, 1986.

[122] ASTM Commitee D-2, Ed., *ASTM Manual for Rating Motor Fuels by Motor and Research Methods*, American Society for Testing and Materials, 1964.

[123] Lancaster D.R., Krieger R.B., and Lienesch J.H., "Measurement and Analysis of Engine Pressure Data", *SAE*, No. 750026, 1975.

[124] Karim G.A. and Al-Alusi Y.H., "Some Considerations of Cyclic Variations in Spark Ignition Engines Fueled with Gaseous Fuels", *SAE*, No. 840232, 1984.

[125] Michael R.S., Mirza J.Y., Zafer D., and Matthew N.S, "The effects of Hydrogen Addition on Natural Gas Engine Operation", *SAE*, No. 932775, 1993.

[126] Fayette Taylor C., *The Internal Combustion Engine in Theory and Practice*, The M.I.T. Press, 1984.

[127] Karim G.A. and Wierzba I., "Comparative Studies of Methane and Propane as Fuels for Spark Ignition and Compression Ignition Engines", *SAE Trans.*, 1984, Vol. 92, pp. 3677–3688.

[128] Soriano B., "Turbulent Combustion", Master's thesis, Department of Mechanical Engineering, University of Calgary, Dec. 1990.

[129] Caris D.F., Mitchell B.J., McDuffie A.D., and Wyczalek F.A., " Mechanical Octanes for Higher Efficiency", *SAE Trans.*, Vol. 64, pp. 76–100, 1956.

[130] Renault F., "A New Technique to Detect and Control Knock Damage", *SAE*, No. 820073, 1982.

[131] Russ S., "A Review of the Effect of Engine Operating Conditions on Borderline Knock", *SAE*, No. 960497, 1997.

[132] Wilde D.J., *Globally Optimum Design*, John Wiley and Sons, New York, 1978.

[133] Haftka R.T. and Gurdal Z., *Elements of Structural Optimization*, Kluwer Academic Publisher., 1992.

[134] Alizadeh Attar A. and Karim G.A., "An Analytical Approach for the Optimization of a Gas Fueled SI Engine Performance Including the Consideration

of Knock", *Proc. of ASME, International Combustion Engine Division*, April 1997, Vol. 28-2, pp. 65–71.

[135] Goldberg D.E., *Genetic Algorithms in Search, Optimization and Machine Learning*, Addison-Wesley, 1989.

[136] Kreinovich V., Quintana C., and Fuentes O., "Genetic Algorithms: What Fitness Scaling is Optimal", *Cybernetics and Systems: An International Journal*, Vol. 24, No. 0196-9722, pp. 9–26, 1993.

[137] De Jong K.A., *An Analysis of the Behavior of a Class of Genetic Adaptive Systems*, PhD thesis, University of Michigan, Ann Arbor, MI., 1975.

[138] Grefenstette J.J., "Optimization of Control Parameters for Genetic Algorithms", *IEEE Trans. Syst., Man, Cyber. SMC-16*, pp. 122–128, 1986.

[139] Cauchy A., "Methode Generale pour la Resolution des Systemes D'equations Simultanees", *Comp. Rend. l'Academie des Sciences Paris*, Vol. 5, pp. 536–538, 1847.

[140] Schaub F.S. and Hubbard R.L., "A Procedure for Calculating Fuel Gas Blend Knock Rating for Large-Bore Gas Engines and Predicting Engine Operation", *Trans. of the ASME*, Vol. 107, pp. 922–930, October 1985.

[141] Karim G.A. and Klat S.R., "The Measurement of the Mass Flow Rate of Different Gases Using a Choked Nozzle", *Int. J. of Laboratory Practice*, Vol. 15, pp. 184, 1966.

Appendices

Appendix A

The physical properties and the chemical kinetics schemes used in the two-zone model

The two-zone predictive model explained in Chapter 3 includes a chemical kinetics scheme of 155 reaction step and 39 species to predict the reactivity of the end-gas. The physical properties of these 39 species are shown in Table A.1. Figure A.1 and Table A.2 show the flow chart and the relevant information of the chemical kinetic scheme.

Table A.1: The physical properties of the species considered in the chemical kinetic scheme

No.	Species	Chemical Formula	Molecular Weight	Element Count			
				C	H	O	N
1	Methane	CH_4	16.0430	1	4	0	0
2	Ethynyl	C_2H	25.0303	2	1	0	0
3	Acetylene	C_2H_2	26.0382	2	2	0	0
4	Vinyl	C_2H_3	27.0462	2	3	0	0
5	Ethylene	C_2H_4	28.0542	2	4	0	0
6	Ethyl	C_2H_5	29.0622	2	5	0	0
7	Ethane	C_2H_6	30.0701	2	6	0	0
8	Methylidene	CH	13.0191	1	1	0	0
9	Methylene	CH_2	14.0270	1	2	0	0
10	Ketene	CH_2CO	42.0376	2	2	1	0
11	Formaldehyde	CH_2O	30.0265	1	2	1	0
12	Methyl	CH_3	15.0351	1	3	0	0
13	Acetaldehyde	CH_3CHO	44.0536	2	4	1	0
14	Acetyl	CH_3CO	43.0456	2	3	1	0
15	Methyloxide	CH_3O	31.0345	1	3	1	0
16	Ketyl	$CHCO$	41.0297	2	1	0	0
17	Carbon Monoxide	CO	28.0106	1	0	1	0
18	Carbon Dioxide	CO_2	44.0100	1	0	2	0
19	Hydrogen Atom	H	1.00797	0	1	0	0
20	Hydrogen Molecule	H_2	2.01594	0	2	0	0
21	Steam	H_2O	18.0153	0	2	1	0
22	Hydrogen Peroxide	H_2O_2	34.0147	0	2	2	0
23	Formyl	HCO	29.0185	1	1	1	0
24	Hydroperoxo	HO_2	33.0068	0	1	2	0
25	Oxygen	O_2	31.9988	0	0	2	0
26	Oxygen Atom	O	15.9994	0	0	1	0
27	Hydroxyl	OH	17.0074	0	1	1	0
28	Carbon	C	12.0110	1	0	0	0
29	Cyanogen	CN	26.0180	1	0	0	1
30	Nitrogen	N_2	28.0134	0	0	0	2
31	Nitrogen Atom	N	14.0067	0	0	0	1
32	Hydrogen Cyanide	HCN	27.0260	1	1	0	1
33	Hydrogen Isocyanate	$HCNO$	43.0250	1	1	1	1
34	Nitric Acid	HNO_3	63.0130	0	1	3	1
35	Imidogen	NH	15.0150	0	1	0	1
36	Nitrogen Oxide	NO	30.0060	0	0	1	1
37	Nitrogen Dioxide	NO_2	46.0060	0	0	2	1
38	Nitrous Oxide	N_2O	44.0130	0	0	1	2
39	Nitrogen Trioxide	NO_3	62.0050	0	0	3	1

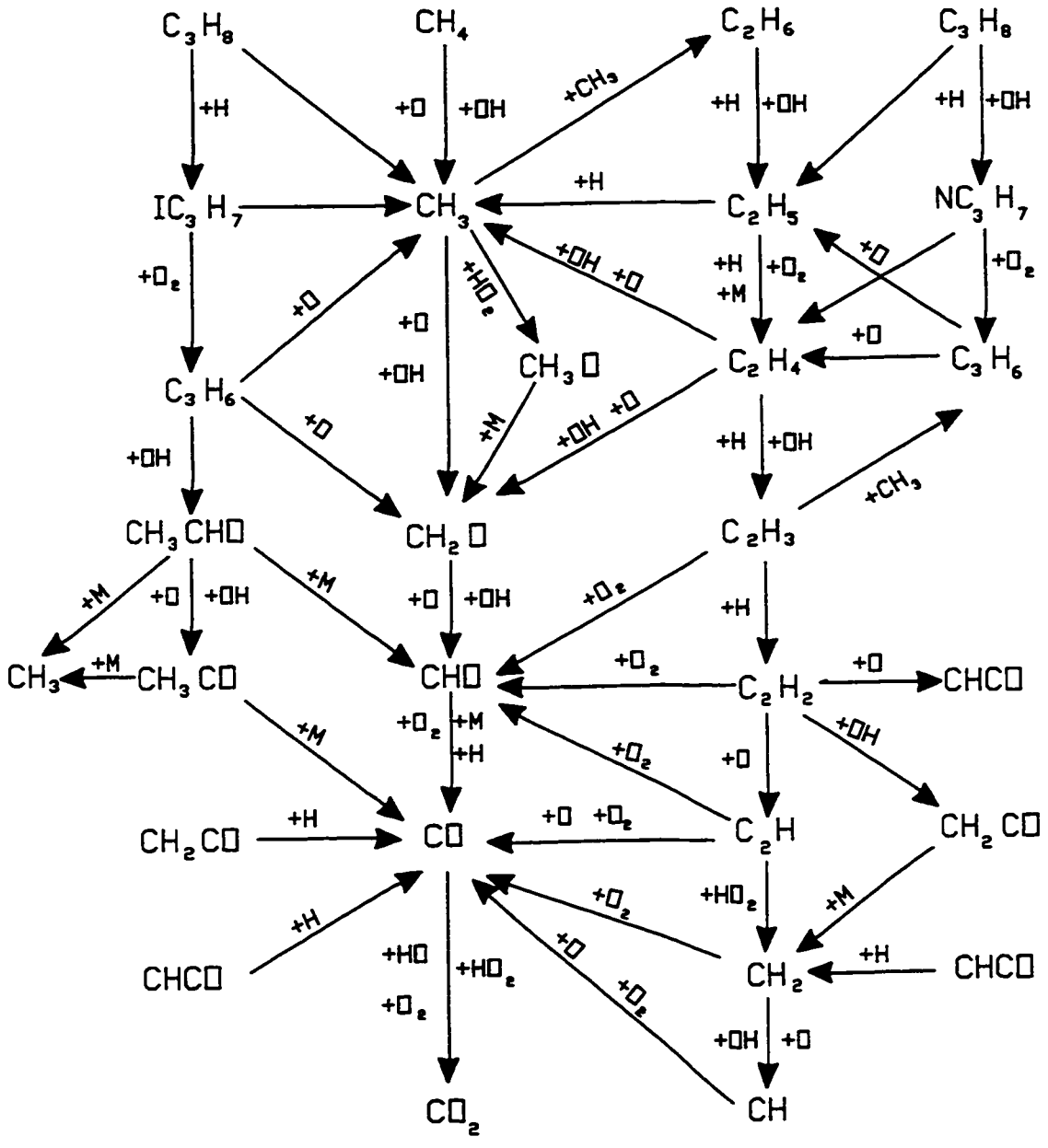

Figure A.1: The flow chart of the chemical kinetic scheme used in the Two-Zone Model.

Table A.2: Chemical kinetic schemes for methane, propane and hydrogen.

No.	Reactions	Forward Reaction Constants			Backward Reaction Constants		
		A_f	B_f	E_f	A_b	B_b	E_b
1	CH4 + OH ⇌ CH3 + H2O	3.460E-03	3.080	8.370E+03	2.990E+07	0.000	8.940E+04
2	CH4 + H ⇌ CH3 + H2	2.200E-02	3.000	3.661E+04	8.330E-04	3.000	3.330E+04
3	CH4 + O ⇌ CH3 + OH	1.200E+01	2.100	3.190E+04	1.990E-01	2.100	2.050E+04
4	CH4 + HO2 ⇌ CH3 + H2O2	1.120E+07	0.000	1.020E+05	7.470E+02	0.000	5.350E+03
5	CH4 + O2 ⇌ CH3 + HO2	7.585E+07	0.000	2.452E+05	1.000E+06	0.000	1.675E+03
6	CH4 ⇌ CH3 + H	6.300E+14	0.000	4.185E+05	1.279E+03	1.000	-1.300E+04
7	CH3 + O ⇌ CH2O + H	1.300E+03	0.000	8.400E+03	1.590E+09	0.000	2.925E+05
8	CH3 + HO2 ⇌ CH3O + OH	3.200E+07	0.000	0.000E+00	2.000E+04	0.000	1.070E+05
9	CH3 + O2 ⇌ CH2O + OH	1.000E+05	0.000	0.000E+00	8.450E+04	0.000	2.117E+05
10	CH2O + OH ⇌ H2O +HCO	7.590E+06	0.000	7.100E+02	4.210E+04	0.490	1.185E+05
11	CH2O + H ⇌ H2 + HCO	3.311E+08	0.000	4.390E+04	2.630E+07	0.000	1.053E+05
12	CH2O + O ⇌ HCO + OH	1.000E+08	0.000	2.220E+04	1.000E+08	0.000	1.460E+05
13	HCO + OH ⇌ CO + H2O	5.000E+07	0.000	0.000E+00	1.170E+08	-0.500	3.824E+05
14	HCO + O2 ⇌ CO + HO2	3.020E+06	0.000	0.000E+00	6.760E+06	0.000	1.351E+05
15	HCO + HO2 ⇌ CH2O + O2	1.000E+08	0.000	1.250E+04	3.630E+09	0.000	1.920E+05
16	CO + OH ⇌ CO2 + H	4.400E+00	1.500	-3.098E+03	1.600E+08	0.000	1.100E+05
17	CO + O2 ⇌ CO2 + O	3.140E+05	0.000	1.570E+05	2.780E+06	0.000	1.830E+05
18	H2 + OH ⇌ H + H2O	2.200E+07	0.000	2.155E+04	9.300E+07	0.000	8.520E+04
19	H2 + O ⇌ H + OH	1.800E+04	1.000	3.711E+04	8.300E+03	1.000	2.900E+04
20	H2 +O2 ⇌ HO2 + H	5.000E+06	0.460	2.240E+05	6.600E+07	0.000	8.930E+03
21	H2 + HO2 ⇌ H +H2O2	7.240E+05	0.000	7.820E+04	1.700E+06	0.000	1.570E+04
22	H + HO2 ⇌ OH + OH	1.500E+08	0.000	4.185E+03	1.530E+04	0.840	1.416E+05
23	H+ H + M ⇌ H2 + M	1.830E+06	-1.000	0.000E+00	6.280E+08	0.000	4.010E+05
24	H+ OH + M ⇌ H2O + M	1.430E+11	-2.000	0.000E+00	1.600E+11	0.000	4.780E+05
25	H+ O2 + M ⇌ HO2 + M	8.000E+05	-1.000	0.000E+00	2.400E+09	0.000	1.900E+05
26	O+ O + M ⇌ O2 + M	4.700E+03	-0.280	0.000E+00	5.100E+09	0.000	4.800E+05

Table A.2: Chemical kinetic schemes for methane, propane and hydrogen (Continued).

No.	Reactions	Forward Reaction Constants			Backward Reaction Constants		
		A_f	B_f	E_f	A_b	B_b	E_b
27	OH+ OH + M ⇌ H2O2 + M	3.200E+10	-2.000	0.000E+00	1.690E+18	-2.000	2.000E+05
28	HO2+ OH ⇌ H2O + O2	1.500E+07	0.000	0.000E+00	1.410E+10	-0.560	2.870E+05
29	H2O+ O ⇌ OH + OH	1.500E+04	1.140	7.213E+04	1.500E+03	1.140	0.000E+00
30	H2O2+ O2 ⇌ HO2 +HO2	1.000E+06	0.000	1.670E+05	2.500E+05	0.000	-5.200E+03
31	H + H2O2 ⇌ H2O + OH	1.000E+07	0.000	1.500E+04	3.340E+06	0.000	3.121E+05
32	H + O2 ⇌ O + OH	5.130E+10	-0.820	6.890E+04	1.300E+07	0.000	2.800E+03
33	C2H6 + H ⇌ C2H5 + H2	5.370E-04	3.500	2.176E+04	9.700E-04	3.500	1.143E+05
34	C2H6 + OH ⇌ C2H5 + H2O	6.300E+00	2.000	2.700E+03	50E-01	2.000	1.000E+05
35	C2H6 + O ⇌ C2H5 + OH	3.000E+01	2.000	2.140E+04	3.140E-01	2.000	4.743E+04
36	C2H6 + O2 ⇌ C2H5 + HO2	4.070E+07	0.000	2.120E+05	1.930E+03	0.590	-2.140E+03
37	C2H6 + HO2 ⇌ H2O2 +C2H5	1.120E+07	0.000	8.100E+04	6.500E+06	0.000	4.300E+04
38	C2H5 + O2 ⇌ C2H4 + HO2	1.500E+05	0.000	0.000E+00	1.330E+05	0.000	5.730E+04
39	C2H5 + H ⇌ CH3 + CH3	3.160E+07	0.000	0.000E+00	3.660E+06	0.000	3.740E+04
40	C2H5 ⇌ C2H4 + H	2.340E+26	-4.240	1.810E+05	1.170E+08	-0.620	7.240E+03
41	C2H5 + O ⇌ CH3CHO+ H	5.000E+07	0.000	0.000E+00	5.360E-01	2.540	2.900E+05
42	C2H4 + OH ⇌ C2H3 + H2O	7.000E+07	0.000	1.255E+04	2.110E+30	-6.580	1.150E+05
43	C2H4 + H ⇌ C2H3 + H2	1.510E+08	0.000	4.270E+04	9.220E+06	0.000	5.845E+04
44	C2H4 + O2 ⇌ C2H3 + HO2	4.220E+07	0.000	2.410E+05	7.760E+03	0.540	-7.177E+03
45	C2H2+ H2 + M ⇌ C2H4 + M	4.600E+00	1.000	1.528E+05	2.600E+11	0.000	3.198E+05
46	C2H3 + O2 ⇌ C2H2 +HO2	1.200E+05	0.000	0.000E+00	1.420E+06	-0.360	4.713E+04
47	C2H3 + H ⇌ C2H2 + H2	2.000E+07	0.000	0.000E+00	3.850E-19	7.390	2.137E+05
48	C2H3 ⇌ C2H2 + H	1.600E+32	-5.500	1.935E+05	8.350E+25	-5.500	4.270E+03
49	C2H + H + M ⇌ C2H2 + M	1.090E-03	1.000	3.220E+03	1.000E+08	0.000	4.770E+05
50	C2H2 + OH ⇌ CH2CO+ H	3.230E+05	0.000	8.370E+02	3.160E+06	0.000	8.732E+04
51	C2H2 + O ⇌ CH2 + CO	6.760E+07	0.000	1.674E+04	1.250E+07	0.000	2.287E+05
52	C2H + O2 ⇌ CO + HCO	2.410E+06	0.000	0.000E+00	2.180E+04	0.540	6.257E+05

Table A.2: Chemical kinetic schemes for methane, propane and hydrogen (Continued).

No.	Reactions	Forward Reaction Constants			Backward Reaction Constants		
		A_f	B_f	E_f	A_b	B_b	E_b
53	C2H + O ⇌ CH + CO	5.000E+07	0.000	0.000E+00	3.160E+07	0.000	2.487E+05
54	CH + O2 ⇌ HCO + O	3.300E+07	0.000	0.000E+00	8.000E+07	-0.070	3.013E+05
55	CH + O ⇌ CO + H	4.000E+07	0.000	0.000E+00	5.490E+08	0.150	7.343E+05
56	CH2 + O2 ⇌ HCO + OH	1.000E+08	0.000	1.148E+04	4.070E+07	0.000	3.204E+05
57	CH2 + O ⇌ CH + OH	1.900E+05	0.680	1.046E+05	5.900E+04	0.680	1.085E+05
58	CH2 + H ⇌ CH + H2	2.690E+05	0.670	1.075E+05	1.900E+05	0.670	1.201E+05
59	CH2 + OH ⇌ CH + H2O	2.690E+05	0.670	1.075E+05	8.120E+05	0.670	1.836E+05
60	CH3CHO+ H ⇌ CH3CO + H2	4.000E+07	0.000	1.757E+04	8.420E+10	-1.370	9.719E+04
61	CH3CHO+ O ⇌ CH3CO + OH	5.000E+06	0.000	7.489E+03	7.390E+09	-1.420	7.979E+04
62	CH3CHO+ OH ⇌ CH3CO + H2O	1.000E+07	0.000	0.000E+00	1.910E+07	0.000	1.532E+05
63	CH3CHO ⇌ CH3 + HCO	7.000E+15	0.000	3.410E+05	3.800E+03	1.000	0.000E+00
64	CH3CO ⇌ CH3 + CO	1.000E+10	0.000	0.000E+00	0.000E+00	0.000	0.000E+00
65	CH2CO+ H ⇌ CH3 + CO	1.090E+07	0.000	1.423E+04	2.310E+06	0.000	1.682E+05
66	CH2CO + O ⇌ HCO + HCO	1.000E+07	0.000	1.000E+04	3.470E+05	0.000	1.400E+05
67	CH2CO + OH ⇌ CH2O + HCO	6.200E+07	0.000	4.000E+03	2.750E+07	0.000	7.740E+04
68	CH2 + CO + M ⇌ CH2CO + M	4.570E-02	0.000	0.000E+00	1.990E+10	0.000	2.510E+05
69	C3H8 ⇌ C2H5 + CH3	1.700E+16	0.000	3.550E+05	1.500E+04	1.000	-1.340E+03
70	C3H8 + O ⇌ IC3H7 + OH	2.820E+07	0.000	2.170E+04	1.870E+06	0.000	4.050E+04
71	C3H8 + O ⇌ NC3H7 + OH	1.130E+08	0.000	3.280E+04	7.500E+06	0.000	5.130E+04
72	C3H8 + H ⇌ NC3H7 + H2	1.300E+00	2.400	1.870E+04	8.900E+03	0.890	6.646E+04
73	C3H8 + H ⇌ IC3H7 + H2	1.320E+00	2.540	2.820E+04	9.120E+03	1.030	6.177E+04
74	C3H8 + OH ⇌ NC3H7 + H2O	5.800E+02	1.400	3.550E+03	1.003E+03	1.250	9.360E+04
75	C3H8 + OH ⇌ IC3H7 + H2O	4.670E+01	1.610	-1.460E+02	3.000E+01	1.610	9.050E+04
76	C3H8 + HO2 ⇌ NC3H7 + H2O2	6.300E+06	0.000	7.400E+04	6.910E+05	0.000	8.100E+04
77	C3H8 + HO2 ⇌ IC3H7 + H2O2	5.600E+06	0.000	6.800E+04	4.160E+05	0.000	7.100E+04
78	C3H8 + CH3 ⇌ NC3H7 + CH4	7.500E+06	0.000	6.250E+04	3.980E+06	0.000	8.350E+04

Table A.2: Chemical kinetic schemes for methane, propane and hydrogen (Continued).

No.	Reactions	Forward Reaction Constants			Backward Reaction Constants		
		A_f	B_f	E_f	A_b	B_b	E_b
79	C3H8 + CH3 ⇌ IC3H7 + CH4	4.306E+06	0.000	5.553E+04	5.830E+06	0.000	8.840E+04
80	C3H8 + C2H5 ⇌ C2H6 + NC3H7	1.000E+05	0.000	4.340E+04	3.630E+04	0.000	4.157E+04
81	C3H8 + C2H5 ⇌ C2H6 + IC3H7	1.000E+05	0.000	4.340E+04	3.630E+04	0.000	4.157E+04
82	NC3H7 + O2 ⇌ C3H6 + HO2	0.000E+00	0.000	0.000E+00	0.000E+00	0.000	7.310E+04
83	IC3H7 + O2 ⇌ C3H6 + HO2	3.000E+06	0.000	1.250E+04	4.141E+04	0.000	5.190E+04
84	NC3H7 ⇌ C3H6 + H	1.250E+14	0.000	1.540E+05	7.940E+06	0.000	1.200E+04
85	IC3H7 ⇌ C3H6 + H	2.000E+14	0.000	1.610E+05	2.890E+08	0.000	1.660E+04
86	NC3H7 ⇌ C2H4 + CH3	9.549E+13	0.000	1.290E+05	2.187E+02	1.000	2.400E+04
87	IC3H7 ⇌ C2H4 + CH3	2.000E+10	0.000	1.230E+05	4.570E-02	1.000	1.800E+04
88	C3H6 + O ⇌ C2H4 + CH2O	6.800E-02	2.560	-4.720E+03	6.600E-02	2.560	3.370E+05
89	C3H6 ⇌ C2H3 + CH3	6.300E+15	0.000	3.580E+05	1.000E+04	1.000	0.000E+00
90	C3H6 + OH ⇌ C2H5 + CH2O	8.000E+06	0.000	0.000E+00	4.600E+07	0.000	7.260E+04
91	CH3 + O2 ⇌ CH3O + O	4.800E+07	0.000	1.210E+05	3.040E+08	0.000	3.070E+03
92	CH2O+ H + M ⇌ CH3O + M	7.700E+20	-6.650	4.050E+04	3.910E+31	-6.650	1.390E+05
93	CH3O + O2 ⇌ CH2O + HO2	6.000E+06	0.000	2.210E+04	2.800E+05	0.000	1.280E+05
94	O + C3H6 ⇌ HCO + C2H5	6.760E-02	2.560	-4.730E+03	1.360E-02	2.560	1.200E+05
95	C3H8 + O2 ⇌ NC3H7 + HO2	4.000E+07	0.000	1.900E+05	2.080E+06	0.000	0.000E+00
96	C3H8 + O2 ⇌ IC3H7 + HO2	4.000E+07	0.000	1.900E+05	2.080E+06	0.000	0.000E+00
97	CO + O + M ⇌ CO2 + M	5.900E+03	0.000	1.715E+04	5.500E+15	-1.000	5.515E+05
98	CO + HO2 ⇌ CO2 + OH	5.800E+07	0.000	9.581E+04	6.600E+08	0.000	3.546E+05
99	CH3 + OH ⇌ CH2O + H2	4.000E+06	0.000	0.000E+00	1.200E+08	0.000	3.043E+05
100	CH2O + HO2 ⇌ H2O2 + HCO	1.000E+06	0.000	3.340E+04	1.090E+05	0.000	2.757E+04
101	CO + H + M ⇌ HCO + M	1.340E+05	-0.930	8.430E+03	2.000E+11	-1.000	7.130E+04
102	C3H6 + OH ⇌ CH3 + CH3CHO	1.000E+05	0.000	0.000E+00	2.800E+05	0.000	8.537E+04
103	C3H6 + O ⇌ CH3 + CH3CO	6.761E-02	2.560	-4.729E+03	1.023E-02	2.560	1.533E+05
104	C3H8 ⇌ NC3H7 + H	4.010E+15	0.000	4.190E+05	2.000E+07	0.000	0.000E+00

Table A.2: Chemical kinetic schemes for methane, propane and hydrogen (Continued).

No.	Reactions	Forward Reaction Constants			Backward Reaction Constants		
		A_f	B_f	E_f	A_b	B_b	E_b
105	C3H8 ⇌ IC3H7 + H	1.570E+15	0.000	4.070E+05	2.000E+07	0.000	0.000E+00
106	C2H4 + O ⇌ CH3 + HCO	2.200E+03	1.200	3.096E+03	1.600E-03	2.370	1.062E+05
107	CH3O + H ⇌ CH3 + OH	4.750E+10	-0.140	8.836E+04	4.500E+08	0.000	6.485E+04
108	C2H5 + O ⇌ OH + C2H4	6.000E+07	0.000	0.000E+00	6.900E+05	0.000	2.680E+05
109	HCO + O ⇌ CO + OH	3.000E+07	0.000	0.000E+00	2.880E+08	0.000	3.678E+05
110	CH3O + OH ⇌ CH2O + H2O	1.810E+07	0.000	0.000E+00	4.620E+03	0.590	4.105E+05
111	C2H2 + O2 ⇌ HCO + HCO	3.980E+06	0.000	1.172E+05	1.000E+05	0.000	2.659E+05
112	C2H2 + O ⇌ C2H + OH	3.230E+09	-0.600	7.113E+04	2.950E+08	-0.600	3.810E+03
113	C2H4 + O ⇌ CH2 + CH2O	4.000E+07	0.000	2.092E+04	3.020E+06	0.000	6.561E+04
114	C2H6 ⇌ CH3 + CH3	6.310E+15	0.000	3.560E+05	1.440E+01	0.000	2.170E+04
115	CHCO + H ⇌ CH2 + CO	3.000E+07	0.000	0.000E+00	6.380E-02	2.200	1.122E+05
116	CHCO + O ⇌ HCO + CO	3.388E+07	0.000	8.370E+03	8.317E+07	0.000	5.367E+05
117	C2H4 + OH ⇌ CH3 + CH2O	4.500E+06	0.000	3.760E+03	1.400E+06	0.000	7.300E+04
118	C2H3+ H + M ⇌ C2H4 + M	2.000E+05	0.000	0.000E+00	6.800E+12	0.000	4.200E+05
119	H2O2 + OH ⇌ H2O + HO2	1.000E+07	0.000	7.500E+03	2.800E+07	0.000	1.378E+05
120	C2H3 + O2 ⇌ CH2O + HCO	4.000E+06	0.000	-1.045E+03	4.000E+06	0.000	3.607E+05
121	C2H2 + O2 ⇌ CH2 + CO2	6.000E+07	0.000	1.674E+05	4.830E-02	0.000	3.753E+05
122	HCO+ H + M ⇌ CH2O + M	6.300E-01	0.000	-1.330E+04	5.000E+10	0.000	3.000E+05
123	H + O + M ⇌ OH + M	1.000E+04	0.000	0.000E+00	8.000E+13	-1.000	4.336E+05
124	HO2 + O ⇌ O2 + OH	2.000E+07	0.000	0.000E+00	2.810E+08	-0.330	2.141E+05
125	C2H6 + CH3 ⇌ C2H5 + CH4	5.500E-07	4.000	3.470E+04	2.290E+08	0.000	1.001E+05
126	IC3H7 + C3H8 ⇌ C3H8 + NC3H7	3.020E+04	0.000	5.400E+04	3.020E+04	0.000	5.400E+04
127	H2 + O2 ⇌ OH + OH	2.500E+06	0.000	1.630E+05	6.000E+04	0.000	8.537E+04
128	C2H3 + C2H5 ⇌ C2H4 + C2H4	1.500E+08	0.000	-1.100E+04	5.000E+08	0.000	2.710E+05
129	CH3 + O ⇌ H2 + HCO	1.000E+08	0.000	0.000E+00	9.372E+07	0.000	3.943E+05
130	C2H4 + H2 ⇌ CH3 + CH3	1.540E+14	-0.750	3.794E+05	5.000E+09	0.000	1.339E+05

Table A.2: Chemical kinetic schemes for methane, propane and hydrogen (Continued).

No.	Reactions	Forward Reaction Constants			Backward Reaction Constants		
		A_f	B_f	E_f	A_b	B_b	E_b
131	CH2O + CH3 ⇌ CH4 + HCO	1.000E+04	0.500	2.512E+04	2.090E+04	0.500	8.851E+04
132	CH3 + HCO ⇌ CH4 + CO	3.000E+05	0.500	0.000E+00	5.140E+07	0.500	3.787E+05
133	HCO + O ⇌ CO2 + H	3.000E+07	0.000	0.000E+00	9.690E+09	0.000	4.611E+05
134	H2O2 + O ⇌ HO2 + OH	2.800E+07	0.000	2.681E+04	9.510E+06	0.000	8.668E+04
135	CH2 + O2 ⇌ CO + H2O	1.870E+04	0.000	-4.184E+03	3.070E+00	1.400	7.276E+05
136	H + HO2 ⇌ O + H2O	3.000E+07	0.000	7.200E+03	2.950E+07	0.000	2.445E+05
137	C2H6 + C2H4 ⇌ C2H5 + C2H5	5.000E+05	0.000	2.500E+05	5.000E+05	0.000	0.000E+00
138	C3H6 ⇌ C3H5 + H	1.000E+13	0.000	3.260E+05	1.000E+05	0.000	0.000E+00
139	C3H6 + HO2 ⇌ C3H5 + H2O2	3.240E+05	0.000	6.220E+04	3.400E+04	0.000	6.150E+04
140	C3H6 + OH ⇌ C3H5 + H2O	2.000E+07	0.000	1.279E+04	3.800E+01	0.000	3.044E+05
141	C3H6 + O2 ⇌ C3H5 + HO2	1.000E+08	0.000	1.632E+05	1.000E+05	0.000	0.000E+00
142	C3H5 ⇌ C3H4 + H	3.981E+13	0.000	2.926E+05	1.000E+02	1.000	0.000E+00
143	C3H5 + O2 ⇌ C3H4 + HO2	6.020E+05	0.000	4.180E+04	1.200E+05	0.000	4.185E+04
144	C3H4 + OH ⇌ CH2O + C2H3	1.000E+06	0.000	0.000E+00	8.490E+05	0.000	1.410E+05
145	C3H4 + O ⇌ HCO + C2H3	1.000E+06	0.000	0.000E+00	2.950E+04	0.000	1.288E+05
146	C3H4 + OH ⇌ HCO + C2H4	1.000E+06	0.000	0.000E+00	5.011E+05	0.000	1.413E+05
147	NO + N1 ⇌ O + N2	3.270E+06	0.300	0.000E+00	1.670E+08	0.000	3.174E+05
148	N1 + O2 ⇌ O + NO	6.400E+03	1.000	2.629E+04	3.880E+06	0.000	1.666E+05
149	N1 + OH ⇌ H + NO	3.800E+07	0.000	0.000E+00	1.200E+08	0.000	2.024E+05
150	NO + HO2 ⇌ NO2 + OH	8.700E+05	0.000	0.000E+00	6.000E+06	0.000	3.350E+04
151	NO + O + M ⇌ NO2 + M	5.800E-02	0.000	-3.580E+04	1.100E+10	0.000	2.720E+05
152	NO2 + O ⇌ NO + O2	1.000E+07	0.000	2.510E+03	2.204E+06	0.000	1.930E+03
153	NO2 + H ⇌ NO + OH	2.900E+07	0.000	0.000E+00	3.500E+05	0.000	1.230E+05
154	NO + O + M ⇌ NO2 + M	5.800E-02	1.000	-3.600E+04	1.100E+10	0.000	2.721E+05
155	NO + NO + O2 ⇌ NO2 + NO2	4.900E-06	1.000	2.512E+03	4.000E+06	0.000	1.130E+05

Appendix B

Air and Fuel Metering

(A) Viscous Flow Air Meter

A laminar flow meter was used for measurement of the air flow rates into the engine. The two pressure taps were connected to an inclined manometer containing "Meriam Oil". The meter was calibrated as installed on the engine using the sharp edged orifice plate method. The calibration of the air meter was carried out in situ, i.e. as installed in the intake air ducting system. During the actual calibration of the meter, a large tank was attached upstream of it to dampen the pulsation. The orifice installation was attached to the side of the tank and upstream of it. A schematic representation of the calibration set-up is shown in Figure B.1.

As the engine was running at a constant speed of 900 RPM, varying the air flow rate was possible by either using a throttle valve installed downstream of the air meter or feeding the engine gaseous fuel from the fuel control panel and therefore fulfilling the breathing capacity of the engine partially with the fuel, resulting in relatively lower air flow rates.

The resulting calibration curve for the air meter is plotted in Figure B.2. It shows also the straight line curve fitting equation, used in this research, to these data.

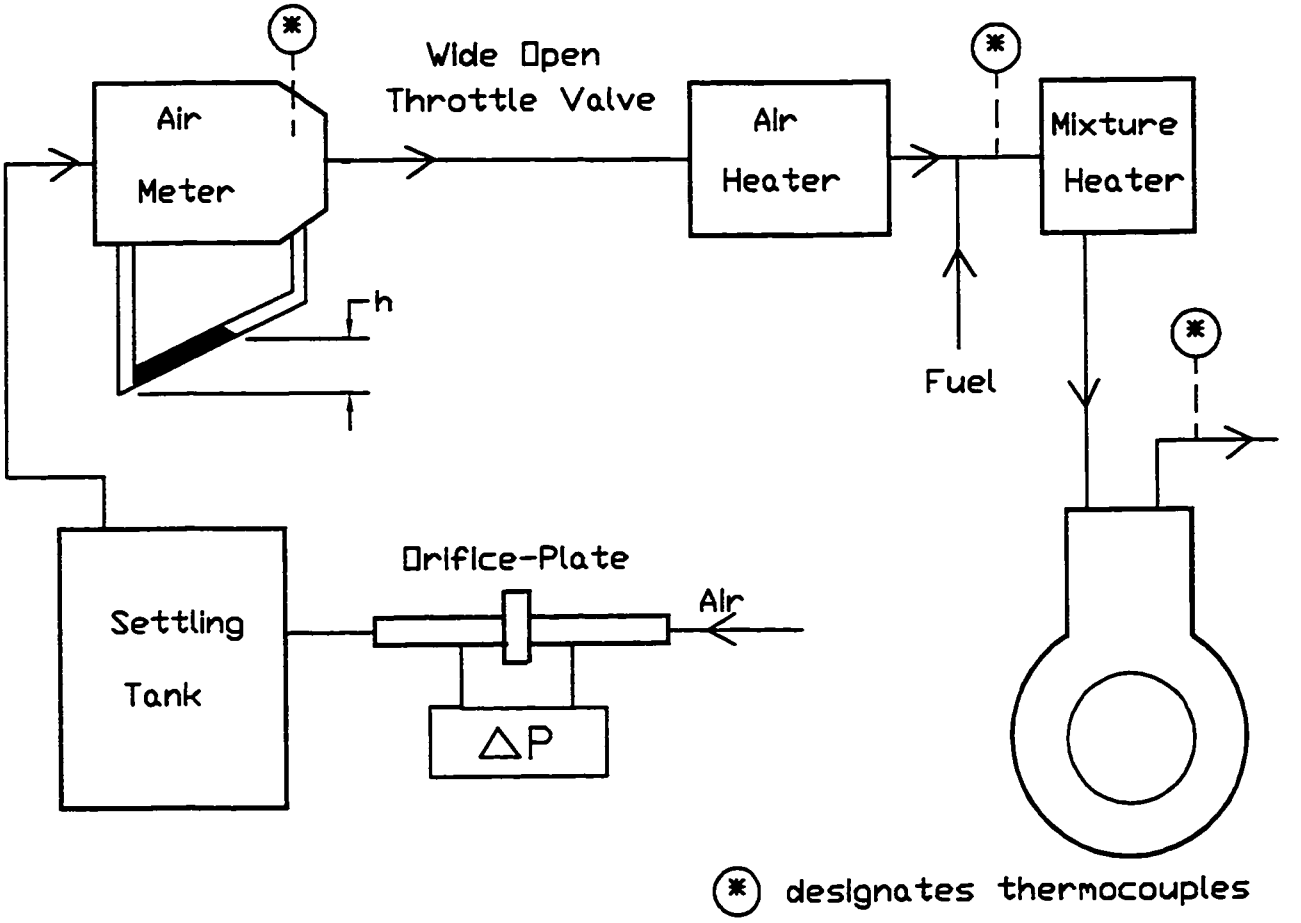

Figure B.1: A schematic diagram of the air meter calibration set-up.

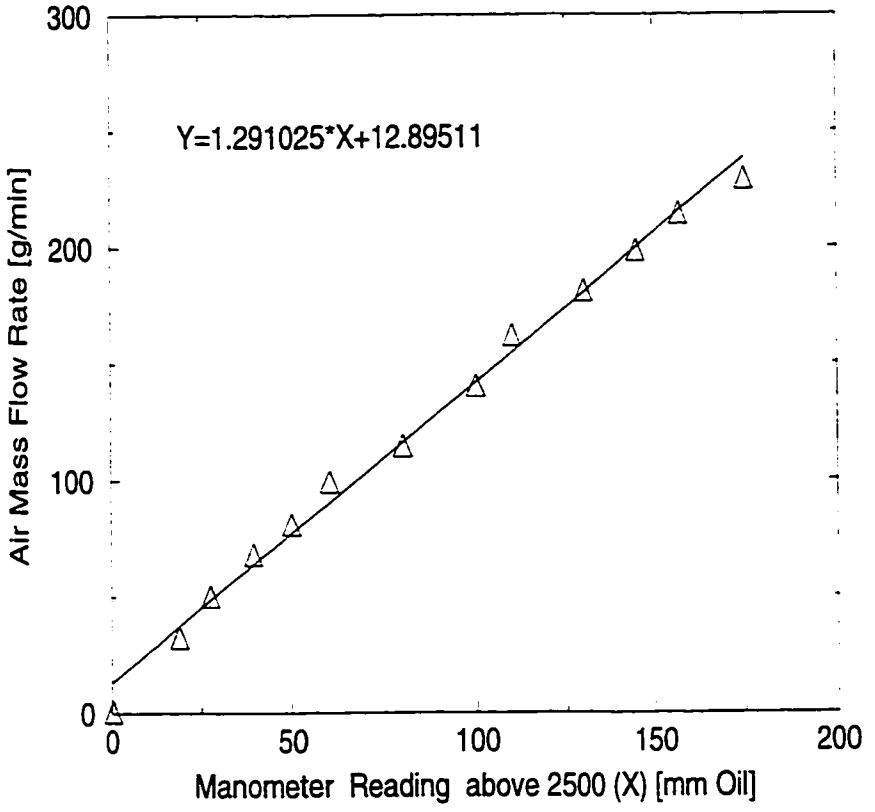

Figure B.2: Calibration curve for the Meriam Oil Manometer.

(b) Fuel Metering System

The engine was operated with processed natural gas as the main fuel. Its composition typically is shown in Appendix (C). The fuel was metered by choked nozzles. These nozzles were calibrated with a wet test meter using air as the working fluid. The results were then converted to yield flow rates for the fuel using the equation suggested by Karim and Klat [141]. Nozzles were manufactured for the fuel as well as for the additive gases to investigate the effects of changes in fuel composition. A separate panel, similar to the fuel metering panel, was used for supplying additives to the engine. It should be noted that the calibration of all choked nozzles were done while they were mounted on the panel where they were eventually used. This assured consistency and eliminated the need to consider the accuracy of the pressure gauges or the effect of the panel piping geometry, etc. on the gas flow rate.

The calibration curve for the processed natural gas nozzle used in this research is shown in Figure B.3.

Figures B.4, B.5 and B.6 show the calibration curves and the corresponding linear curve fitting equations for the additives line.

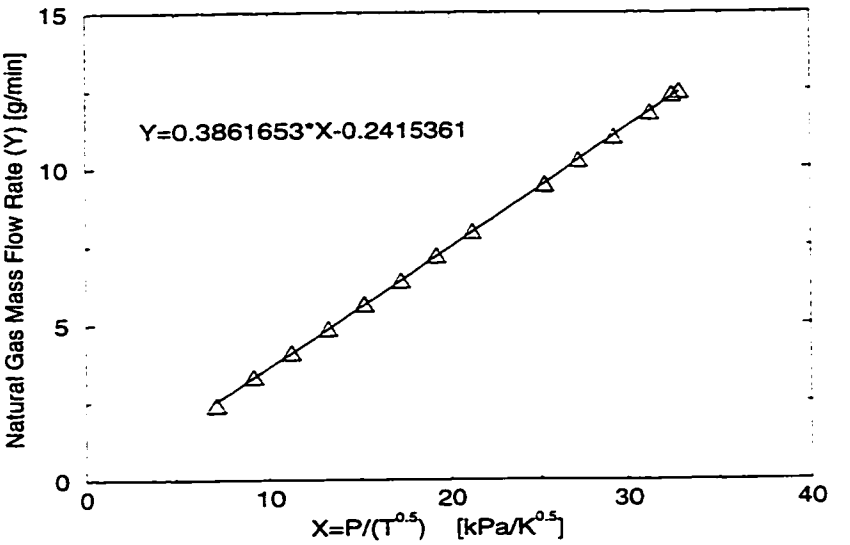

Figure B.3: Calibration curve for Natural Gas line.

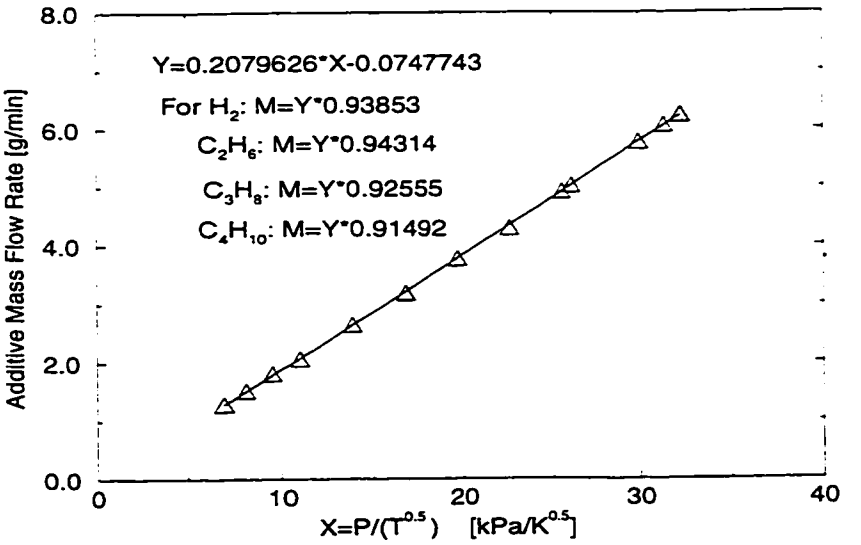

Figure B.4: Calibration curve for Additives, Nozzle 1.

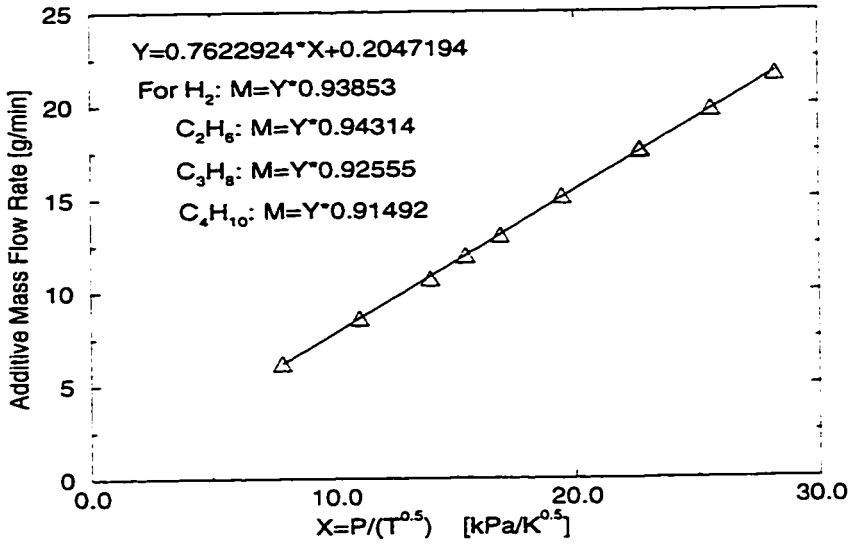

Figure B.5: Calibration curve for Additives, Nozzle 2.

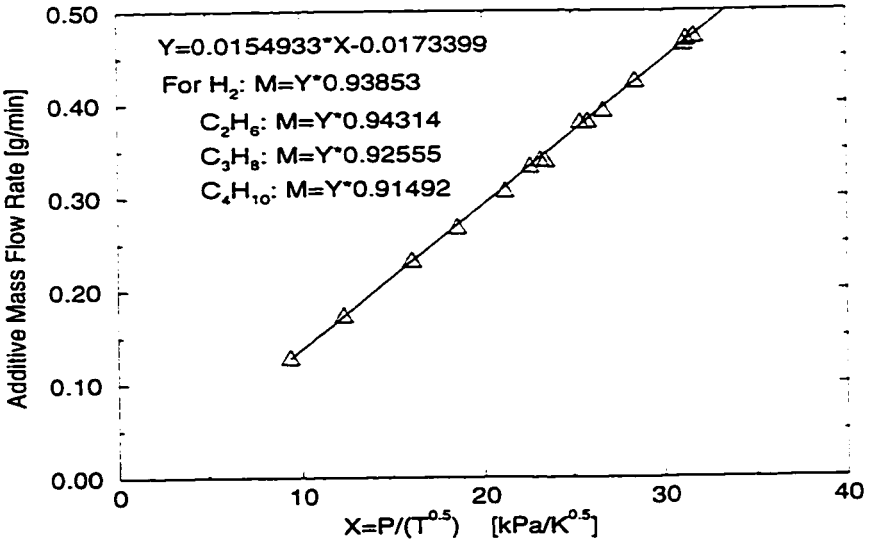

Figure B.6: Calibration curve for Additives, Nozzle 3.

Appendix C

Fuel Composition

The gaseous fuels used are processed natural gas, hydrogen, ethane, propane and butane. The typical composition of the processed natural gas is listed in the following table. The others have more than 99% purity and are considered to be pure hydrogen, propane, ethane and butane.

Composition of the Processed Natural Gas

Specie	Formula	Molar Concentration
Methane	CH_4	93.07%
Ethane	C_2H_6	5.74%
Carbon Dioxide	CO_2	0.16%
Nitrogen	N_2	1.03%

IMAGE EVALUATION
TEST TARGET (QA-3)

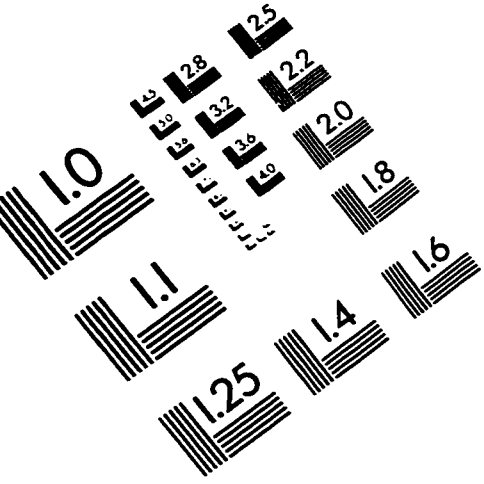

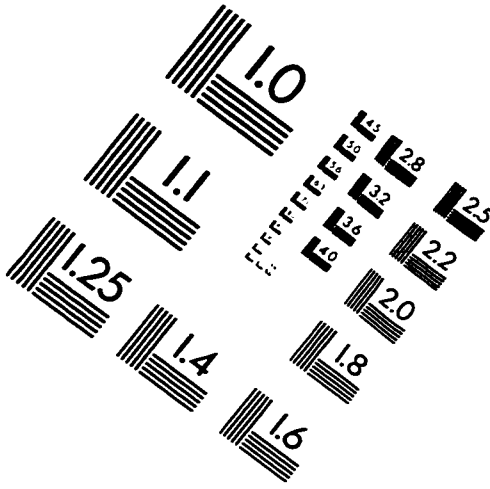

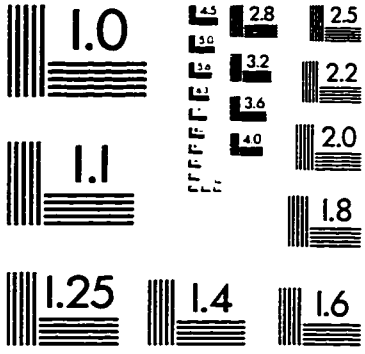

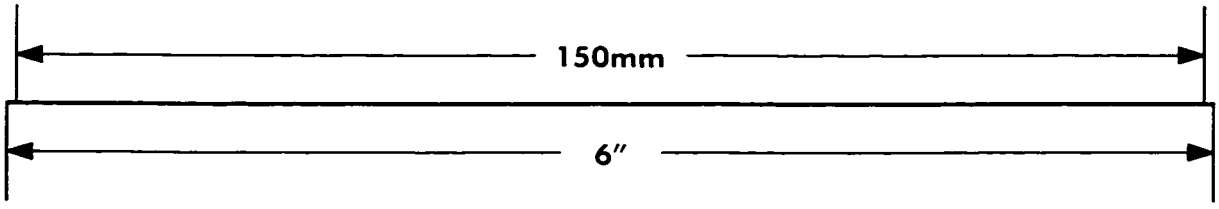

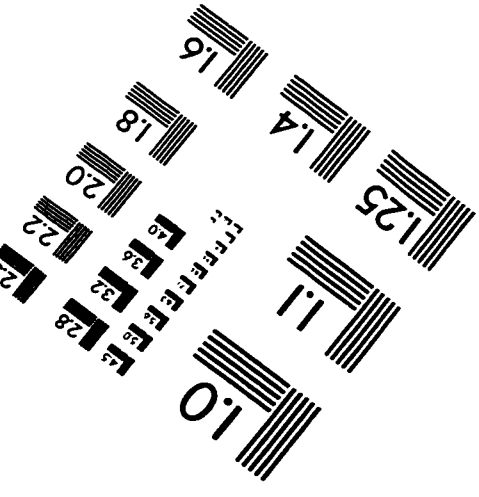

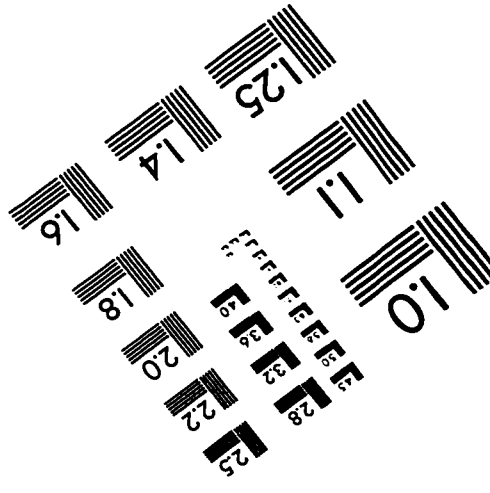

APPLIED IMAGE, Inc
1653 East Main Street
Rochester, NY 14609 USA
Phone: 716/482-0300
Fax: 716/288-5989